2017

Development of Cathode Materials for Room Temperature Lithium/Sulfur Batteries

Mohammad Rejaul Kaiser
University of Wollongong

UNIVERSITY OF WOLLONGONG

Institute for Superconducting and Electronic Materials

(ISEM)

Development of Cathode Materials for Room Temperature Lithium/Sulfur Batteries

Mohammad Rejaul Kaiser

This thesis is presented as part of the requirements for the Award of the

Degree of Doctor of Philosophy

of the University of Wollongong

January, 2017

Declaration

I, Mohammad Rejaul Kaiser, declare that this thesis, submitted in fulfilment of the requirements for the award of Doctor of Philosophy, in the Institute for Superconducting and Electronic Materials, Faculty of Engineering, University of Wollongong, is wholly original work unless otherwise referenced or acknowledged. This thesis has not been submitted for qualifications at any other academic institution.

Mohammad Rejaul Kaiser

January, 2017

Dedication

To my friends and family who stand by me all the time

Abstract

The demand for high energy batteries is increasing day by day due to recent advances in portable electronic devices, which require high energy and power to run. Current Li-ion technology that has been predominant for the last 20 years has reached its limit and can hardly deliver a specific capacity of 170 mA h g^{-1}. Moreover, recent electric vehicle (EV) and hybrid electric vehicle (HEV) technology demands high gravimetric and volumetric energy density batteries so that the vehicle can run for 400 to 500 km with a single charge. Considering all these facts, there is a crying need to find an alternative material that has high theoretical energy density along with low cost and environmental benignity.

Elemental sulfur, which is abundant in nature, is produced as a by-product of oil extraction, and every year, hundreds of millions of tons are accumulated at the oil extraction sites. Sulfur has a theoretical specific capacity of 1675 mA h g^{-1}, which is only surpassed by silicon, and a gravimetric energy density of 2600 Wh/kg. Moreover, sulfur is considered as only a slightly toxic type of material, belonging to Toxicity Class III, based on the rules of the United States Environmental Protection Agency. These alluring features (abundance, low cost, environment friendliness, high capacity and energy) make it very promising for the next generation of cathode materials for rechargeable batteries technologies. Despite the above-mentioned advantages, there are a number of intricate challenges that must be overcome to make the sulfur cathode suitable for battery use and commercially available. The most fatal challenges for lithium-sulfur batteries are: (i) the low conductivity of elemental sulfur, which leads to low active material (sulfur) utilization and poor rate capability in the cathode; (ii) the electrochemical reduction is not a single step process and generates various forms of intermediate lithium polysulfides, which are highly soluble in organic electrolyte and induce the well-known shuttle effect, as well as causing the formation of an insulating layer on the anode surface, while the precipitation of active materials causes irreversible loss of sulfur

active material over repeated cycles; and (iii) the change in volume when sulfur is converted to sulfide (because of the density difference) during cycling leads to its mechanical rupturing and consequent rapid degradation of the electrochemical performance.

These challenges can be minimize by modifying the anode, electrolyte and cathode. There are numbers of attempt has been tried to solve the problems but yet to resolve completely. In my doctoral work, I focused on the cathode to minimize the aforementioned problems by adopting different fabrication methods of sulfur-carbon composite and lithium sulfide-carbon composite along with inserting carbon inter layer and applying new charging technique.

The whole of this thesis work can be divided into two parts. In the first part, the high energy ball-milling method was applied to fabricate sulfur-carbon and lithium sulfide-carbon composites from different carbon sources, combined with optimization of the processing parameters and suitable composites. Finally, to improve the cycling performance and capacity retention, a free-standing layer of single-walled carbon nanotubes was inserted between the cathode and separator, and used in conjunction with fixed capacity charging. With the help of this, an initial discharge capacity of 1670 mAh/g was achieved with very high capacity retention.

In the second part, sulfur-carbon composite was chemically synthesized from a thiosulfate and polysulfide solution by spray precipitation and the reverse microemulsion method. In the spray precipitation method, I synthesized carbon-sulfur composite by using a modified chemical process, which can be considered as an industry-oriented, facile method to produce high-surface-area sulfur particles and to obtain a homogeneous dispersion of sulfur in carbon black. In this chemical process, sodium thiosulfate solution was sprayed into an oxalic acid – carbon black (CB) solution to achieve precipitation of sulfur in the carbon black solution. It was found that spray-precipitated carbon-sulfur composite showed better discharge capacity

and capacity retention compared to the products of the conventional method, in which a pipette is used to drop thiosulfate solution onto acid solution. This conventional method is known as the drop precipitation method.

In the reverse microemulsion method, sulfur was precipitated out from a functionalized graphene-containing sodium polysulfide solution when reacted with hydrochloric acid. The reaction occurred through a reverse microemulsion process, where small droplets of aqueous phase were homogeneously dispersed into oil phase that contained carbo-oxylated functionalized hydrophilic graphene to make a microemulsion. A second microemulsion was also prepared, where a hydrochloric-acid-containing aqueous phase was homogeneously dispersed into oil phase. These two emulsions were then mixed together so that the aqueous phases could mix with each other and react. The reaction product was sulfur which was firmly adhered to functionalized graphene. This functionalized sulfur-graphene composite can effectively minimize the shuttle behaviour and showed a very high and stable discharge capacity with extremely low capacity fading after several hundred cycles. Furthermore, to increase the active material content, boron and nitrogen-doped 3-D carbon cloth was used where more than 8mg of sulfur was loaded in a 1cm diameter carbon cloth. Finally, this high active material loaded carbon cloth showed discharge capacity of ~1200 mAh/g with 98% capacity retention.

Acknowledgements

First of all, I would like to express my deepest appreciation to my supervisors, Prof. Jiazhao Wang, Prof. Shixue Dou and Prof. Huakun Liu, for their academic supervision and guidance, constant support and encouragement, and invaluable advice during my PhD study in Wollongong.I also would like to thank Prof. Chunsheng Wang who provided me with supervision and support during my visit to the University of Maryland, College Park, USA. Many thanks go to Dr. Tania Silver as well, who always critically read every manuscript during my Ph.D study.

Financial support provided by an Excellerate Australia (Former Auto CRC) Project (Auto CRC-2020). I also would like to thank the University of Wollongong as sponsor of my University Postgraduate Award and International Postgraduate Tuition Award.

Moreover, I would like to thank the staff members and technicians at ISEM for their kind assistance, including Dr. Shahriar Hossain, Dr. Germanas Peleckis (XRD), Dr. Mitchel (TEM), Dr. Kosta Konstantinov (BET, TGA/DTA), Dr. Mitchell Nancarrow (SEM), Mr. Tony Romeo (SEM, EDS), Mrs. Crystal Longin, Mrs. Narelle Badger, Ms. Joanne George (OH&S), Mr. Robert Morgan, Mr. Mathew Davis, and Mrs. Candace Gabelish.

Many thanks to Dr. Xin Liang, Dr. Majharul Haque Khan, Mr. Nazrul Islam, Mr. Monirul Islam, Dr. Yunxiao Wang, Dr. Zhijia Zhang, Dr. Jiantie Xu, Mr. Yuede Pan, Dr. Jun Wang, Dr. Lili Liu, Dr. Weijie Li, Dr. Xuanwen Gao, Dr. Wenbin Luo, Dr. Azrin Akter, Dr. Parvez Mannan, Dr. Mansur Ahmed, Mr. Shaon Barua, Mr. Shazed Aziz, Mrs. Bidita, Mrs. Faizunnesa and other students and staff in ISEM.

Table of Contents

Nomenclature

List of Abbreviations

Abbreviation	Full name
3D	Three-dimensional
a.u.	Arbitrary unit
BET	Brunauer-Emmett-Teller
CNT	Carbon nanotube
CV	Cyclic voltammetry
DTA	Differential thermal analysis
EDS	Energy dispersive X-ray spectroscopy
EIS	Electrochemical impedance spectroscopy
EVs	Electric vehicles
FESEM	Field-emission scanning electron microscopy
HEVs	Hybrid electric vehicles
GO	Graphene oxide
HRTEM	High-resolution transmission electron microscopy
LIBs	Lithium-ion batteries
LSB	Lithium-Sulfur Battery
MWCNT	Multi-walled carbon nanotube
NMP	1-methyl-2-pyrrolidinone
PPy	Polypyrrole
Py	Pyrrole
PTS Na	Sodium p-toluenesulphonate

Nomenclature

PVDF	Polyvinylidene fluoride
SAED	Selected area electron diffraction
SDBS	sodium dodecyl benzene sulphonate
SEI	Solid electrolyte interphase
SEM	Scanning electron microscopy
SWCNT	Single-walled carbon nanotube
TEM	Transmission electron microscopy
TGA	Thermogravimetric analysis
XRD	X-ray diffraction

List of Symbols

Symbol	Name	Units
2θ	Detection angle in XRD	°/Degree
C-rate	Charge or discharge rate	mA g^{-1}
m	Active material weight	G
P	Relative pressure	Pa
P_0	Saturation pressure	Pa
S_{BET}	Specific BET surface area	m^2 g^{-1}
SE	Specific energy	Wh kg^{-1}
SP	Specific power	W kg^{-1}
T	Temperature	K or °C
t	Time	h or s
λ	X-ray wavelength	Å

List of Organizations

Abbreviation	Full name
AIIM	Australian Institute for Innovative Materials
EMC	Electron Microscopy Centre
ISEM	Institute for Superconducting and Electronic Materials
UOW	University of Wollongong
UMD	University of Maryland

List of Figures

List of Tables

Chapter 1. Introduction

1.1.Background and motivation

Li-ion battery (LIB) technologies have become an indispensable part of our daily lives since they were introduced by Sony in 1991. With the emergence of new portable electronic devices (e.g. smart phones, tablets, laptop computers, cameras, hover-boards, drones, etc.), the consumption of LIBs has increased significantly, and in 2015 it was more than five billion [1]. With the successful usage of LIBs in portable electronics, the focus has now been shifted to plug-in electric vehicles (EVs) and hybrid electric vehicles (HEVs) to reduce the dependency on fossil fuels and to reduce CO_2 emissions. Moreover, scientists and policy makers predicted that a pivotal role can be played by batteries to reduce the dependency on fossil fuels, if a successful integration of solar, wind, and hydro energy with batteries is possible. The current LIBs can deliver the energy density of 100-150 Wh/kg, which is twice as much as with the primitive version introduced by Sony, but it is still not high enough to use in EVs and in power grids. It has been accepted by the scientific community that the current LIBs have reached their limit, and it seems impossible to extend their energy density further. Thus, it is necessary to explore and develop new materials that can fulfil and satisfy current and future energy needs in portable electronics, and in the transportation and power grid sectors. Thus, there is a crying need to develop a next-generation battery that can store and deliver a higher amount of energy within a short period of time. The quest for high energy materials has brought sulfur into the limelight in the scientific community. Sulfur, which is one of the oldest known elements in the periodic table, has the highest theoretical specific capacity (~1675 mAh/g) among all the known solid cathode materials and shows very high energy density (~2500 Wh/kg) when coupled with lithium metal anode. In addition, sulfur is the seventeenth richest element in the Earth's crust and does not need too much

processing to purify it, which makes it available at low cost [2, 3]. Another significant feature for elemental sulphur is its very low toxicity. According to US environmental protection agency (EPA), sulfur is categorize in group three which belongs to the only slightly toxic category, which makes it outstanding among all the materials that have been used for batteries and other electronic devices. Although sulfur shows a number of promising features as a cathode material, as was mentioned earlier, it also suffers from several drawbacks and challenges that must be overcome to make the sulfur cathode suitable for battery use. The following are the main challenges that impede the commercialization of the lithium/sulfur battery: (i) the low conductivity of sulfur leads to low sulfur utilization and poor rate capability in the cathode; (ii) the multistep electrochemical reduction processes generate various forms of soluble intermediate lithium polysulfides, which dissolve in the electrolyte, induce the so-called shuttle effect, and cause irreversible loss of sulfur active material over the course of cycling; and (iii) the change in volume (~76% increase) when sulfur is converted to sulfide during cycling leads to its mechanical rupturing and consequently, rapid degradation of its electrochemical performance [4-8]. So, to commercialize and to make the lithium/sulfur battery industrially viable, extensive research efforts need to be undertaken.

1.2. Objectives of the research

This doctoral research is focused on to mitigate the aforementioned challenges by understanding the basic structure property relationships between materials such as sulfur, carbon, lithium, etc. and their synthesis methods.

To deal with the first challenge, which is the low conductivity of sulfur, is the first objective of this work. The electrical conductivity of elemental sulfur at room temperature is 5×10^{-30} $S \cdot cm^{-1}$, which means that sulfur falls into the category of insulating materials. To use any material as cathode for a battery, it must have very high electrical and ionic conductivity, so that it can transport electrons and ions to keep the battery active. Unfortunately, this scenario

is totally opposite for sulfur, and to use sulfur as a cathode material in the Li/S system, conducting additives must be added. Moreover, it also needs to be confirmed that each single grain of sulfur is attached to some conducting additive to make use of 100% sulfur utilization [9, 10]. To fulfil that requirement, it is necessary to find conductive materials that are inert with respect to the active materials of the battery and also have very low density (to reduce the overall weight of the battery). After careful scrutiny, the scientific community decided to use conductive carbon, which satisfies the above requirements. There are numbers of different conductive carbons commercially available, however, and among them, only a few are attractive to researchers due to their particularly high conductivity, surface area, and specialized morphology. The designers' choices of conductive carbons are mesoporous carbon, activated carbon, single and multi-walled carbon nanotubes, carbon fibre, reduced graphene oxide, and carbon black [11-33]. In my first doctoral subproject, I carefully chose three different carbon sources, carbon black, activated carbon, and mesoporous carbon. These carbons were chosen based on my fabrication method for sulfur-carbon composite, which was the high energy ball milling method. After careful evaluation of their morphology and electrochemistry, the best conducting carbon was selected among these three. In the second, third, and fourth subprojects, carbon black, multi-walled carbon nanotube (MWCNT), and functionalized graphene were chosen for experimental benefits that later would be reflected in performance also.

To handle the second challenge, which is to reduce the polysulfide shuttle behaviour, was the second objective of this doctoral work. The most stable form of sulfur at room temperature is octa-sulfur (S_8), and when it reacts with lithium ions, it forms polysulfides with longer linear chains. Longer chain polysulfides are soluble in the electrolyte and are reduced to Li_2S on the lithium anode surface. Li_2S does not dissolve in the electrolyte, and for this reason, it either passivates the anode or precipitate out of the electrolyte, leading to both material loss and an

increase in impedance. In extreme cases, it totally impedes the lithium ions, resulting in the death of the battery. Moreover, the dissolution and precipitation process alters the morphology of the cathode in each cycle, which induces strain inside the electrode and degrades the cycle life [34]. The dissolution of polysulfides also results in the so-called shuttle effect, where long chain polysulfides (LCPs) diffuse to the surface of the lithium anode and are reduced to short chain polysulfides (SCPs). The SCPs can then move back to the cathode and be oxidized to LCPs. This parasitic process takes place continuously, creating an internal ‘‘shuttle’’ phenomenon. It decreases the active mass utilization in the discharge process and markedly reduces the Coulombic efficiency [35, 36]. In this thesis, the first two and the fourth subprojects used single-walled carbon nanotube (SWCNT) as an interlayer between the cathode and the separator to capture and to prevent the release of LCPs for further reduction on the anode side. In the thired subproject, carbo-oxylated functionalized graphene was used to prevent LCPs reduction.

To address the volume expansion when elemental sulfur is reduced to lithium sulphide (Li_2S) is the fourth objective of my doctoral work. Elemental sulfur has a density of 2.03 g/cm^3, while Li_2S has a density of 1.66 g/cm^3. As a result, when sulfur is fully reduced to Li_2S the overall volume is expanded by 76%. This volume change leads to cracking or structural failure on the cathode surface and in some cases, pulverization of the active materials, which leads to fast capacity decay [37]. In this thesis, in my fourth subproject, I used Li_2S as an active material instead of elemental sulfur. Li_2S is the fully lithiated state of sulfur, and there will be no volume expansion rather than contraction. In the other three subprojects in this thesis, I also considered the volume expansion problem and carefully chose other additives that can accommodate the expansion.

In a nutshell, the research effort in this doctoral work has been directed towards sulfur cathode materials for lithium/sulfur batteries. It can be stated in terms of different directions:

(1) modify the elemental sulfur via different methods to engineer the morphology; (2) introduce and select various carbon sources to synthesize sulfur/carbon composites through a simple and commercially viable method; (3) prepare and apply a free-standing SWCNT layer to capture polysulfides; (4) employ spray precipitation and the reverse microemulsion method to synthesize various morphologies and carbon/sulfur composites, (5) apply fully lithiated sulfur (Li_2S) as an active material; (6) apply a new charging method to improve the cycling performance of the lithium/sulfur batteries.

1.3. Thesis structure

This doctoral thesis is composed of eight chapters. A brief overview of these chapters is outlined as follows:

Chapter 1 introduces the general background, promising features, major challenges, and some approaches for improving the electrochemical performance of lithium/sulfur batteries. It explains the objectives of this research and gives an outline of the thesis.

Chapter 2 presents a comprehensive literature review on lithium/sulfur batteries and specifically on sulfur-based cathode, including a basic introduction to lithium/sulfur batteries, the challenges to be faced for commercializing lithium/sulfur batteries, and the ongoing approaches to overcome these challenges.

Chapter 3 presents the chemicals and methods that have been used to synthesize ball-milled sulfur/carbon composite with suitable ball-milling parameters, spray-precipitated and drop precipitated sulfur/carbon composites, ball-milled Li_2S/C composite, and reverse microemulsion-based functionalized graphene/sulfur composite. This chapter also briefly introduces the instrumental analysis techniques that have been used to characterize the electrode materials, including X-ray diffraction (XRD), thermogravimetric analysis (TGA), Raman spectroscopy, scanning electron microscopy (SEM), field emission scanning electron

microscopy (FESEM), transmission electron microscopy (TEM), energy dispersive X-ray spectroscopy (EDS), Fourier transform infrared spectroscopy (FTIR), Brunauer-Emmett-Teller (BET) surface area measurements, and electrochemical measurements, including cyclic voltammetry (CV), galvanostatic charge-discharge cycling, and electrochemical impedance spectroscopy (EIS).

Chapter 4 investigates a systematic approach to a synthesis method for S-C composite that is suitable for large-scale production. In addition, a conductive single-walled carbon nanotube (SWCNT) free-standing layer with a refined, woven-like structure is inserted in between the cathode and the separator to improve the capacity and cyclability. This carbon layer was fabricated by ultrasonic dispersion followed by vacuum filtration. Finally, the fixed capacity charging method was applied to improve the capacity retention.

Chapter 5 reports on the synthesis of carbon-sulfur composite by using a modified chemical process denoted as spray precipitation, which can be considered as an industry-oriented, facile method to produce high-surface-area sulfur particles and to obtain a homogeneous dispersion of sulfur in carbon black. In this chemical process, sodium thiosulfate solution was sprayed into an oxalic acid – carbon black (CB) solution to achieve precipitation of sulfur in the carbon black solution. It was expected that spray-precipitated carbon-sulfur composite will show better discharge capacity and capacity retention compared to the products of the conventional method, in which a pipette is used to drop thiosulfate solution onto acid solution. This conventional method is designated as the drop precipitation method.

In Chapter 6, sulfur was precipitated out and adhered to graphene via the reverse microemulsion method. In this method, small droplets of aqueous phase were homogeneously dispersed into oil phase that contained carbo-oxylated functionalized hydrophilic graphene to make a microemulsion solution. A second microemulsion was also prepared, where

hydrochloric-acid-containing aqueous phase was homogeneously dispersed into oil phase. These two emulsions were then mixed together so that the aqueous phases could mix with each other and react. The reaction product is sulfur, which is firmly adhered to the functionalized graphene. This functionalized sulfur-graphene composite can effectively minimize shuttle behaviour effectively and shows a very high and stable discharge capacity with extremely low capacity fading after several hundred cycles. Moreover, heteroatom-doped 3-D carbon cloth was also used to increase the active material content as well as to increase capacity retention.

Chapter 7 presents microsized Li_2S powders that were ball milled with four different carbon sources to synthesize Li_2S-C composites, where smaller size Li_2S particles were mixed uniformly with conductive carbon. Based on physical and morphological examination, the most suitable carbon source was selected among the four carbons. The fabricated composites were then capillary-deposited in three-dimensional (3-D) multi-layered Ni foam from a dioxolane (DOL)-containing mixture with high amount of active material. To facilitate the electrochemical activation of Li_2S-C composite by reducing the initial potential barrier, in the 1^{st} cycle, the cells were charged to 3.5 V with a very low current density. In addition, a conductive, single-walled carbon nanotube (SWCNT) free-standing layer with a refined, woven-like structure was inserted in between the cathode and the separator to improve the initial capacity and capacity retention. Finally, a comparative study was conducted to analyse the effects of the binder and 3-D multi-layered Ni foam.

In Chapter 8, the general conclusions are summarized, and recommendations for further research work based on this doctoral work are discussed as well.

References are listed after Chapter 8, followed by publications and awards received during the period of my PhD study.

Chapter 2. Literature Review

2.1. Principles of the lithium / sulfur rechargeable battery system

It is well-known that a battery is an electrochemical device that can store electrical energy through chemical means and can deliver the electrical energy through chemical reaction when needed. In the lithium-sulfur batteries (LSB) electrical energy can be stored in the sulphur electrode through the chemical reaction of lithium and sulfur. Like all other rechargeable batteries, the LSB consists of a number of components in a single cell, depending on the design, working principles and battery type. The components can be classified into two groups, with the first group assigned as essential and the second one as supporting. The components and the operation principles of a LSB are shown in Figure 2.1.

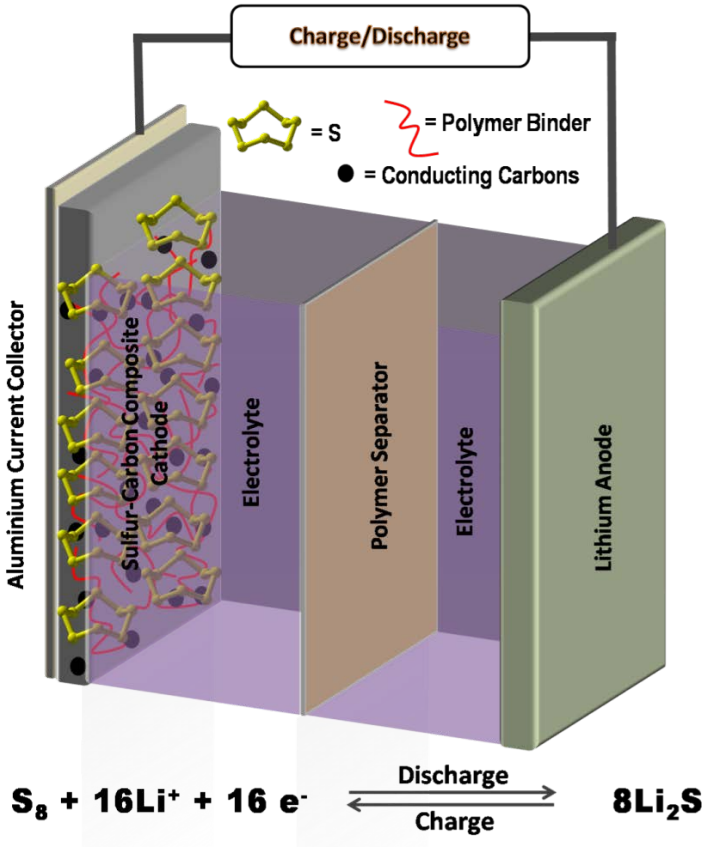

Figure 2.1 Schematic diagram of lithium-sulfur (Li-S) cell showing its components and the reversible chemical reaction.

There are three essential components of a conventional Li-S cell which are:

1) Anode: In almost every case, metallic lithium is used as anode in a Li-S cell except for some works where lithium metal was modified or treated [38, 39] to increase the performance of the cell.
2) Electrolyte: Organic electrolyte has been chosen due to its compatibility with the anode (lithium) and the sulfur-based cathode, as well as the intermediates of sulfur that are produced during charging and discharging processes. Besides the compatibility with electrodes, other important properties (e.g. voltage window, ionic conductivity, viscosity, etc.) need to be considered for selection of an electrolyte. There has been comprehensive research to find a suitable electrolyte for the Li-S system [6, 40-46]. So far, it has been considered that the electrolyte composed of 1,3-dioxolane (DOL) and 1,2-dimethoxyethane (DME), with a volume ratio of 1:1, containing 1 M lithium bis(trifluoromethanesulfonyl)imide (LiTFSI) and 0.1 M lithium nitrate ($LiNO_3$) shows better compatibility, properties, and performance than the alternatives when used in a Li-S cell.
3) Cathode: Elemental sulfur-based cathode is used in almost all Li-S batteries, although some work has been done where lithium-sulphide-based (Li_2S) cathode was used to fabricate Li-S batteries [47-49].

In addition to the three essential components there are a number of other components which have been used in the LSB, depending on material fabrication method, cell design, and mode and method of charging. In this thesis, these components are designated as supporting components, which are listed below.

1) Current collector: The current collector is only used for the cathode in a Li-S cell, where all the active material is coated on the surface. In most cases, aluminium (Al)

foil has been used as the current collector due to its high electronic conductivity, low cost, and ability to form an oxide layer, which prevents corrosion during charging and discharging. There are a few works where different current collectors (e.g. carbon paper, carbon cloth, nickel-foam, graphene, etc.) were used instead of Al-foil [50-53].

2) Conductive additives: In a Li-S system, researchers sometime consider conductive additives as an essential component rather than a supporting component. Due to the insulating nature of sulfur, 100% sulfur cannot be used as cathode. A certain proportion of conductive additive needs to be added to transport the electrons and ions to the sulfur and the current collector. Most of the works that have been done on the Li-S system used carbon as the conductive additive due to its low cost, high conductivity, and inertness.
3) Binder: In the Li-S system, the binder is also an important component, which is used for firmly bonding the sulfur, conductive carbon, and current collector. There are three well-known binders, polyvinylidene fluoride (PVDF), carboxymethyl cellulose (CMC), and alginate, which are frequently used in a Li-S cell.
4) Separator: Separator is another important component made from insulating materials with millions of small pores. Its purpose is to prevent short-circuiting which is can occur through direct contact of the anode and cathode. There are a number of different separators made from different polymers, glass fibers, and other insulating materials. The selection of the separator strongly depends on the cell design and electrolyte, however. A highly viscous electrolyte needs a glass separator to absorb the electrolyte and maintain sufficient contact between the anode and the cathode [43]. The most popular separator for Li-S cell is polypropylene film (Celgard) with different pore sizes and densities.

A fabricated Li-S cell is in the charged state and will discharge when connected with a load. During discharging, oxidation takes place at the anode surface, where lithium metal forms lithium ions (Li^+) by the loss of one electron. The electrons then pass through the loads and reach the cathode, where reduction of sulfur takes place by accepting electrons and lithium ions and forming lithium sulfide. During charging, however, the opposite phenomena occur through oxidation of the cathode and reduction of the anode. The reaction of the half cells and the overall reaction during discharging are shown below.

Oxidation reaction on anode surface:

$$16Li \longrightarrow 16Li^+ + 16e^- \text{ ……..(1)}$$

Reduction reaction on cathode surface:

$$S_8 + 16Li^+ + 16e^- \longrightarrow 8Li_2S \text{ …….(2)}$$

The overall reaction is:

$$S_8 + 16Li \longrightarrow 8Li_2S\text{……..(3)}$$

Even though the overall reaction has been shown as a single step, in the real case the reaction has multiple steps. The capacity calculation of a Li-S full cell is shown below.

Theoretical capacity of any element is = nF/atomic mass

Where, n = Number of electrons transferred per atom and

F = Faraday's constant = 96485 Coulomb ≈ 26.8 Ah ≈ 26800 mAh

Theoretical capacity of lithium = (1×26800)/6.94 ≈ 3862 mAh/g

Theoretical capacity of sulfur = (2×26800)/32 ≈ 1675 mAh/g

So, the theoretical capacity (Q) of a Li-S full cell is,

$1/Q = (1/3862) + (1/1675)$; $Q \approx 1166$ mAh/g ≈ 1166 Ah/kg

The average discharge voltage plateau (discharge shows multiple plateau) is 2.2V.

So, the gravimetric energy density of a Li-S cell is = 2.2 × 1166 ≈ 2600 Wh/kg.

As mentioned earlier, the reduction of sulfur has multiple steps which include both single phase and two phase reduction. The details of the reduction products, steps, and mechanism are stated below and also shown in Figure 2.2.

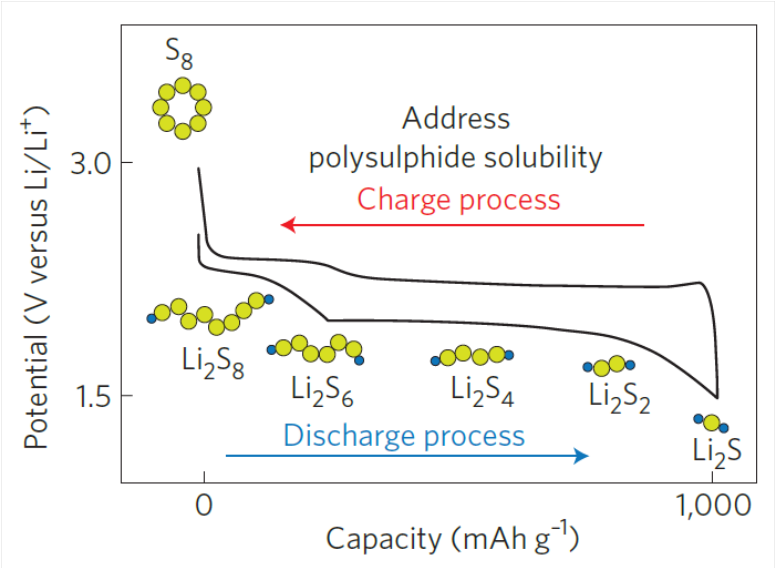

Figure 2.2 The charge discharge curve shows the oxidation and reduction of sulfur [54].

Step 1: A solid-liquid two-phase reaction where S_8 is reduced to Li_2S_8. The reduction product, which is Li_2S_8, is highly soluble in liquid organic electrolyte due to its high polarity. This liquid solution acts as a catholyte for further reduction.

Step 2: A liquid-liquid single-phase reduction where dissolved Li_2S_8 is reduced to Li_2S_6 and Li_2S_4.

Step 3: A liquid-solid two-phase reaction where the dissolved Li_2S_6 and Li_2S_4 polysulfides are further reduced to insoluble Li_2S_2.

Step 4: A solid-solid single phase reaction where insoluble Li_2S_2 is reduced to Li_2S.

There is a huge controversy about the reaction mechanism and steps of the Li-S system. Little *in-situ* characterization has been done, but it was found that the formation of Li_2S_6 along with Li_2S_8 occurs at the very first step. Moreover, each individual step does not produce any specific product rather than multiple reduction products [55]. Researchers are still struggling to find concrete proof the reduction mechanism. Very recently Wild et al. [8] published a critical review on the reduction mechanism and tried to model the polysulfides. The reduction products and the corresponding voltages are the output of his model, which is shown below.

Step	Corresponding reaction	Voltage
1	$S_8 + 2Li^+ + 2e^- \leftrightarrow Li_2S_8$ $3Li_2S_8 + 2Li^+ + 2e^- \leftrightarrow 4Li_2S_6$	> 2.3V
2	$2Li_2S_6 + 2Li^+ + 2e^- \leftrightarrow 3Li_2S_4$	2.3 to 2.1V
3	$Li_2S_4 + 2Li^+ + 2e^- \leftrightarrow 2Li_2S_2$ $Li_2S_4 + 6Li^+ + 6e^- \leftrightarrow 4Li_2S$	1.9 to 2.1V
4	$Li_2S_2 + 2Li^+ + 2e^- \leftrightarrow 2Li_2S$	< 1.9V

In a simplified form, it can be said that the first two steps, which involve reduction of S_8 to S_8^{2-} S_6^{2-}, and S_4^{2-}, resemble the 1st plateau of the discharge curve; and the last two steps where S_4^{2-} is reduced to S_2^{2-} and S^{2-} form the 2nd plateau of the discharge curve that is shown in Figure 2.2.

2.2. Materials and technical challenges for Li-S system

So far, it the promising features and the principles of LSB have been discussed, including the very high theoretical capacity, high volumetric and gravimetric energy, low-cost active materials and very low impact on the environment. However, Li-S system suffers from

several daunting challenges in all three major components, the lithium anode, organic electrolyte, and sulfur cathode. A brief description of these challenges is presented below.

2.2.1. Lithium metal anode

Lithium metal, which shows a -3.04 V reduction potential (vs. standard hydrogen electrode), is lightweight (density is 0.59 gm/cm^3) and has extremely high theoretical capacity. It has been studied as an anode material for last forty years [7]. However, there are two major barriers for lithium anode which are the formation of dendrites, resulting in a safety hazard, and low coulombic efficiency, which reduces the cycle life of the battery. The second challenge can be overcome by putting excess lithium on the anode side, but the dendrite formation issue is still a big challenge for commercialization of lithium metal anode [56]. Researchers found that the formation of lithium dendrites can be minimized by either the formation of a thick solid electrolyte interphase (SEI) on the anode surface or the usage of a low voltage window [57, 58]. It has been observed in Li-S cells that the dissolved polysulfide that evolves during discharging can "chemically dissolve" the lithium dendrites with a very high surface area. In addition, the solid discharge products (Li_2S and Li_2S_2) produced during the reaction between the polysulfide and the dendritic lithium can form a dense layer on the anode surface, which will slow down or even fully inhibit the growth of lithium dendrites [59].

2.2.2. Electrolyte

The electrolyte is an organic liquid that may contain one or more organic solvents along with an organo-metallic salt. The most common organic solvents are esters, carbonates, phosphates, and ethers. The solvents must meet certain criteria to be used in an electrolyte. The ideal electrolyte solvent for lithium/ sulfur batteries should meet the following requirements: (1) has very low melting point and very high boiling point; (2) be chemically stable against polysulfide anions, polysulfide anionic radicals, and the lithium anode; (3) has

high polysulfide solubility; (4) has low viscosity in polysulfide solution; (5) has a voltage window that is suitable for Li and sulphur; (6) has high a dielectric constant and high donor number; (7) has very high ionic conductivity and low electrical conductivity; and finally (8), remains stable over a big temperature range (both high and low temperatures). Nevertheless, most of the carbonate, ester, and phosphate-based solvents react with polysulfides and cannot be used as electrolyte solvent for the Li-S system [6, 40]. Extensive research has been conducted to find the most suitable ether solvent for the Li-S system, and it has been found that suitable electrolyte solvents for lithium/sulfur batteries are limited to the linear and cyclic ethers, such as poly(ethylene glycol) dimethyl ether (M_n = 500) [60], tetraethylene glycol dimethyl ether [21], 1,2- dimethoxyethane (DME), and 1,3-dioxolane (DOL) [11, 12, 16, 19, 25, 33, 61-64]. Among them, DME and DOL in a volume ratio of 1:1 have been used by most of the researchers, considering the electrochemical performance and the cost.

Like the solvent, lithium-based salts should meet certain criteria. An ideal electrolyte salt for room temperature rechargeable lithium batteries should (1) be able to completely dissolve and dissociate in the solvent. (2) The anion should be stable against oxidative decomposition at the cathode. (3) The anion should be inert towards electrolyte solvents. (4) Both the anion and the cation should remain inert towards the other cell components, such as the separator and electrode substrate. As the lithium polysulfides can react with most of the conventional lithium salts that have been used in the Li-ion battery system over the years, such as lithium hexafluorophosohate ($LiPF_6$), lithium tetrafluoroborate ($LiBF_4$), lithium bisoxalatoborate (LiBOB), and lithium difluoro(oxalato)borate ($LiBF_2C_2O_4$), the choice of lithium salt is also very limited [65]. It was observed that lithium triflate **(**$LiSO_3CF_3$) [63], lithium bistrifluorosulfonylimide ($LiN(SO_2CF_3)_2$) [20, 66], and a few other salts meet the criteria and show better performance in a Li-S cell. Thus, these salts have been exclusively used in the ether-based solvent for LSBs.

2.2.3. Sulfur-based cathode

Elemental sulfur has been known and used for several thousands of years. It has been used as a cathode, however, since 1962, when Herbet and Ulam fabricated a sulfur-based electric dry cell [67]. Over the next forty years, the sulfur battery didn't gain too much attention and was only used as primary battery due to its intricate chemistry. With advances in technology and organic chemistry, however, the Li-S system become rejuvenated and attractive to researchers in the early 2000s. Although the Li-S system is a hot topic in current research, and thousands of researchers all over the world are working on it, work is still needed to solve all the challenges and to commercialize it. There are three main challenges that need to be solved for commercialization of LSBs.

The first challenge is the insulating behaviour of sulfur. It is not electrically conductive at all and shows an electrical conductivity of 5×10^{-30} $S \cdot cm^{-1}$ [68-74], which leads to poor electrochemical accessibility and low utilization of the sulfur in the electrode. The second challenge is the reduction products of S. When sulfur is fully reduced during discharging, it forms lithium sulfide (Li_2S) which is not only electronically insulating but also ionically insulating [75-78]. In addition, when Li_2S form, it starts to be deposited on the surface of the cathode, and once a thin Li_2S layer completely covers the whole electrode, further lithiation will be largely impeded, and the voltage decreases rapidly. Thus, complete conversion of sulfur to Li_2S rarely happens, and in every case, the discharge capacity is less than 80% of the theoretical capacity. The third and the most fatal challenge by far is the polysulfide dissolution into electrolyte. The polysulfide anions, which are readily formed as the reaction intermediates, are highly soluble in the organic electrolyte solvent [77] and form a concentration gradient in the electrolyte, so that they move to the anode surface through diffusion. These soluble species are then reduced to Li_2S, which is insoluble in the electrolyte, precipitates out of the electrolyte and forms a passivation layer at the lithium

anode surface, causing loss of active material and increasing the impedance of the Li-S cell. Furthermore, the polysulfide dissolution and the precipitation process alter the morphology of the cathode in each cycle, and it does not return to its initial morphological structure, which induces strain inside the electrode and results in low active material utilization and poor cycle life [79-82]. Polysulfide dissolution is also responsible for the well-known "shuttle phenomenon", where long chain polysulfides diffuse to the surface of the lithium anode due to the concentration gradient and are reduced to short chain polysulfides. They also create a concentration gradient on the anode side. The short chain polysulfides can then move back to the cathode and are oxidized to long chain polysulfides, again creating a concentration gradient. This parasitic process takes place continuously and creates an internal ''shuttle'' phenomenon [83-99]. The mechanism of the shuttle phenomenon is shown in Figure 2.3.

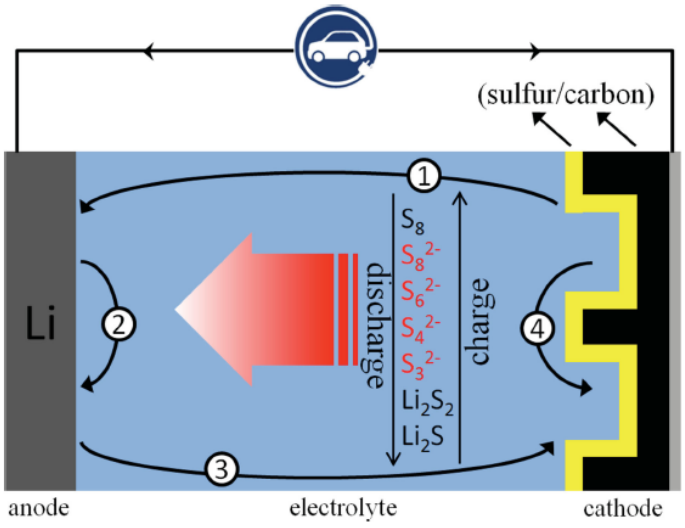

Figure 2.3 Schematic diagram of the shuttle effect of polysulfides in Li–S batteries during charge-discharge [46].

To be concise, it can be said that this shuttle phenomenon along with its parasitic reactions causes the following problems (1) consumption or loss of active material, (2) corrosion of the Li metal anode, and (3) polarization of the Li anode when insoluble Li_2S and Li_2S_2 are formed and deposited on the Li surface. In other words, this shuttle phenomenon causes low

active material utilization, low coulombic efficiency, and short cycle life in the Li-S system [100, 101].

2.2.4. Lithium sulfide (Li_2S) cathode

Despite these advances on Li-S battery, the use of elemental lithium as the anode in Li-S batteries is a major concern. The formation of lithium dendrites during cycling that can penetrate through the separator and lead to thermal runaway which may cause overheating and explosion [102]. Moreover, lithium metal can react with the polysulfide ions diffused from the cathode, which limits capacity retention and cycle life of Li-S battery. To avoid these problems in the lithium/sulfur system, it is necessary to use a high-capacity anode material (e.g. Si, Sn, Sb or metal oxides) other than elemental lithium while replacing sulfur by lithium sulfide (Li_2S) in the cathode. Li_2S has a theoretical capacity of 1166 mAh g^{-1} which is more than three times higher than conventional metal oxide batteries. On the other hand, compared with elemental sulfur, Li_2S has lowest density (~1.66 g/cm^3) and higher melting point (~938 ^oC) helps it to perform at higher temperature. However, low electrical conductivity, large particle size, sensitivity to moisture and high initial activation potential (~4V) making the manufacturing process intricate and expensive [103, 104].

A conventional Li-S battery consists of a sulfur cathode, lithium-metal anode and a non-aqueous Li^+ conducting electrolyte. Overall, the electrochemical reaction can be described as follows, assuming the formation of Li_2S from elemental sulfur during discharge and vice versa:

$$S_8 + 16Li \underset{\text{Charge}}{\overset{\text{Discharge}}{\rightleftharpoons}} 8Li_2S \quad \text{.....(4)}$$

If Li metal foil is replaced by an alloy type anode material M (M: silicon, tin, etc.), and then this kind of anode is combined with a Li_2S cathode to make a new sulfur-based battery, this new electrochemical storage system is called the Li-ion sulfur batteries.

$$Li_2S + xM \underset{\text{Discharge}}{\overset{\text{Charge}}{\rightleftharpoons}} S + Li_2M_x \text{.....(5)}$$

Recently, lithium sulfide (Li_2S) has received much attention not only because of its high theoretical capacity but also with the capability of being paired with lithium-metal-free anodes, such as "insertion" and "alloying" anode materials. Moreover, unlike sulfur, which expands 80% during initial lithiation, Li_2S initially shrinks as it is delithiated, generating empty space for subsequent volumetric expansion during lithiation, thus mitigating against structural damage to the electrode. The Li_2S cathode has met several challenges in practice which need to overcome.

Commercial Li_2S is electronically and ionically insulating, which leads to poor electrochemical accessibility and low utilization of the Li_2S in the electrode. To increase the capacity or active material utilization, it is necessary to increase the conductivity of Li_2S by adding conductive materials. Various efforts have been made to improve the contact between Li_2S and the current collector by using conductive additives such as metal and carbon materials. Cui's group reported a lithium-free cell containing of a Li_2S-mesoporous carbon composite as the cathode, and the Li_2S was better utilized by incorporating it within the small pores of CMK-3 mesoporous carbon [102]. Improved performance of electrodes made from ball-milled Li_2S powders (~10 μm) and Super-P carbon was reported by Scrosati's group [105].

Lithium polysulfides, which are formed as the reaction intermediates, are soluble in organic solvent based electrolyte, which causes the rapid irreversible loss of active materials over repeated cycles. Three strategies are generally used to solve this problem for Li-S batteries: (1) using a conductive adsorbent in the cathode, such as porous carbon, so that polysulfides can be captured on the adsorbent, reducing the diffusion of polysulfide from the cathode into the electrolyte, (2) coating with a protection layer, so that the polysulfides could be confined

within the internal conductive matrix, (3) using solid–state electrolyte to reduce dissolution of polysulfide [106]. These promising strategies used for improving the performance of Li-S batteries are also suitable for the Li-ion sulfur battery. Development of Li-ion sulfur batteries system is in its early stages, and these promising strategies have not been systematically studied.

2.2.5. Self-discharging

The self-discharging problem is also an important challenge for the Li-S system that does not get enough attention from the scientific community. This is because the self-discharging problem strongly related to the dissolution problem of the sulfur cathode. Self-discharging occurs due to the diffusion in the concentration gradient of the electrolyte. It is found that, during resting of a Li-S cell, the active material gradually dissolves into the organic electrolyte and migrates to the lithium anode [107]. Like conventional nickel-cadmium and nickel metal hydride batteries, the LSB shows strong self-discharge behaviour, which is shown in Figure 2.4.

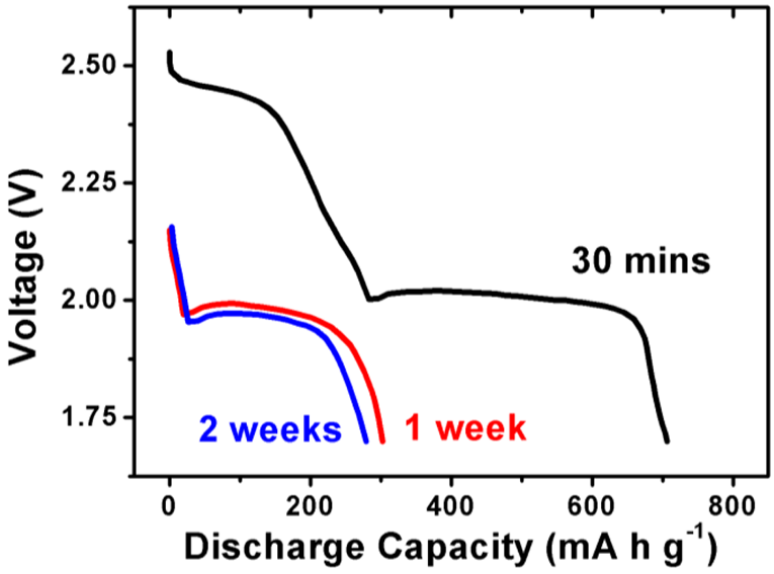

Figure 2.4 Self discharging after different aging periods [5].

2.3. Methods to overcome the challenges

Different approaches and methods have been applied and introduced to overcome the challenges for the Li-S system. Most of the research was focused on the sulfur cathode or, more specifically, the fabrication of sulfur/carbon and sulfur/conducting polymer composites [21, 60, 108-127]. The addition of metal oxides such as Al_2O_3 and TiO_2, and metal organic frameworks have also been investigated extensively to reduce or to eliminate the challenges [128-136]. Besides the sulfur-carbon composite, there have also been attempts to minimize the challenges for the lithium anode and electrolyte by applying a protective film on the lithium anode [137] and by modification of the electrolyte [138] by adding different salts, solvents, and additive materials. This dissertation is only concentrated on the sulfur-carbon cathode, and hence, this literature review will also be only focused on the sulfur-carbon cathode.

2.3.1. Modification of sulfur cathode

2.3.1.1. Synthesis of sulfur-carbon composite

It has been mentioned earlier that one important role of carbon is to attach itself to the sulfur so that electrons and ions can reach each sulfur particle. Carbon was selected for this role due to its high conductivity, low density, low cost, and inertness over a long voltage window. Later, it was also found that carbon can adsorb polysulfide species, which makes it unique as a supportive material for sulfur [14, 18, 23, 101, 108, 112, 139-155]. There are a number of ways to synthesize sulfur-carbon (S-C) composites, however; all the synthesis techniques can be classified into three groups. The first technique is heat treatment, where sulfur is heated to a certain temperature and then filled or deposited into carbon [19, 21, 22, 100, 156, 157]. The heat-treatment technique is classified into two sub-techniques: a) melt infusion and b) vapour deposition. The second technique is a chemical treatment, where sulfur is deposited through chemical reaction or from a chemical solution [15, 16, 64, 158]. This chemical technique is

also classified into two types: a) chemical precipitation and b) solution evaporation. The third technique is a mechanical treatment, where sulfur and carbon are mixed in a mechanical mixer (e.g. hand milling, ball milling etc.) [159-162].

2.3.1.1.1. Heat treatment technique

Heat treatment techniques are generally classified as melt infusion and vapour deposition. In melt infusion process, a sulfur-carbon mixture is heated above the melting temperature of sulfur (M.P of sulfur is ~115 ^{o}C), so that the molten sulfur can infuse into the pores in the carbon. The general melt infusion temperature is 155-160 ^{o}C. This temperature was chosen due to the unique behaviour of sulfur as the temperature rises. Sulfur shows its lowest viscosity in that temperature range, which facilitates filling of the carbon pores through capillary deposition. There are hundreds of paper that has been published on melt-infusion methods, and among them, some notable works are discussed in this subsection.

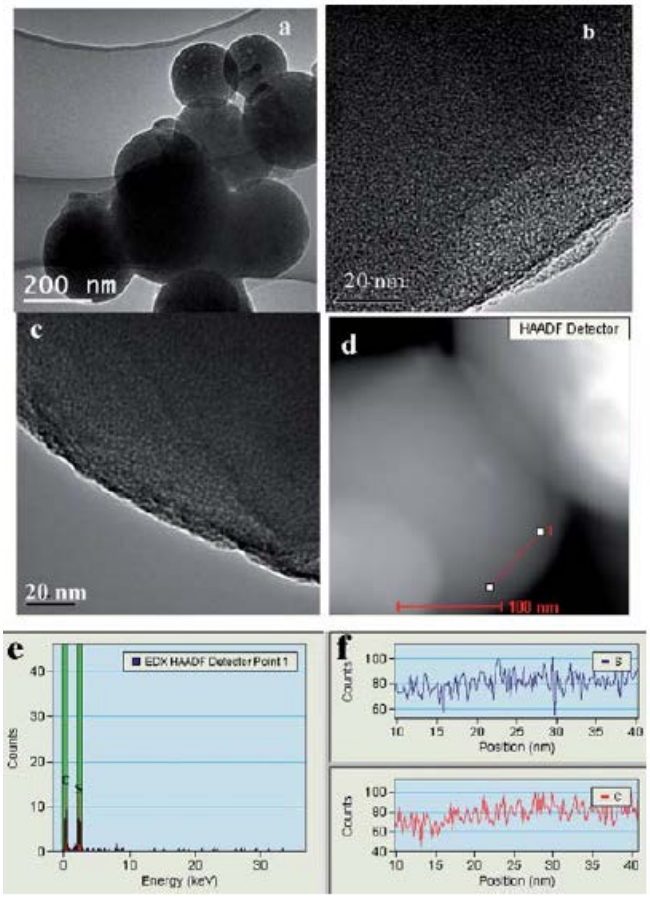

Figure 2.5 TEM image of carbon spheres (a, b), and the sulfur–carbon-sphere composite (c). High-angle annular dark field − scanning TEM (HAADF-STEM) image (d) with EDX spectrum (e) and corresponding line-scans [100].

Zhang et al., [100] used the melt infusion method to enhance the long-term stability of sulfur cathode by encapsulating sulfur into micropores of carbon spheres. Figure 2.5 shows transmission electron microscope (TEM) images of microporous carbon spheres along with energy dispersive spectroscopy (EDS), which confirms the successful penetration of sulfur. This engineered S-C composite structure is very stable and features a high discharge capacity, up to 500 cycles.

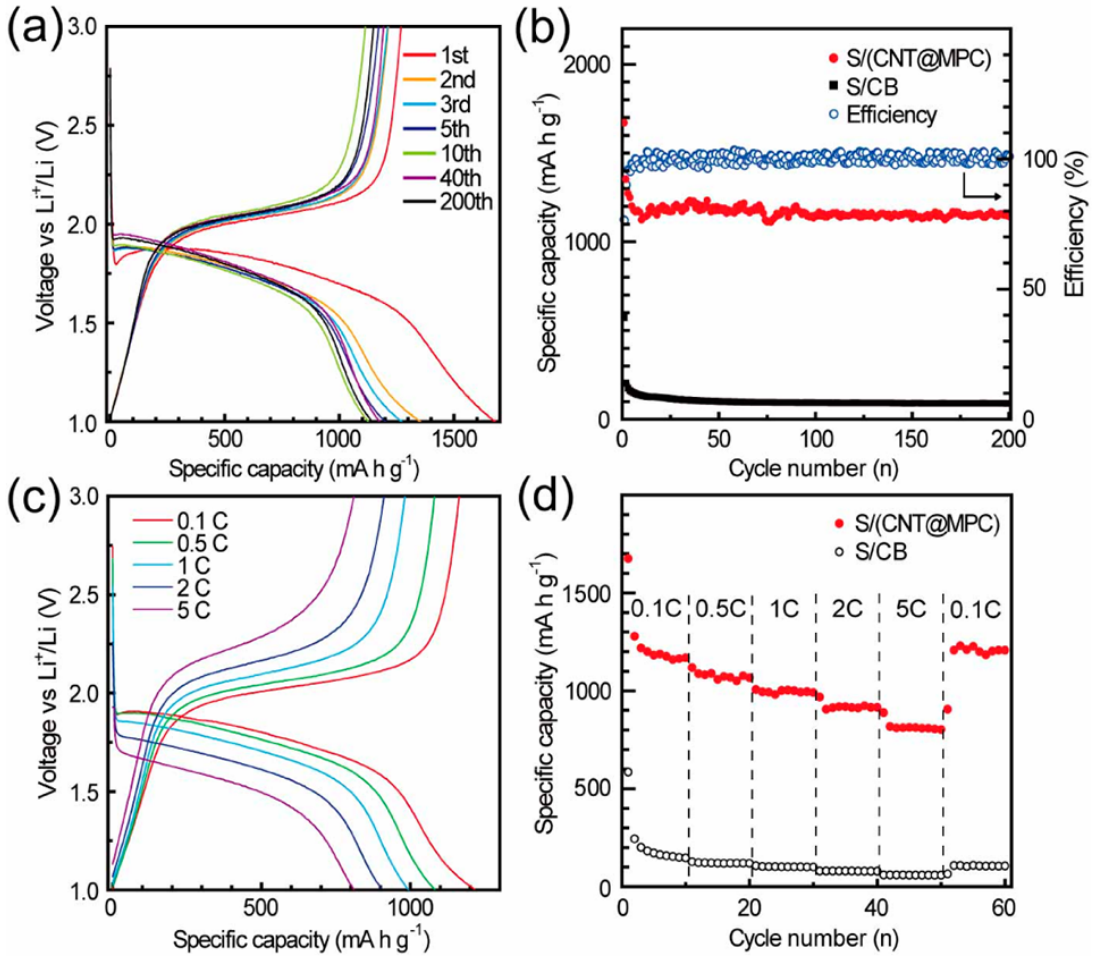

Figure 2.6 Electrochemical performance of S/(CNT@MPC) composite and comparison with conventional S/CB composite [163].

Xin and her co-workers [163] confined metastable small sulfur molecules in a microporous carbon matrix through melt infusion. The electrochemical performance shown in Figure 2.6 of their fabricated composite features very high and stable discharge capacity compared to conventional sulfur-carbon black (CB) composite. The rate capability data shows that this newly developed composite can has higher capacity even at very high current density.

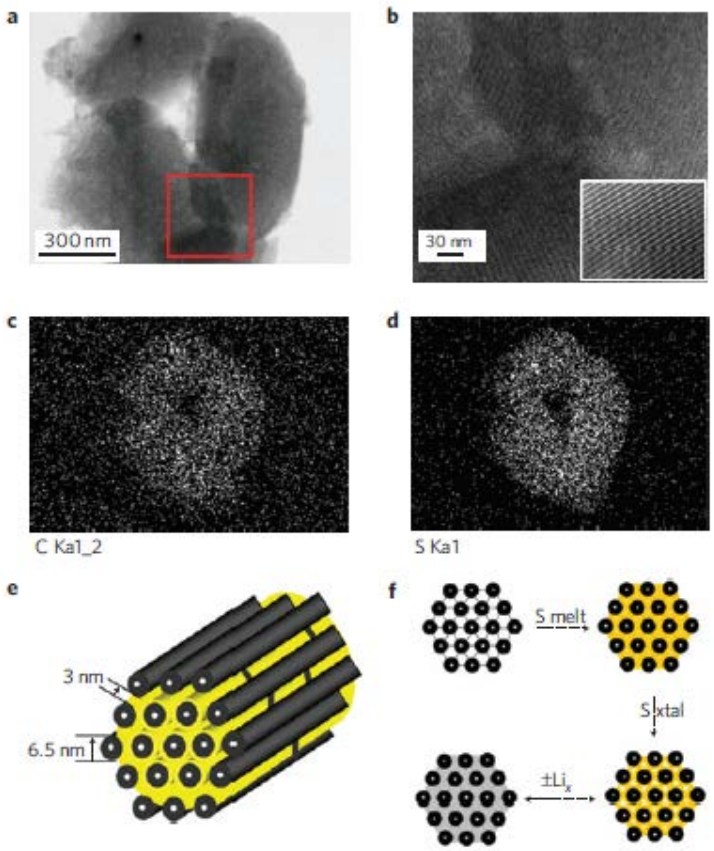

Figure 2.7 TEM image (a) and elemental maps (b-d) of a CMK-3/S-155 composite particle, and schematic diagrams of the structure and redox processes [164].

Ji et al., [164] reported a mesoporous carbon–sulphur (CMK-3-S) composite created by melt diffusion, which is shown in Figure 2.7 and displayed all of the benefits of confinement effects at a small length scale. The stable nanoscale conductive carbon framework can not only accommodate excellent accessibility of the active material, but also serves as a miniature electrochemical reaction chamber. The successful confinement of the active materials

ensured that a more complete redox process took place and resulted in enhanced utilization of the active sulphur material.

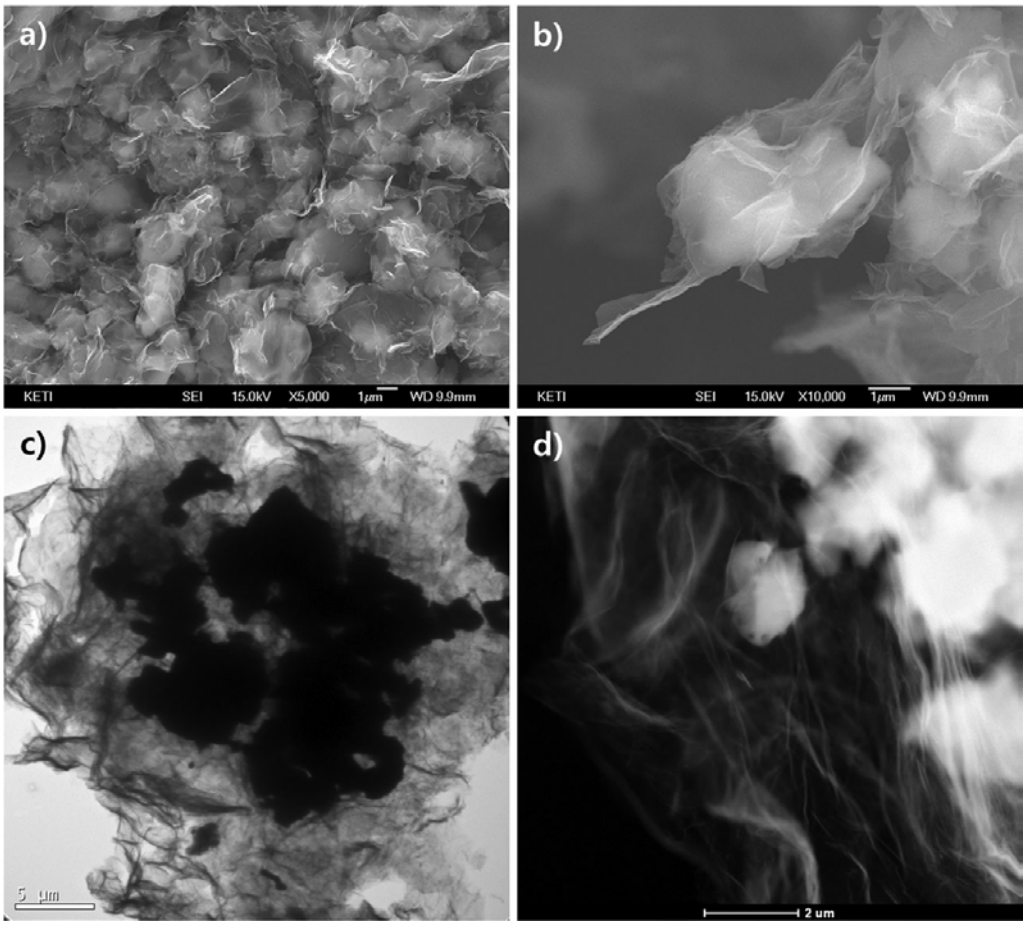

Figure 2.8 (a) and (b) FESEM images of S-impregnated graphene composite at different magnifications; (c) and (d) TEM images of the S-impregnated graphene composite [27].

A one-step synthesis of sulfur impregnated graphene cathode was developed by Park et al. [27]. They investigated whether the use of the sulfur-impregnated graphene composite through melt infusion as a cathode could confine the active sulfur and prevent the dissolution of soluble polysulfides, while providing sufficient electrical conduction. A high first cycle discharge capacity of 1237 mA h g^{-1} was achieved, along with a good capacity retention of

67% after 50 cycles. The SEM image in Figure 2.8 shows successful impregnation of sulfur into the graphene.

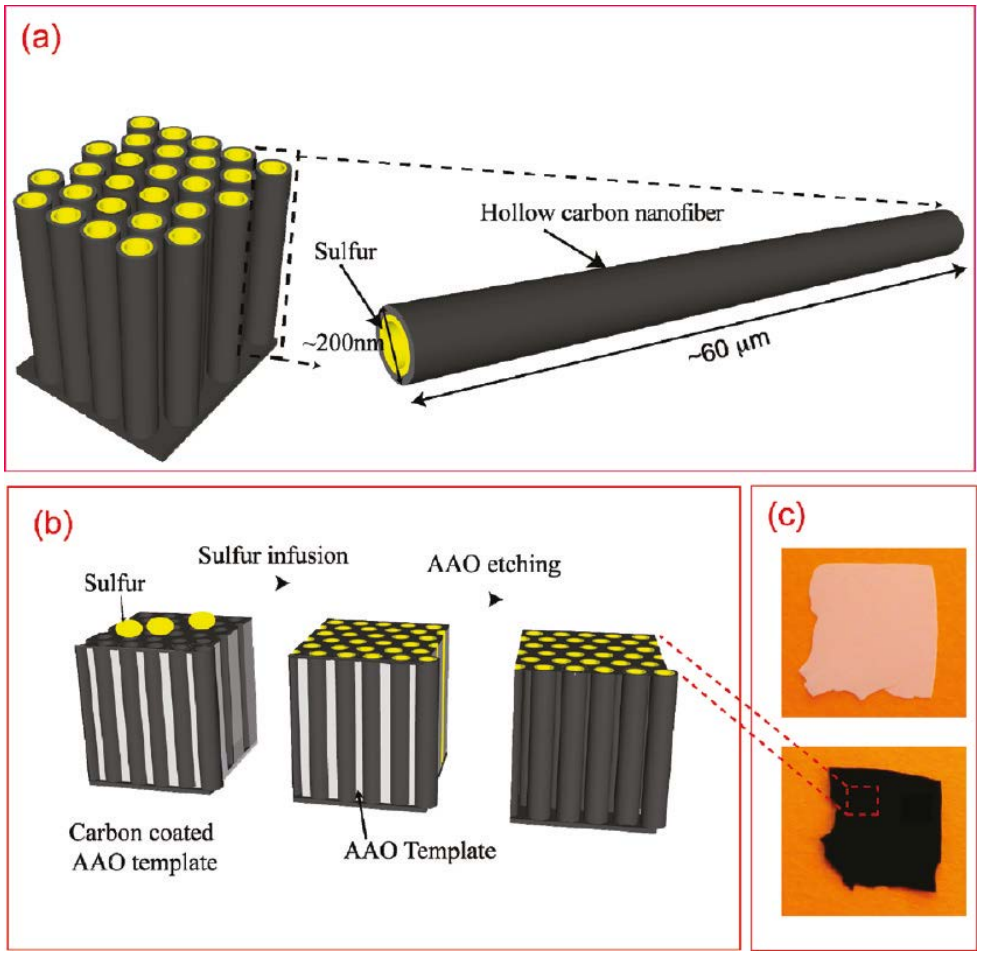

Figure 2.9 Schematic illustration of the design and fabrication process for hollow carbon nanofibers/sulfur composite structure [15].

Zheng et al. [15] reported a hollow carbon nanofiber-encapsulated sulfur cathode through melt infusion for effective trapping of polysulfides and excellent electrochemical cycling of the cells. A schematic diagram of the hollow carbon nanofibers/sulfur composite is shown in Figure 2.9. Anodic aluminium oxide (AAO) templates were used to synthesize hollow carbon nanofibers, through thermal carbonization of polystyrene. The AAO template also helped to facilitates sulfur infusion into the hollow fibers and prevented the sulfur from adhering onto the exterior of the carbon walls. The high aspect ratio (length to diameter ratio) of the carbon

nanofibers provides a useful structure for trapping polysulfides that causes faster capacity decay. Moreover, the thin carbon wall promotes rapid transport of lithium ions.

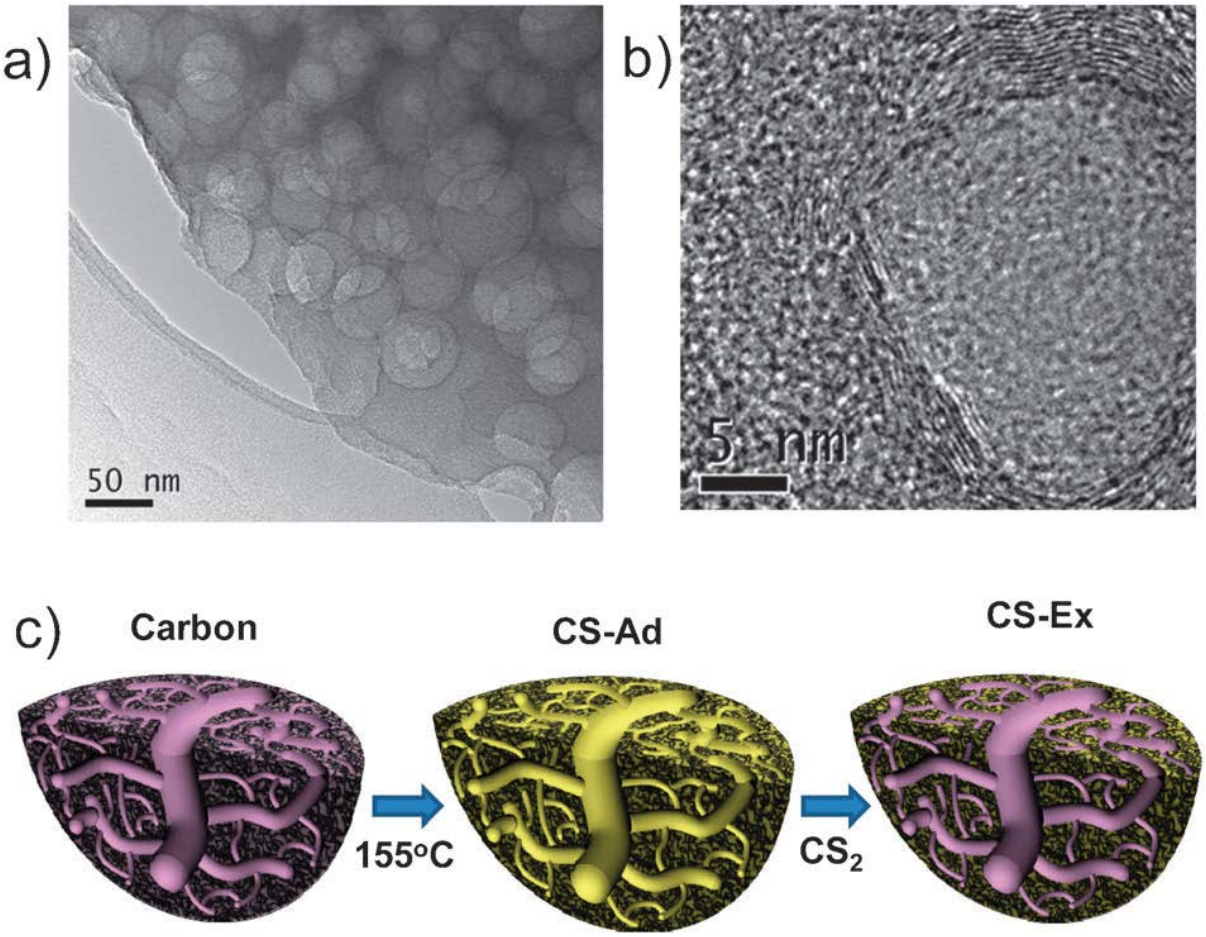

Figure 2.10 TEM images and schematic illustration of the adsorption and extraction of sulfur, towards mostly sub-nanometre sulfur immobilization [165].

Wang and his co-workers [165] investigated the use of microporous–mesoporous carbon with graphitic structure as the sulfur immobilizer for a high rate, stable Li–S cathode in a carbonate electrolyte. TEM images and schematic illustration of the microporous–mesoporous carbon with graphitic structure is shown in Figure 2.10. The sulfur was confined in micropores through the melt infusion process, and its stability was tested over 800 cycles in an aggressive carbonate electrolyte. The high rate capability of this cathode was excellent, allowing a practical four minute recharge operation. The authors believe that the graphitic

structure and microporous framework invigorate the high rate performance through facilitating both ion and electron transport.

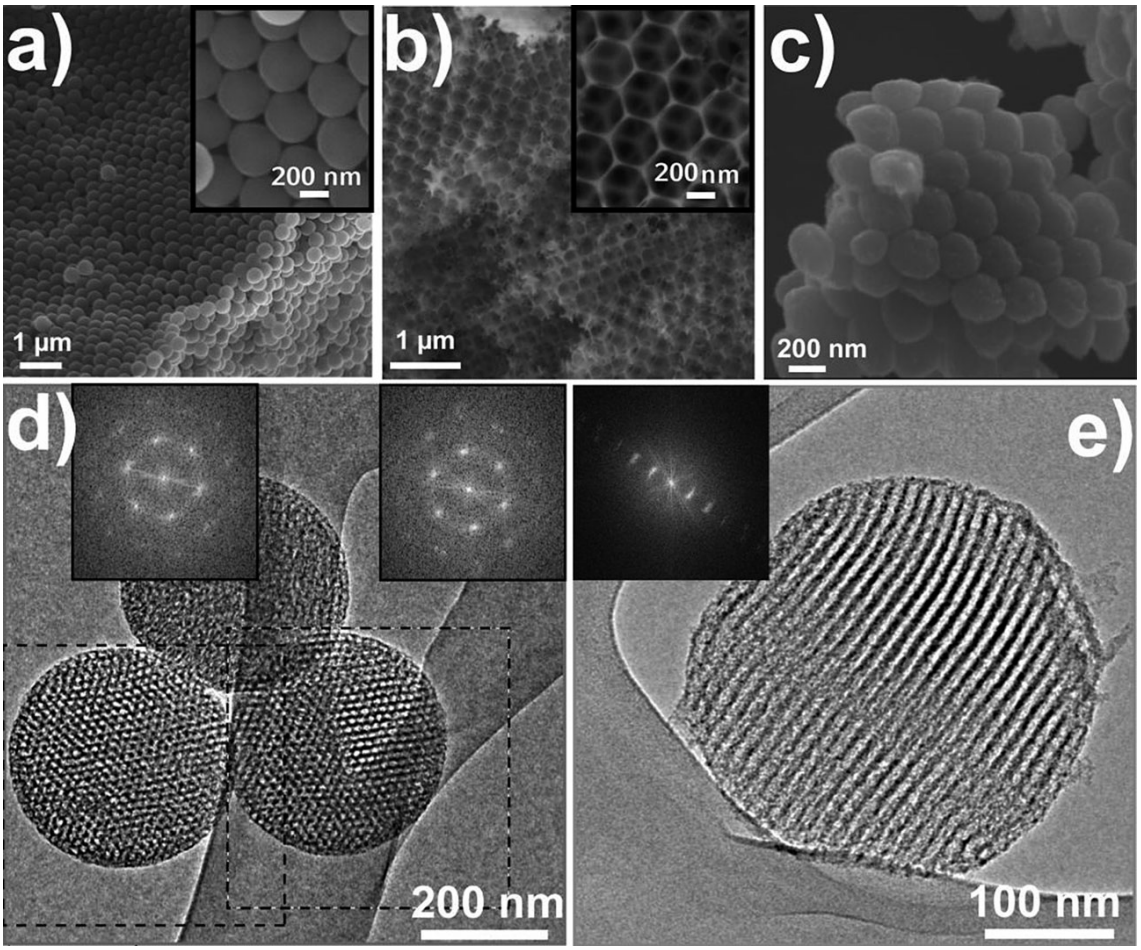

Figure 2.11 SEM images of:(a) poly(methyl methacrylate) (PMMA) spheres with ordered close packing (b) silica inverse opal structure (c,d,e) TEM images of spherical OMC nanoparticles, with the insets showing the corresponding selected area electron diffraction (SAED) patterns [156].

Guang He et al. [156] prepared an ordered mesoporous carbon (OMC) structure with very high bimodal porosity, which is shown in Figure 2.11. These OMC structures were filled with sulfur particles through melt adsorption and were investigated as a cathode material. The electrochemical performance showed very high initial discharge capacity and good

cyclability without sacrificing rate capability. Unlike bulk porous carbon this specially synthesized OMC did not display significant capacity fading.

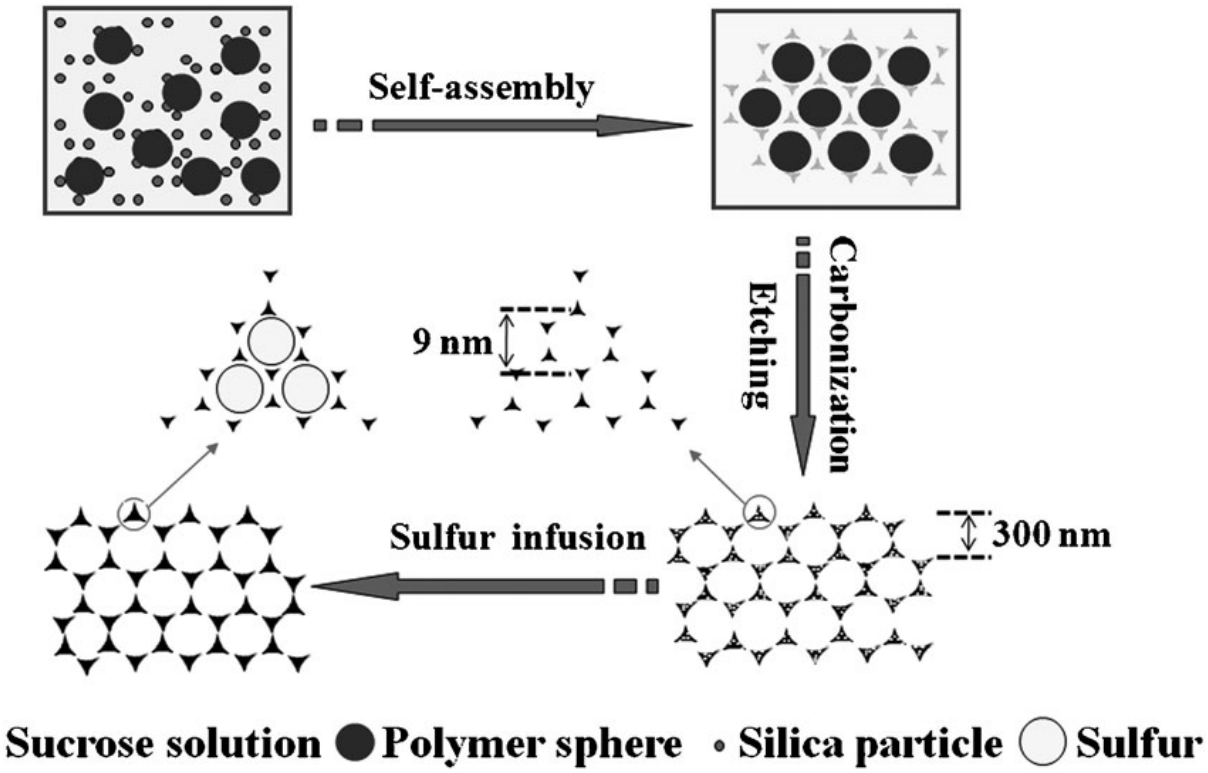

Figure 2.12 Schematic diagram of the preparation of hierarchical ordered porous carbon (HOPC) and HOPC/sulfur nanocomposite [121].

Three-dimensional hierarchical ordered porous carbon (HOPC) with mesoporous walls and interconnected micropores was prepared by Ding and his co-workers [121] through *in-situ* self-assembly of colloidal polymer and silica spheres, where sucrose was used as the carbon source, as is is shown in Figure 2.12. The as-prepared porous carbon shows very high surface area and pore volume, which were later filled by melted sulfur. Electrochemical tests showed that the HOPC/S nanocomposite with well-defined nanostructure had a high initial specific discharge capacity of 1193 mA h $g^{-1}$and a stable capacity of 884 mA h g^{-1} after 50 cycles with a current density of 0.1 C. In addition, the HOPC/S nanocomposite exhibited high reversible capacity at high current density. They proposed that the excellent electrochemical

performance is due to the beneficial integration of the mesopores for the electrochemical reactions and the macropores for ion transport.

In vapour deposition process, a sulfur-carbon mixture is heated above the boiling temperature of sulfur (B.P of sulfur: ~444.6 ^{o}C), so that the gaseous sulfur can be deposited inside the pores or on any preferred surfaces of the conductive additives. There is no general or fixed temperature for vapour deposition process because the boiling temperature strongly dependent on pressure. The lower the pressure, the lower the temperature needed to vaporize the sulfur.

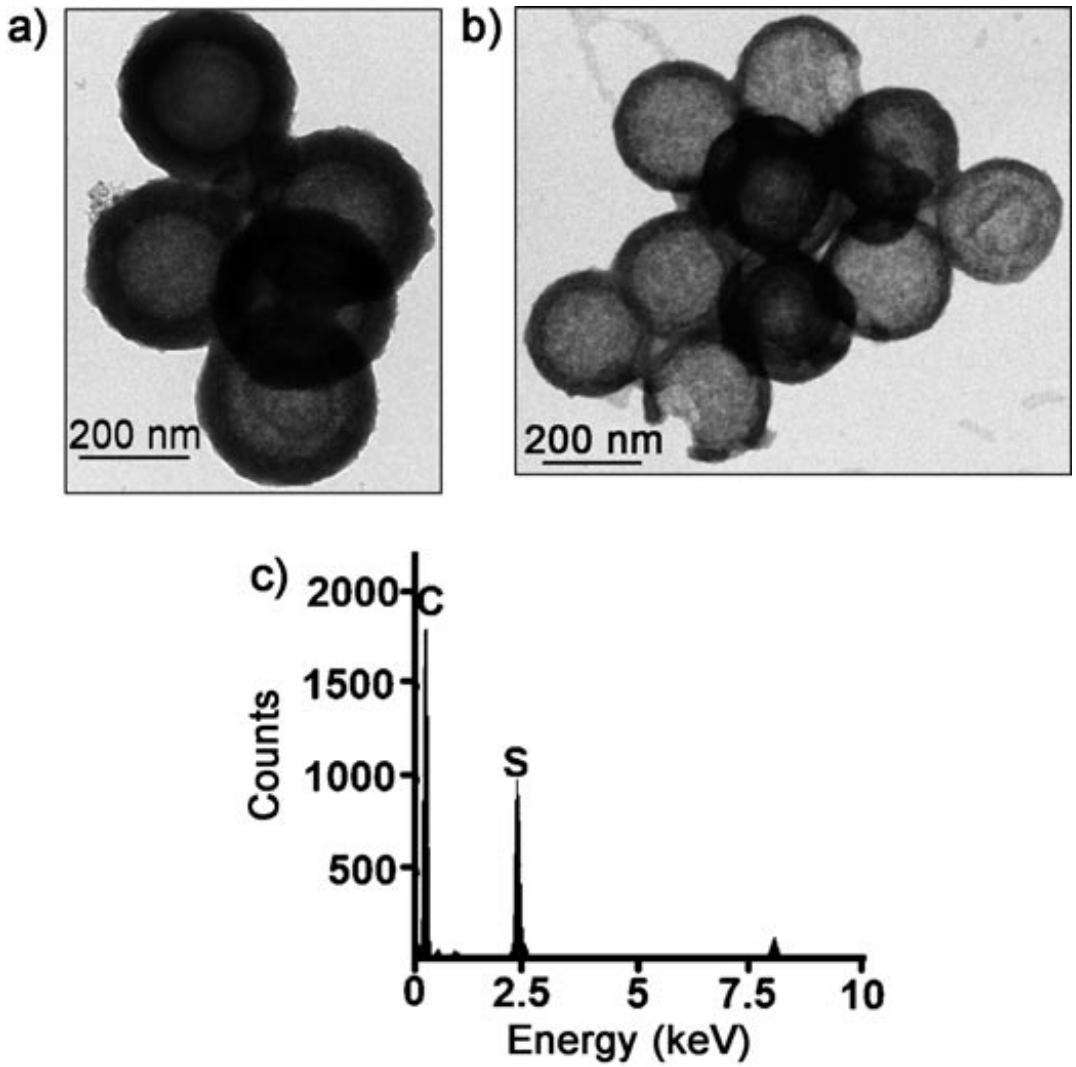

Figure 2.13 TEM image and EDS analysis of hollow spheres C@S nanocomposite [166].

Jayaprakash et al. [166] reported a facile, scalable approach for synthesizing mesoporous hollow carbon capsules that encapsulate and sequester elemental sulfur through vapour deposition in their interior and porous shells. The SEM and EDS analysis of this new C@S nanocomposite is shown in Figure 2.13. The as prepared C@S nanocomposite was used as cathode and demonstrated promising electrochemical behaviour after extended cycling for 100 cycles at 0.5C.

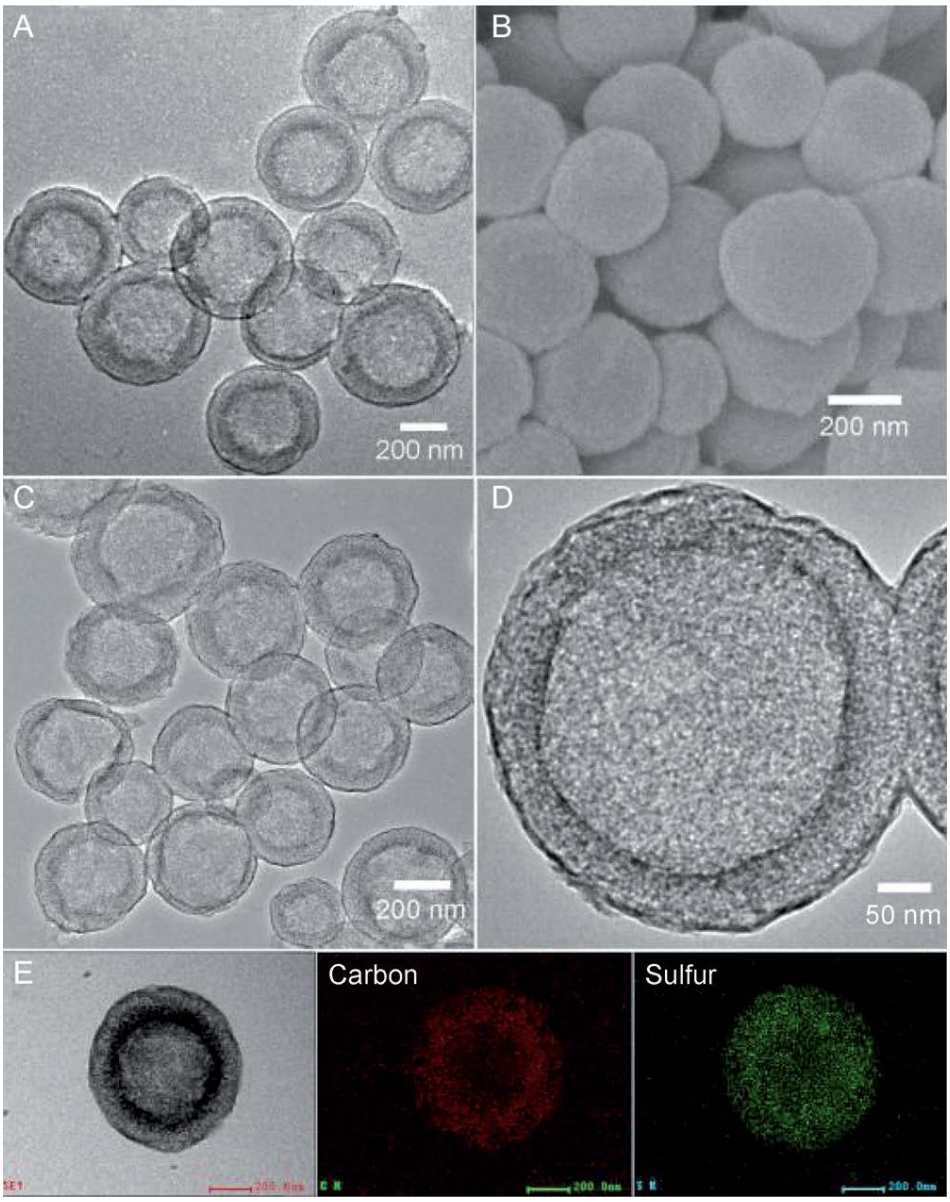

Figure 2.14 TEM and FESEM images and their corresponding elemental analysis of double-shelled hollow carbon spheres-sulfur (DHCS-S) composite [167].

Zhang et al. [167] reported the rational design and synthesis of a new sulfur‑carbon nanocomposite, made by confining sulfur through vapour deposition in double-shelled hollow carbon spheres (DHCSs). The FESEM, TEM, and EDS analysis of the DHCSs is shown in Figure 2.14. Such hollow carbon spheres with complex shell structures help to maximize the advantages of hollow nanostructures. This DHCS-S composite shows a significant improvement in electrochemical performance when used as the cathode material in a Li-S cell.

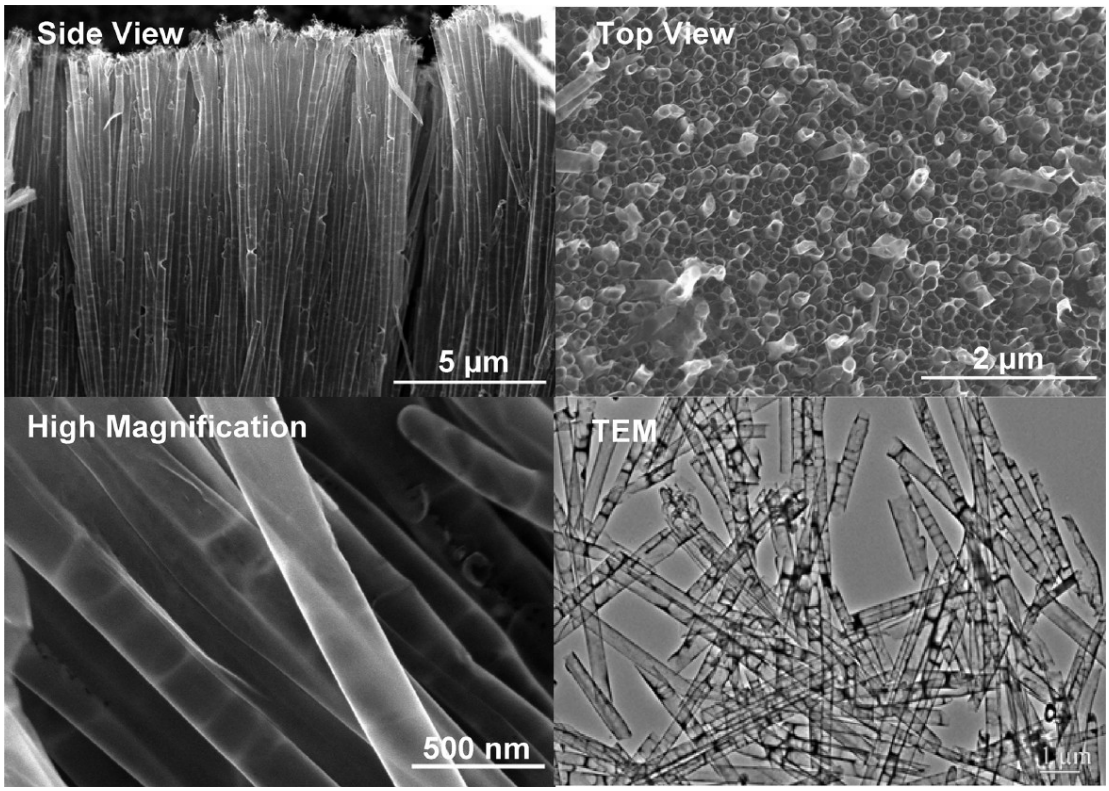

Figure 2.15 SEM and TEM images of the disordered carbon nanotubes prepared by the template wetting method [168].

Gou et al. [168] synthesized disordered carbon nanotubes (DCNT) by a template wetting technique using commercial anodic aluminum oxide (AAO) membranes as the template. SEM and TEM images of the DCNTs are shown in Figure 2.15. The synthesized DCNTs

were impregnated with sulfur through the vapour deposition technique at 500 ^{o}C. This DCNT composite with sulfur shows improved electrochemical performance.

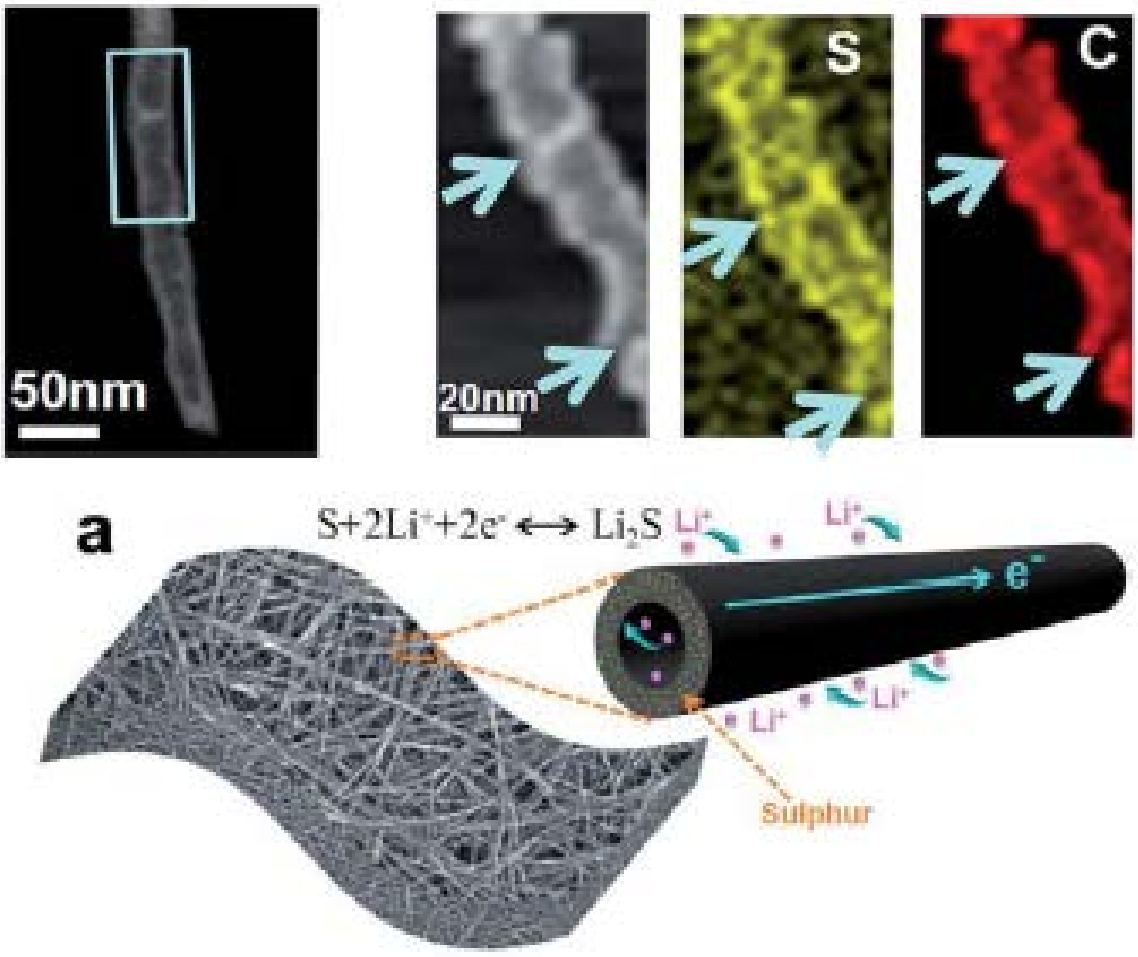

Figure 2.16 STEM analysis and elemental mapping of S-CNT composite [11].

Zhou et al., [11] reported the template-directed synthesis of sulphur–carbon nanotubes and used them to form a membrane that was binder-free, highly conductive, and flexible. The sulfur was impregnated through vaporization, which was confirmed through STEM analysis and elemental mapping, as shown in Figure 2.16. This nanostructured membrane is then used as a self-supporting cathode without metal current-collectors for Li-S batteries. The membrane cathode has high electrical conductivity and supports a long lifetime of sulphur of over 100 charge–discharge cycles.

2.3.1.1.2. Chemical techniques

2.3.1.1.2.1. Chemical precipitation

In this technique sulfur is precipitated out of a sulfur containing compound. The general and most common reaction is when sodium thiosulfate reacts with hydrochloric acid, and elemental sulfur is precipitated out of the solution along with water, sodium chloride, and sulfur dioxide. Beside this reaction, there are a few other reactions where sulfur can be precipitated out like, for example, when polysulfide reacts with acid it forms salt, elemental sulfur, and hydrogen sulfide gas. The chemical reactions are shown below.

$$Na_2S_2O_3 + 2HCl \leftrightarrow 2NaCl + S\downarrow + H_2O + SO_2\uparrow$$

$$Na_2S_x \,/\, Li_2S_x + 2HCl \leftrightarrow 2NaCl \,/\, 2LiCl + S_x\downarrow + H_2S\uparrow$$

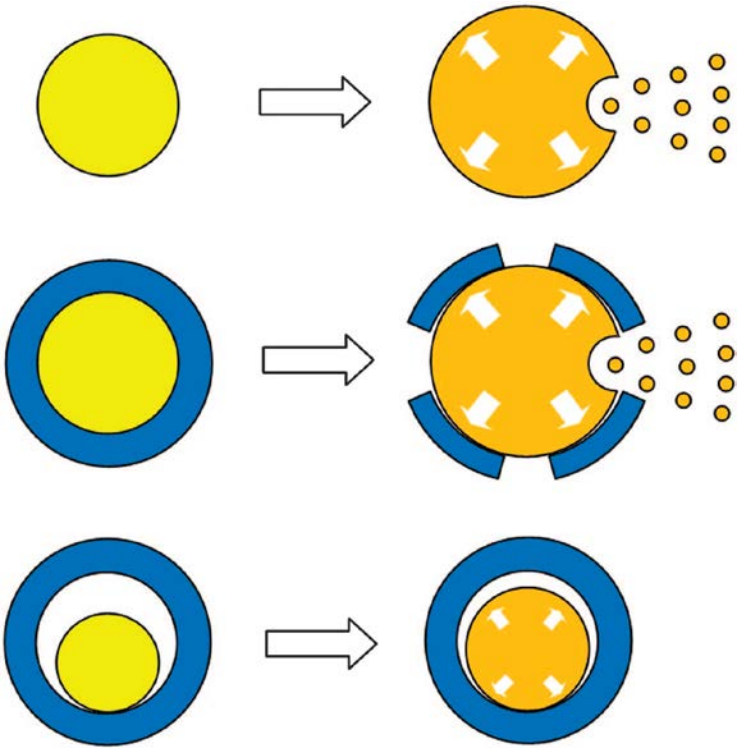

Figure 2.17 Schematic illustration of the working mechanisms of bare sulfur particles and yolk–shell TiO_2-S particles [129].

Seh et al. [129] designed a sulphur–TiO_2 yolk–shell nanoarchitecture, as shown in Figure 2.17, for stable and prolonged cycling over 1,000 charge/discharge cycles in lithium–sulphur batteries. Sulfur acts as the yolk, which is chemically precipitated inside a TiO_2 shell. The unique advantage of the yolk–shell morphology lies in the presence of internal void space to accommodate the large volumetric expansion of sulphur during lithiation, thus preserving the structural integrity of the shell to minimize polysulphide dissolution.

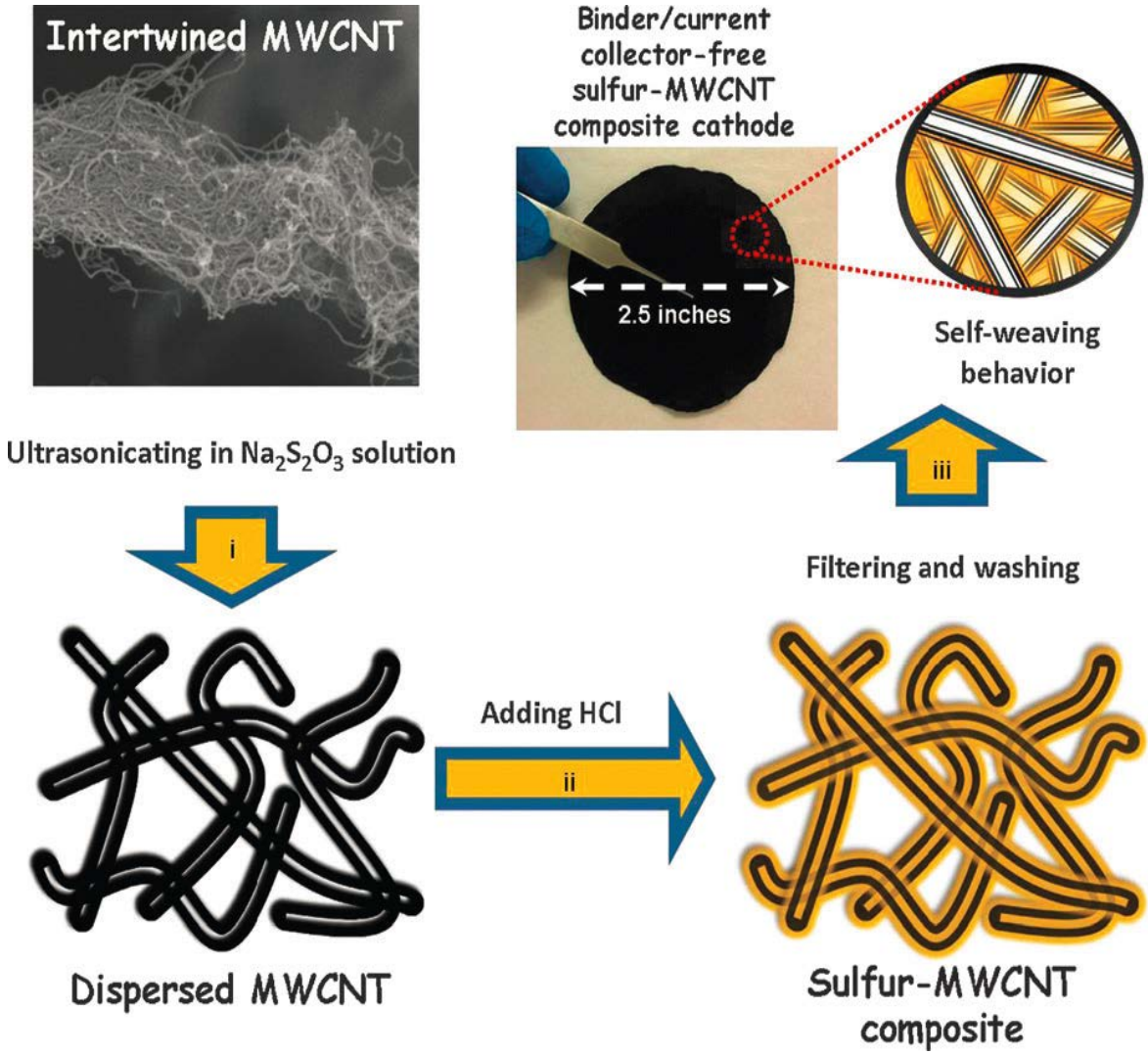

Figure 2.18 Schematic fabrication process for a self-weaving sulfur–MWCNT composite cathode synthesized by an in situ sulfur deposition method [12].

Figure 2.18 shows a in situ fabrication process of sulfur- multi-walled carbon nanotube (MWCNT) composite reported by Su et al., [12]. This sulfur–MWCNT composite cathode with its unique structure and morphology shows outstanding electrochemical performance.

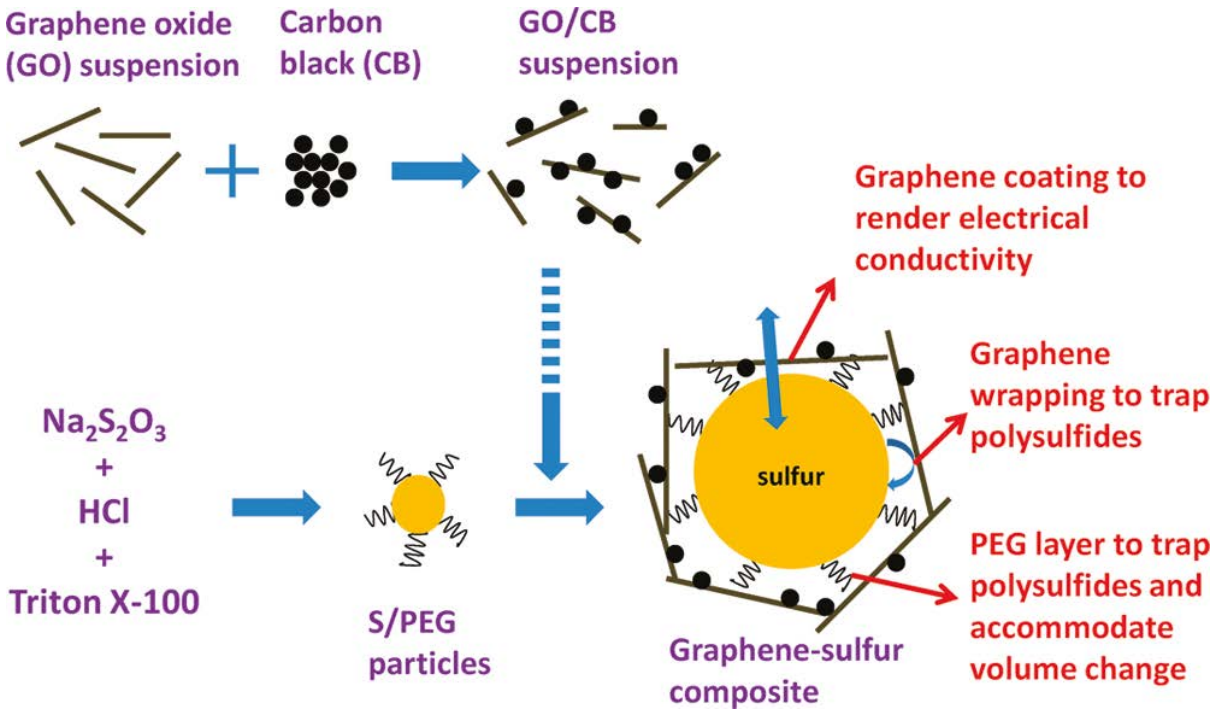

Figure 2.19 Schematic illustration of the synthesis of sulfur-wrapped graphene composite [169].

Wang et al. [169] reported the synthesis of a graphene-sulfur composite material by wrapping poly(ethylene glycol) (PEG) coated submicrometer-sized sulfur particles with mildly oxidized graphene oxide sheets decorated by carbon black nanoparticles, as is shown in Figure 2.19. The sulfur particles were precipitated out through the reaction of sodium thiosulfate and hydrochloric acid. The PEG and graphene coating layers help to compensate for the volume expansion of sulfur particles during discharge along with trapping soluble polysulfide intermediates and rendering the sulfur particles electrically conducting. The fabricated composite showed high and stable specific capacity up to 100 cycles.

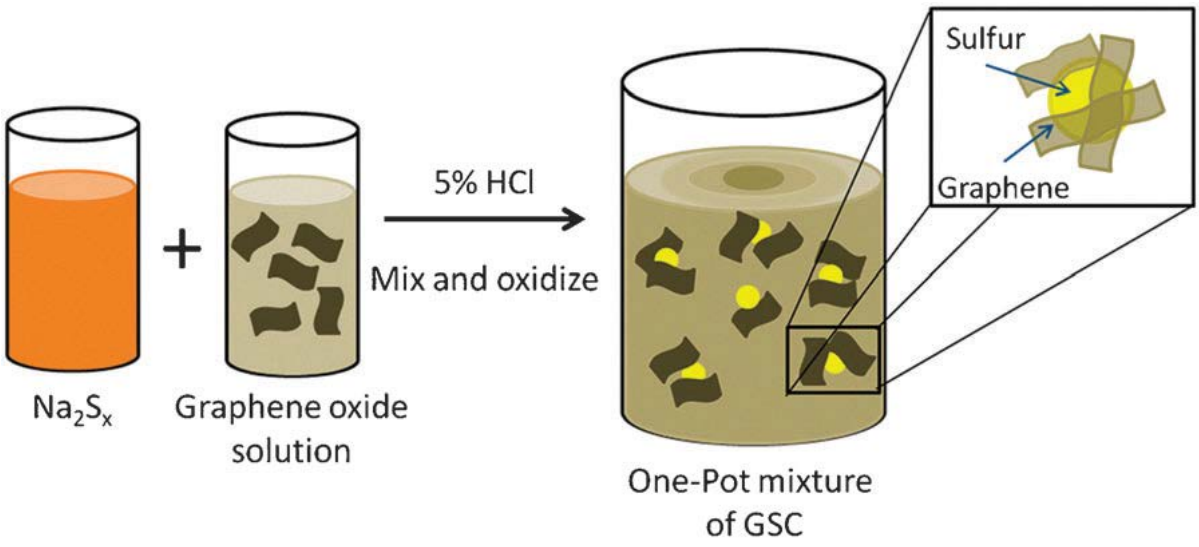

Figure 2.20 Schematic illustration of one pot synthesis of sulfur/graphene composite [28].

Evers and Nazar [28] reported a highly scalable graphene‑sulfur composite (GSC) cathode material that exhibited very high sulfur loading (87 wt%). Reduced graphene oxide (rGO) was used to envelop micron-sized sulfur particles, to form a highly conductive network around the sulfur particles and trap the polysulfides through favourable hydrophilic-hydrophilic interactions. The synthesis of the graphene-sulfur composite (GSC) was easily accomplished by combining a mixture of graphene oxide and soluble polysulfide ($Na_2S_{\sim 2.4}$), and carrying out oxidation in situ as a one pot reaction, as described in Figure 2.20.

Sun et al. [170] have developed a new one-pot wet chemical method to encapsulate sulfur uniformly into the interlayer galleries of graphene sheets, forming a novel sulfur − reduced-graphene-oxide composite. In this method, the formation of the composite is achieved through the simultaneous oxidation of sulfide and reduction of graphene oxide (GO), which is shown schematically in Figure 2.21. The as-prepared sulfur − reduced-graphene-oxide composite (SGC) enhances the transportation of lithium ions and electrons due to the high conductivity of the graphene and the uniform dispersion of sulfur in the interlayer galleries of the graphene sheets.

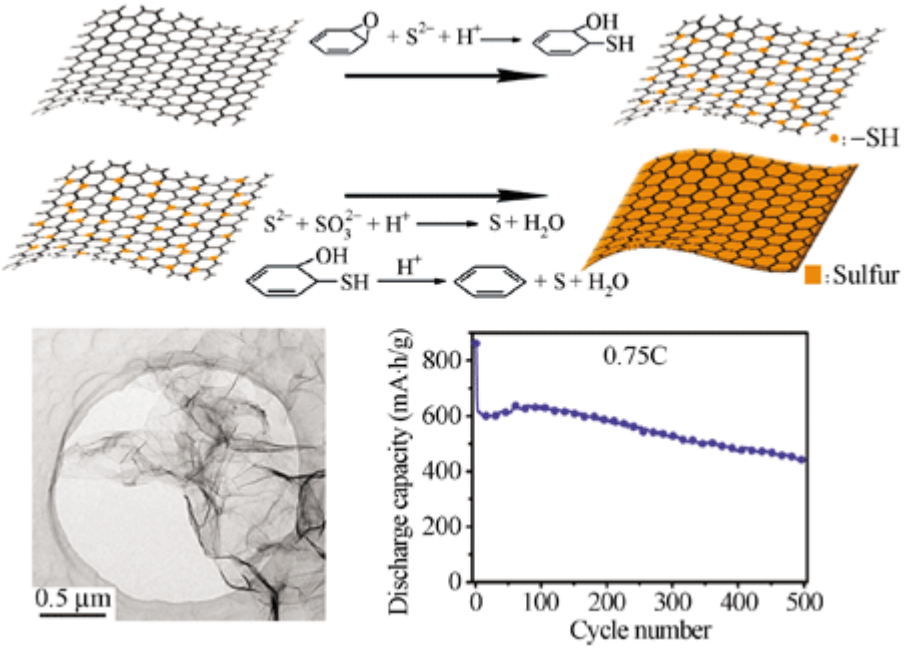

Figure 2.21 Schematic representation of the synthesis processes for sulfur − reduced-graphene-oxide composites [170]

2.3.1.1.2.2. Solvent evaporation

Elemental sulfur that has an orthorhombic lattice structure and features the S_8 crown-shaped molecular structure is nonpolar. This is why, in general, sulfur is dissolved in all the nonpolar solvents, although its solubility also depends on the molecular structure of the solvent. Among all the nonpolar solvents, carbon disulfide (CS_2) has the highest solubility of 34.8 wt% at room temperature. The Pauli electronegativity of sulfur and carbon are 2.58 and 2.55, respectively, and because of this, the carbon-sulfur bond is slightly polarized. Furthermore, CS_2 is a linear molecule and results in no net dipole moment of the CS_2, which is responsible for the high solubility of sulfur at room temperature. Other common organic solvents having high solubility are: benzene (~2.1 wt%), toluene (~2.17 wt%), aniline (1.26 wt%), cyclohexane (~1.26 wt%), chloroform (~1.16 wt%), nitrobenzene (~0.86 wt%), carbon tetrachloride (~0.83 wt%), n-hexane (~0.4 wt%), dimethylformamide (~0.19%), diethyl ether (~0.18 wt%), acetone (~0.08%), and ethanol (~0.07%) [2].

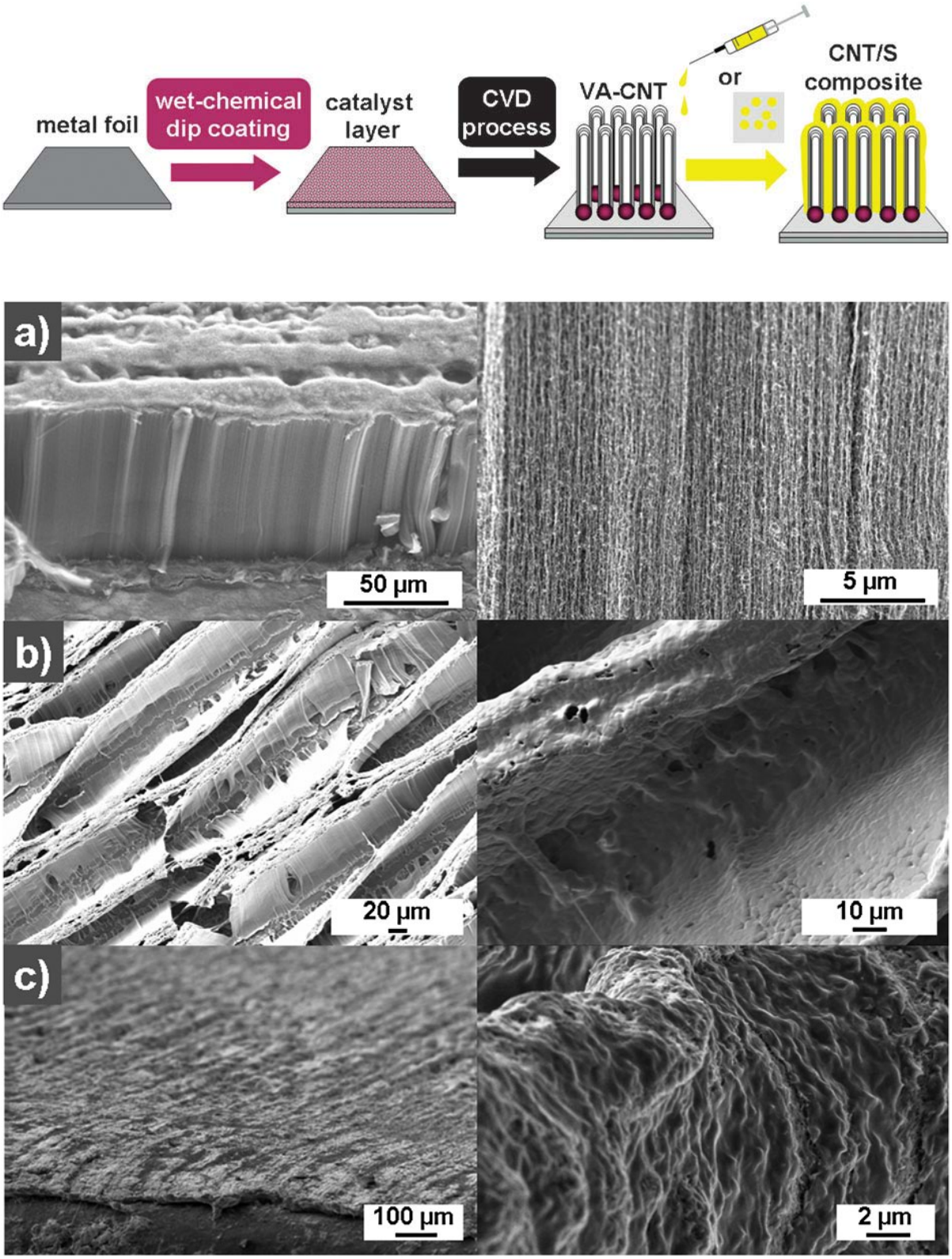

Figure 2.22 Schematic illustration of electrode preparation through chemical vapour deposition of CNT and infiltration of sulfur solution, and SEM images of the electrode [171].

Dorfler et al., [171] report a new approach based on binder free carbon nanotube (CNT)/sulfur composite, which was synthesized through the chemical vapour deposition (CVD) method and loading the CNTs with sulfur w through dip coating. The synthesis process and SEM images of the composite are shown in Figure 2.22. The fabricated electrodes enable high sulfur loadings up to 70 wt% and deliver discharge capacities higher than 800 mAh g^{-1}, with respect to the composite electrode mass.

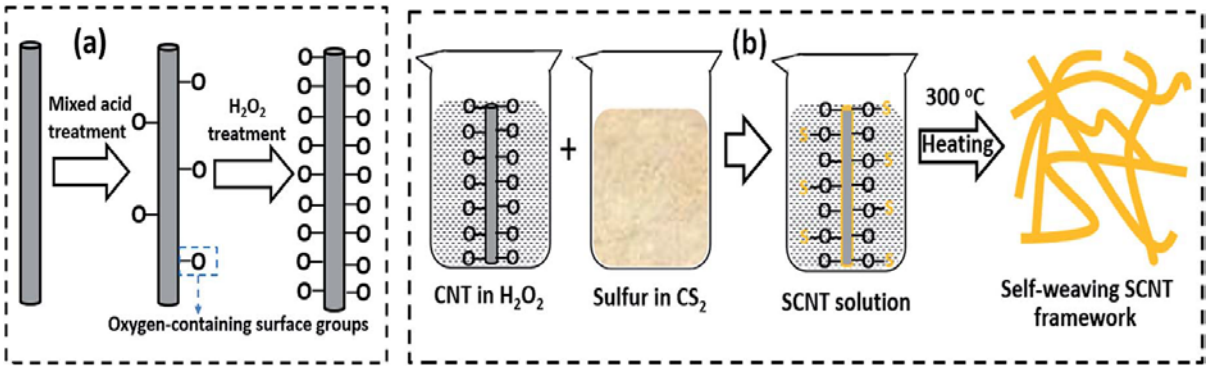

Figure 2.23 Schematic illustrations of (a) treatment for integrating oxygen-containing surface groups into CNTs, and (b) the proposed strategy for grafting sulphur onto CNTs [144].

Yan et al. [144] reported sulfurized carbon nanotube (SCNT) cathodes in a Li-S cell that could demonstrate long-life and high-efficiency. They tried to develop a new synthesis method to fabricate SCNT materials with a high sulfur content (~68 wt%) at the relatively low temperature of 300 ^{o}C, by functionalizing the CNTs and using a solvent exchange method to graft sulfur chains onto the CNTs. The solvent evaporation method was used to load sulfur into the SCNT, as is shown in Figure 2.23. Their SCNT cathodes exhibited very long cycle life (exceeding 1300 cycles with a current density of 1/3 C) with ultrahigh capacity retention (67.8% over 1300 cycles, from a discharge capacity of 809 to 549 mA h g^{-1}). Moreover, their Li–S cells showed excellent rate capability up to 2 C, and their Coulombic efficiency was higher than 95.5%.

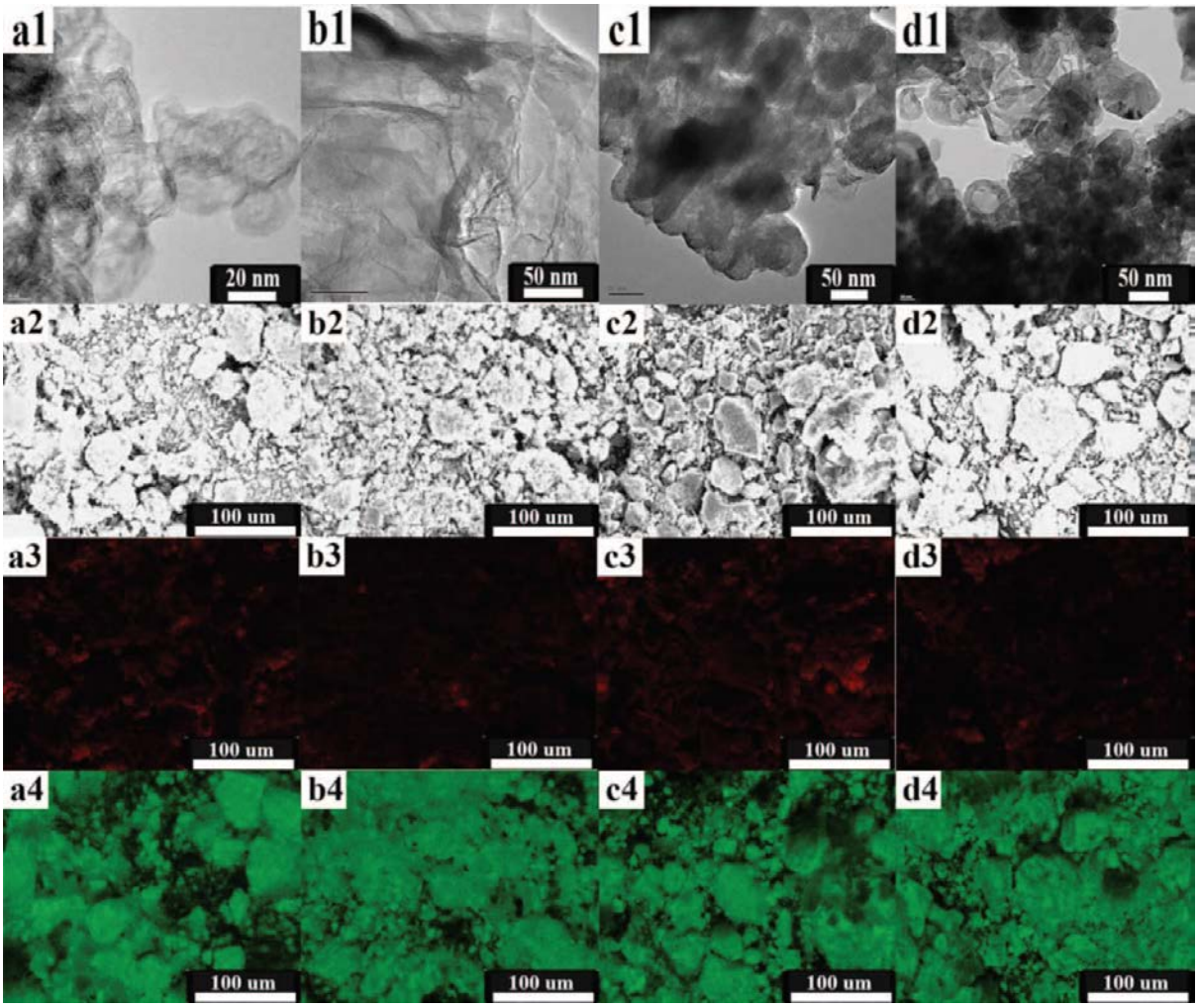

Figure 2.24 TEM images, SEM images, and elemental maps (carbon in red and sulfur in green) of different C/S composites [172].

Zheng and his co-workers [172] carefully chose four different types of carbon, Ketjenblack (KB, high surface area and porous), graphene (high surface area but nonporous), acetylene black (AB, low surface area and nonporous) and hollow carbon nanospheres (HCNS, low surface area and porous), to construct S-C composites. They loaded sulfur from sulfur containing CS_2 solution to investigate the influences of the different carbon sources with different surface areas, pore volumes, and architectures. The sulfur content in all C/S composites in this work was controlled at ~80 wt%, and the sulfur loading on the electrode was about 1 mg cm^{-2}.

2.3.1.1.3. Mechanical treatment

In this method, a carbon-sulfur mixture was mechanically treated with a ball mill, hand mill, sonicator, magnetic stirrer, or any other mechanical means. Due to mechanical forces, sulfur and carbon firmly adhere to each other. These mechanical treatments are also used to reduce the particle size of sulfur, which facilitates higher surface area of the sulfur particles and helps to increase the contact area between the sulfur and the carbon.

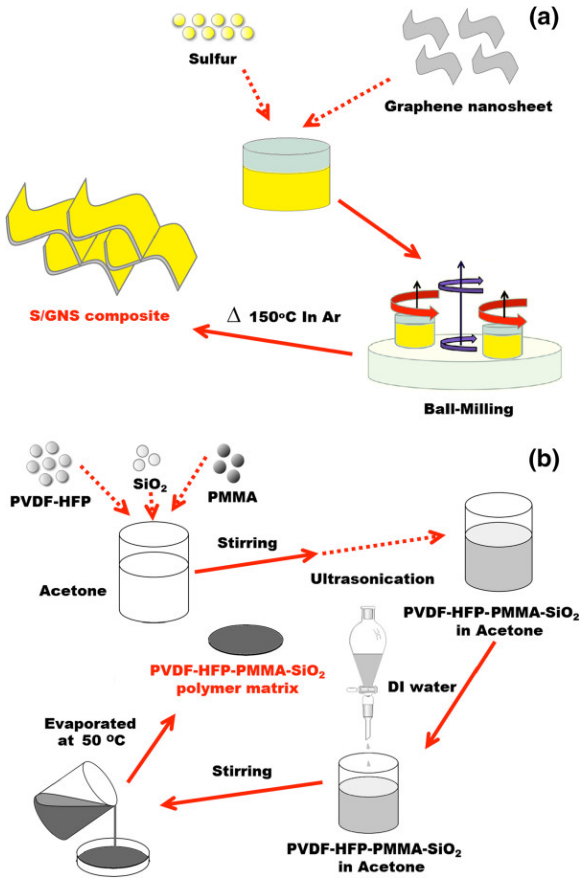

Figure 2.25 Schematic diagram of the synthesis of (a) S/GNS composite and (b) PVDF-HFP/PMMA/SiO_2 polymer matrix [173].

Zheng et al. [173] reported on the preparation of a novel sulfur/graphene nanosheet (S/GNS) composite via simple ball milling of sulfur and commercial multi-layer graphene nanosheets, followed by a heat treatment, and investigated its physical and electrochemical properties as a cathode for Li-S batteries, as is shown in Figure 2.25. The electrochemical performance of

their battery features a discharge capacity of 809 mAh g^{-1} in the 1st cycle and can retain capacity up to 413 mAh g^{-1} after 50 cycles at 0.2 C with high coulombic efficiency.

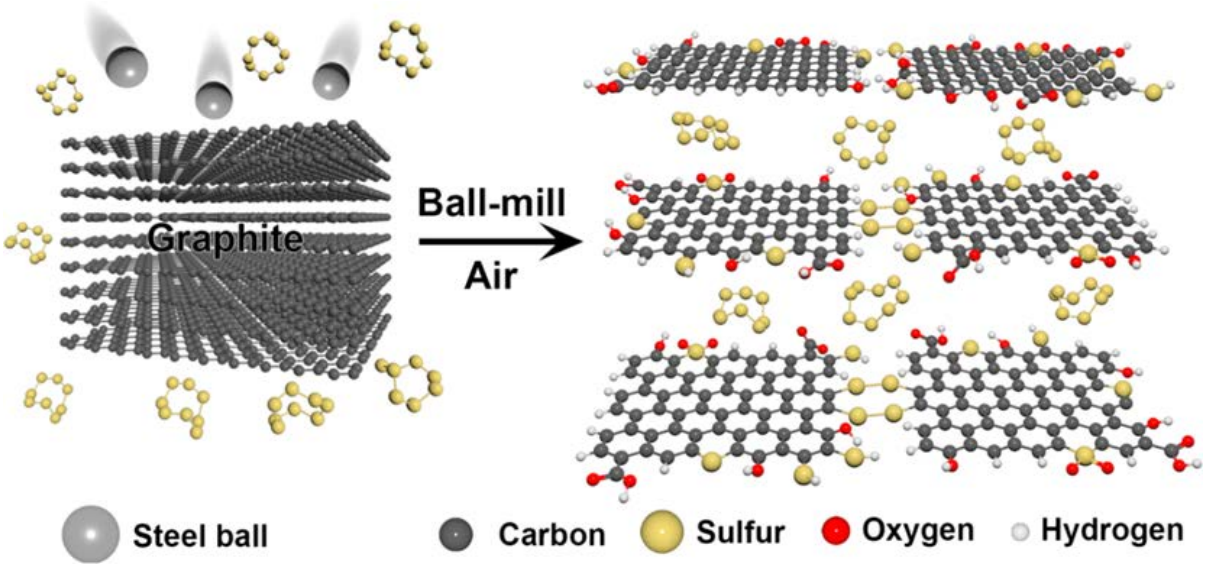

Figure 2.26 Schematic representation of ball-milled sulfur-graphene nanocomposite fabrication [160].

Xu et al., [160] developed a simple, low-cost, but effective and eco-friendly ball-milling method for large-scale production of various graphene nanoplatelets (GnPs). A schematic illustration of the synthesis of GnPs is shown in Figure 2.26. These GnPs were edge-functionalized with different moieties without any basal-plane damage, which led to good electrical/thermal conductivities. They also demonstrated in the present study that sulfur could edge-selectively functionalize GnPs (S-GnPs) with a concomitant homogeneous adsorption on and within the GnP structure, leading to highly efficient LSB cathode materials. The electrochemical performance of S-GnPs with different compositions shows that 70%S-30%GnPs have excellent discharge capacity and capacity retention.

2.3.2. Application of a carbon free-standing layer

The polysulfide shuttle phenomenon which is one of the most notorious challenges for the Li-S cell can be mitigated by placing a free-standing carbon layer in between the cathode and the

separator. It was speculated that this interlayer can act like a fishing net and can capture longer chain polysulfides in its net-like structure, significantly minimizing the shuttle phenomenon.

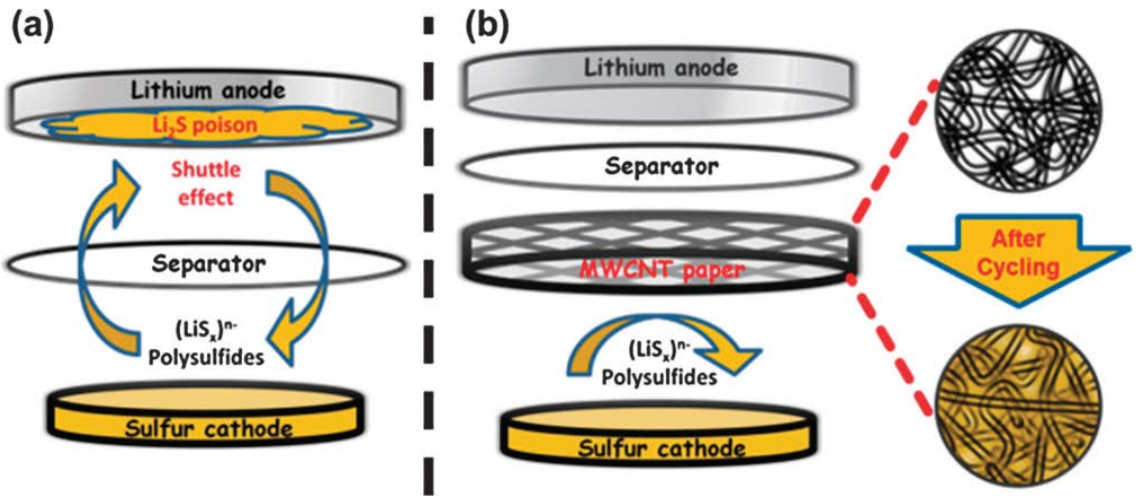

Figure 2.27 Schematic illustration of cell configurations of rechargeable Li–S batteries:(a) traditional configuration, and (b) new configuration with the MWCNT interlayer [174].

The Manthirum group [174] first demonstrated this idea by placing a multi-walled carbon nanotube (MWCNT) interlayer between the cathode and the separator, as is shown in Figure 2.27. In their work they demonstrated that inserting a bi-functional, conductive, porous MWCNT paper between the cathode and the separator leads to an enhancement in both the specific capacity and the cyclability of Li–S batteries. This free-standing MWCNT paper was first fabricated by an ultrasonic dispersion of synthesized MWCNTs, followed by a simple vacuum filtration without the addition of binders. Later, this idea was also adopted by other groups [36, 162].

2.3.3. Implementation of fixed capacity charging

Another way to reduce the polysulfide dissolution problem and shuttling phenomenon is to prevent the formation of longer chain polysulfides, which are soluble in organic electrolyte. As is well known, the general electrochemical window for the Li-S system is 1.5 to 3.0 V.

During discharging, longer chain polysulfides start to form at 2.4 to 2.3 V, and shorter chain polysulfides form at around 2.1 V. On the contrary, during charging, shorter chain polysulfides are oxidized to longer chain polysulfides within that voltage range. In this method, Li-S cell will discharge down to 1.5 V but will be charged to a fixed lower capacity instead of 3 V, which will prevent the formation of longer chain polysulfides.

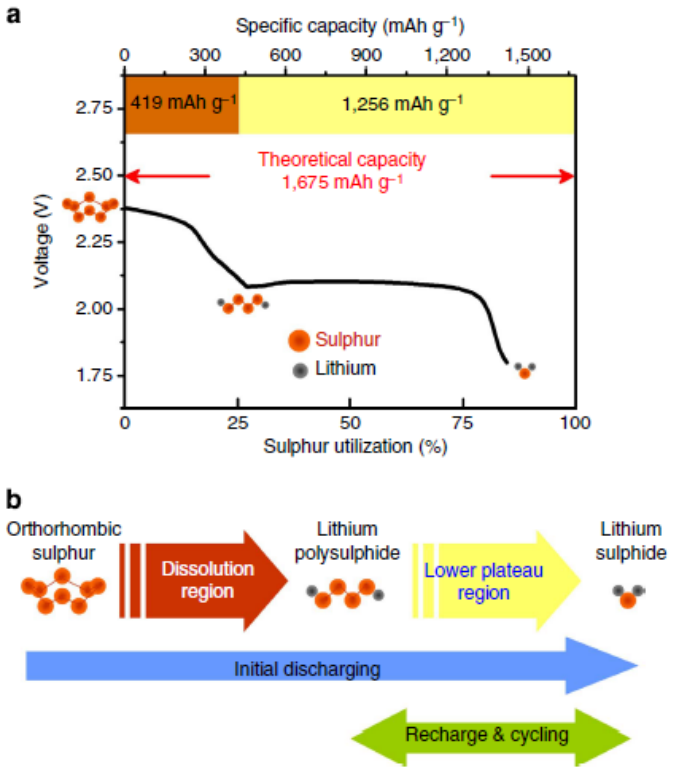

Figure 2.28 (a) Typical discharge profile of the Li-S battery (b) The strategic approach to recharging Li-S batteries. The lower plateau possesses a theoretical capacity of 1,256 mA h g-1 [175].

Su et al. [175] first reported this new fixed capacity charging method, and the mechanism behind this method is shown in Figure 2.28. In their work, they reported an applicable way to recharge lithium-sulphur cells by simple charge operation control, which offers tremendous improvement for various lithium-sulfur battery systems. Adjusting the charging condition from voltage window to fixed capacity leads to long cycle life (over 500 cycles) with

excellent capacity retention (> 99%) by inhibiting electrochemical reactions accompanied by severe polysulphide dissolution.

Finally, it is important to mention here that besides these methods, there are numbers of different methods that scientists have tried to solve the challenges for the Li-S system. Modification of anode, usage of ionic liquids as electrolyte, addition of different additives and salts in the electrolyte, usage of different binders and conductive polymer are the most notable attempts. Even though the challenges are yet to fully overcome, there has been significant improvement so far, and it is expected that, by the next decade, the Li-S system will be fully commercialized.

Chapter 3. Experimental

3.1. Overview

In this doctoral work, different methods were adopted to synthesize elemental sulfur and sulfur-carbon composite. The mechanical method that has been used multiple times for synthesizing and modifying the active materials is the high energy ball-milling method. Beside this, spray precipitation and reverse microemulsion methods were also used for the synthesis of active materials. After synthesizing the materials, a series of physical characterizations, morphological characterizations, and electrochemical characterizations were conducted to find the structure − property relationship between materials and performance. The common physical and morphological characterization tools that have been used are: X-ray diffraction (XRD), field emission scanning electron microscopy (FESEM), transmission electron microscopy (TEM), energy dispersive X-ray spectroscopy (EDS), thermogravimetric analysis (TGA), differential scanning calorimetry (DSC), Fourier transform infrared spectroscopy (FTIR), Raman spectroscopy, and the Brunauer-Emmett-Teller (BET) surface area analysis technique. After these two types of characterization, if a material showed the desired structure, spectra, and properties, then it was used as an active material for the preparation of electrodes and cells. Finally, the cells were electrochemically tested to evaluate the material's performance as part of an electrochemical cell. The common electrochemical characterization techniques that have been used are: cycling performance testing, rate capability testing (different current densities), galvanostatic charge-discharge testing, cyclic voltammetry (CV), and electrochemical impedance spectroscopy (EIS). The logical flow of the experimental route along with characterizations is shown in Figure 3.1 below.

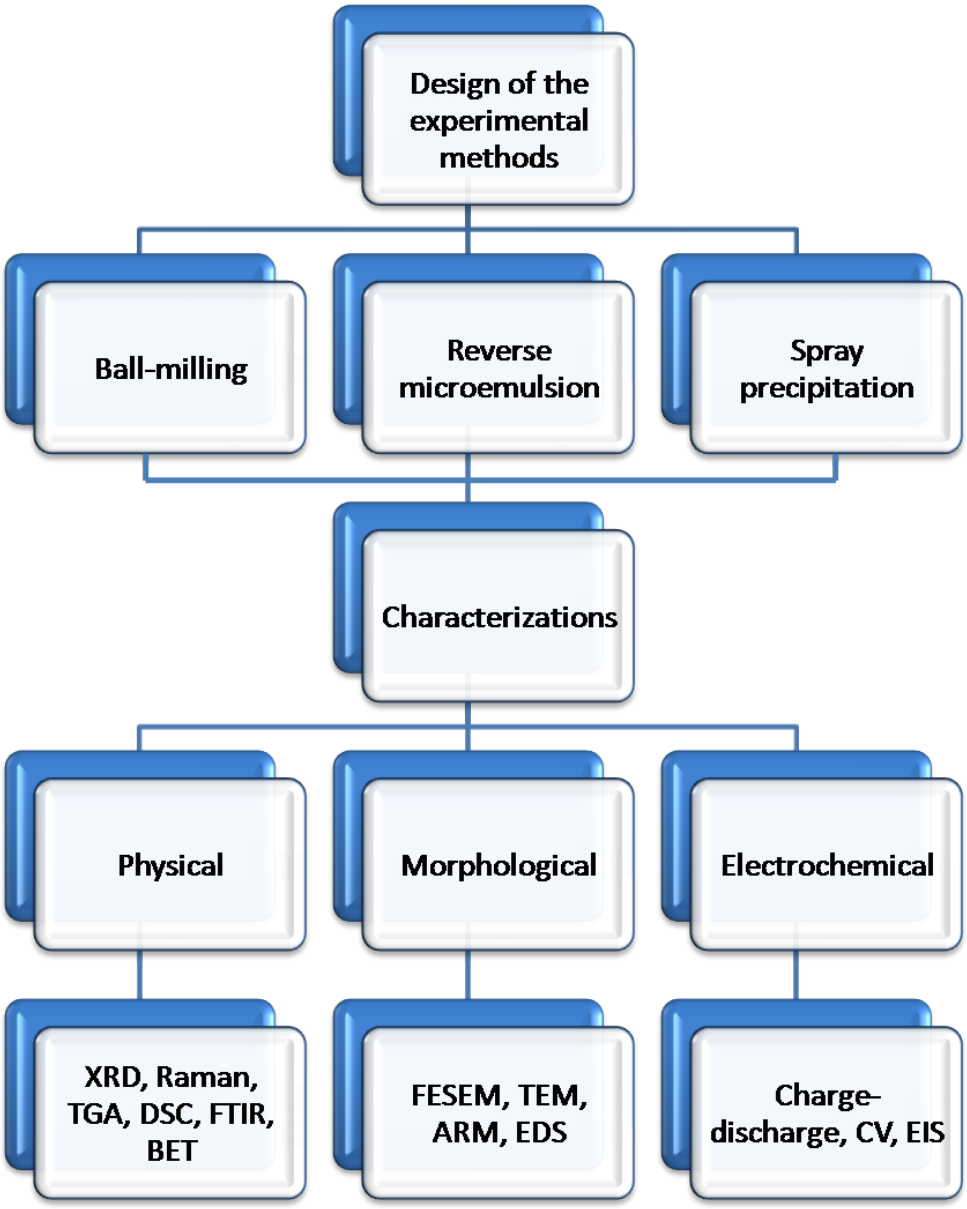

Figure 3.1 Outline of the experimental procedures and characterization techniques used in this thesis.

3.2. Chemicals and materials

The important chemicals and materials that have been used during the experiments are listed in the following table along with their suppliers, purity, and chemical formula. It is important to mention here that not all chemicals are listed in the tables and the chemical may not follow IUPAC rule in every case.

Table 3.1 List of chemicals, with formulas, purity, and suppliers.

Materials/Chemicals	**Formula**	**Purity (%)**	**Supplier**
1,3-dioxolane	$C_3H_6O_2$	99	Sigma Aldrich, Australia
1-methyl-2-pyrrolidinone (NMP)	C_5H_9NO	99.5	Sigma Aldrich, Australia
Acetone	CH_3COCH_3	99	Sigma Aldrich, Australia
Activated Carbon	C	99	Sigma Aldrich, Australia
Aluminium foil	Al	N/A	China
n-Butanol	$C_4H_{10}O$	99.8	Sigma Aldrich, USA
Carbon black	C	N/A	Timcal, Belgium
CR2032 type coin cells	N/A	N/A	China
Cyclohexane	C_6H_{12}	99	Sigma Aldrich, USA
Dimethoxy ethane	$C_4H_{10}O_2$	99	Sigma Aldrich, Australia
Ethanol	C_2H_5OH	Reagent	Q-store, Australia
Graphite	C	N/A	Sigma Aldrich, Australia
Graphene nanoplatelet	C	N/A	Sigma Aldrich, USA
Hydrochloric acid	HCl	36.5	Sigma Aldrich, Australia
Iron (III) chloride	$FeCl_3$	97	Sigma Aldrich, Australia
Lithiumbis(trifluoromethanesulfonyl)imide	$CF_3SO_2NLiSO_2CF_3$	N/A	Sigma Aldrich, Australia
Lithium metal	Li	99.9	Sigma Aldrich, Australia
Lithium nitrate	$LiNO_3$	99	Sigma Aldrich, Australia
Multi-walled carbon	C	99	Shen Zhen Nanotech

nanotubes (CNTs)			Port.
Nano-graphite carbon	C	99	Sigma Aldrich, Australia
Oxalic acid	$H_2C_2O_4$	99	Sigma Aldrich, Australia
Polypropylene separator	$(C_3H_6)_n$	Celgard 2500	Hoechst Celanese Corporation, USA
Polyvinylidene difluoride (PVDF)	$(CH_2CF_2)_n$	N/A	Sigma Aldrich, Australia
Pure ethanol	C_2H_5OH	99.95% absolute	Sigma Aldrich, Australia
Pyrrole	C_4H_5N	98	Sigma Aldrich, Australia
Singled-Walled CNT	C	99	Nanocore, USA
Sodium thiosulphate	$Na_2S_2O_3$	99	Sigma Aldrich, Australia
Sodium p-toluenesulfonate	$CH_3C_6H_4SO_3Na$	95	Sigma Aldrich, Australia
Span 80	$C_{24}H_{44}O_6$	>60	Sigma Aldrich, USA
Sulfur	S	99.5+	Sigma Aldrich, Australia
Triton X-100	$C_{34}H_{62}O_{11}$	99	Sigma Aldrich, USA
Tween 80	$C_{32}H_{60}O_{10}$	>60	Sigma Aldrich, USA

3.3. Materials preparation

Materials preparation and synthesis were conducted by using the ball-milling, spray precipitation, and reverse microemulsion methods. All the methods will be elaborated in the individual chapters.

3.4. Physical and morphological characterization techniques

The physical and morphological characterization techniques that were used to characterize the synthesized materials are briefly discussed in the following sections.

3.4.1. X-ray diffraction

X-ray diffraction (XRD) is widely used to detect a material's crystal structural and grain size. X-rays are electromagnetic wave radiation with very short wavelengths and high energy. In this thesis, X-ray powder diffraction was conducted on a GBC MMA diffractometer in UOW. This XRD device uses Cu Kα radiation, λ = 1.54056 Å.

3.4.2. Raman spectroscopy

Raman analysis is a spectroscopic technique to observe vibrational, rotational, and other low-frequency modes in a system, which can be employed to identify the components of materials [176]. In a Raman spectrometer, the energy shift of some laser photons, caused by the interaction between laser light and molecular vibrations, phonons, or other excitations, gives information on the phonon modes in the system. In this thesis, Raman spectra were recorded on a JOBIN Yvon Horiba Raman 57 Spectrometer model HR800 in UOW.

3.4.3. Brunauer-Emmett-Teller (BET) technique

The Brunauer-Emmett-Teller (BET) method has been widely used to measure the specific surface area and the pore size distribution of materials [177].The BET surface areas of samples can be calculated based on the experimental points at a relative pressure of P/P_0 = 0.05 – 0.25, and the pore size distributions can be calculated by the Barrett-Joyner-Halenda (BJH) method, based on the amount of nitrogen adsorbed at a relative pressure of P/P_0 = 0.99. In this doctoral work, nitrogen sorption was measured on a Quanta Chrome Nova 1000 in UOW in liquid nitrogen.

3.4.4. Thermogravimetric analysis

Thermogravimetric analysis (TGA) is a technique for analysis of the chemical changes or physical weight changes in materials with increasing temperature [178]. TGA can provide information on physical phenomena, such as vaporization, sublimation, absorption, and desorption, and also can provide information on chemical phenomena, such as chemisorption, dehydration, decomposition, and solid-gas reactions. In this doctoral work, TGA was used to determine the sulfur percentage and the carbon ratio in the composite materials. TGA was performed on a SETARAM Thermogravimetric Analyzer (France). The sample was placed in an alumina crucible with loading mass of 5-10 mg, depending on the density of the composite materials.

3.4.5. Scanning electron microscopy and energy dispersive spectroscopy

Scanning electron microscopy (SEM) is a microscopy technique used to produce images by scanning a sample with a focused beam of electrons. The interaction between the electrons and the atoms in the sample can give the information about the topography, composition, and other properties of the sample surface, such as electrical conductivity. The types of signals produced by a SEM include secondary electrons (SE), back-scattered electrons (BSE), characteristic X-rays, specimen currents under illumination, and transmitted electrons. All SEMs have the standard secondary electron detectors, but the other detectors for all possible signals are only installed together in a machine as options. The signals result from interactions of the electron beam with atoms at or near the surface of the sample. Due to the very narrow electron beam, with the most common standard technique, secondary electron imaging (SEI) micrographs allow a large depth of field, so that a characteristic three-dimensional appearance of the surface structure of a sample can be obtained. The powder samples in this work were either dispersed in ethanol or directly loaded onto an aluminium holder using carbon conductive tape for SEM observation.

Energy-dispersive X-ray spectroscopy (EDS) is commonly used for the elemental analysis or chemical characterization of materials. It is based on the interaction between some source of X-ray excitation and the sample. As each element has a unique atomic structure, it features a unique set of peaks on its X-ray spectrum. In this thesis, the morphology, structure, and elemental mapping of the samples were detected with a field-emission scanning electron microscope (FESEM; JEOL 7500 in UOW).

3.4.6. Transmission electron microscopy

Transmission electron microscopy (TEM) is a microscopy technique to investigate the morphology, crystal structure, and electronic structure of the materials. In TEM, a beam of electrons is transmitted through an ultra-thin specimen, and the TEM image is formed from the interaction between the electrons and the specimen when it passes through. In this thesis, the samples were dispersed in ethanol and then loaded onto a holey carbon support film on a copper grid, and the TEM images of the samples were collected by a JEOL 2011, 200 kV in UOW.

3.5. Electrochemical characterizations

3.5.1. Electrode preparation

Before discussing electrochemical characterization techniques, it is necessary briefly describe the preparation of the electrodes. Generally, the electrode slurry consists of a mixture of active materials, conductive carbon (e.g. carbon black or Super P), and binder (e.g. polyvinylidene difluoride (PVDF) in N-methyl-2-pyrrolidone (NMP)). This slurry was vigorously mixed in a ball mill or by hand with a mortar and pastel. The obtained homogeneous slurry was coated onto the current collector (usually aluminium foil) which is then dried in a vacuum oven at 50-60 °C for 24 hours. It is then pressed at moderate pressure and cut into appropriate sizes.

3.5.2. Battery assembly

The assembly of Li-S cells was carried out in an Ar-filled glove box using CR2032-type coin cells. The stacking components of a CR2032 coin cell are shown in Figure 3.2. In my CR 2032 coin-type cells, they were assembled in the following order: (1) the working electrode disc was placed at the positive cap followed by the addition of 1-2 drops of organic electrolyte; (2) the separator was then evenly immersed in the electrolyte and placed in the cell, and an extra 1-2 drops of electrolyte were dripped in; (3) the lithium foil was placed onto the separator followed by the stainless steel spacer, spring, and negative cap; and (4) finally, the coin cell is tightly sealed, and then rested for at least 12 hours before electrochemical testing.

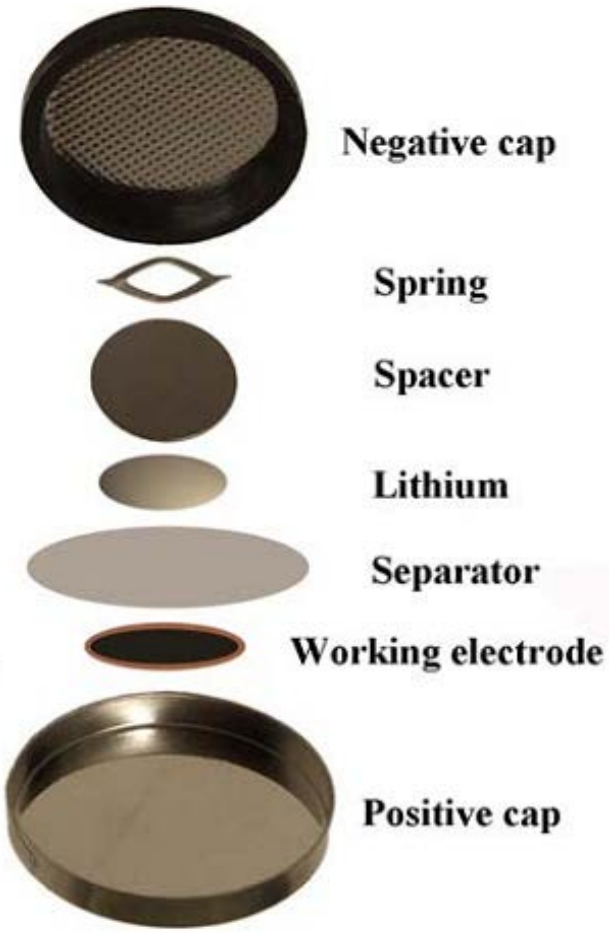

Figure 3.2 Stacking components of a CR2032 coin cell [179].

3.5.3. Electrochemical characterization

The electrochemical characterization techniques that have been used to characterize the performance of the electrodes in lithium/sulfur batteries are cyclic voltammetry (CV), galvanostatic charge-discharge measurements, and electrochemical impedance spectroscopy (EIS).

3.5.3.1. Cyclic voltammetry

Cyclic voltammetry (CV) is widely used to study a variety of redox processes and for determining the stability of reaction products and the presence of intermediates in oxidation-reduction reactions in a coin cell, which are marked by pairs of peaks that are observed in both anodic and cathodic curves when a redox reaction occurs. CV is conducted by recording the response current when cycling the potential of a working electrode at a specified scan rate. In this doctoral work, the CV data were acquired on a Biologic VMP-3 electrochemical workstation in UOW.

3.5.3.2. Galvanostatic charge-discharge

The cycling performance, the rate capability, and the charge-discharge profile of the materials were investigated by galvanostatic charge-discharge tests, in which the cell is charged and discharged within a certain cut-off voltage range at a constant current. In this thesis, the 2032 coin cells were galvanostatically charged and discharged using an automatic Land®battery tester system in UOW.

3.5.3.3. Electrochemical impedance spectroscopy

Electrochemical Impedance Spectroscopy (EIS) is applied to test the internal resistance, which includes the electrolyte resistance, the charge transfer resistance, and the interfacial resistance of a coin cell. In the impedance spectrum, the high-frequency semicircle is related to the kinetic processes, which indicate the charge transfer resistance and the double layer

capacitance; the low-frequency linear tail reflects the solid-state diffusion of lithium ions into the bulk of the active materials. In this thesis, EIS data were collected on a Biologic VMP-3 electrochemical workstation in UOW.

Chapter 4. A Systematic Approach to High and Stable Discharge Capacity for Scaling Up the Lithium-Sulfur Battery

4.1. Introduction

With the advancement of portable electronics devices, electric cars, and hybrid electric vehicles, it is necessary to endow their energy storage devices with higher energy densities. Commercially available lithium-ion batteries exhibit specific energy of approximately 400 Wh/kg, which is inadequate for current needs [3]. Sulfur, which exhibits 2600 Wh/kg specific energy, could be a better option in terms of availability, cost, and performance, if it is possible to achieve high discharge capacity by reducing capacity fading and minimizing the insulating behavior. The latter problem can be minimized by using different types, shapes, and properties of conductive materials, specifically carbon-based materials [164]. Improving the discharge capacity, however, to near to the theoretical level and minimizing the capacity fading phenomenon are the burning questions that need to be solved, which involve solving the problems of polysulfide dissolution and the shuttling effect of polysulfide [180]. Extensive research has been conducted on different techniques: loading the sulfur onto carbon materials [37, 48, 181-184], engineering the cathode surface [119, 185, 186], using different electrolytes and binders [187, 188], and applying different additives, specifically conductive polymers [110, 189], to minimize the problems.

Previously published works on sulfur-carbon cathode material, where the sulfur was loaded either by melt diffusion or wet chemical precipitation [141, 190-193], managed to achieve better specific capacity with allowable capacity fading, however, the synthesis methods that were adopted are complicated and laboratory oriented. To commercialize lithium sulfur batteries, it is important to develop a large-scale fabrication method for the production of S-C composites. Recently, Hui-Ming Cheng's group studied the large-scale fabrication of

graphene-sulfur composites [191, 194] to obtain a high-performance long-life Li-S battery. In their work, they produced a unique Sulfur-graphene sandwich structure and managed to achieve higher capacity retention. Their large-scale sulfur-graphene sandwich fabrication method is less facile and accessible, however, compared to the ball-milling method.

Ball milling is a simple, inexpensive, environmentally friendly, and industrially oriented method, which had been studied for mechanical mixing of materials for the Li-ion battery [195-198] since the beginning of the last decade. Moreover, this method is also extensively used in Li-ion battery research for manufacturing nanostructured materials [199], increasing reactivity [200], fabricating composites [201], and obviously improving rate capability and discharge capacity [202].It has never been optimized, however, in terms of processing parameters and carbon sources for the Li-S battery. Sulfur and sulfur-carbon composites that were synthesized by un-optimized ball-milling processes failed to achieve higher specific capacity (even though they were better than commercial sulfur) and better capacity retention than with other synthesis methods [16, 31, 32], which makes them of less interest to the researcher.

Changing the physical and morphological characteristics of S-C composite is not the only way to improve the performance of the Li-S battery. The construction of the cell and the method of charging also play a pivotal role in better performance. A new approach has been established to improve cycling performance by inserting a free-standing carbon interlayer between the cathode and the separator [35, 203, 204]. With this new approach, it was possible to obtain 1400 to 1500 mAh/g initial discharge capacity, which is the maximum initial capacity that has been reported in the literature. By using that carbon layer, it was also possible to control capacity fading behavior. Jeong et al. [204] used an acetylene black free-standing layer and claimed that this free-standing layer acts as a fishing net that can capture

polysulfide and inhibit the shuttle phenomenon. With the free-standing layer, they managed to reduce the capacity fading to 30-35% after 50 cycles.

On the other hand, very recently, Manthiram's group [34] achieved a breakthrough in the abatement of capacity fading by using a new charging method. With the help of that method, they managed to reduce capacity fading to as low as 1%. In their method, they charged the cell up to a certain capacity rather than using the conventional voltage window. They discovered that the first plateau of the discharge curve of sulfur, where the larger polysulfides (Li_2S_8, Li_2S_6) are formed, is responsible for the polysulfide dissolution and the shuttle phenomenon. So, they charged a Li-S cell up to a level such that the first plateau could not be formed and then allowed the cell to discharge. They found that the discharge capacity was almost equal to the charge capacity, which is definitely the maximum capacity retention for a Li-S battery ever recorded.

In this study, a systematic approach has been developed wherein a large-scale production method is used for the synthesis of S-C composite. In addition, a conductive single-walled carbon nanotube (SWCNT) free-standing layer with a refined, woven-like structure is inserted in between the cathode and the separator to improve the capacity and cyclability. This carbon layer was fabricated by ultrasonic dispersion followed by vacuum filtration [205]. Finally, the fixed capacity charging method was applied to improve the capacity retention.

4.2. Experimental

4.2.1. Synthesis of Carbon-Sulfur Composite: Commercial sulfur purchased from Sigma-Aldrich with 100 µm mesh size was used for ball milling in a planetary ball mill for different milling times (3, 6 and12 hours), at 100 rpm and with a 10:1 ball to sulfur weight ratio. Then, the ball-milled sulfur was morphologically, physically, and electrochemically characterized

by FESEM, the Brunauer-Emmett-Teller (BET) technique, and battery testing with a Land automatic battery tester to find the best dwell time. The optimum dwell time, along with the best rotational speed and sample-to-ball weight ratio from the literature, was used for finding the best carbon sources. Carbon black (CB), activated carbon (AC) and mesoporous carbon (MC) were ball milled with sulfur in a 30:70 weight ratio [206], and the resultant composites were denoted as carbon black–sulfur composite (CBS), activated carbon–sulfur composite (ACS), and mesoporous carbon–sulfur (MCS) composite.

4.2.2. Fabrication of SWCNT free-standing layer: 15 mg of SWCNT with 500 ml de-ionized water were poured into a beaker, and 500 mg of Triton-X100 surfactant was added. Then, the solution was probe sonicated for 1 hour with a 2 second pause time, followed by vacuum filtration and washing with de-ionized water and ethanol. The polytetrafluoroethylene (PTFE) filter paper with the SWCNT layer was dried under vacuum overnight at 60 ^{o}C, and finally, the SWCNT layer was easily peeled off from the filter paper [205]. Figure 4.1 shows the easy peeling of the FSL.

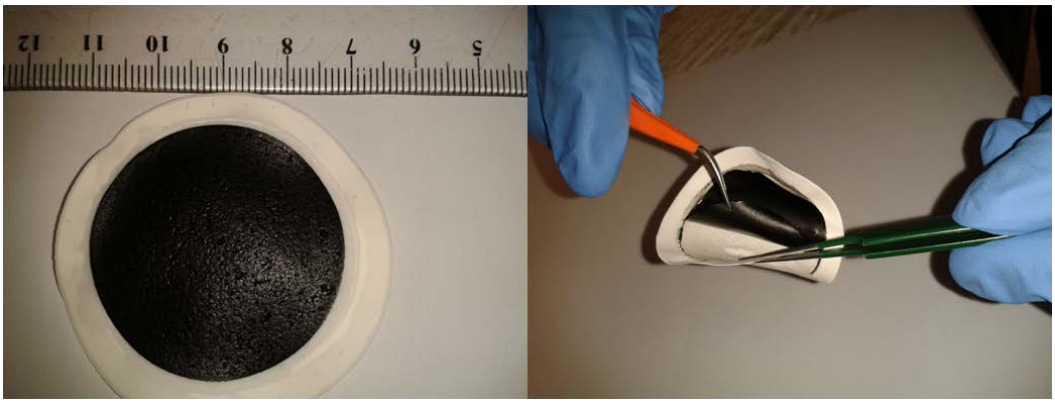

Figure 4.1 Easy peeling of FSL.

4.2.3. Fabrication of cells: For assembling the cells, we first prepared the cathode, which was based on carbon-sulfur composite, and the preparation method for all three carbon-sulfur composites was the same. The cathode was fabricated by using CBS/ACS/MCS, Super-P,

and PVDF in an 80:10:10 ratio, which means that the active materials in the cathode amount to 56 wt% (70% × 80%). This mixture was manually mixed for 10 minutes, followed by mixing in a Kurabo MAZERUSTAR planetary mixer KK-250S for 15 minutes with the addition of N-methyl-2-pyrrolidone (NMP). The obtained slurry was coated on Al foil, and the coated Al foil was dried at 50 °C for 24 hours under vacuum. Then, the electrode was cut into 9.5 mm diameter discs where each disc contains around 1 mg of sulfur and was pressed at about 2 MPa. The fabricated disc electrodes were dried again at 50 °C for a few hours before use. The CR 2032 coin-type cells were assembled in an Ar-filled glove box where discs of Li foil were used as counter electrode and reference electrode. The electrolyte was prepared by dissolving 1 M LiTFSI and 0.1 M $LiNO_3$ in the co-solvents 1,3-dioxolane (DOL) and 1,2-dimethoxyethane (DME), with a volume ratio of 1:1.A porous polypropylene film was used as the separator. The sequence of electrodes, electrolyte, separator, and FSL is shown in Figure 4.2.

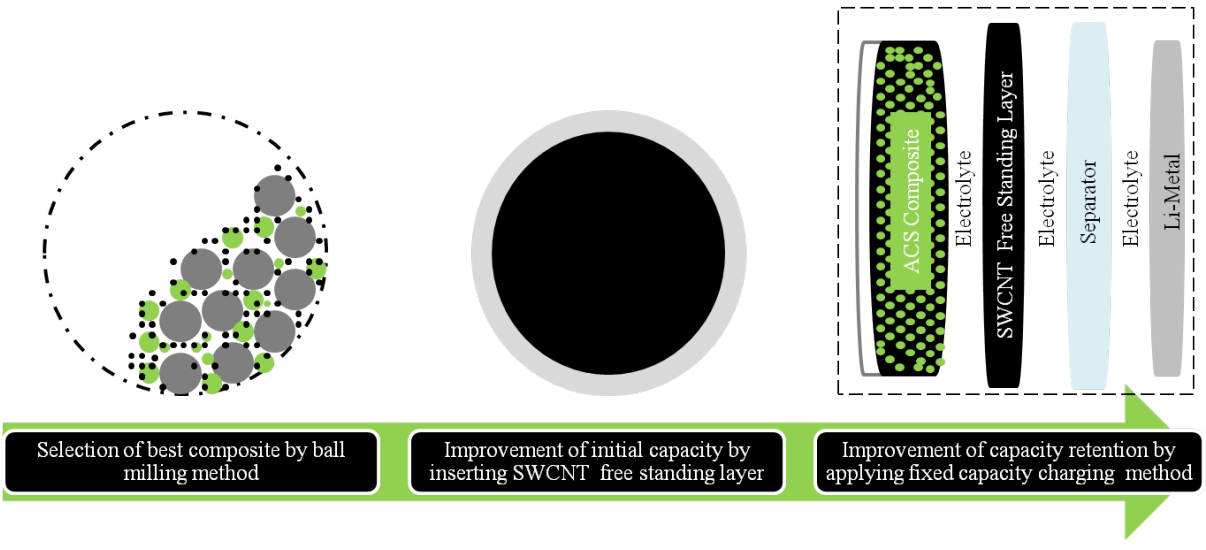

Figure 4.2 Systematic approach and structural sequence inside cell.

4.2.4 Characterization: To characterize the ball-milled sulfur, carbon-sulfur composites, SWCNT free-standing layer, and Li-S cells, different analytical tools were used. For physical

and morphological characterization of the ball-milled sulfur and carbon-sulfur composites, field emission scanning electron microscopy (SEM; JEOL FESEM-7500) and the 15 point N_2 absorption Brunauer-Emmett-Teller (BET) method on a Quanta Chrome Nova 1000 were used. For electrochemical performance evaluation of Li-S cells, an automatic battery tester system (Land®, China) was used at various current densities in the range of 1.5–3 V at room temperature.

4.3. Results and discussion

For the exploration of optimum processing parameters, such as the ball-to-sample weight ratio, the speed (rpm), and the dwell time in the ball-milling process is the first step in this systematic approach. These ball-milling parameters mainly depend on the physical properties of the pure sulfur [207]. To discover the most suitable parameters, an extensive literature survey was conducted, but it failed to find any papers that describe the ball milling of pure sulfur except for Takacs [208]. Among these three parameters, the ball-to-sample weight ratio and speed that were used in our work are 10:1 and 100 rpm, respectively, which are frequently used as ball milling parameters for other materials [195, 197, 209]. To determine the appropriate dwell time, which is one of the most important parameters for ball milling, we set the other two parameters as stated above and changed the dwell time to 3-hours, 6-hours, and 12-hours. The ball-milled sulfur was characterized physically, morphologically, and electrochemically to determine the most suitable dwell time.

Table 4.1 Specific surface area (BET) against dwell time.

Dwell Time	Specific Surface Area(m^2/g)
0 hours (commercial)	0.2637
3hours	0.3190
6 hours	0.4346
12 hours	0.3202

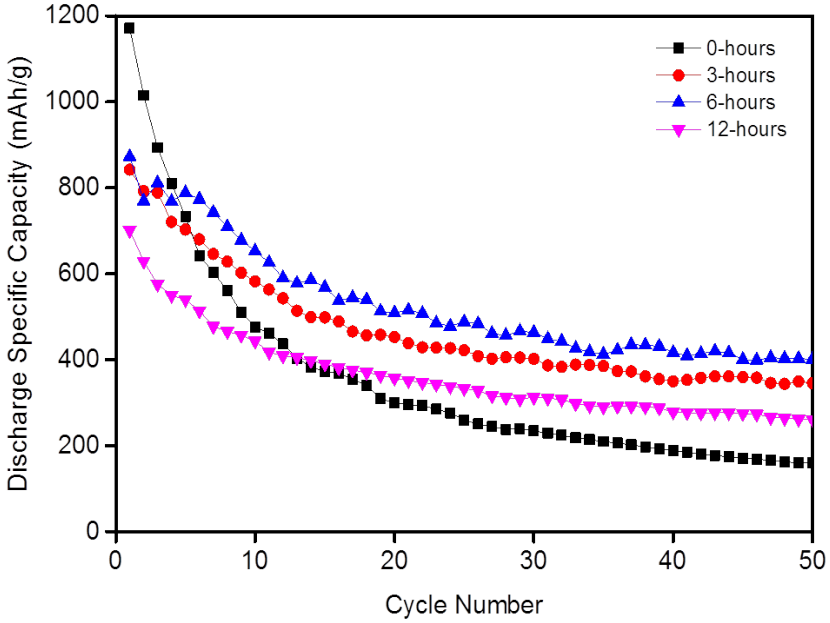

Figure 4. 3 Cycling performance of ball-milled sulfur electrode with different dwell times.

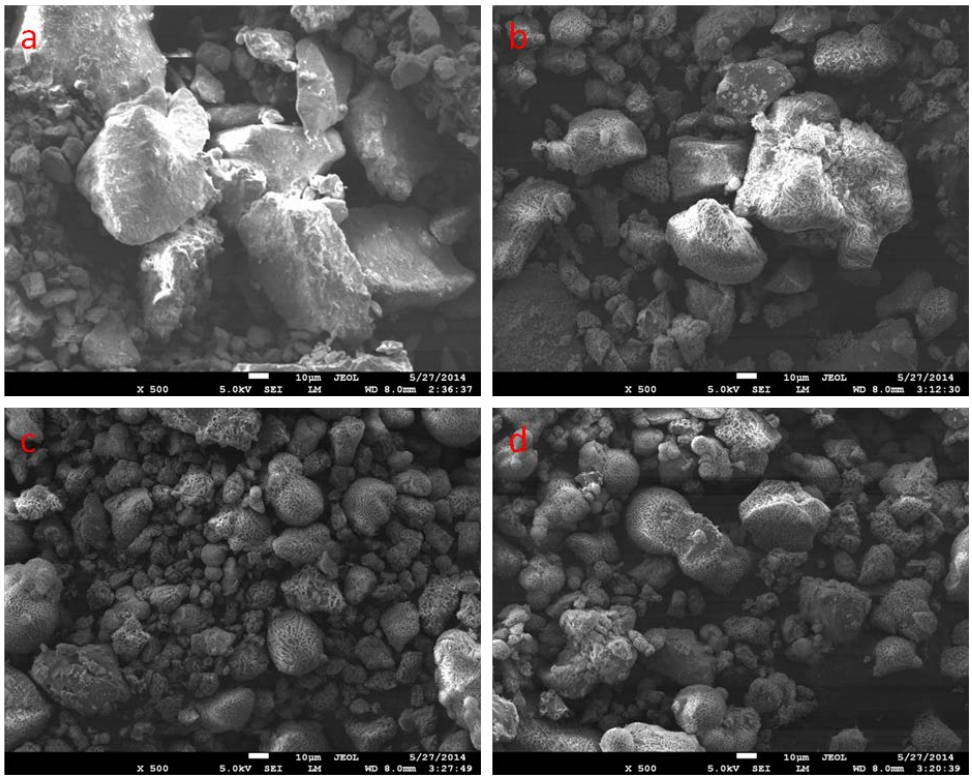

Figure 4.4 FESEM images of ball-milled sulfur after different dwell times: a) 0 hours, b) 3 hours, c) 6 hours, and d) 12 hours.

Figure 4.3 shows the cycling performance of sulfur electrodes with different dwell times, where the electrode with 6-hours dwell time exhibits discharge capacity of 401.2 mAh/g after fifty cycles, which is better than that of the other samples. Physical and morphological modification of sulfur due to different dwell time is the key factor for achieving better capacity. Figure 4.4 in the shows the morphological behavior of ball milled sulfur. Dwell time of 6 and 12 hours gives a smaller particle size and more porous structure than 0 hours (commercial sulfur) and 3 hours. Figure 4.4 also indicates that there is no significant difference between the results for dwell time of 6 and 12 hours except for slight agglomeration of the sulfur due to the higher dwell time. The morphological observations are also supported by Brunauer-Emmett-Teller (BET) testing, and the BET specific surface areas are presented in Table 4.1, where the dwell time of 6 hours gives the maximum specific surface area, followed by 12, 3 and 0 hours. It has been established that porous sulfur that shows higher specific surface area can confine carbon additives and inhibit shuttling behavior, resulting in better electrochemical performance [10]. From these results it can be deduced that 6-hours dwell time is the optimum parameter for the ball milling of sulfur, in combination with a 10:1 ball-to-sample weight ratio and 100 rpm speed.

Table 4.2 Specific surface areas (BET) of carbon-sulfur composites.

Sample Name	Denotation	Specific Surface Area (m^2/g)
Carbon Black–Sulfur Composite	CBS	16.05
Activated Carbon–Sulfur Composite	ACS	3.17
Mesoporous Carbon–Sulfur Composite	MCS	18.52

After obtaining the optimum parameters for the ball milling of sulfur, our next step was to find the best carbon source among carbon black (CB), activated carbon (AC), and mesoporous carbon (MC) to manufacture carbon-sulfur composite, which is frequently used with sulfur for Li-S battery. It should be mentioned that for manufacturing carbon-sulfur composites, we used the ball-milling method with the optimized parameters that we determined in the first part, and the resultant composites are denoted as CBS, ACS, and MCS, respectively, which are described in Table 4.2. All these three carbons have very high specific surface area (> 500 m^2/g), but when they are coupled with sulfur, their surface area drops significantly due to confinement of carbon in the sulfur pores. Table 1 shows the specific surface areas of the three composites and that among them, the activated carbon–sulfur composite has the lowest specific surface area, followed by CBS and MCS. The lower surface area of the composites is an indication of successful penetration of the carbon source into the sulfur pores.

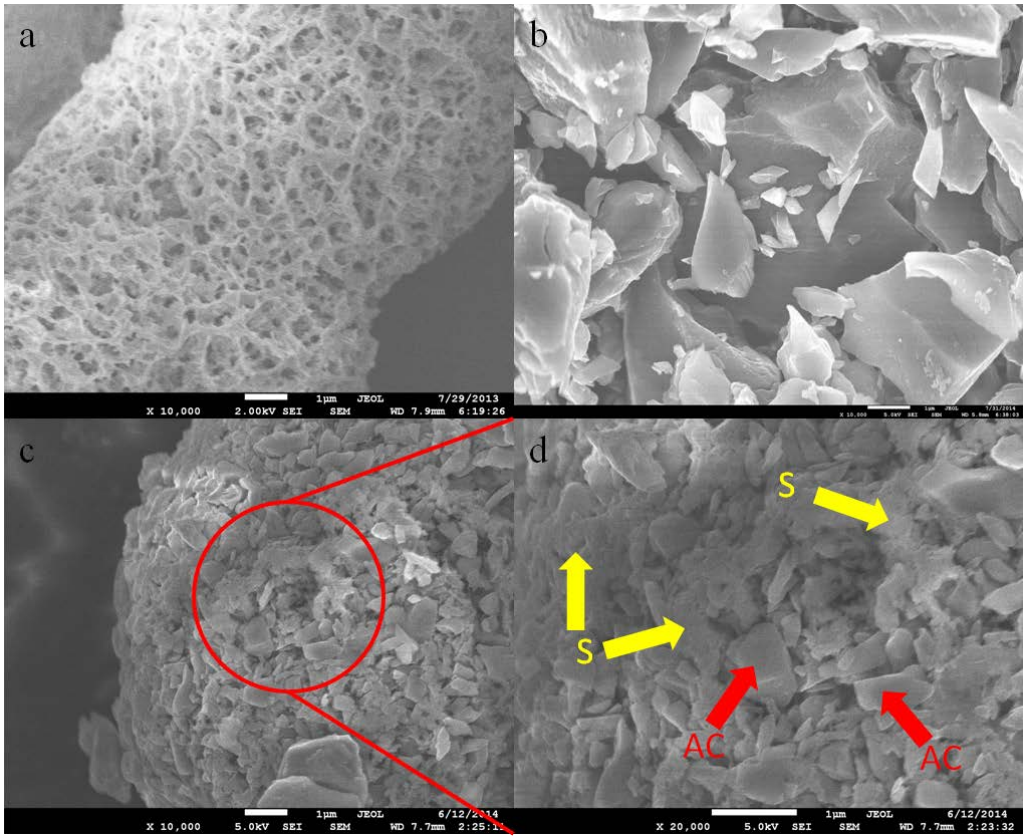

Figure 4.5 FESEM micrograph of a) pure sulfur (S), b) pure activated carbon (AC), c) & d) ball-milled ACS composite at different magnifications. The yellow arrows in (d) point the sulfur particles, and the red arrows point the activated carbon.

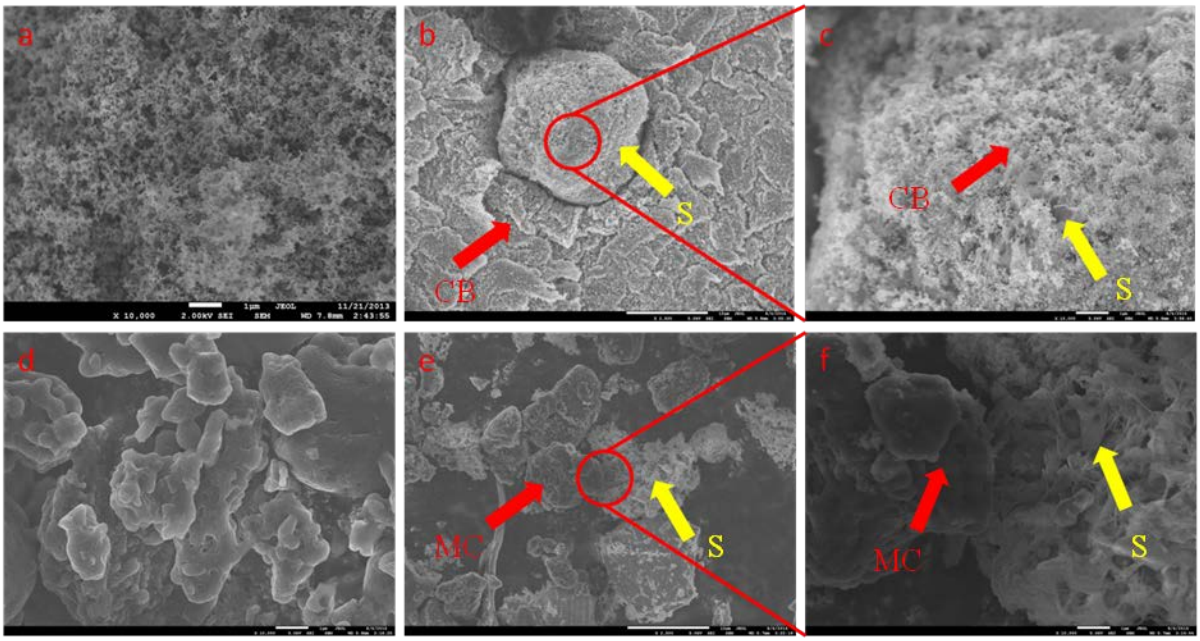

Figure 4.6 FESEM images of ball-milled carbon-sulfur composites: a) pure carbon black (CB), b) CBS (lower magnification), c) CBS (higher magnification), d) pure mesoporous carbon (MC), e) MCS (lower magnification) and f) MCS (higher magnification). The yellow arrows point the sulfur particles, and the red arrows point the carbon.

Figure 4.5 shows that submicron size AC flakes can easily penetrate the sulfur pores, and Figure 4.6 shows field emission SEM (FESEM) images of CBS and MCS composites where sulfur (yellow arrows) and carbons (red arrows) can easily be identified. MCS shows very low adhesion in between the carbon source and the sulfur, while on the other hand, CBS shows much better adhesion compared to MCS, but penetration of the carbon source into the sulfur pores is quite low. ACS, however, shows much more penetration of AC into the pores in the sulfur. From the FESEM image, we can infer that in ACS composite, the carbon is more confined by the sulfur due to the arbitrary size and shape of its particles than in the CBS

and MCS composites. This result is also supported by the literature [164, 190], where it was reported that it is difficult to confine carbon black and mesoporous carbon in sulfur pores through a mechanical mixing process. To support the BET results and morphological analysis, and to find the best composite among these three, we conducted cycling performance and rate capability testing of these three composites, the results of which are shown in Figure 4.7.

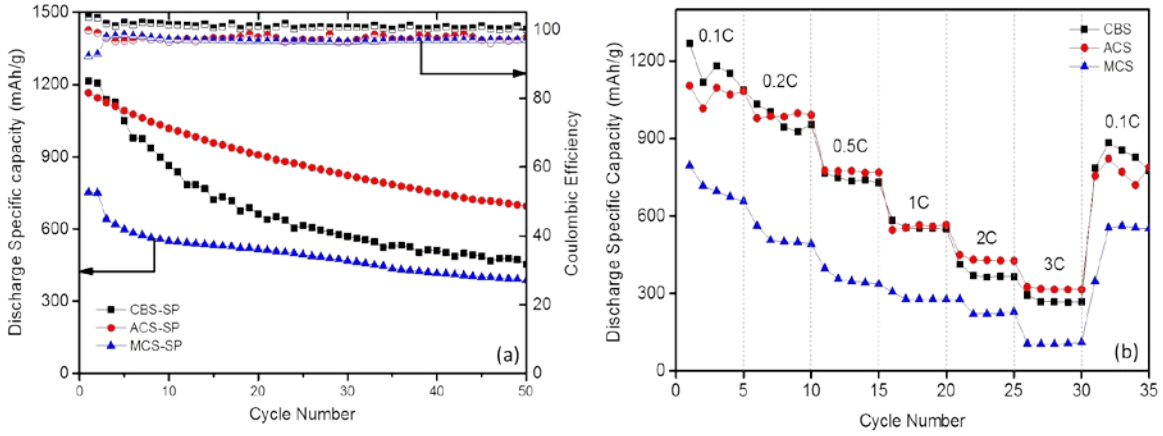

Figure 4.7 Cycling performance (left) and rate capability (right) of ball-milled carbon-sulfur composite.

The cycling results show that, the initial capacity of CBS is 1200 mAh/g, but it drops to 450 mAh/g after fifty cycles, which is about 34% of initial capacity. On the other hand, the initial capacity of ACS is 1172 mAh/g, and the capacity after fifty cycles is 698 mAh/g, which is about 60% of its initial capacity. Beside these two, MCS shows neither high initial capacity nor better capacity retention. The rate capability also indicates that CBS and ACS exhibit better performance at different current densities. It is notable that at higher current densities (2 C and 3 C), ACS shows much better capacity than CBS, which helped us to choose between these two composites for our next step. It can be inferred from the cycling performance that, the ACS composite is better than the other two in terms of capacity

retention and higher current rates. Furthermore, it should be mentioned that neither the ball-milled sulfur nor the carbon-sulfur composites show high discharge capacity and better capacity retention with respect to theoretical capacity. So, in the next phase, we will focus on the improvement of the capacity of ACS composite along with capacity retention.

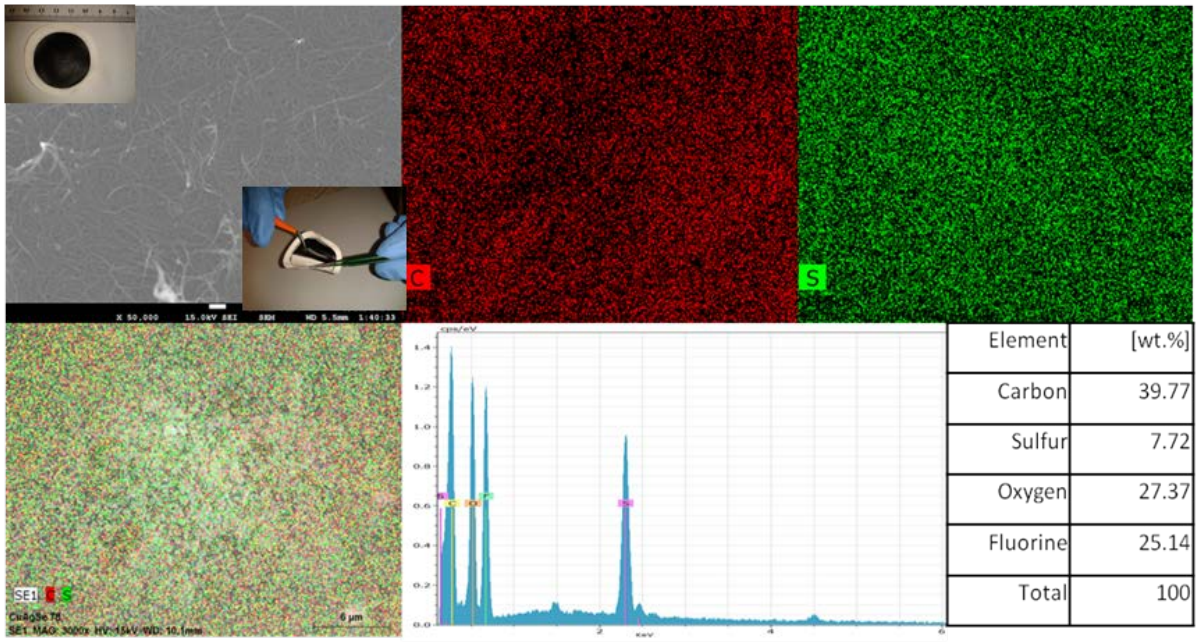

Figure 4.8 FESEM micrograph of SWCNT free standing layer before cycling(top left), with the insets showing photographs of the carbon interlayer, and energy dispersive spectroscopy (EDS) maps, spectrum, and elemental analysis of the carbon interlayer after cycling.

To improve the initial capacity of the composite (ACS), we inserted a SWCNT free-standing layer (FSL) in between the separator and the cathode, which was fabricated through a vacuum filtration process. This approach was first introduced by Manthiram's group [203] by using multi-walled carbon nanotube (MWCNT) as a free-standing layer. Later, Kim [204] used acetylene black mesh as a FSL to capture dissolved polysulfide. Both of them managed to increase the initial capacity up-to 1450 mAh/g, but failed to achieve the theoretical capacity. This sort of FSL acts as a filter paper to trap the dissolved long chain polysulfides, preventing them from reaching the anode, and successfully reduces the polysulfide shuttle

phenomenon. SWCNT, which has nanotubes with very small diameters (~10 nm), can form a woven-like structure that can act as a perfect filter paper for the filtration of polysulfide. Figure 4.8 shows the elemental mapping and quantitative analysis of the FSL after cycling, and it is clear that the sulfur is distributed homogeneously throughout the SWCNT free standing layer. Quantitative analysis shows that about 8% sulfur content is still present in the FSL after cycling, which is an indication of successful sequestering of longer chain polysulfide. There are two more peaks shown in the quantitative analysis, which belong to oxygen and fluorine. The fluorine comes from the polyvinylidene fluoride (PVDF) binder, and the oxygen comes from air.

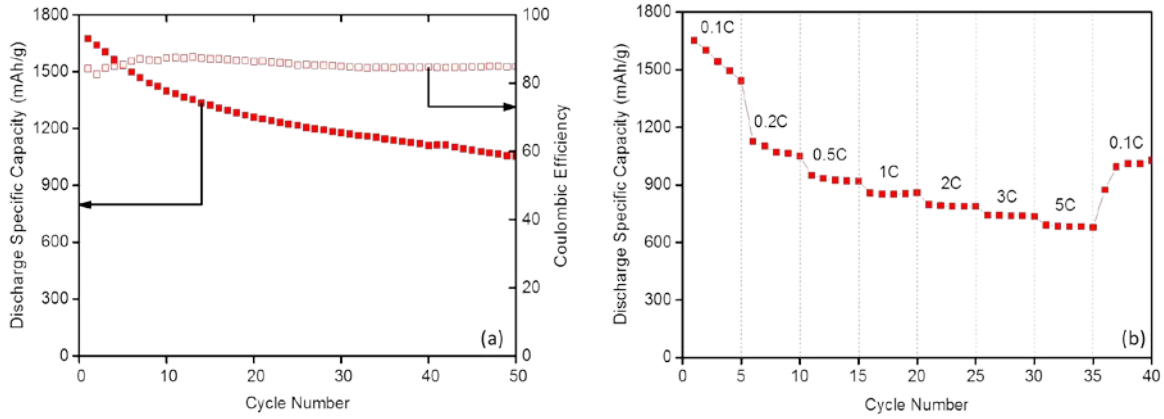

Figure 4.9 Cycling performance (left) and rate capability (right) of C-S composite with SWCNT free-standing layer.

To confirm the effects of the FSL, the cycling performance was examined with fixed and different current densities. Figure 4.9 (right) presents the discharge specific capacity of the sulfur composite with the FSL at different C-rates (1 C = 1675 mAh/g). By inserting the SWCNT FSL, we managed to achieve an initial capacity of 1674 mAh/g at 0.1 C, which is the maximum capacity that has ever been reported for Li-S battery, and 1052 mAh/g was retained after fifty cycles. However, the coulombic efficiency is considerably low which may occur due to unreacted polysulfides that pass through CNT layer and failed to oxidised

charging due to the prevention of CNT layer. The FSL can improve the capacity not only at lower current density, but also at higher current density. It should be noted that the decrease in capacity does not have a linear relationship with increasing current density. It can be observed (Fig. 4.9) that at 3 C and 5 C, 700-800 mAh/g capacity is achieved, which is about half of the initial capacity at 0.1C. From Figure 4.9, we can also observe that although very high initial capacity has been achieved, the capacity retention is about 63% after fifty cycles, which means that the polysulfide dissolution problem was reduced to a certain extent, but the problem failed to be eradicated by using the SWCNT layer, which is a big hurdle for commercialization.

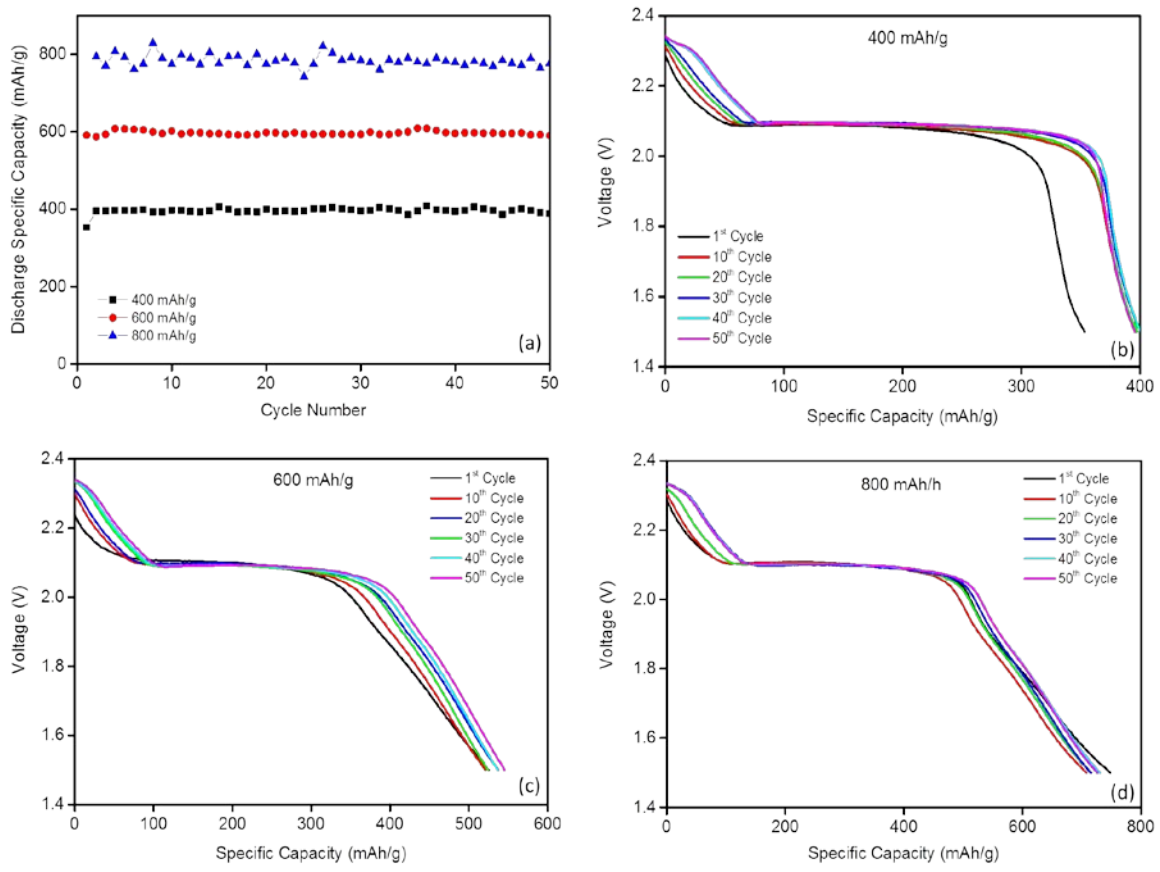

Figure 4.10 Fixed capacity cycling performance (top left) and voltage profiles for selected cycles of ACS with FSL at capacities limited to 400 mAh/g (top right), 600 mAh/g (bottom left), and 800 mAh/g (bottom right).

To improve the capacity retention, the new charging method developed by Manthiram's group [34] was followed, where the cells were charged up-to a certain capacity rather than using the conventional voltage window. It should be noted that the purpose of the new charging method is to prevent the formation of longer chain polysulfides that can be dissolved in the electrolyte and are responsible for the shuttle phenomenon. The longer chain polysulfides appear at the first plateau of the discharge curve, and to avoid that plateau, we must charge only up to a certain level where the first plateau cannot be formed. Manthiram's group found that the theoretical capacity of the 1^{st} and 2^{nd} plateau is 419 mAh/g and 1256 mAh/g, respectively. So, to get a stable capacity, it is necessary to charge the Li-S cell to lower than 1256 mAh/g, and for this purpose, we charged our cells at three different capacities (400, 600, and 800 mAh/g), which are lower than 1256 mAh/g, with 0.1 C current density and allowed them to discharge to observe the capacity retention. Figure 4.10 (top left) shows the cycling performance and voltage change with increasing cycle number. It is clearly demonstrated that the capacity retention is independent of the charge capacity, so long as it is under 1256 mAh/g, for ACS composite with FSL, and in this case, the retention is almost 99% after fifty cycles for the three different charge capacities that were used. The change in voltage with cycle number is also significantly low, which indicates a very stable cycling performance. It should be noted that the deterioration of specific capacity is usually very intense for the first 20 or 50 cycles for any cells. If the capacity retention is not significantly reduced within this period, the cell is going to show higher capacity retention as cycling continues.

It can be concluded from the above discussion that the insertion of a SWCNT free-standing layer combined with the new charging technique can significantly improve the performance of the Li-S battery. Using the free-standing layer, however, will make the manufacturing process complicated and add to the cost. Therefore, we have tried to explore whether there is

any possibility of only using the new charging technique to improve the capacity and cycling stability of commercial sulfur and ball-milled carbon-sulfur composite. Hence, we applied the new charging method to commercial sulfur and ball-milled carbon-sulfur composite; although unfortunately, the commercial sulfur failed to retain capacity, even at very low (~400 mAh/g) charge capacity. The voltage was varied frequently and eventually raised to over 3 V, where the capacity faded after a few cycles. The low capacity of the second plateau and the low initial discharge capacity are responsible for this. The ball-milled carbon-sulfur composite, however, showed quite stable discharge capacity at low (~500 mAh/g) charge capacity, but it was unstable at higher charge capacity compare to free standing layer contained ACS composite.

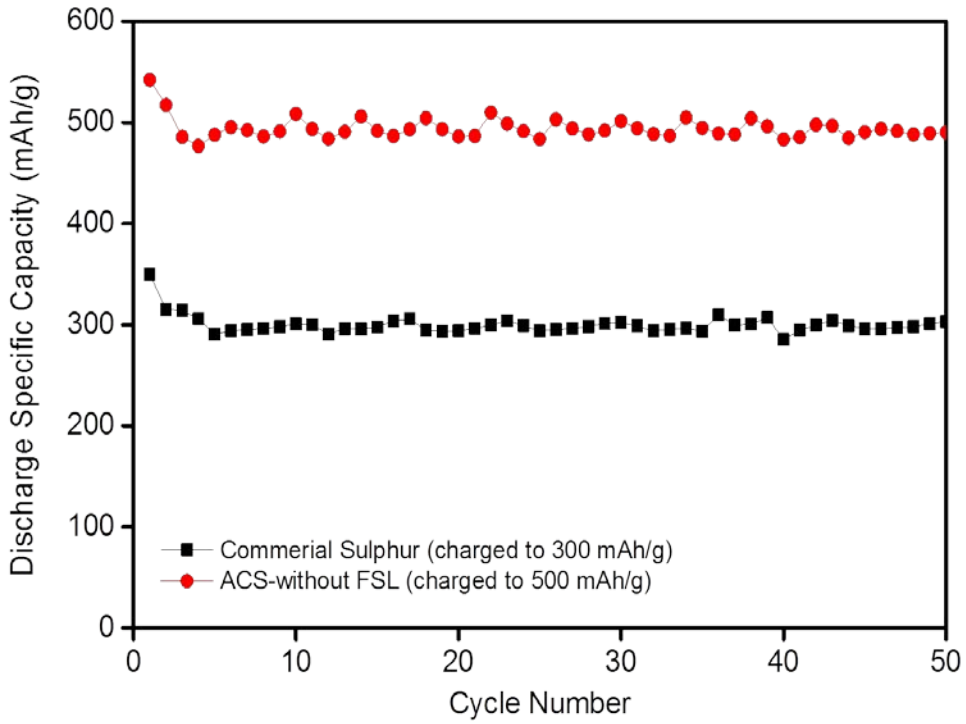

Figure 4.11 Cycling performances of commercial sulfur and ACS with fixed charge capacity.

Figure 4.11 shows the cycling performance of both commercial sulfur and ball-milled ACS composite with the fixed charging method, where the commercial sulfur and ACS composite

show stable discharge capacity when charged to 300 mAh/g and 500 mAh/g, respectively. This result also confirms that the formation of porous sulfur via ball milling has a significant impact on the electrochemical properties. It can be inferred from the above discussion that the SWCNT free-standing layer helps to raise the initial capacity and to enlarge the second plateau to achieve better capacity retention at higher charge capacity.

4.4. Conclusion

It can be concluded that a systematic way of fabricating Li-S batteries that is suitable for large-scale production has been demonstrated by applying a series of facile methods (Figure 4.2). The fabrication of porous sulfur was achieved by the industrially-oriented ball-milling method, followed by identification of better carbon sources for that porous sulfur, by observing their physical, morphological, and electrochemical behavior. After that, the SWCNT free-standing layer was inserted to raise the discharge capacity of the best composite-the activated carbon–sulfur composite. By inserting the SWCNT free-standing layer, the initial capacity is raised to 1674 mAh/g, which is the maximum initial capacity recorded in the literature at this time. Finally, to retain the capacity for a higher number of cycles, a new charging method was applied, which helped to retain the capacity at about 99%. We believe that this method will help to make the Li-S battery commercially viable in the near future, representing a major advance for energy storage device.

Chapter 5. A Facile Synthesis of High Surface Area Sulfur-Carbon Composite for Li/S Batteries

5.1. Introduction

The demand for high energy batteries has been increasing rapidly due to the emergence of new portable electronic devices, and of hybrid and electric vehicles into our daily lives. Moreover, storing energy when it is abundant and available also requires high energy batteries. Conventional metal oxide batteries which have been in use since 1991 and show specific energy of 400 $Whkg^{-1}$are unable to meet the current requirements [3]. To solve this problem, researchers have concentrated on different cathode materials that have high theoretical capacity, such as sulfur [54].

Sulfur, which is cheap, easily available, and non-toxic, exhibits 2600 $Whkg^{-1}$ specific energy, so that it could be a better alternative to the existing cathode materials. The poor electrical conductivity of sulfur, however, the dissolution of long chain polysulfides into electrolyte, and the changes in volume during the sulfur to sulfides transformation are obstructing its progress [164]. Extensive research has been conducted to reduce the impact of these problems by applying different techniques to load sulfur onto carbon materials [37, 48, 181-184]. Engineered sulfur-based cathode materials [119, 185, 186, 210], as well as different electrolytes, binders [187, 188], and additives [60, 108, 110, 189, 211], are also being meticulously studied to solve these problems. Researchers have found that, by improving the conductivity of sulfur and the surface area of S-C composite, it is possible to ameliorate the problems and to achieve better capacity. In most of the published works on sulfur-carbon cathode materials, the sulfur was loaded either by melt-diffusion [37, 164, 212, 213] or by a wet chemical process [141, 190-193]. Using a chemical process to load sulfur into a carbon matrix for fabrication of S-C composite is the predominant method to fabricate small-size and

arbitrary-shaped sulfur particles. Recently, several groups have focused on the fabrication of very fine sulfur particles with high surface area for the Li-S battery to achieve better electrochemical performance [214-217]. In their methods, they used different surfactants,such as Triton-X100, cetyltrimethyl ammonium bromide (CTAB), and sodium dodecyl benzene sulfonate (SDBS), for the refinement of sulfur. Surfactants, which are usually organic compounds and amphiphilic in nature, are used to reduce the interfacial tension for the dispersion of a compound in a solution [216]. These high molecular weight surfactants are expensive and environmentally hazardous. Moreover, removing the surfactant from the synthesized product is time-consuming and tiresome work. In most cases, the synthesized product needs to be rinsed several times in distilled water to remove the surfactant. During rinsing, the synthesized product sometimes is washed out and may give an unwanted and inaccurate sulfur-carbon ratio.

In order to avoid using surfactant, controlling the physicochemical properties of the reactants, such as their concentrations, the temperature, the presence of catalyst, the rate of stirring, and the particle size, plays a significant role in the fabrication of high-surface-area materials via chemical precipitation [218, 219]. In our study, we reduced the size of the droplets of one of the reactants (thiosulfate) by using a nozzle. The nozzle can spray very fine droplets, and these were sprayed over another reactant (oxalic acid) and produced a high-surface-area product. This method, involving manipulation of the reactant droplet size by using a nozzle and the fabrication of high-surface-area arbitrary-shaped product, is herein denoted as the spray precipitation method. This spray precipitation method is a modified chemical process method, and a simple, single-step, and industry-oriented method. In this method, thiosulfate solution is sprayed onto a carbon-black-containing acid solution with a nozzle, and the high surface area sulfur particles are precipitated throughout the carbon black solution. The possible reaction mechanism can be explained as follows: the atomized thiosulfate creates

numerous nucleation sites where the surrounding nuclei, along with the carbon, inhibit the growth process of the sulfur and help to produce submicron-sized elemental sulfur particles with higher surface area compared to conventional methods. Moreover, the higher number of nucleation sites helps to achieve a homogeneous distribution of sulfur particles with better adhesion to the carbon black, which helps to increase the conductivity of the sulfur and results in higher utilization of the active material [220]. It is expected that the newly developed high-surface-area spray-precipitated carbon-sulfur composite will show superior electrochemical performance.

Development of new electrode materials by changing their physical and morphological characteristics is not the only way to improve their performance. The construction of the cell and the method of charging also play a pivotal role in better performance. Few new approaches have been established to improve cycling performance. Among them, insertion of a free-standing carbon interlayer between the cathode and the separator [35, 203, 204], and applying fixed capacity charging [34, 162] are very recent and significant inventions to achieve higher and more stable discharge capacity. According to the fixed capacity charging method, the cell has to be charged upto a certain capacity rather than within a fixed voltage window. (For the Li-S battery, the conventional voltage window is 1.5-3V.) It has been found that the longer chain polysulfides (Li_2S_8, Li_2S_6) which are formed in the first plateau of the discharge curve are responsible for capacity fading, and by preventing the formation of longer chain polysulfides, it is possible to achieve better cycling performance [175].

In this work we have tried to synthesize carbon-sulfur composite by using a modified chemical process denoted as spray precipitation, which can be considered as an industry-oriented, facile method to produce high-surface-area sulfur particles and to obtain a homogeneous dispersion of sulfur in carbon black. In this chemical process, sodium

thiosulfate solution was sprayed into an oxalic acid – carbon black (CB) solution to achieve precipitation of sulfur in the carbon black solution. It is expected that spray-precipitated carbon-sulfur composite will show better discharge capacity and capacity retention compared to the products of the conventional method, in which a pipette is used to drop thiosulfate solution onto acid solution. This conventional method is designated as the drop precipitation method.

5.2. Experimental

5.2.1. Synthesis of Carbon-Sulfur (S-C) Composite: All the chemicals were bought from Sigma-Aldrich and used with no further modification. In a beaker, 300ml of 0.5M sodium thiosulphate ($Na_2S_2O_3$) solution was prepared, and in an another beaker, 300ml of 1M oxalic acid ($H_2C_2O_4$) solution was also prepared. 2.0571 g carbon black was added into the oxalic acid solution. The amount of carbon black was calculated in such a way that the ratio of sulfur to carbon black was 70:30. After that, the $Na_2S_2O_3$ solution was sprayed into the oxalic acid, which was stirred at 360 rpm to homogenize the sulfur precipitation. The precipitated solution was washed with de-ionized water and ethanol, followed by vacuum drying at 50 °C for 24 hours. A similar procedure was applied for the fabrication of drop-precipitated S-C composite. The only exception is that the $Na_2S_2O_3$ solution was dropped into the oxalic acid by using a dropper rather than by spraying. After that, a similar washing and drying procedure was followed. The chemical reaction for sulfur precipitation is: $Na_2S_2O_3 + H_2C_2O_4 \rightarrow Na_2C_2O_4 + S\downarrow + SO_2\uparrow + H_2O$.

5.2.2. Fabrication of SWCNT Free-Standing Layer: 25 mg SWCNT was added into 50 ml de-ionized water (DI-water) in a beaker. 500.25 mg Triton X-100 surfactant, which was 1wt% of total weight (~50.25 mg; 1ml of water = 1g) was added into the mixture. The mixture was then probe-sonicated for two hours with a two second pulse and work time.

During sonication, the temperature of the mixture was kept at less than 5 °C by putting the beaker into an ice bath. After sonication, the mixture underwent vacuum filtration onto a polytetrafluoroethylene (PTFE) filter paper. After filtration, the filter paper was washed with DI-water and ethanol several times. Then, the filter paper was dried at 60 °C for 12 hours. The fabrication process for the SWCNT free-standing layer is shown in Figure 5.1. After drying, the SWCNT carbon layer was easily peeled off and cut into 10 mm diameter discs, which were used as the free-standing layers.

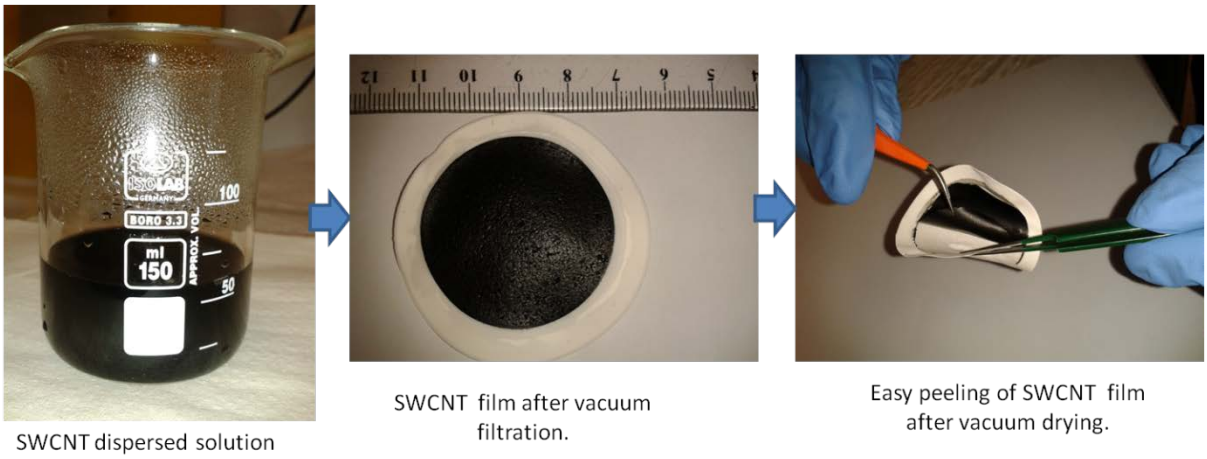

Figure 5.1 Fabrication of SWCNT free-standing layer.

5.2.3. Fabrication of cells: For assembling the cells, we first prepared the cathode, which was based on spray-precipitated carbon-sulfur composite. The cathode was fabricated by using the carbon black (CB) – sulfur precipitated composite, Super-P, and polyvinylidene difluoride (PVDF). The PVDF was added to the amount of 10 wt%, and the amount of Super-P was dependent on the amount of sulfur, which was maintained at 50% of the total amount. It should be noted that according to the synthesis technique, the amount of active material (sulfur) should be 70 wt% in carbon-sulfur composite, however, from TGA analysis, the sulfur content was found to be 64.5 wt%. The S-C composite, Super-P, and PVDF mixture was manually mixed for 10 minutes, followed by processing in a Kurabo MAZERUSTAR

planetary mixer, model KK-250S, for 15 min with the addition of an appropriate amount of N-methyl-2-pyrrolidone (NMP). The obtained slurry was coated on Al foil to a thickness of 100 microns, and was then dried at 50 °C for 24 hours under vacuum. Then, the electrode was cut into 10 mm diameter discs and pressed at about 2 MPa. Each 10 mm disc contained around 1 mg of active materials (sulfur).The fabricated disc electrodes were dried again at 50 °C for a few hours before use. The CR 2032 coin-type cells were assembled in an Ar-filled glove box, where discs of Li foil were used as the counter electrode and reference electrode. The electrolyte was prepared by dissolving 1 M lithium bis(trifluoromethane sulfonyl)imide (LiTFSI) and 0.1M $LiNO_3$ in co-solvents of 1,3-dioxolane (DOL) and 1,2-dimethoxyethane (DME), with a volume ratio of 1:1. A porous polypropylene film was used as the separator. The sequence of anode, separator, free-standing layer, and cathode is shown in Figure 5.2.

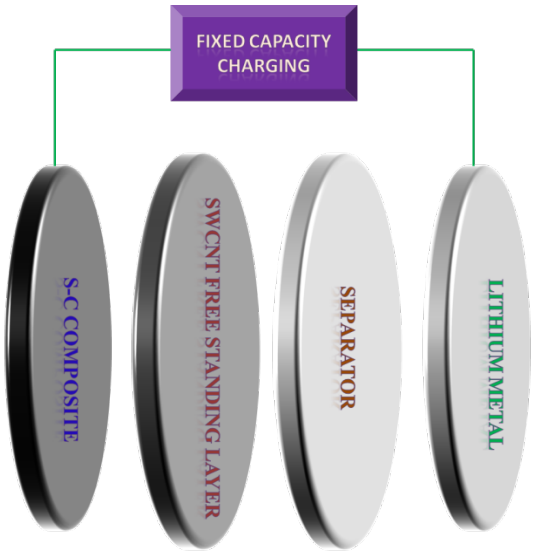

Figure 5.2 Assembly of cell.

5.2.4. Characterization: To characterize the spray-precipitated C-S composite and Li-S cells, different analytical tools were used. For physical and morphological characterization of spray precipitated C-S composite, X-ray diffraction (XRD, GBC MMA 017), Raman spectroscopy (JOBIN YVON HR800 Confocal Raman system with 632.8 nm diode laser

excitation on a 300 lines/mm grating at room temperature), field emission scanning electron microscopy (SEM; JEOL: FESEM-7500), and the 15 point N_2 absorption Brunauer-Emmett-Teller (BET) method conducted on a Quanta Chrome Nova 1000 were used. Moreover, a JEOL JEM-ARM200F 200 kV transmission electron microscope was used for scanning transmission imaging and for conducting large-area EDS mapping. For electrochemical performance evaluation of the Li-S cell, an automatic battery tester system (Land®, China) at various current densities at room temperature was used. Electrochemical impedance spectroscopy (EIS) and cyclic voltammetry (CV) measurements were performed on a Biologic VMP 3 electrochemical workstation over a frequency range of 10 mHz to 100 kHz, and the scan rate was 0.1mV/s within a 1.5V to 3V voltage window.

5.3. Results and discussion

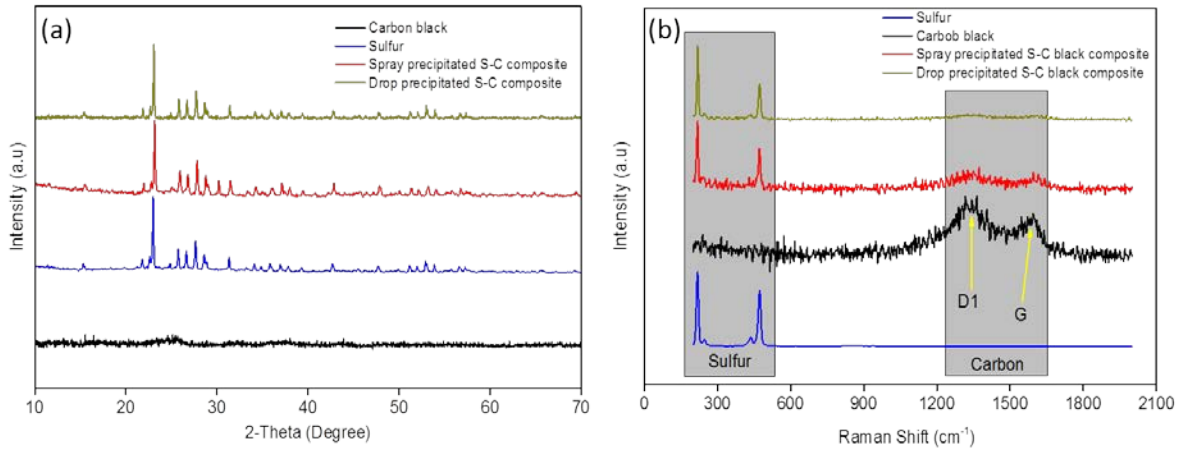

Figure 5.3 (a) XRD patterns and (b) Raman spectra of spray- and drop-precipitated sulfur.

X-ray diffraction (XRD) patterns of drop- and spray-precipitated sulfur, along with pure sulfur and carbon black, are shown in Figure 5.3a. Both drop- and spray-precipitated sulfur exhibit a sharp peak around 23.1°, which is a characteristic peak of crystalline octa-sulfur (S_8) that is diffracted from the (222) plane. The crystallite sizes of both the composites were also determined from that characteristic peak by using the Scherrer equation and are shown in Table 5.1 (The size factor (*K*) that was used for calculating the crystallite size is 0.89). As

expected, the spray-precipitated composite shows smaller crystallite size than the drop-precipitated composite. On the other hand, the Raman spectra (Fig. 5.3b) also show similar patterns for both the drop-precipitated and the spray-precipitated sulfur, in that both of them show sharp peaks at 219.1 cm^{-1} and 473.2 cm^{-1}, which reflect the bending and the stretching of S-S bonds, respectively [221]. Moreover, the drop-precipitated and spray-precipitated S-C composites show small peaks around 1400 cm^{-1} and 1600 cm^{-1}, which are the characteristic peaks for carbon. These two peaks are well-known as the D1-band and the G-band, respectively [222]. In the drop-precipitated S-C composite, the D1 and G bands are relatively less intense compared to spray-precipitated S-C composite, which is an indication of better confinement of sulfur in the carbon black for the spray-precipitated S-C composite.

Table 5.1 Determination of crystallite size using Scherrer equation.

Samples	**Peak position (2θ, °)**	**FWHM (°)**	**Calculated crystallite size (nm)** $\tau = \frac{K\lambda}{\beta \cos\theta}$
Commercial Sulfur	23.10	0.14	-
Drop-precipitated S-C composite		0.17	267.25
Spray-precipitated S-C composite		0.20	133.66

Fabrication of precipitated sulfur from thiosulfate is a very old and conventional technique, where thiosulfate and acid are mixed together and elemental sulfur comes out as a precipitate. To accelerate the reaction rate and to refine the grain size, however, it is necessary to have multiple nucleation sites, which can be achieved by spraying the thiosulfate into the acid. Using organic acid (e.g. oxalic acid) has an additional advantage, however, which is that it can achieve higher surface area [220]. Moreover, it is found that the sodium oxalate salt, which forms as a by-product of the sodium thiosulfate and oxalic acid reaction, has a significant effect on the architecture and particle size of the precipitated sulfur [220]. The

fabrication of sulfur and sulfur-carbon composite by the drop precipitation method and the spray precipitation method are illustrated in Figure 5.4. The mechanism for the manipulation of the particle size and adhesion between the precipitated sulfur and the carbon are also depicted in the illustrations, which are confirmed by the field emission scanning electron microscope (FESEM) micrographs. The micrographs show that the morphology of the drop-precipitated sulfur (Fig. 5.4a) and its composite (Fig. 5.4b) features a minimum number of nucleation sites and larger droplets, resulting in very large sulfur particles with uniform rectangular shapes compared to the spray-precipitated sulfur and its composite, where abundant nucleation sites with very fine droplets of reactant help to form finer and more arbitrary-shaped sulfur particles [220].Therefore, using the spray method can produce fine and arbitrary-shaped sulfur particles.

Figure 5.4a also shows that the drop-precipitated sulfur particles are not fully covered and adhered to by their respective carbon black particles due to their larger shape and size. The large and uniform-shaped drop-precipitated sulfur particles show lower surface area, which has an adverse effect on adhesion between the carbon black and the sulfur. Moreover, it is difficult to cover larger size sulfur particles with a small amount of smaller size carbon black. On the contrary, the spray-precipitated sulfur (Fig. 5.4c) and its respective composite (Fig. 5.4d) show the formation of fine and arbitrary-shaped sulfur particles. These sulfur particles are fully covered and adhered to by carbon black due to their favorable size, shapes, and surface area, which can only be formed by using the spray-precipitation method [219]. This is because in the spray method, very fine droplets of sodium thiosulfate are sprayed onto an oxalic acid solution, which creates multiple nucleation sites, and these impede each other during the growth process. Due to the impeded growth process, the shapes of the precipitated sulfur become asymmetric and arbitrary. Moreover, in the presence of carbon, the growth process is further impeded, resulting in the formation of very fine, high-surface-area, and

arbitrary-shaped grains which are firmly adhered to by the carbon. On the contrary, the drop precipitation method results in a smaller number of sulfur nucleation sites, which have sufficient space for growth. Due to the favorable conditions for growth, drop-precipitated sulfur shows larger and more oval-shape grains, resulting in a low surface area.

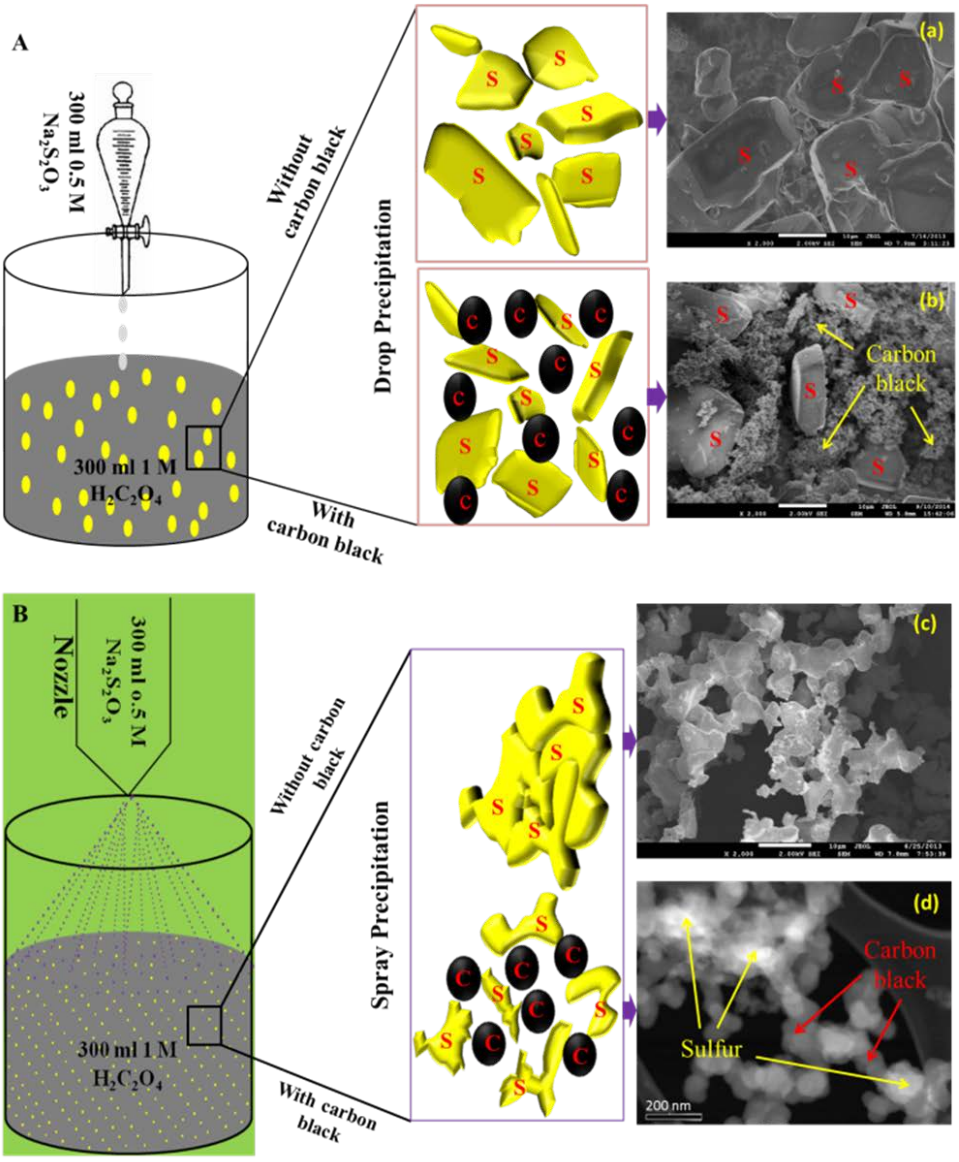

Figure 5.4 Schematic diagram showing the fabrication of (A) drop-precipitated material: FESEM image of (a) drop-precipitated sulfur and (b) drop-precipitated S-C composite; and (B) spray-precipitated material: (c) FESEM image of spray-precipitated sulfur and (d) HAADF image of spray-precipitated S-C composite.

High-angle annular dark field (HAADF) transmission electron microscope (TEM) images (Fig. 5.4d) also show the coexistence of sulfur and carbon black. The brighter spots which are created due to charging (because sulfur is electrically nonconductive) indicate sulfur, and the darker spots indicate carbon black, which is highly conductive. Both HAADF and secondary electron (SE) imaging, which are shown in Figure 5.5, confirm that the spray-precipitated sulfur particles are adhered to and confined by their respective carbon black particles, which will increase the conductivity of the sulfur along with active the material utilization during charge and discharge.

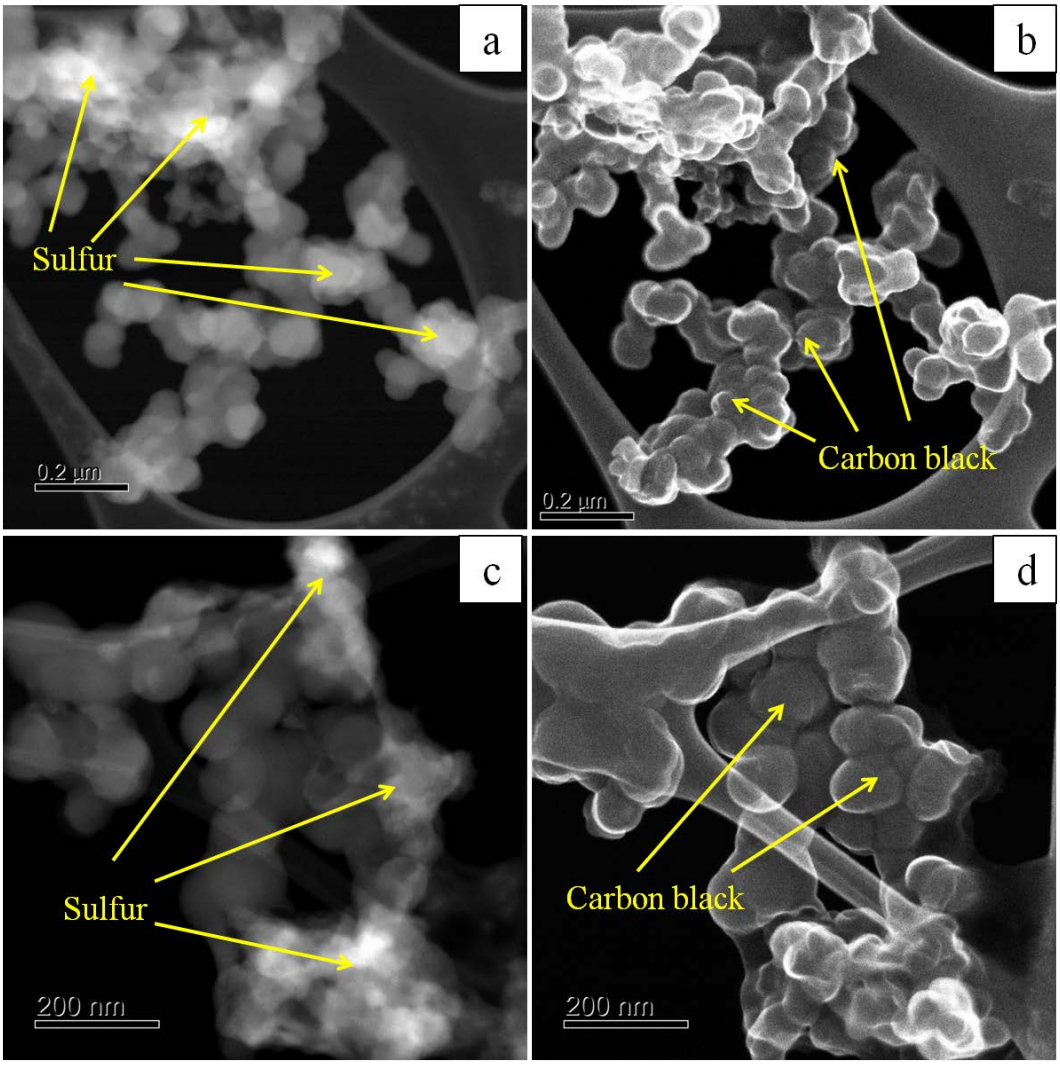

Figure 5.5 (a,c) HAADF images and (b,d) SE images of spray-precipitated S-C composite.

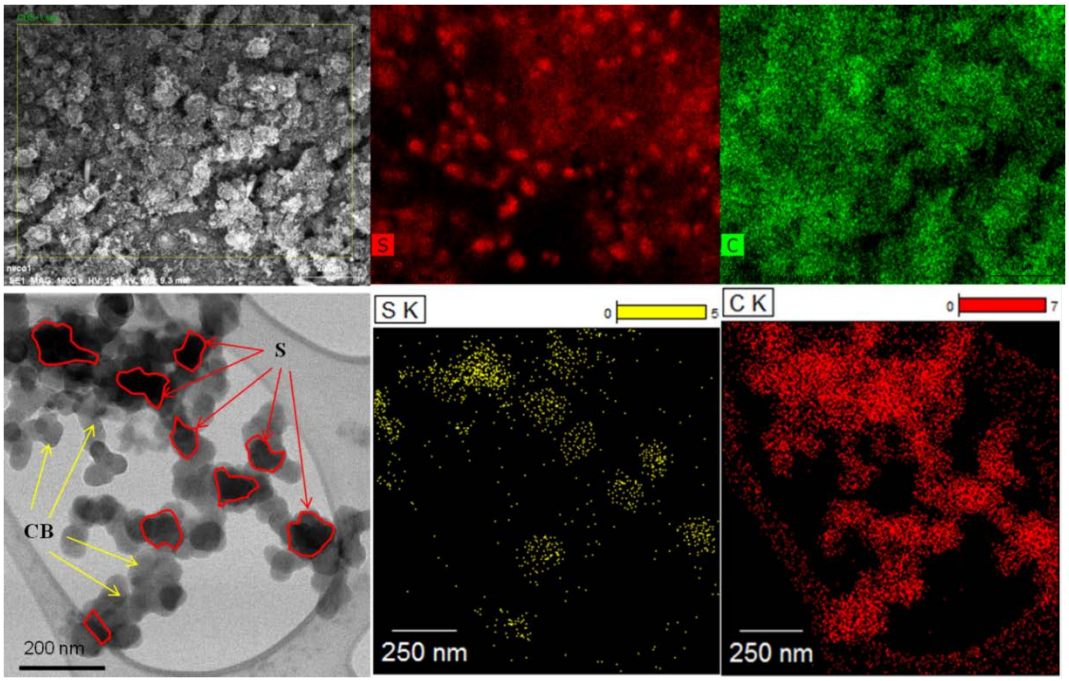

Figure 5.6 EDS analysis and TEM imaging of spray-precipitated S-C composite.

For further confirmation, energy dispersive X-ray spectroscopy (EDS) mapping from both FESEM and TEM was conducted, along with bright-field TEM analysis, and the results are shown in Figure 5.6. The top three images of Figure 5.6 show that the spray-precipitated sample entirely consists of loosely bound groups of sulfur particles which are covered with carbon black and form a core-shell structure. Transmission electron microscopy along with high resolution EDS analysis (in the bottom images) also shows that the arbitrary shaped and smaller size sulfur particles, as indicated by the outlines in the lower left TEM image, are well dispersed and embedded inside the carbon black as in a core-shell structure.

The Brunauer-Emmett-Teller (BET) surface area measurements confirm that the spray-precipitated sulfur (2.48 m^2g^{-1}) shows almost 11 times higher surface area than the drop-precipitated sulfur (0.23 m^2g^{-1}), because the particle size in the spray-precipitated sulfur is much smaller than in the conventionally precipitated sulfur.

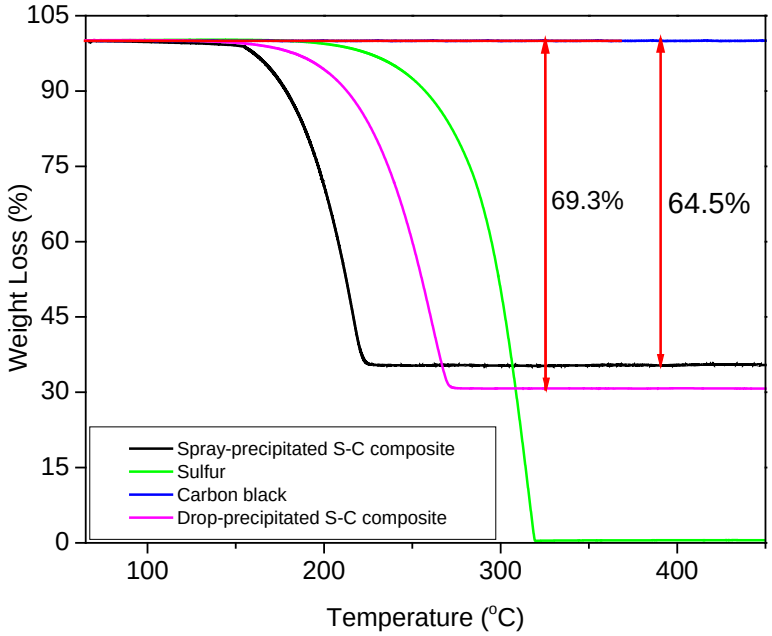

Figure 5.7 Thermogravimetric analyses (TGA) of both drop- and spray-precipitated composites.

According to the morphological analysis, it is expected that the electrochemical performance of the spray-precipitated materials should be better than that of the drop-precipitated materials. To confirm this, the cycling performances of both the drop-precipitated and the spray-precipitated S-C composites needed to be investigated. For measuring the cycling performance, it was first necessary to conduct thermogravimetric analysis(TGA)to measure the sulfur content in both composites. Figure 5.7 shows the TGA curves of both the drop- and the spray-precipitated composites. According to the stoichiometry, the sulfur content should be 70 wt%, however, the TGA results show that the sulfur content is about 64.5% and 69.3% for the spray-precipitated and the drop-precipitated S-C composites, respectively. It should also be mentioned that in the spray-precipitated composite, the loss was about 5.5%, which is much higher comparing to the drop-precipitated composite (~0.7%).

It is obvious that finer particles are easier to washout than larger particles, and for this reason, it is assumed that the loss of sulfur occurs during the washing and handling in the synthesis process. It would be expected that in the spray-precipitated method with finer particles, the loss would be higher compared to the drop-precipitated method.

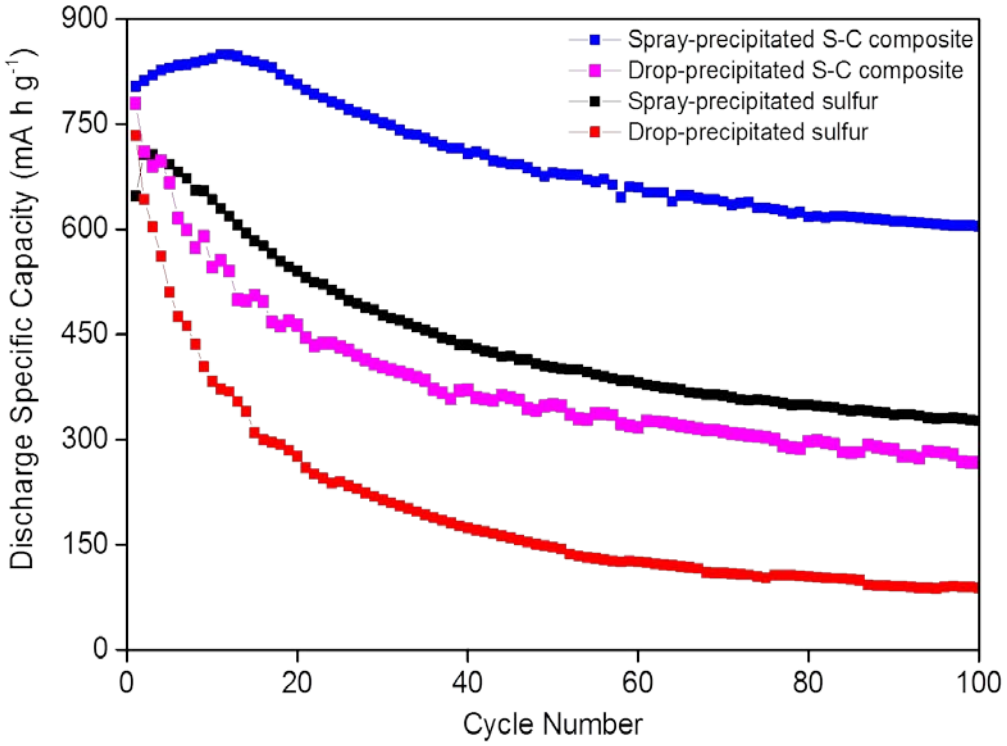

Figure 5.8 Cycling performances of both drop and spray-precipitated pure sulfur and composites.

Figure 5.8 shows the specific discharge capacities of the samples prepared by both the drop-precipitated and the spray precipitated methods with a current density of 0.1C. Spray-precipitated sulfur shows 330 mA h g^{-1} discharge capacity after 100 cycles, which is 48% of its initial discharge capacity. On the contrary, drop-precipitated sulfur shows only 12% of its initial capacity after 100 cycles, which is much lower than that of the spray-precipitated sulfur. The particle size, shape, and surface area of sulfur are responsible for this distinct electrochemical performance. A similar trend is found for the cycling performances of both

the spray- and the drop-precipitated S-C composites, where the spray-precipitated S-C composite shows 800 mA h g^{-1} initial discharge capacity and manages to retain 75% of its initial capacity after 100 cycles, which is about 45% higher than for the drop-precipitated sulfur.

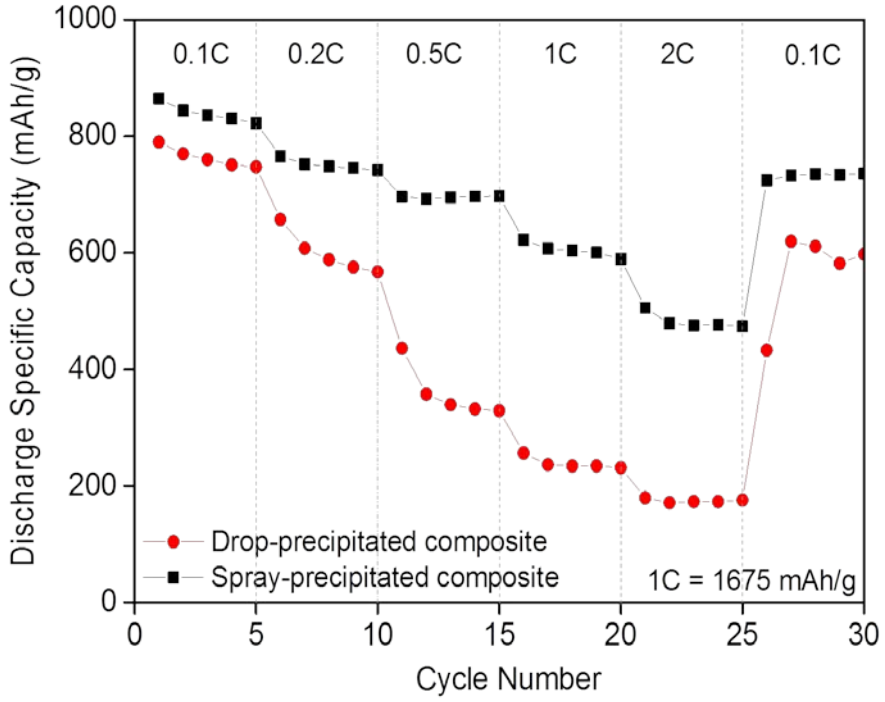

Figure 5.9 Rate performance of spray- and drop-precipitated sulfur-carbon composite.

It is believed that the homogeneous dispersion of the active materials in the carbon black helps to increase the active material utilization, resulting in better discharge capacity and capacity retention. Moreover, the large surface area of spray-precipitated S-C composite may ameliorate volume expansion during the sulfur to sulfide conversion, which could also play a vital role in better cycling performance. The rate performances of both spray- and drop-precipitated S-C composites are shown in Figure 5.9, where the spray-precipitated composite shows much better stability at higher current densities than the drop-precipitated composite. From the above discussion, we can infer that the spray precipitation method can successfully

produce high-surface-area sulfur and sulfur-carbon composite. For further confirmation, a comparative study was conducted on the fabrication processes for sulfur and sulfur-carbon composite between the conventional chemical methods and the spray precipitation method, resulting in different properties, which are listed in Table 5.2. Table 5.2 clearly shows that most of the conventional methods for the fabrication of high-surface-area sulfur particles and their composites use surfactant and require multiple steps to produce fine sulfur particles with high surface area. The spray-precipitation method, however, shows higher surface area for both sulfur and sulfur-carbon composite. Moreover, the capacity retention, which is 75% for spray-precipitated S-C, is also much higher than for the other methods.

Table 5.2 Comparison of properties and performance between the conventional chemical methods and the spray-precipitation method.

Chemicals used for sulfur fabrication	Surfactant use	BET surface area of sulfur (m^2g^{-1})	Conductive carbons and additives	Steps involved for S-C composite fabrication	BET surface area of S-C composite (m^2g^{-1})	Capacity retention after 100 cycles (%)	References
$Na_2S_2O_3$, HCl, Triton X-100, PEG	Yes	NA	Graphene oxide, carbon black	2	NA	~64% at 0.1C	[169]
$Na_2S_2O_3$, HCl, Triton X-100, PEG	Yes	NA	MWCNT	3	NA	~60% at 1C	[12]
$Na_2S_2O_3$, HCl, isopropyl alcohol	Yes	NA	Carbon black	1	NA	~50% at 0.1C	[223]
$Na_2S_2O_3$, HCl, Triton X-100	Yes	NA	Graphene sheet	2	NA	~63% at 0.1C	[224]
Na_2S_4, HCl, Oil bath, Anhydrous ethanol	Yes	NA	Carbon black	2	73 (the carbon black surface area is 1269 m^2/gm)	~67% at 0.1C	[225]
Commercial sulfur	No	0.20	NA	NA	NA	~30% at 0.1C	[226]
Drop-precipitated sulfur ($Na_2S_2O_3$, $H_2C_2O_4$)	No	0.23	Carbon black	1	8.82 (the carbon black surface area is 487 m^2/gm)	~53% at 0.1C	This work
Spray-precipitated sulfur ($Na_2S_2O_3$, $H_2C_2O_4$)	No	2.48	Carbon black	1	23.31 (the carbon black surface area is 487 m^2/gm)	~75% at 0.1C	This work

Besides the cycling performance, to evaluate the effects of particle size and shape, it is also necessary to conduct cyclic voltammetry (CV) and electrochemical impedance spectroscopy (EIS) to understand the reaction mechanisms inside the cell during charge and discharge, and to justify the obtained results. Figure 5.10a and 5.10d shows cyclic voltammograms of drop-precipitated and spray-precipitated composites for the first 4 cycles with 0.1 mV s^{-1} scan rate. Both panels show two reduction peaks and one oxidation peak, with a small deviation in intensity with increasing cycle number. The first reduction peak appearing at 2.3-2.4V is related to the change from elemental sulfur to long chain lithium polysulfide (Li_2S_n, $n \geq 4$), and the second reduction peak appearing at 1.9-2.0 V is responsible for the reduction of long chain lithium polysulfide to short chain lithium polysulfide (Li_2S_n, $n<4$). Figure 5.10c and 5.10f confirms the above statement because two different plateaus appear during the discharge and one plateau is formed during charging [139]. The intensity of the peaks remains constant for the spray- and drop-precipitated composites with increasing cycle number, however, the second reduction peak of the drop-precipitated composite is much broader compared to that for the spray-precipitated composite [227]. This peak broadening reflects the lower discharge capacity of the drop-precipitated composite. The reverse phenomenon is found for the oxidation peak, where the drop-precipitated composite shows a sharp and intense peak compared to the spray-precipitated composite. The sharp oxidation peak, which is created during charging, is an indication of polarization. A lower oxidation peak indicates little polarization and is an indicator of good electrochemical performance [228]. It should also be mentioned that the oxidation peak of the spray precipitated composite shows a broad shoulder, which fades away with increasing cycle number. This phenomenon can be explained as follows. For the first few cycles, the active materials may not have sufficient contact with the electrolyte, which slows the oxidation process. As a result of this, a broad shoulder appears in the oxidation curve rather than a sharp peak. After several cycles,

the electrolyte may have sufficient contact with the sulfur particles, which facilitates the oxidation process, and for this reason, the broad shoulder gradually disappears. It is notable that the drop-precipitated composite, which is not totally confined by the carbon black and electrolyte, can easily come to contact with the active materials and doesn't show this phenomenon, which also supports our explanation. This assumption is also confirmed by the cycling performance curve (Figure 5.8), where the discharge capacity gradually increases with cycle number (for the first 15 cycles) for the spray-precipitated composite, while the opposite trend occurs for the drop-precipitated composite. To confirm the CV results, the capacity vs. voltage curves are plotted for both charge and discharge, and are presented in Figure 5.10c and 5.10f. The figure shows that the discharge curve has two plateaus, which reflect the two reduction peaks, while the charge curve shows one plateau, which reflects the single oxidation peak for both the drop- and the spray-precipitated composites. Interestingly, the cathode prepared by the spray technique showed a lower voltage plateau compared to the cathode from the drop method. The reason for the lower voltage plateau of the spray precipitated composite is because this electrode was aged for longer. The spray precipitated cell had to wait a few days for the cycling test due to lack of available testing channels. As a result of its longer aging, self-discharging occurred that causes lower open circuit voltage. In the following cycles (cycle numbers two to four), however, the plateaus go back to normal as is shown in Figure 5.10c and 5.10f. The impedance curve of the spray-precipitated composite shows higher impedance at the first cycle compared to the next four cycles which supports the previous statement. From the CV analysis, it is clear that the spray-precipitated composite shows low polarization and better discharge capacity than the drop-precipitated composite.

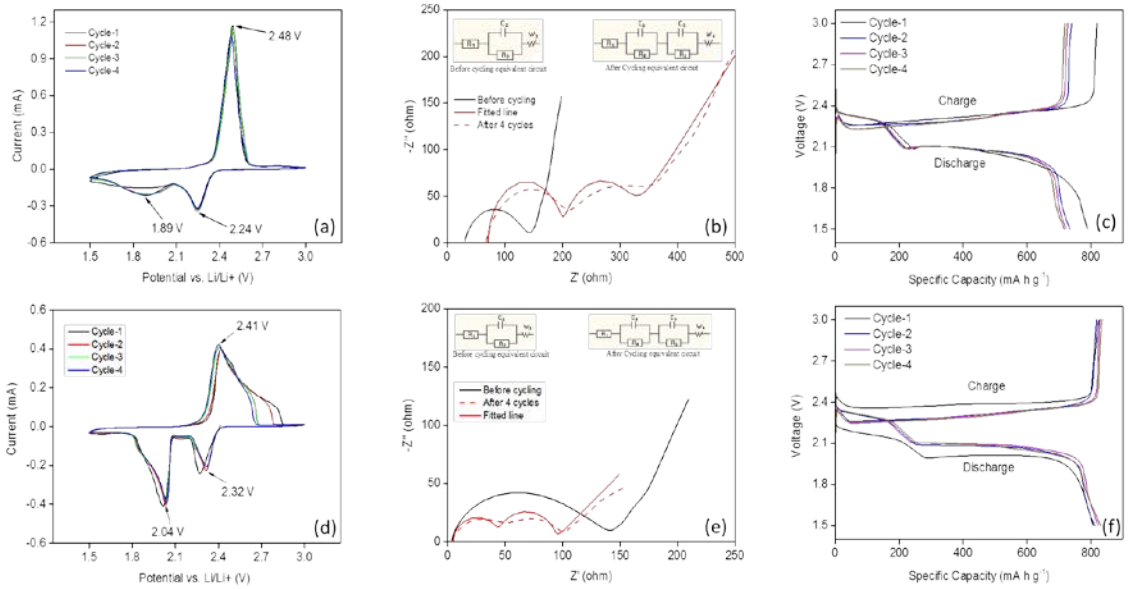

Figure 5.10 Cyclic voltammetry (CV) curves for the first 4 cycles, electrochemical impedance spectra (EIS), and first cycle charge-discharge curves of drop-precipitated (a, b, c) and spray-precipitated (d, e, f) composites, respectively. The insets to the EIS spectra are the equivalent circuits.

The EIS results shown in Figure 5.10b and 5.10e present the impedance spectra of both the drop-precipitated and the spray-precipitated composites as cathode. Figure 5.10b and 5.10e also shows the fitted equivalent circuits of both composites, where the resistance (R), constant phase element (CPE ≈*C*), and Warburg impedance element (W) are included. R_e(~R_1), R_{ct} (R_2), and R_{sf} (R_3) represent the solution resistance of the electrolyte, the charge transfer resistance, and the surface resistance, respectively. C_1 and C_2 which are representedby CPE1 and CPE2 are related to the solid-state diffusion of Li^+ due to the formation of a double layer capacitor between the electrolyte and the cathode interface. W is the Warburg impedance element attributable to the diffusion of lithium ions in the active materials. The first cycle the EIS curve shows a depressed semicircle in the middle frequency region, which reflects the impedance associated with charge transfer. The impedance spectra

after four cycles exhibit two depressed semicircles, where the higher frequency region semicircle (left) is ascribed to the charge transfer resistance and the lower frequency region semicircle (right) is attributed to the formation of Li_2S [110, 229]. The fitted results for both composites are listed in Table 5.3, where the solution resistance for the drop-precipitated composite is much higher than that of the spray-precipitated composite. Moreover, the increase in the solution resistance after four cycles is very small for the spray-precipitated composite, however, for the drop-precipitated composite, the solution resistance increases by more than 3 times after four cycles. The increased solution resistance occurs due to the dissolution of polysulfide into the electrolyte after several cycles. On the other hand, the initial charge transfer resistance of the drop-precipitated composite is 68.37 Ω, and after 4 cycles, it increases to 126.5 Ω, which means that the movement of Li^+ ions from anode to cathode becomes more restricted and finally reduces the capacity. On the other hand, the spray-precipitated composite shows 111 Ω initial charge transfer resistance, but it drops down to 38.99 Ω after four cycles, which indicates the easy movement of Li^+ ions and increased capacity. The EIS data for the spray-precipitated composite also agree with the cycling performance, where the discharge capacity increases in the first few cycles and then decreases. Another important parameter that can be extracted from Table 5.3 is the Warburg impedance element (W). The Warburg impedance is very high for the drop-precipitated composite comparing to the spray-precipitated composite. This means that, the diffusion of Li^+ from the electrolyte-cathode interface to the cathode is easier for the spray-precipitated composite and difficult for the drop-precipitated composite. This result also confirms that the solid electrolyte interphase (SEI) for the drop-precipitated composite is much thicker compared to the spray-precipitated composite and impedes Li^+ diffusion.

Table 5.3 Z-fitted EIS results for the drop-precipitated and spray-precipitated S-C composite before and after four cycles.

	Impedance values	**R_e (Ω)**	**R_{ct} (Ω)**	**CPE1 (μF)**	**R_{sf} (Ω)**	**CPE2 (μF)**	**W ($\Omega.S^{-0.5}$)**
Drop-precipitated S-C composite	**Before cycling**	19.15	68.37	2.106	-	-	284.7
	After 4 cycles	70.51	126.5	2.418	102.1	97.4	82.65
Spray-precipitated S-C composite	**Before cycling**	4.081	111	2.056	-	-	29.15
	After 4 cycles	4.818	38.99	2.464	47.86	95.28	14.47

It should be mentioned that although the spray-precipitated composite shows better cycling performance compared to the drop-precipitated composite, the discharge capacity graph still (Figure 5.8) shows a negative slope, which means that capacity decay will continue with increasing cycle number. This phenomenon will be a stumbling block for commercialization and large-scale fabrication of Li-S batteries by this facile method. To make this Li-S battery compatible and commercially viable, it is necessary to increase the capacity retention by more than 90%. To do so, it is important to discover the reason behind the capacity fading. Manthiram's group [34] suggested that the long chain polysulfides (Li_2S_8 and Li_2S_6) which form during the first plateau of the discharge curve are responsible for capacity fading. These long-chain polysulfides dissolve in the electrolyte, diminish the reaction rate, and also intensify the shuttle phenomenon, which leads to huge capacity fading. By preventing the formation of longer chain polysulfides, it is possible to mitigate these problems and to improve capacity retention. To prevent the formation of longer chain polysulfides, Manthiram's group introduced a new charging method, whereby the cells were charged up to a certain capacity rather than within the conventional voltage window, so that the first plateau

could not be formed. They then allowed the charged cell to discharge. They found that with this new charging technique, it is possible to achieve very high capacity retention. Manthiram's group used this new charging technique along with a free carbon interlayer in between the separator and the sulfur cathode. The carbon interlayer also had a significant role in the prevention of polysulfides. We applied this new charging method with the spray-precipitated composite to enhance the capacity retention.

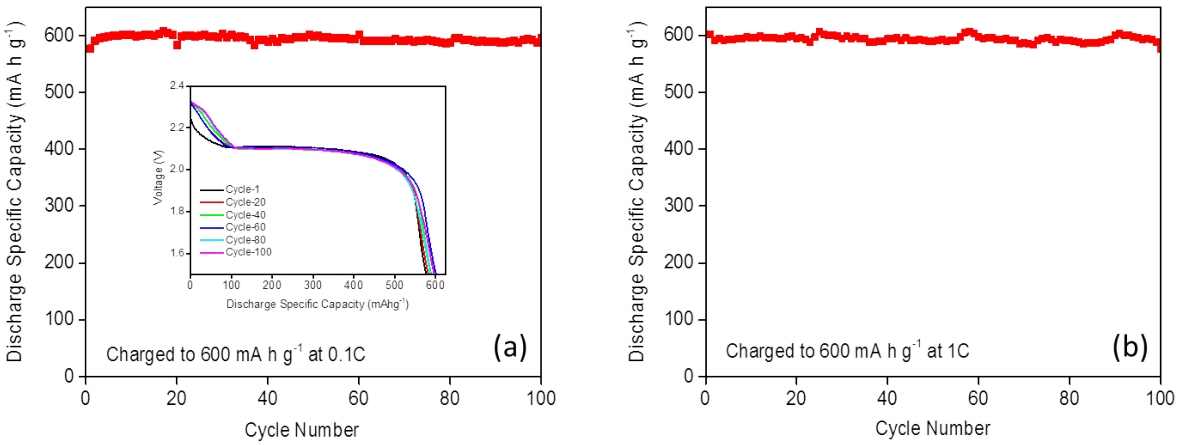

Figure 5.11 Discharge specific capacity with fixed charging (a) at low current density and (b) at high current density. The inset in (a) shows the voltage dependence on discharge specific capacity for selected cycles.

Figure 5.11a and 5.11b shows the effect of the new charging technique on the discharge capacity of the spray-precipitated composite at different current densities. By applying different current densities (0.1C and 1C), the cells were charged to 600 mA h g^{-1} and allowed to discharge. The outcome was phenomenal, and the cells showed very stable discharge capacity, regardless of current density, so that the capacity retention was more than 99% after100 cycles. It is worthwhile to show the change in voltage with cycle number because the discharge capacity can be made to remain steady by sacrificing voltage. The above statement means that the voltage should also remain steady with cycle number during

charging and discharging when the new charging technique is applied. For this reason, the inset in Figure 5.12b shows the change in voltage with cycle number at 0.1C.It is clear that no first plateau was formed, and the voltage remained constant between 2.25 and 2.35V for 100 cycles. It can be inferred that by applying the new charging technique, it is possible to prevent the formation of longer chain polysulfides, so that the initial capacity is retained.

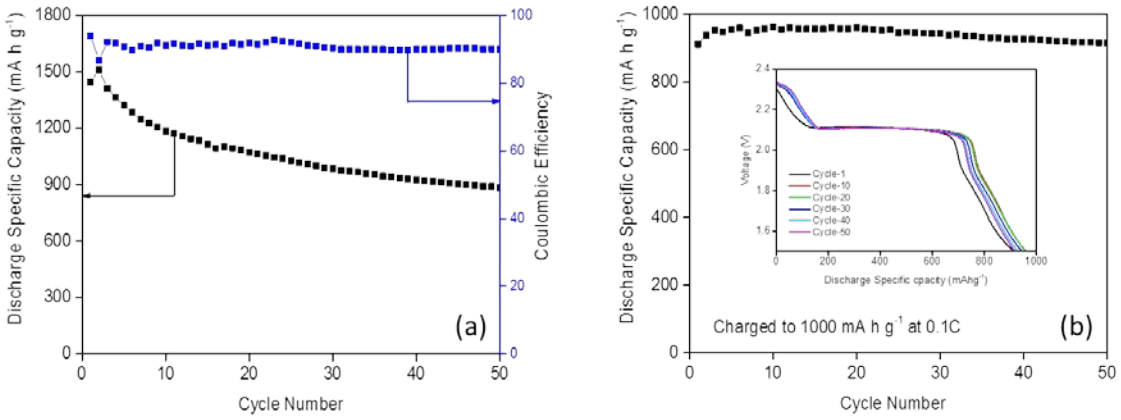

Figure 5.12 Discharge specific capacity of spray-precipitated composite (a) with free-standing layer and (b) with free-standing layer in combination with fixed capacity charging. The inset in (b) shows the voltage dependence on the discharge capacity for selected cycles.

It is also necessary to mention that with the combination of the spray-precipitation method and fixed capacity charging, we managed to achieve 35.8% of sulfur's theoretical capacity, which is only twice as high as in a commercial battery. To improve the capacity further, a free-standing layer (FSL) of single-walled carbon nanotube (SWCNT) was inserted in between the separator and the cathode, which helped to increase the conductivity of the sulfur along with the prevention of longer chain polysulfides. This new approach was also introduced by Manthiram's group [203], and later, it was also adopted by other groups [35, 204] to raise the initial capacity as close to the theoretical capacity as possible.

Figure 5.12a shows the cycling performance of the spray-precipitated composite with a SWCNT free-standing layer in between the cathode and the separator. The initial discharge capacity rose to 1444 mA h g^{-1}, and capacity of 841 mA h g^{-1} was retained after fifty cycles. Although the initial capacity was increased with the help of the free-standing layer, the capacity retention was 58.2%, which is 16.8% lower than that without the free-standing layer. To increase the capacity retention for the spray-precipitated composite with the free-standing layer, the new charging technique was also applied, and this time, the cells were charged to 1000 $mAhg^{-1}$ (because the initial capacity is increased due to insertion of the free-standing layer). The results are shown in Figure 5.12b, where the capacity retention is 91.6% and the capacity is increased by almost 40% with the help of the new charging technique after fifty cycles. The inset in Figure 5.12b shows the voltage vs. discharge capacity curves to demonstrate the change in the voltage with cycle number. It was found that this 91.6% capacity retention was achieved without much fluctuation of voltage.

5.4. Conclusion

A modified chemical method has been developed for the fabrication of sulfur-carbon composite, which is denoted as the spray precipitation method. This newly developed method can produce fine and arbitrary-shaped sulfur particles. This method can also successfully fabricate a carbon-sulfur composite, denoted as spray-precipitated carbon-sulfur composite, which shows high specific surface area along with a homogeneous distribution of sulfur in the carbon. With the combination of these two properties, the spray-precipitated composite shows high discharge capacity with acceptable (~75%) capacity retention. With the combination of the spray precipitation method and the new capacity-limited charging technique (charging up to 600 mA h g^{-1}), we managed to achieve more than 99% capacity retention after 100 cycles. For further improvement of the discharge capacity and capacity retention, a free-standing layer of SWCNT was applied along with the new charging

technique (charging to 1000 mA h g^{-1}), and we managed to retain 91.6% of the initial capacity. Considering the significantly improved discharge capacity and capacity retention, we believe that this spray-precipitation technique, along with the fixed charging method, will represent a quantum leap for the large-scale production and commercialization of the Li-S battery.

Chapter 6. Synthesis of Sulfur/Graphene Composite by Reverse Microemulsion Method for Enhancing the Stability of the Lithium/Sulfur Battery

6.1. Introduction

The demand for efficient energy storage devices is increasing day by day due to the continual improvement of portable electronics and the inclination of the automotive industry towards electric and hybrid electric technologies[230]. The limited global fossil fuel energy supply and the environmental impact of CO_2 release from the transportation sector have invigorated the trend towards renewable energy harvesting and storage [231]. The conventional Li-ion technology which has been dominant for the last two and half decades can satisfy the energy demands of portable devices (e.g. smart phones, laptop computers, cameras, etc.), but it barely can meet the energy and power requirements for electric and hybrid electric vehicles [232]. The current Li-ion batteries can deliver gravimetric energy density of 160-190 Wh/kg, which can hardly run an electric vehicle for 150 to 200km. The main hurdle for low energy density Li-ion batteries comes from the cathode side, where transition metal oxides are used as active cathode materials that can deliver a theoretical capacity of 150-170 mAh/g [54].

Sulfur, which exhibits 2600 $Wh \cdot kg^{-1}$ specific energy, is inexpensive, naturally abundant, and environmentally benign, so it could be a better and more promising alternative to the existing cathode materials. Even though the Li/S system has been under investigation for the last thirty years, it is yet to be commercialized due to its poor cycling performance, specifically, its low cycling stability [164]. Researchers have found that there are three main reasons behind the low cycling performance of the Li/S system, which are:(i) the very low electrical conductivity of sulfur, leading to limited active material utilization; (ii) dissolution of long chain polysulfides and the polysulfide shuttle, which causes low cycling stability; and (iii) volume changes in the active material during charge and discharge, which causes precipitation of the active materials and degradation of the cathode. Extensive research has

been conducted by applying different techniques to load sulfur onto different conductive carbon materials[161, 162, 210, 233, 234],in combination with the usage of different electrolytes [45, 235], binders [187, 188], and additives [60, 108, 110, 189, 211].In most cases, a high initial capacity (>1000 mAh/g) was achieved, but the researchers failed to achieve higher cycling stability.

Graphene, along with its derivatives (reduced graphene, functionalized graphene, heteroatom doped graphene, etc.), which show excellent electronic conductivity and high surface area, is considered one of the most promising carbons that could be used to ameliorate the challenges of the Li/S system [194, 236, 237]. Considerable research has been conducted on graphene/sulfur composites to increase the capacity and stability of the Li/S system. In most cases, however, the graphene/sulfur composites were fabricated either by mechanical milling or by chemical precipitation methods [66, 237, 238], where the graphene was not exfoliated or firmly adhered to the sulfur. To improve the cycling performance and stability, it is important to have better adhesion between the sulfur and the graphene, which will not only help the active material utilization, but also will maintain the structural integrity during expansion and contraction of the sulfur.

Herein, we report an old nanomaterial synthesis technique for synthesising sulfur/graphene composite, which is commonly known as the water-in-oil microemulsion (w/o microemulsion) or reverse microemulsion method. This method is commonly used for the synthesis of metal nanoparticles from their respective salt solutions [239, 240]. In this method, an aqueous solution containing metal salts is dispersed in an organic oil phase with the help of a surfactant, and this microemulsion is designated as microemulsion-1, while another microemulsion (designated as microemulsion-2) is prepared, in which an aqueous solution containing a reducing agent is dispersed in the same oil phase. Then, these two emulsions are mixed together, and the aqueous phases merge and react with each other to

form metal nanoparticles [240]. A similar approach has been applied in our work, where carboxylated-graphene containing sodium polysulfide aqueous solution was added to cyclohexane oil to prepared microemulsion-1, whereas in microemulsion-2, an aqueous solution of hydrochloric acid was added to cyclohexane. These two emulsions were mixed to form graphene-adhered sulfur. It is important to mention here that this method has been used by the scientific community for the last sixty years in different fields [241-243], but it is yet to be used for the synthesis of sulfur/carbon composite.

This is because the synthesized sulfur from the reverse microemulsion method is a nonpolar molecule and dissolves in almost all organic nonpolar solvents that generally have been used as the oil phase in the reverse microemulsion method. From a literature review, it was been found that only Gou et al.[244] had used this method for the fabrication of monoclinic sulfur, although their claim is questionable for several reasons. The first discrepancy is the oil that they used in their reverse microemulsion method. The name of the oil is “theolio”, and there is no such oil with this name in the open sources. Even if it exists, sulfur should be highly soluble in it, which was not mentioned in the paper. The second discrepancy is the room temperature stabilization of monoclinic sulfur. From both the phase diagram of sulfur and the literature, it is well-known that monoclinic sulfur only exists above 95 ^{o}C.

In our work, we used cyclohexane as the oil phase, which also has a sulfur solubility of 1.185 wt%. In our method, however, sulfur-dissolved saturated cyclohexane was used as the oil phase, so that the synthesized sulfur could not dissolve in the cyclohexane. Later, a three-dimensional (3-D) heteroatom-doped carbon cloth current collector was used to increase the loading of active materials. It has been observed that a 3-D carbon cloth cathode can contain more than 8 mg/cm^2 active material with improved capacity and stability. Moreover, the weight of the carbon cloth (per square centimetre) is much lower than that of Al-foil, which also will help to increase the gravimetric capacity of the Li/S system.

6.2. Experimental

6.2.1. Preparation of carboxylated-graphene/sodium polysulfide solution: 6.4 g commercial sulfur was added into a 50 ml 2M Na_2S aqueous solution. Then, the solution was stirred for several hours until all the sulfur reacted with the Na_2S to form Na_2S_x.There was some unreacted sulfur residue powder in the solution, which was filtered out to obtain a clear red coloured Na_2S_x solution. 100 g carboxylated-graphene was added into this solution, and it was sonicated for 10 min to form a homogeneously dispersed graphene/polysulfide solution. All the chemicals, the sulfur, the Na_2S, and the carboxylated-graphene were purchased from Sigma Aldrich. The following chemical reaction occurred for the formation of polysulfides.

$$(x\text{-}1)S_8 + 8Na_2S \rightarrow 8Na_2S_x$$

6.2.2. Preparation of microemulsions and graphene/sulfur composite: 30 g of a mixture of sorbitan monooleate (Span®80) and polyethylene glycol (PEG-20) sorbitan monooleate (Tween®80) in a ratio of 8:1, along with 10 ml n-butanol, was added into 450 ml of sulfur-saturated cyclohexane. Both Span80 and Tween80 act as surfactants, whereas n-butanol and cyclohexane act as a cosurfactant and the oil, respectively. Then, the mixture was homogenized by a Sonic Ruptor-400 ultrasonic homogenizer for 1 hour. The homogenized mixture was equally divided into two beakers for preparing two reverse microemulsion solutions. In the first beaker, 12.5ml of carboxylated-graphene containing Na_2S_x was poured in, and the microemulsion was sonicated again for 10 to 15 minutes, whereas, in the second beaker, 12.5 ml of 4M HCl was added, and this microemulsion was also sonicated for 10 to 15 minutes. Finally, these two reverse microemulsions were mixed together and stirred for 2 to 3 hours to form the graphene/sulfur composite. The following reaction occurred when the sulfur precipitated out and formed the graphene/sulfur composite.

$$8Na_2S_x + 16HCl \rightarrow 16NaCl + 8H_2S + (x\text{-}1)S_8\downarrow$$

The composite was then separated by centrifugation at 5000 rpm and repeatedly washed with acetone and water to remove all the oils and salts. A schematic illustration of this method is shown in Figure 6.1, and Figure 6.2 shows the photographs of the different steps. All the chemicals in this case were also purchased from Sigma and directly used without any purification.

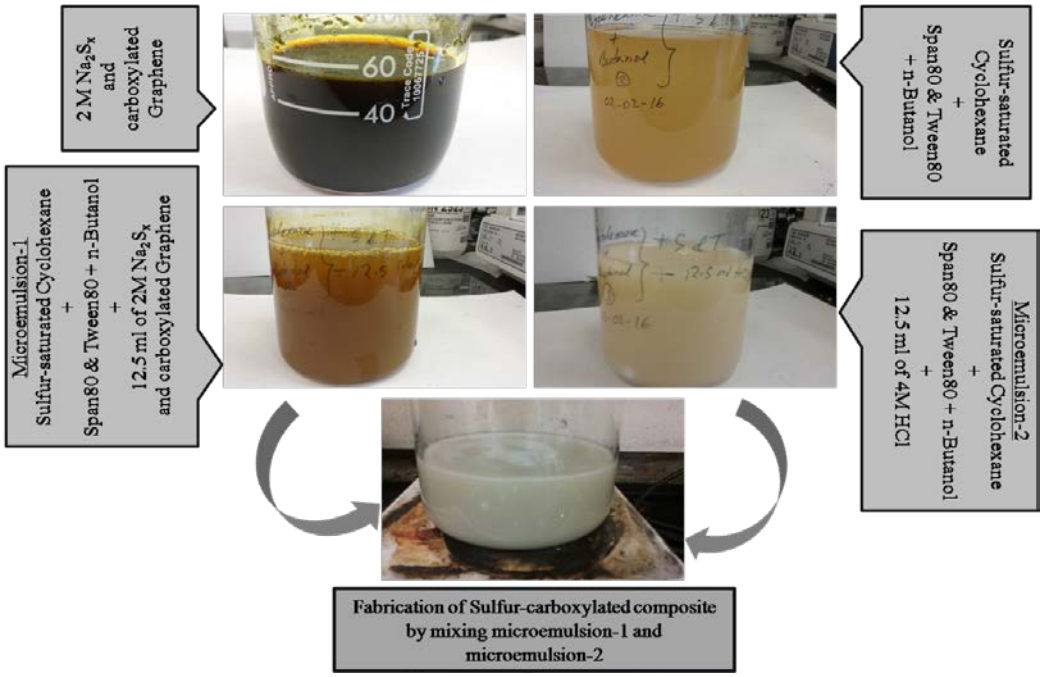

Figure 6. 1: Photographs of the different steps in the reverse microemulsion method and synthesis of the sulfur-graphene composite.

6.2.3. Fabrication of boron- and nitrogen-doped carbon cloth: For the synthesis of boron- and nitrogen-doped carbon cloth we followed Yuan's method for preparing boron, nitrogen doped graphene [245]. To do so, small diameter (5 mm) carbon cloth discs were cut and submerged in1-ethyl-3-methylimidazolium tetrafluoroborate ([Emim]BF_4) ionic liquid in an argon filled glove box. Then, the fully soaked carbon cloths were put into a quartz boat and transferred into a furnace for heat treatment at 330 °C under vacuum. After the heat treatment, the carbon cloths were further annealed at 400 °C in argon to form boron- and nitrogen-doped carbon cloth.

6.2.4. Fabrication of electrodes and coin cells: The aluminum-current-collector-based cathode was fabricated by using the carboxylated graphene–sulfur precipitated composite, carbon black, and polyvinylidene difluoride (PVDF). The PVDF was added in the amount of 10 wt%, and the amount of carbon black was dependent on the amount of sulfur, which was maintained at 50 wt% of the total amount. The composite, carbon black, and PVDF mixture was manually mixed for 20 to 30 minutes with the addition of an appropriate amount of N-methyl-2-pyrrolidone (NMP). The obtained slurry was coated on Al foil to a thickness of 90 microns and was then dried at 50 °C for 24 hours under vacuum. Then, the electrode was cut into 10 mm diameter discs. Each 10 mm disc contained around 1 mg of active materials (sulfur).The fabricated disc electrodes were dried again at 50 °C for a few hours before use. For the carbon-cloth current-collector-based cathode, the slurry was prepared with the addition of carbon black and PVDF, where the sulfur content was 80 wt% along with 10 wt% PVDF and 10 wt% graphene and carbon black. 5 mm diameter carbon cloth discs were dipped into the slurry and dried in a vacuum oven for 24 hours at 50 ^{o}C. Each 5 mm diameter carbon cloth disc contained 7.5 to 8.5 mg of sulfur. These discs were then directly used as cathode in the coin cells. The CR 2032 coin-type cells were assembled in an Ar-filled glove box, where discs of Li foil were used as the counter electrode and reference electrode. The electrolyte was prepared by dissolving 1 M lithium bis(trifluoromethane sulfonyl)imide (LiTFSI) and 0.1 wt% $LiNO_3$ in co-solvents of 1,3-dioxolane (DOL) and 1,2-dimethoxyethane (DME), in a volume ratio of 1:1. A porous polypropylene film was used as the separator.

6.2.5. Characterization: To characterize the sulfur-graphene composite and Li-S cells, different analytical tools were used. For physical characterization of the composite, we conducted X-ray diffraction (XRD; Bruker Smart-1000, Bruker AXS Inc., USA, using Cu Kα radiation), Raman spectroscopy (Horiba Jobin Yvon Labram Aramis using a 532 nm diode-

pumped solid-state laser), Fourier transform infrared spectroscopy (FTIR;NEXUS 670 FT-IR), thermogravimetric analysis (TGA; Netzsch STA 449F3, Germany, in an argon environment with a heating rate of 5 °C/min), and four probe conductivity measurements (Signatone SP4). For morphological analysis, scanning electron microscopy (SEM) and transmission electron microscopy (TEM) were conducted on a Hitachi SU-70 analytical SEM (Japan) and a JEOL (Japan) 2100F field emission TEM, respectively. The scanning electron microscope was also used for conducting large-area energy dispersive X-ray spectroscopy (EDS) mapping. For electrochemical performance evaluation of the Li-S cell, an automatic battery tester system (Land®, China) was used at various current densities at room temperature with a conventional voltage window (1.5-3 V). Electrochemical impedance spectroscopy (EIS) and cyclic voltammetry (CV) measurements were performed on a Gamry Reference 3000 Potentiostat/Galvanostat/ZRA with a scan rate of 0.1 mV s^{-1} (within a voltage window of 1.5 V to 3 V), and for impedance analysis, a frequency range of 10 mHz to 100 kHz was applied.

6.3. Results and discussion:

6.3.1. Reverse microemulsion and selection of materials: A dispersion consists of water, oil, and surfactant(s), which constitute a thermodynamically stable system that is isotropic. A dispersion with a with dispersed domain diameter of~1 to 100 nm is called a microemulsion. If the dispersed phase is water or an aqueous solution and the continuous phase is an organic liquid (an "oil"), it is called a water-in-oil (w/o) microemulsion or reverse microemulsion [246]. In this method, the selection of materials is extremely important, specifically, the surfactants, oil phase, and aqueous phase. In our method, 2M Na_2S_xsolution mixed with carboxylated-graphene was used as the aqueous phase. The carboxylated-graphene was chosen due to its ability to form hydrogen bonds with water, which helps it to disperse uniformly in water. On the other hand, Na_2S_x was chosen because of its reaction products

(when reacted with HCl), which are hydrogen sulfide (H_2S) and sodium chloride (NaCl). H_2S, which is a gas, doesn't affect the ratio of aqueous phase to oil phase. In the case of sodium thiosulphate ($Na_2S_2O_3$), however, which is a very common salt for synthesizing sulfur, water (H_2O) is produced as a by-product when it reacts with HCl, which changes the ratio of aqueous phase to oil phase and is hence inappropriate for this reverse microemulsion method.

Table 6.1: Solubility of sulfur in common organic solvents [2].

Solvent	**Solubility (wt%)**	**Solvent**	**Solubility (wt%)**
Ethanol	0.066	Acetone	0.079
Carbon tetrachloride	0.832	Nitrobenzene	0.856
Cyclohexane	1.185	Chloroform	1.164
Benzene	2.093	Diethyl formamide	0.191
n-Hexane	0.40	Aniline	1.259
Xylene	2.051	Diethyl ether	0.181
Toluene	2.070	Chlorobenzene	2.370
Carbon-di-sulfide	34.8	Bromoform	3.64

Selection of the oil is one of the prime tasks in this method. The oil must be nonpolar, hydrophobic, and feature extremely low solubility of sulfur. In addition, the oil must have a very good compatibility with the surfactant and cosurfactant to produce a uniform microemulsion. No such organic oil is available that can fulfil all these requirements. Almost all the nonpolar solvents feature high solubility of sulfur, and those which have less solubility do not form a stable and uniform microemulsion. Table 6.1 shows the solubility limit of sulfur in common organic solvents, and the left column shows the solubility of sulfur in nonpolar solvents apart from ethanol. Among them, carbon tetrachloride and n-hexane show the lowest solubility of sulfur, but they cannot form a stable and uniform microemulsion.

Cyclohexane, which has 1.185 wt% solubility of sulfur, can form an extremely stable and uniform microemulsion with Span®80 and Tween®80 surfactants [247]. These two surfactants have very low surface tension, with a hydrophilic-lipophilic balance (HLB) of 4.3 and 15, respectively. A lower HLB number indicates higher hydrophobicity and vice-versa. In the reverse microemulsion method, a large amount of oil and small amount of water are generally used, and because of that, a ratio of 8:1 of Span80 and Tween80 surfactants was used in 450 ml of cyclohexane. Moreover, it was found that, to form a stable reverse microemulsion, the HLB of the surfactant should be in the range of 3 to 6 [248]. Figure 7.2 presents a schematic illustration of the preparation of the reverse microemulsions and synthesis of the sulfur-graphene composite from these emulsions. It is important to mention here that, in this method, the cyclohexane was saturated with sulfur before it was used as an oil phase.

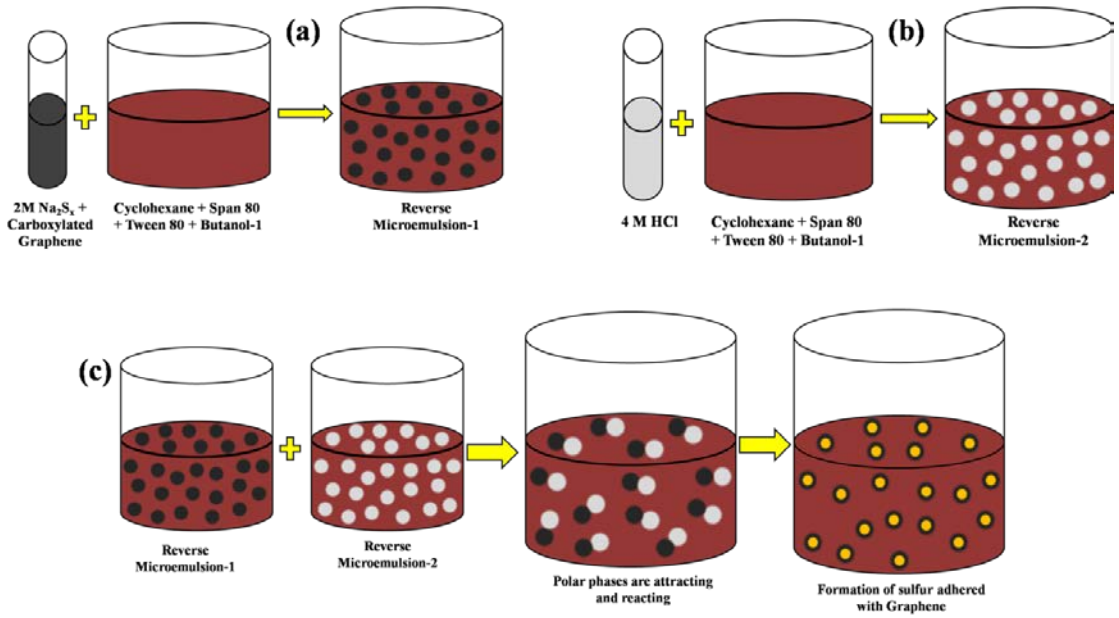

Figure 6.2: Schematic illustration of the reverse microemulsion method: a) preparing microemulsion-1, b) preparing microemulsion-2, and c) synthesis of sulfur/graphene composite.

6.3.2. Physical and morphological characterization of synthesized sulfur-graphene composite: The main reason for using the reverse microemulsion method to synthesize sulfur-graphene composite is to obtain nanosized sulfur with better adhesion to carboxylated-graphene. The combination of these two features can enhance the cycling performance by improving the electronic conductivity of the sulfur and the active material utilization. Moreover, carboxylfunctional groups can attract the polysulfides to reduce the shuttle effect. The conductivity of the synthesized composite, along with those of carboxylated-graphene, commercial sulfur, and hand-mixed sulfur-graphene composite, was measured with a four probe Signatone conductivity tester, and the results are shown in Table 6.2. The conductivity of hand-milled sulfur graphene composite with the same weight percent of graphene was measured to compare the effects of graphene dispersion and adhesion due to the reverse microemulsion method. The graphene content in our sulfur/graphene composite is 6.1 wt%, which was measured by thermogravimetric analysis (TGA) (Figure 6.3) under flowing argon gas.

Table 6.2: Four probe conductivity data.

Sample	**Conductivity S/cm**	**Sample**	**Conductivity S/cm**
Pure Sulfur	3.32×10^{-25}	Reverse microemulsion sulfur-graphene (RM-S/G) composite	7.92×10^{4}
Carboxylated-graphene	4.09×10^{7}	Hand-mixed sulfur-graphene composite	3.27×10^{2}

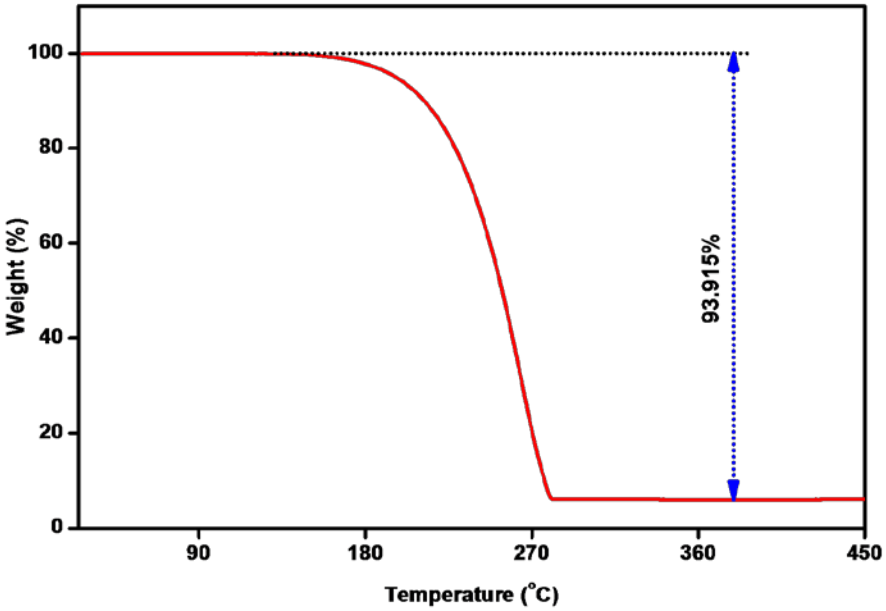

Figure 6.3: Thermogravimetric analysis (TGA) of sulfur-graphene composite

Table 6.2 shows that, the conductivity of the RM-S/G composite is two orders of magnitude higher than that of hand-mixed sulfur-graphene composite, even though the graphene percentage is the same for both composites. The increased conductivity is due to better adhesion and exfoliation of graphene in the sulfur. To observe the particle sizes and morphology, the synthesized sulfur-graphene composite was observed under scanning electron microscopy (SEM). The SEM micrograph in Figure-6.4(a,b) shows the graphene firmly adheres to the surface of the sulfur particles, although the sulfur particles, which are expected to be in nanometer range, are found to be micrometer-sized (around 10 to 20 micrometers). It is important to know that the size of the micelles created by Span80 and Tween80 in cyclohexane oil is approximately 7 to 100 nm [247], which means that either the sulfur particles are agglomerated during the nucleation and growth of the sulfur, or the micelles of Span80 and Tween80 are unstable and inhomogeneous in cyclohexane. It has been determined, however, that the cyclohexane, Span80, and Tween80 system is one of the most stable microemulsions with uniform micelle size [247].In the former case, if the sulfur

particles are agglomerated during the nucleation and growth process, graphene should be trapped inside the big agglomerated sulfur particles.

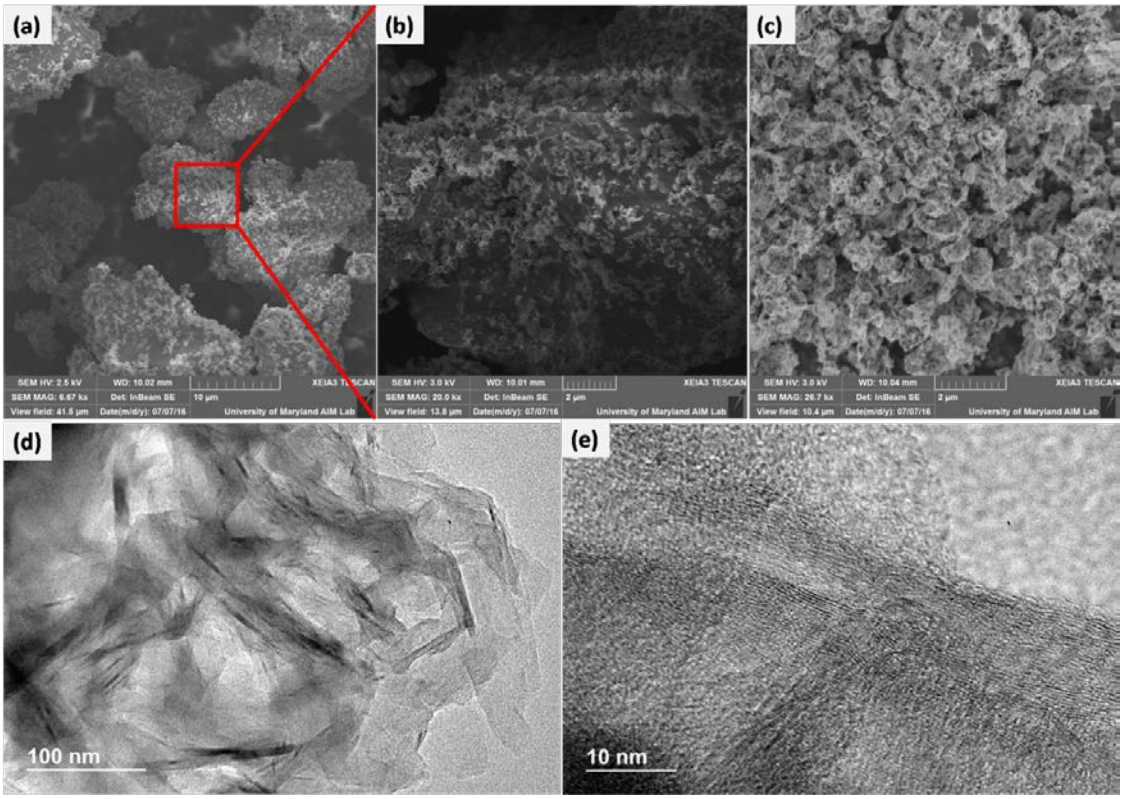

Figure 6.4: SEM and TEM micrographs of RM-S/G: a,b) the as-synthesized composite at different magnifications, c) ball-milled RM-S/G composite, d,e) presence and exfoliation of graphene inside the sulfur.

Figure 6.4(d,e) shows TEM micrographs of the RM-S/G composite, and it is clear that the graphene sheets are exfoliated and well-distributed inside the sulfur particles. In addition, Figure 6.4e also shows a moiré pattern, which confirms the dispersion of crystalline graphene. For further confirmation of entrapment of graphene in sulfur, a sample of the microsized sulfur/graphene composite was ball-milled, so that all the graphene sheets that were entrapped inside the sulfur particles could be exposed. The SEM micrograph of RM-S/G composite in Figure 6.4c shows a large number of graphene sheets, along with smaller size sulfur/graphene composite particles that were exposed after ball milling.

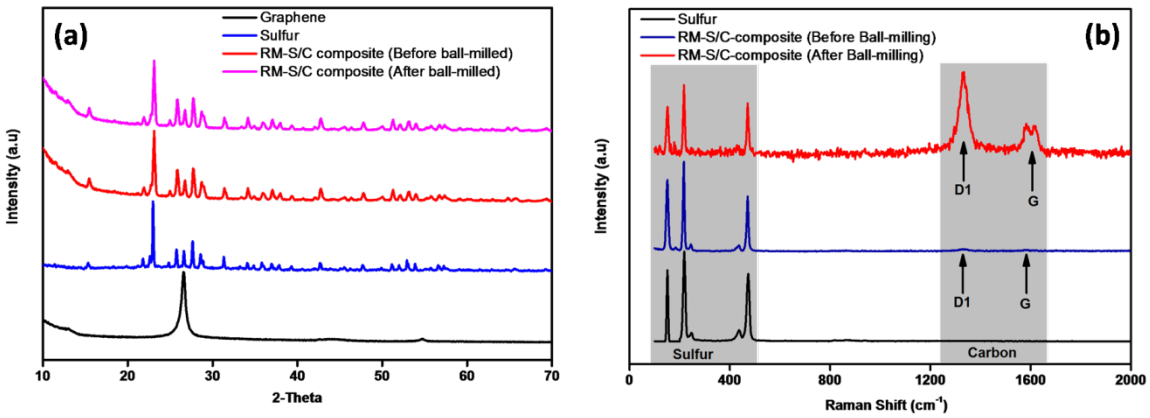

Figure 6.5: XRD patterns (a) and Raman spectra (b) of RM-S/G composite before and after ball-milling.

Figure 6.5a shows the X-ray diffraction patterns of RM-S/G composite along with that of graphene. Along with other small peaks, RM-S/G exhibits a sharp peak around 23.1°, which is a characteristic peak of crystalline octa-sulfur (S_8) that is diffracted from the (222) planes. It is also noticeable that this characteristic peak is broadened for RM-S/G composite compared to commercial sulfur, which indicates smaller particle size.The Raman spectra of pure sulfur and RM-S/G composite are presented in Figure 6.5b, and all the spectra show sharp peaks at 219.1 cm^{-1} and 473.2 cm^{-1}, which reflect the bending and the stretching of nonpolar S-S bonds, respectively [221]. Moreover, RM-S/G composite shows small peaks around 1400 cm^{-1} and 1600 cm^{-1}, which are the characteristic peaks for carbon. These two peaks are well-known as the D1band and the G band, respectively [222]. It is important to note here that, in ball-milled RM-S/G composite, the D1 and G bands are relatively more intense compared to theRM-S/G composite that was not ball milled, which is also an indication of agglomeration of sulfur particles and exfoliation of graphene in the sulfur. After ball milling, the graphene sheets are exposed to the laser radiation and exhibit higher intensity. Another factor here is that, because of the confinement and exfoliation of graphene, electrons can not only strike the surface of the sulfur/graphene composite, but also can pass

through, and hence, RM-S/G composite shows higher conductivity compared to hand-mixed sulfur-graphene composite, where the graphene only adheres to the surface of the sulfur particles.

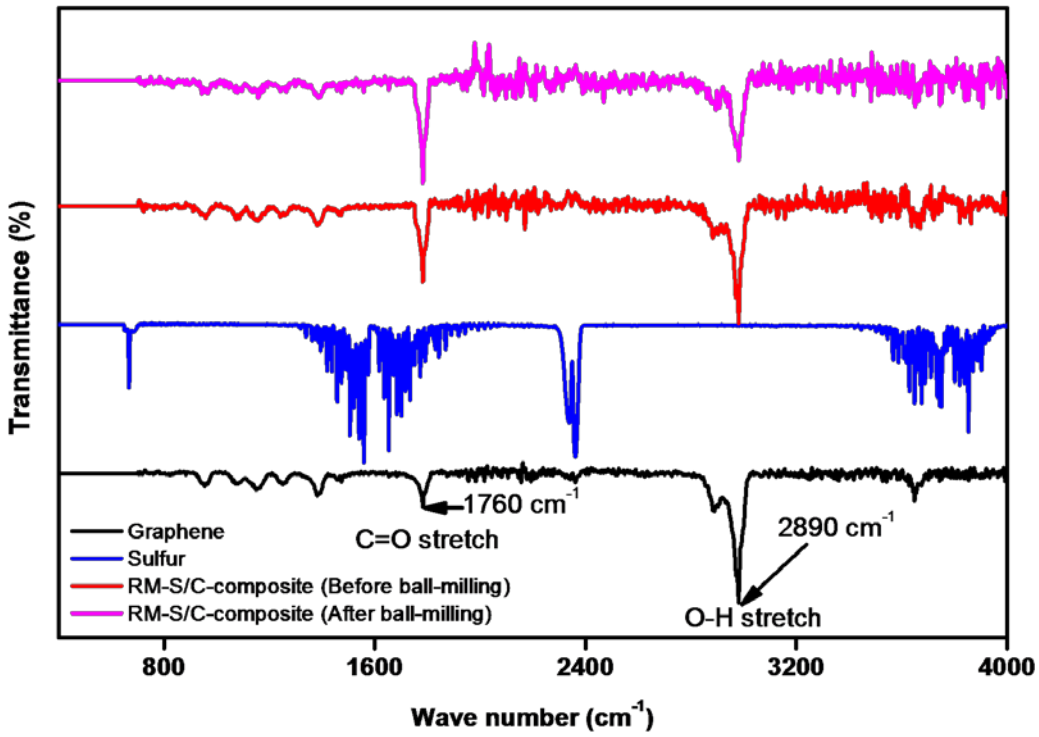

Figure 6.6: FTIR spectra of sulfur, graphene and RM-S/G composite.

Before evaluating the electrochemical performance of RM-S/G composite, it is necessary to confirm the presence of carboxyl groups in graphene after the reverse microemulsion method. These carboxyl groups not only can play a pivotal role in the exfoliation and good dispersion of graphene in aqueous solution, but also can play a significant role in capacity stabilization by reducing the shuttle effect. Figure 6.6 shows the Fourier transform infrared (FTIR) spectrum of RM-S/G composite. It is shown that both graphene and RM-S/G composite feature two sharp peaks at 1760 cm^{-1} and 2890 cm^{-1}, which are characteristic peaks of C=O stretching and O-H stretching for carboxyl groups. The FTIR spectrum of elemental sulfur is also shown in Figure 6.6 for comparison with RM-S/G composite and carboxylated-

graphene. The nonpolar and symmetric S-S bonds should not be detected through IR radiation; a very sharp peak appears at 2400 cm^{-1}, however, which may represent the symmetric stretching of water (H_2O) that comes from moisture.

6.3.3. Electrochemical performance evaluation of RM-S/G composite: The electrochemical performance of the RM-S/G composite was evaluated by galvanostatic charge-discharge cycling at different current densities and by cyclic voltammetry. The cycling behaviour at a current density of 0.1 C of RM-S/G composite, hand-milled sulfur/graphene composite, and commercial sulfur is shown in Figure 6.7a.It is important to mention here that both the hand-milled sulfur-graphene composite and the RM-S/G composite cathodes consist of 6 wt% graphene, 34 wt% carbon black, 50 wt% sulfur, and 10 wt% PVDF. On the other hand, commercial sulfur contains no graphene, but the sulfur content remains the same (~50 wt%). Commercial sulfur cathode shows an initial discharge capacity of 823 mAh/g(based on sulfur) and drops to 248 mAh/g after 200 cycles, which is 30.13% of the initial capacity. In another sense, it can be said that the capacity fading is around 70% after 200 cycles. A similar trend can be detected for hand-milled sulfur/graphene composite, where 17.5% capacity retention (or 82.5% capacity fading) is observed with an initial discharge capacity of 587 mAh/g (based on sulfur). In both cases, the conventional Li/S battery discharge behaviour is observed, where the capacity fades rapidly for the first few cycles due to low active material utilization and polysulfide dissolution, and then stabilizes. It is believed that, in the hand-milled sulfur/graphene composite where 6 wt% graphene was used, the graphene didn’t exfoliate well during hand milling, so that it behaves as graphite, which not only reduces the specific surface area of the graphene, but also reduces the conductivity of the composite. On the other hand, commercial sulfur cathode, which contains only 40 wt% of high surface area carbon black, did not experience the exfoliation phenomenon, so it shows better initial discharge capacity and capacity retention compared to

the hand-milled composite. Compared to these two, RM-S/G composite shows an initial discharge capacity of 914 mAh/g (based on sulfur), but manages to retain discharge capacity of 731 mAh/g after 200 cycles. The capacity retention of RM-S/G composite (around 80%) is 62% higher than that of the hand-milled composite. It can be speculated that the increased discharge capacity and capacity retention is due to the better exfoliation and adhesion of graphene in the sulfur particles, which not only increases the active material utilization, but also reduces the shuttle phenomenon. In addition, the RM-S/G composite shows excellent Coulombic efficiency which is more than 99%.

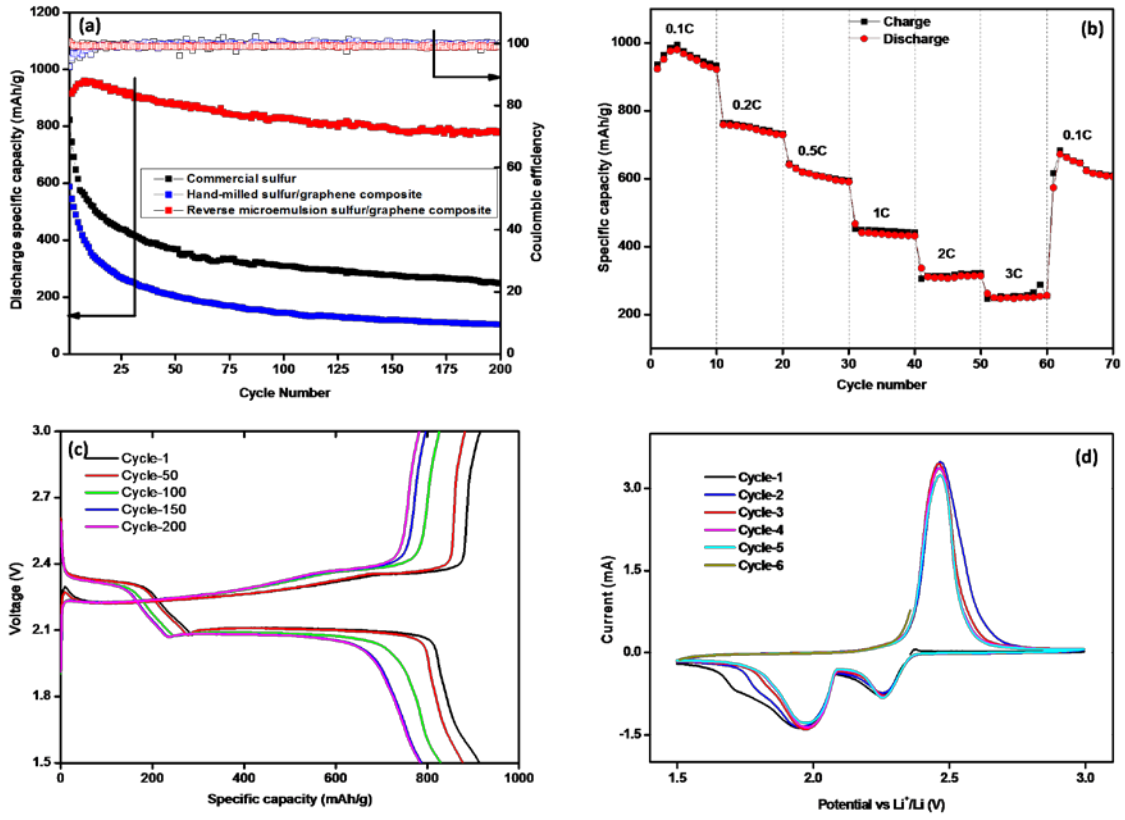

Figure 6.7: Electrochemical performance of RM-S/G composite: a) comparison of cycling performance of RM-S/G composite with hand-milled sulfur/graphene composite and commercial sulfur at a current density of 0.1C, b) rate capability of RM-S/G composite at different current densities, c) charge-discharge curves for selected cycles of RM-S/G

composite at 0.1C,and d) cyclic voltammograms for the first 6 cycles of RM-S/G composite at a scan rate of 0.1 mV s^{-1}.

The rate performance of RM-S/G composite shown in Figure 6.7b demonstrates that, even at higher current density, this composite cathode can deliver adequate discharge capacity and can regain its capacity when a lower current is applied. Charge-discharge profiles and cyclic voltammograms are presented in Figure 6.7c and 6.7d, respectively. In the cyclic voltammograms, two reduction peaks and one oxidation peak are observed, with a small deviation in intensity with increasing cycle number. The first reduction peak appearing at 2.3-2.4V is related to the change from elemental sulfur to long chain lithium polysulfides (Li_2S_n, $n \geq 4$), and the second reduction peak appearing at 1.9-2.0 V reflects the reduction of long chain lithium polysulfides to short chain lithium polysulfides (Li_2S_n, $n<4$). The discharge profile in Figure 6.7c confirms the above statement because two different plateaus appear during the discharge and one plateau is formed during charging [139]. It is important to note here that the second reduction peak in the cyclic voltammograms (CVs) shows a small bump at 1.7 V for the first two cycles, which resembles what appears in CVs for the reduction of $LiNO_3$ salt, an additive that can help to form a stable solid electrolyte interphase (SEI) on the lithium metal surface [249]. This SEI helps to reduce the shuttle phenomenon and to promote active material utilization.

It can be inferred from the above discussion that this reverse microemulsion method can help to achieve high capacity and better capacity retention. The active material content in each electrode is quite low (~1mg/cm^2), however, which makes it unfavorable for scaling up. It has been calculated that, to surpass the current Li-ion technology, it is necessary to load more than 4mg/cm^2 of active material in a cathode [9]. With the conventional aluminum (Al) foil current collector, it is hard to load such a large amount. A three-dimensional (3-D) interconnected conductive network such as carbon cloth has a large accessible surface area

with high electrical conductivity, and can accommodate and utilize high amounts of active material. Researchers from all over the world [250-252] have focused their attention on 3-D network structures to load larger amounts of active material while maintaining higher electrical conductivity, thermal stability, and structural integrity. They found that a 3-D interconnected network is an ideal means to allow the transport of electrons and ions during charging and discharging of a battery. Recently, Yuan et al.[245] reported that, heteroatom-doped (boron and nitrogen) carbon can enhance the cycling performance and stability of the Li/S system by minimizing the polysulfide shuttle phenomenon. Here, to increase the active material content as well as to improve the cycling performance, we introduced boron, nitrogen-doped carbon cloth as a current collector and active material host.

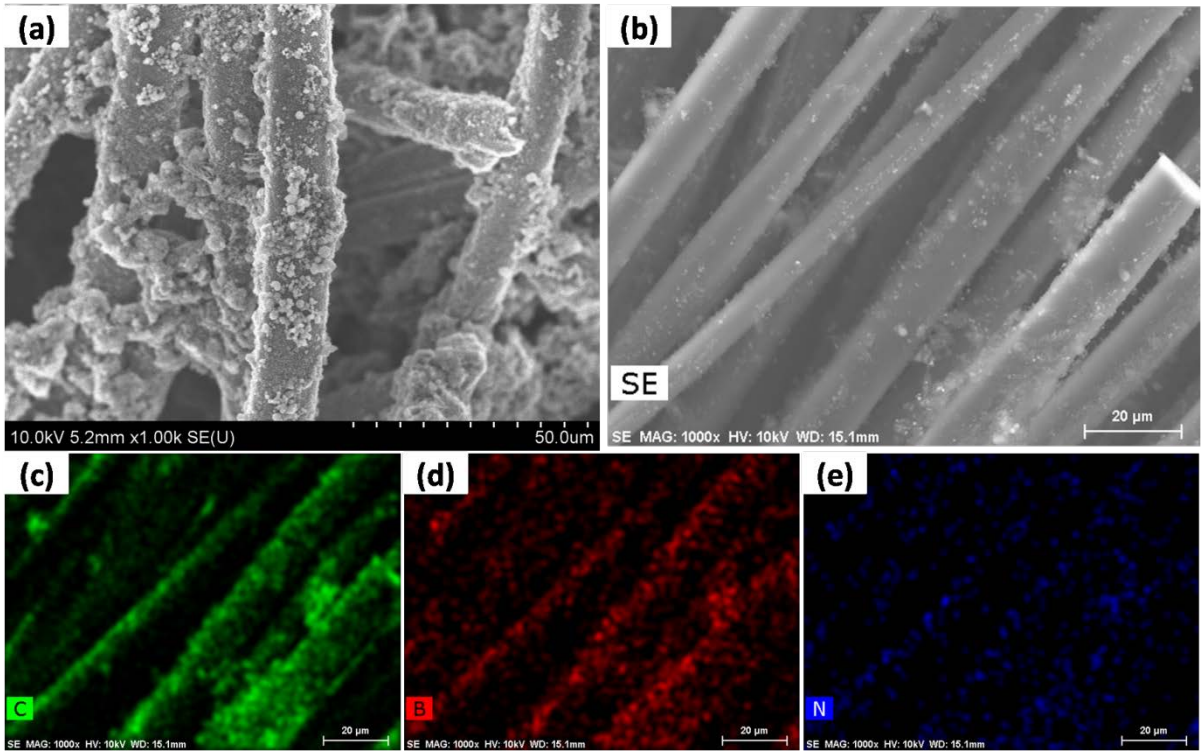

Figure 6.8: (a) SEM and (b-e) energy dispersive spectroscopy (EDS) analysis of boron, nitrogen-doped carbon cloth.

Figure 6.8 shows the morphology and the EDS mapping of RM-S/G composite-loaded B,N-doped carbon cloth, which confirms the presence of boron and nitrogen in the carbon cloth. It is important to mention here that the boron and nitrogen come from the tetrafluoroborate anion and the1-ethyl-3-methylimidazolium cation, respectively. Figure 6.8 also shows the interaction between RM-S/G composite and the carbon cloth, which firmly adhere to each other and compose a stable 3-D interconnected network. It is expected that this RM-S/G composite loaded on boron, nitrogen-doped carbon cloth will show better electrochemical performance along with high active material loading.

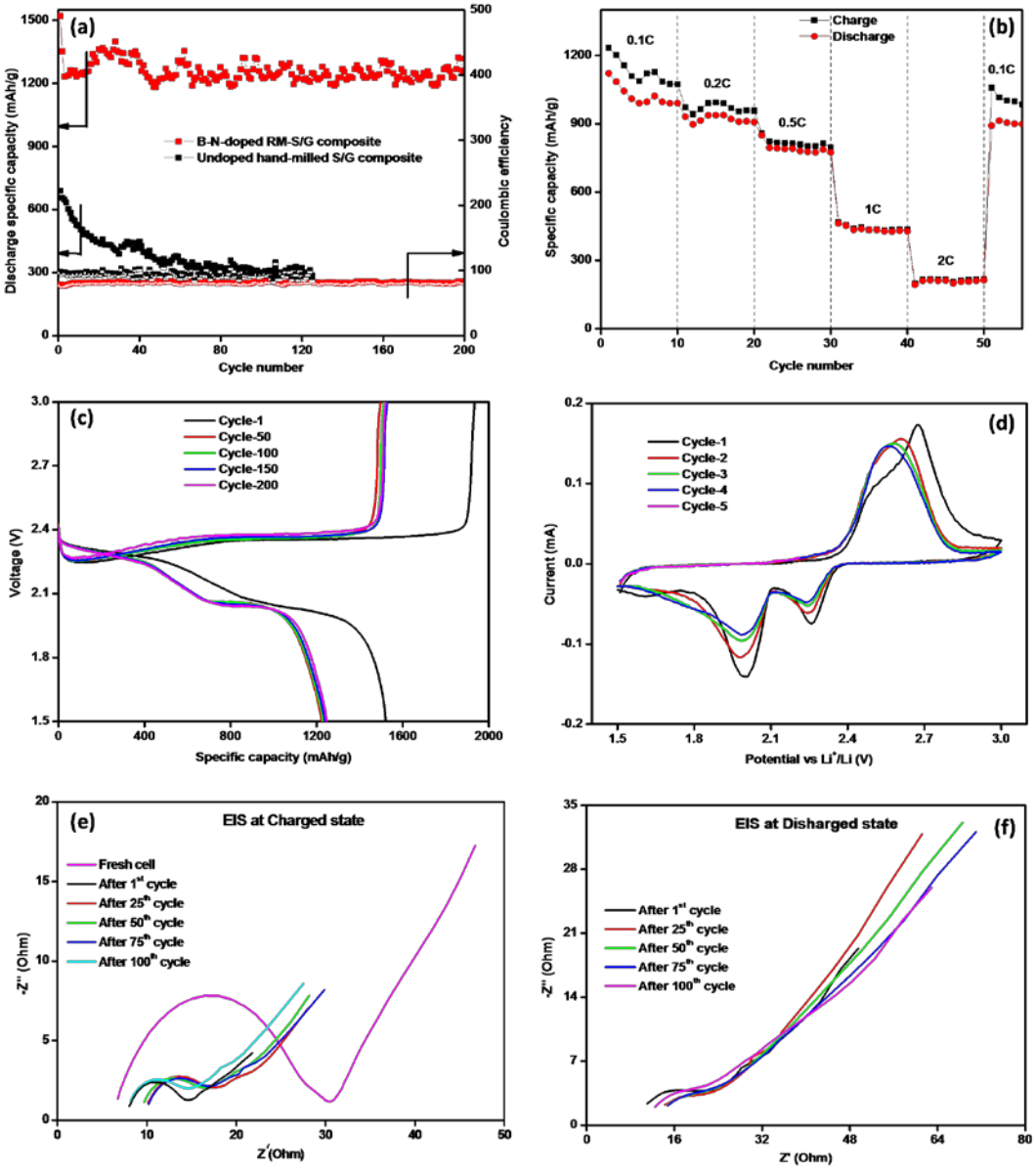

Figure 6.9: Electrochemical performance of RM-S/G composite loaded on boron, nitrogen-doped carbon cloth: a) comparison of cycling performance of B,N-doped RM-S/G composite with hand-milled undoped-sulfur/graphene at a current density of 0.1C, b) rate capability of doped-RM-S/G composite at different current densities, c) charge-discharge curves for selected cycles of doped-RM-S/G composite at 0.1C, d) cyclic voltammograms for the first 5 cycles of doped-RM-S/G composite at a scan rate of 0.1 mV s^{-1}, and e,f) EIS curves in the charged and discharged states for selected cycles.

Figure 6.9 shows the electrochemical performance of the RM-S/G-composite-loaded B,N-doped carbon cloth cathode, where each cathode contains more than eight milligrams of active materials (~8-9 mg/cm^2). The cycling performance shows that, even at higher loading, 1256 mAh/g specific discharge capacity was obtained after 200 cycles at a current density of 0.1C. Considering the performance from the second cycle, 99% capacity retention was achieved with moderate coulombic efficiency. To understand the effects of doping and the benefits of the reverse microemulsion method, the cycling performance of hand-milled undoped-sulfur/graphene composite was also evaluated. The hand-milled undoped-sulfur/graphene composite cathode was shown to exhibit a discharge capacity of 300 mAh/g after 100 cycles with capacity retention of 40% at 0.1C current density. It can be deduced from the cycling performance that the doped 3-D carbon cloth and the reverse microemulsion method make a significant contribution to achieving higher capacity and better capacity retention. The rate performance of the RM-S/G-composite-loaded B,N-doped carbon cloth cathode (Figure 6.9b) also shows that, even at higher current density, this cathode can deliver acceptable discharge capacity and can regain its capacity when low current density is restored. The charge-discharge profile and CV curves show that, with the addition of doped-carbon cloth, there are no negative effects on the cell chemistry. The well-known two

reduction peaks and one oxidation peak were observed in the CV curves, and two discharge plateaus and one charge plateau were observed in the discharge-charge curves, respectively.

For sulfur cathode with high active material content (generally more than 5 mg/cm^2), precipitation of the active material is observed due to loss of contact between the current collector and the active material, which increases the internal impedance of the cell [253]. To analyse this, electrochemical impedance spectroscopy (EIS) was used to measure the electrolytic resistance (R_e) along with charge transfer resistance (R_{ct}) and diffusion. Figure 5e and 5f shows the EIS curves of RM-S/G composite-loaded B,N-doped carbon cloth cathode in the charged and discharged states. In both cases, the curves show a depressed semicircle followed by an inclined straight line, which reflect the charge transfer resistance and diffusion, respectively. It can be seen from the EIS curves that the fresh cell has an electrolytic resistance (R_e) of 7Ω and a charge transfer resistance of 23Ω. The R_e value remains almost constant at different cycle numbers, however, but the R_{ct} is reduced significantly from 23Ω to 8Ω, even after 100 cycles in the charged state. A similar trend was observed in the discharged state, where both the R_e and R_{ct} values remain same at different cycle numbers, which indicates that the active materials didn't precipitate out to the electrolyte and maintained a firm adhesion to the carbon cloth.

6.4. Conclusion

It can be concluded from all of these results that the reverse microemulsion method can effectively exfoliate the carboxylated-graphene and form a sulfur/graphene composite, where the graphene sheets adhere to the surfaces of the sulfur particles as well as being well-dispersed inside the agglomerated sulfur particles. This synthesized composite shows high and stable cycling performance. The active material loading was only 1 mg/cm^2, however, which was not sufficient for scaling up. B,N-doped 3-D carbon cloth was introduced to increase the active material loading as well as further improving the discharge capacity. With

the help of 3-D carbon cloth, we successfully incorporated more than 8 mg/cm^2 of active material, achieving 1256 mAh/g discharge capacity and more than 99% capacity retention.

Chapter 7. A Methodical approach for Fabrication of Binder-free Li_2S-C composite Cathode with High Loading of Active Material for Li-S Battery

7.1. Introduction

It is now a great challenge to the scientific committee to improve the capacity of existing energy storage devices due to the advent of new electronic devices, electric cars, and hybrid electric vehicles. Commercially available rechargeable batteries show specific energy of 400 Wh kg^{-1} which is almost to their theoretical limit but still falls far short of expectations for high energy applications [3, 164]. It seems impossible to increase the specific energy of these existing batteries due to the inherent capacity limitations of the materials. Therefore, it is necessary to introduce new materials for high energy battery applications.

Among all the promising rechargeable batteries, the Li/S system is considered a strong candidate to replace the currently available commercial batteries, due to its availability, low cost, and high performance. The poor electrical conductivity of sulfur, however, the dissolution of long chain polysulfides into electrolyte, and the expansion in volume during the sulfur to sulfide transformation are the limiting factors for sulfur-based battery systems [54]. Extensive research has been conducted to reduce the impact of these problems by applying different techniques to load sulfur onto carbon materials [37, 48, 181-184]. Engineered sulfur-based cathode materials [185, 210, 226], as well as different electrolytes, binders [187, 188], and additives [60, 108, 110, 189, 211], are also being meticulously studied to solve these problems, but yet to be successful. Moreover, in the Li/S system, it is necessary to achieve full lithiation of the sulfur during discharging to achieve higher discharge capacity. Unfortunately, this is unlikely to happen with elemental sulfur-based cathode, which negatively affects the performance of the Li/S cell. On top of that, the

metallic lithium that has been used as anode for the Li/S system forms dendritic structures during operation, which penetrate through the separator and can cause short circuits and fire. Besides this major safety concern, metallic lithium is highly reactive, so it reacts with the electrolyte and degrades the cell performance. Considering all the shortcomings of elemental sulfur-based cathode, the performance and the safety concerns for the Li/S battery can be ameliorated by using prelithiated cathode, which helps to avoid the direct use of metallic lithium [254].

Lithium sulfide (Li_2S) has about four times higher theoretical capacity (1166 mAh/g) than that of commercial cathode materials, and also has a very high melting point (938 ^oC), which allows it to perform even at higher temperature. With the advantages of full lithiation of sulfur, Li_2S can also be paired with different anodes (e.g. tin, silicon, etc.) which eliminate dendrite formation and the safety issues of metallic lithium [47]. Moreover, Li_2S, which has a low density than sulfur, undergoes volumetric contraction rather than expansion during charging and discharging, resulting in less structural damage to the cathode. Although Li_2S has a number of advantages over sulfur, it also has some challenges to overcome. Unlike sulfur, Li_2S is very sensitive to moisture and needs to be activated when coupled with anodes. It is also electronically and ionically nonconductive and has very large particle sizes [255].

Few efforts have been directed towards mitigating the aforementioned shortcomings of Li_2S. Among them, Yang et al. [256] ball milled Li_2S and Al_2O_3 to reduce the size of the Li_2S particles and to increase the conductivity of the Li_2S. Similar ball-milling approaches along with cathode fabrication in inert environment (glove box), high 1^{st} cycle activation voltage (~4V) were adopted by other groups [48, 255, 257] to fabricate Li_2S-C composites with different carbon sources, to prevent moisture absorption and to activate the active material. Besides mechanical mixing and grinding processes, *in-situ* chemical processes were also

adopted to fabricate fine-grained Li_2S-C composite with increased conductivity [258, 259]. However, none of their works focused on suitable carbon material selection through ball milling method along with high active material content.

In their methods, both the mechanical and the chemical processes, however, the electrodes were prepared by the conventional slurry casting method where a large proportion (~around 50%) of the slurry consists of binder (e.g., poly(vinylide difluoride) (PVDF) and carboxymethyl cellulose (CMC)), solvents (e.g. N-methyl-2-pyrrolidone (NMP), and other conductive additives which has no positive contribution on discharge capacity. In some cases, the active material content is reduced to 30-40 wt% to accommodate the various additives. It has been found that, among these inactive materials, the binder has some adverse effects on cell performance. Most of the binders are insulating in nature and increase the internal resistance of the cell. Moreover, at high temperature, binders (e.g. PVDF) decompose into toxic compounds (e.g. hydrofluoric acid, fluorocarbons, etc.) [51, 260].

Eliminating the binder content is not the only way to increase the active material content and to achieve better capacity. A three-dimensional (3-D) interconnected metallic network such as nickel (Ni) foam has a large accessible surface area with high electrical conductivity, and can accommodate and utilize high amounts of active material. Researchers from all over the world [250-252] have focused their attention on 3-D network structures to load larger amounts of active material while maintain higher electrical conductivity, thermal stability, and structural integrity. They found that a 3-D interconnected network is an ideal means to allow the transport of electrons and ions during charging and discharging of a battery [50, 261-263]. It is necessary, however, to develop a systematic approach to finding suitable carbon sources for fabrication of Li_2S-C composite through the ball-milling process. The usage of 3-D multi-layered Ni foam for encapsulation of Li_2S-C composite to produce high

active material content binder-free 3-D-structured cathode is reported for the first time here. In this work, microsized Li_2S powder was ball milled with four different carbon sources to synthesize Li_2S-C composites, where smaller size Li_2S particles were mixed uniformly with conductive carbons. From physical and morphological examination, suitable carbon source was selected among the four carbons. The fabricated composites were then capillary-deposited in 3-D multi-layered Ni-foam from a dioxolane (DOL)-containing mixture with high amount active material. To facilitated the electrochemical activation of Li_2S-C composite by reducing the initial potential barrier, in the 1st cycle the cells were charged to 3.5V with a very low current density. In addition, a conductive, single-walled carbon nanotube (SWCNT) free-standing layer with a refined, woven-like structure was inserted in between the cathode and the separator to improve the initial capacity and capacity retention. Finally, a comparative study was conducted to analyze the effects of binder and 3-D multi-layered Ni-foam.

7.2. Experimental

7.2.1. Synthesis of Li_2S-Carbon Composite: Due to the sensitivity of Li_2S to moisture and air, the fabrication process and materials preparation were conducted inside an argon-filled glove-box. Commercial Li_2S was purchased from Sigma-Aldrich with larger mesh size (10-20 µm), and a carbon source were ball-milled together in a planetary ball mill at 100 rpm, with a 10:1 ball to Li_2S weight ratio, to synthesize the Li_2S-C composite. Same procedure and similar parameter were used for fabricating Li_2S-C composite for four different carbon sources. The other ball-milling parameters were chosen from our previous work on Li-S [162]. The ratio of Li_2S to carbon was 70:30. Four different carbon sources, carbon black (CB), activated carbon (AC), graphene (GP), and multi-walled carbon nanotube (MWCNT) were used for synthesizing four different Li_2S-C composites. Among the four carbon sources,

GP was synthesized in our laboratory through a modified Hummers' method [264], and the other three are commercial grade purchased from Sigma Aldrich.

7.2.2. Fabrication of Li_2S-C composites encapsulated in 3-D Ni-foam electrode: First, the Ni foam was cut into circular disks with a diameter of 9.5 mm. The average areal weight of each Ni-foam disk is around 25 mg/cm^2. The disks were then washed with distilled water followed by ethanol. Then, the disks were put into an ethanol-containing beaker and sonicated for 10 minutes to remove all microsized contaminations. Then, the disks were dried at 80 ^oC for 24 hours under vacuum and transferred to the glove box. Before encapsulating the Li_2S-C composites in the Ni-foam disks, the weight of the each disk was measured, in order to calculate the amount of active material that was loaded into each disk. For encapsulation of the active material, a certain amount of Li_2S-C composite was mixed with DOL in a mortar. Then, the disks were dipped into the slurry to encapsulate the active material. Through capillary action, the pores of the Ni foam were filled with active material-contained DOL which were later dried inside the glove box at room temperature. It should be noted that DOL, which is an organic compound, can sublime easily at room temperature. After the evaporation of DOL, the disks were mechanically pressed to entrap the active materials in the 3-D Ni-foam. Each 9.5 mm disk electrode contained ~5-6 mg of active materials (Li_2S-C).

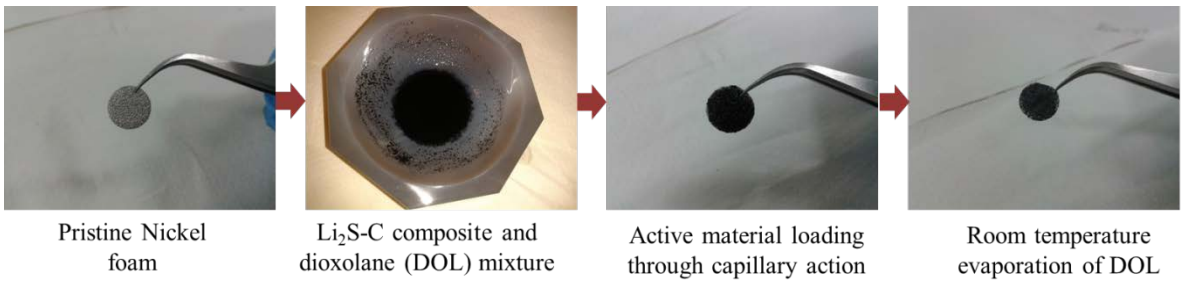

Figure 7.1 Encapsulation of active materials in 3-D Ni foam.

The sequence of active material loading into the Ni foam is shown in Figure 7.1. For fabrication of Li_2S-C composites with binder, polyvinylidene fluoride (PVDF) was added into the composite in such a way that the ratio of Li_2S to carbon to PVDF was kept at 60:30:10. A certain amount of mixture was mixed in a mortar with NMP to make slurry. When the PVDF was dissolved in the NMP, the disks were dipped into the mixture, which was followed by vacuum drying at 80 ^oC for 48 hours.

7.2.3. Fabrication of SWCNT free-standing layer: 15 mg SWCNT with 500 ml de-ionized water were poured into a beaker, and 500 mg Triton-X100 surfactant was added. Then, the solution was probe-sonicated for 1 h with a 2 s pause time, followed by vacuum filtration and washing with de-ionized water and ethanol. The polytetrafluoroethylene (PTFE) filter paper with the SWCNT layer was dried under vacuum overnight at 60 ^oC, and finally, the SWCNT layer was easily peeled off from the filter paper [205, 265].

7.2.4. Fabrication of cells: The CR 2032 coin-type cells were assembled in an Ar-filled glove box, where discs of Li foil were used as the counter electrode and reference electrode. The electrolyte was prepared by dissolving 1 M lithium bis(trifluoromethane sulfonyl)imide (LiTFSI) and 0.1 M $LiNO_3$ in co-solvents of 1,3-dioxolane (DOL) and 1,2-dimethoxyethane (DME), with a volume ratio of 1:1 and the amount that was used for each coin cell was around 100-200 µL. A porous polypropylene film was used as the separator. A SWCNT free-standing layer with an areal mass of 1.5 mg/cm^2 and 1~3 µm thickness was inserted in between the cathode and the separator in some cells.

7.2.5. Characterization: To characterize the Li_2S-C composite and Li-S cells, different analytical tools were used. For physical and morphological characterization of the composite, X-ray diffraction (XRD, GBC MMA 017) and field emission scanning electron microscopy (SEM; JEOL: FESEM-7500) were used. A scanning electron microscope was also used for

conducting large-area energy dispersive X-ray spectroscopy (EDS) mapping. For electrochemical performance evaluation of the Li-S cell, an automatic battery tester system (Land®, China) was used at various current densities at room temperature. For testing the cycling performance, the cell was activated by charging it to 3.5V with very low current density (C/200, 1 C = 1166 mAh/g_{Li_2S}). From the following cycle, a conventional voltage window (1.7-3 V) was applied. Electrochemical impedance spectroscopy (EIS) and cyclic voltammetry (CV) measurements were performed on a Biologic VMP 3 electrochemical workstation over a frequency range of 10 mHz to 100 kHz, and the scan rate was 0.05 mV within a 1.5 V to 4 V voltage window.

7.3. Results and discussion

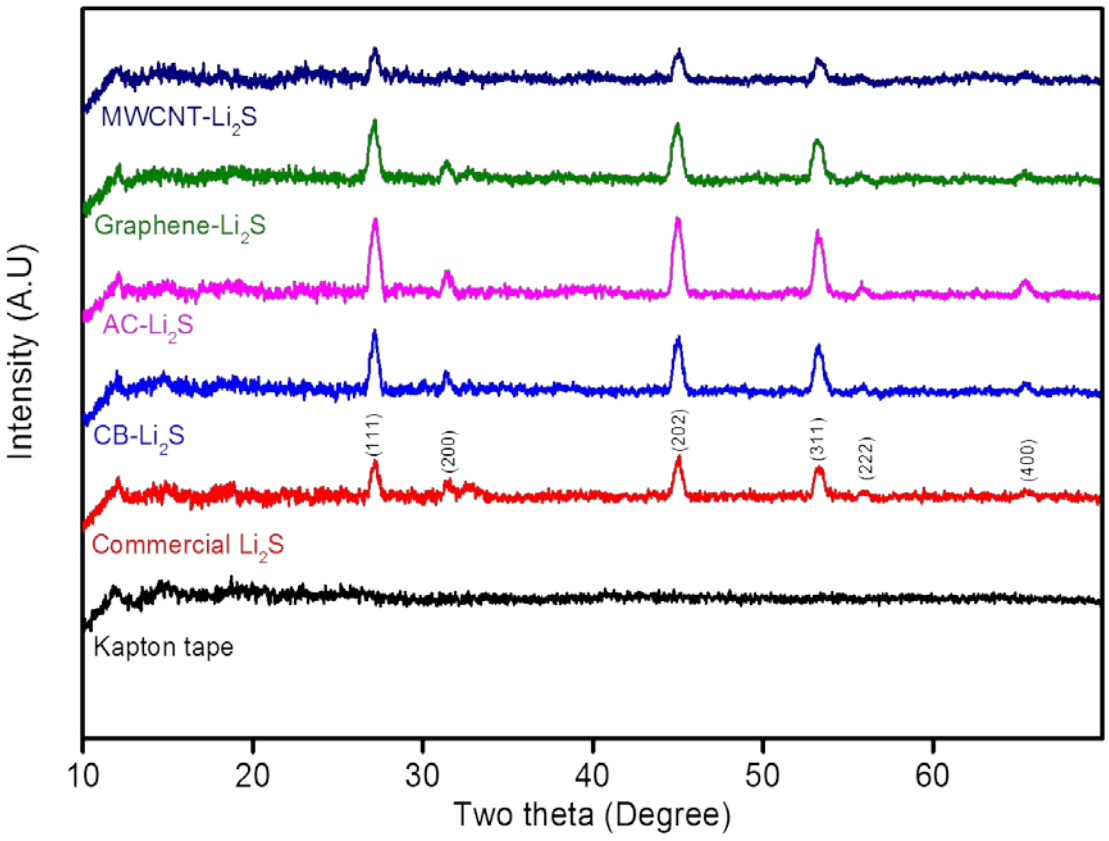

Figure 7.2 XRD patterns of Li_2S-C composites.

The X-ray diffraction (XRD) patterns of all Li_2S-C composites, along with commercial Li_2S, are shown in Figure 7.2, which clearly shows that all four composites exhibit characteristics peaks of Li_2S. As is well known, Li_2S has an antifluorite structure and has higher atomic packing density on the (111), (200), and (311) planes, and for this reason, all the major peaks for Li_2S come from the (111), (200), and (311) planes [266]. The intensity of the peaks for all four composites looks similar, however, except for Li_2S-MWCNT, where the peak intensities are much smaller than for the other composites, which means that, in Li_2S-MWCNT composite, Li_2S has less favorable condition to reflect the X-ray beams from those particular planes. In other words, it can be said that MWCNT, which has a very high aspect ratio (length to diameter ratio), managed to adhere and successfully cover the Li_2S particles, reducing the intensity. It should be mentioned that all the samples were covered with Kaptontape before the XRD analysis due to the sensitivity to moisture and air of Li_2S. Figure 7.3 shows the XRD sample preparation using Kapton tape.

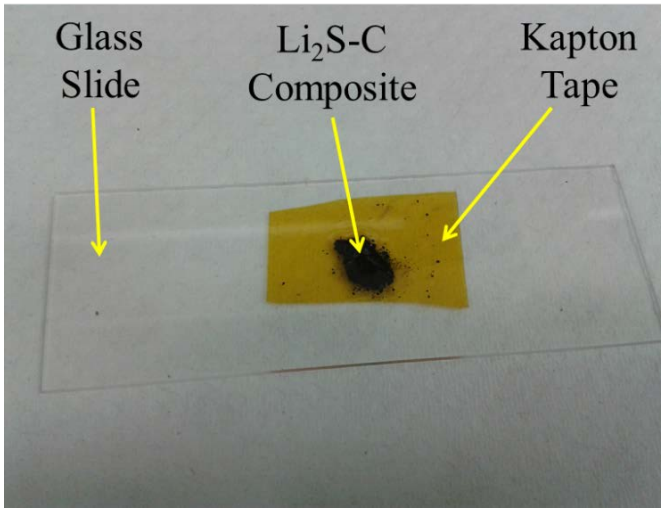

Figure 7.3 Sample prepared for XRD analysis.

Field emission SEM (FESEM) micrographs of the four carbon sources are presented in Figure 7.4, which clearly shows the sizes and structures of the four different carbons. CB

particles look spherical, whereas AC particles have an arbitrary flake shape. On the other hand, GP is in the form of agglomerated two-dimensional sheets, and MWCNT has a fiber-like structure with a very high aspect (length to diameter) ratio. These FESEM images were of help in analyzing the morphology of the ball-milled Li_2S-C composites that have been fabricated using those four carbon sources.

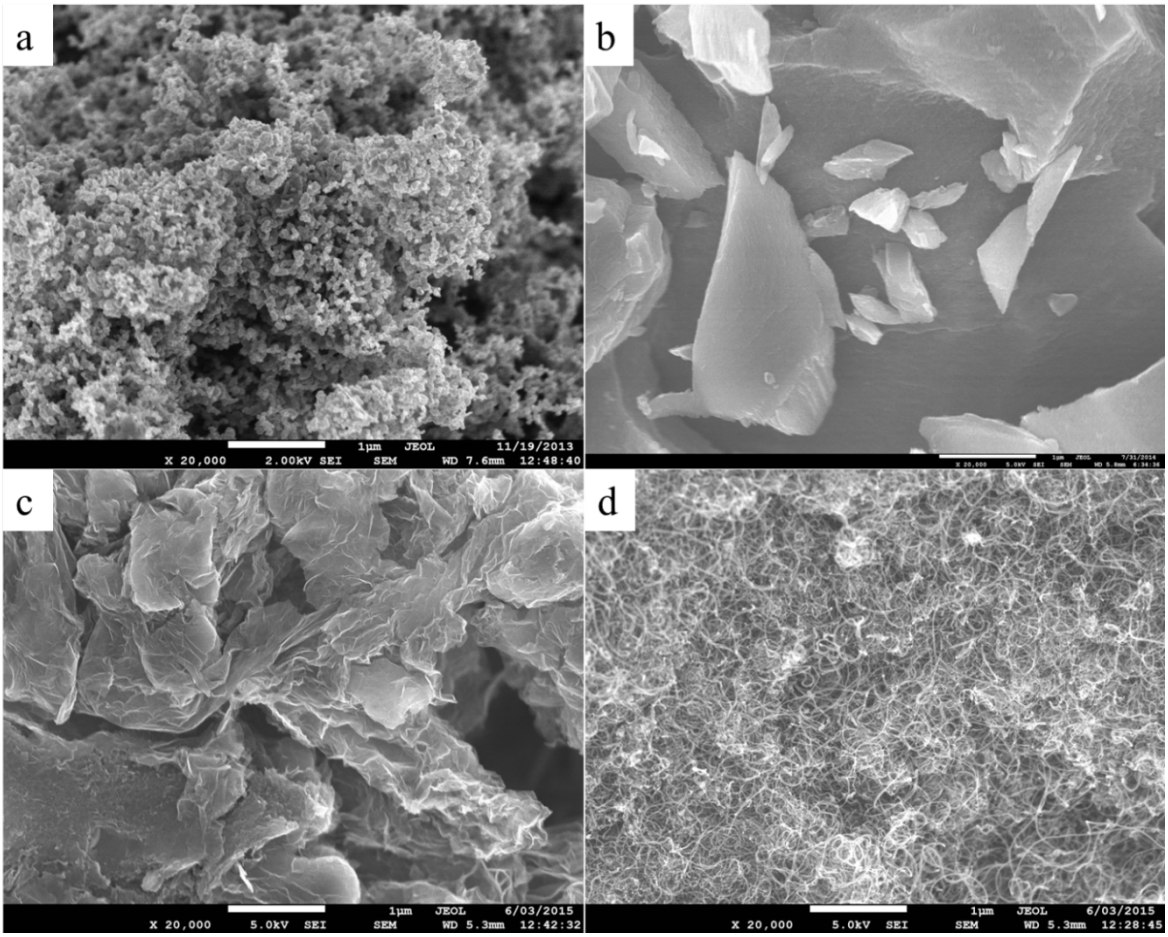

Figure 7.4 FESEM images of a) carbon black (CB), b) activated carbon (AC), c) graphene (GP), and d) multi-walled carbon nanotube (MWCNT) (Scale bars for all the figures are 1 μm).

Figure 7.5 shows the morphology of the ball-milled composites along with pristine Li_2S. It is clearly shown in Figure 7.5b and 7.5c that CB and AC are discretely dispersed and do not adhere to the Li_2S particles. This is because the CB and AC are much smaller in size

compared to Li_2S, and the percentage of carbon that has been added into the composite, which is 30 wt%, is not sufficient to cover the larger size Li_2S particles. On the other hand, the same amounts (30 wt%) of GP and MWCNT not only firmly adhere to the Li_2S, but also covers the Li_2S particles, as is shown in Figure 7.5d and 7.5e. Moreover, the MWCNT covers each Li_2S particles completely because of its very high aspect ratio, which can reduce the insulation problem with Li_2S. From the FESEM micrograph, it can be predicted that the Li_2S-MWCNT composite should have better electrochemical performance compared to the remaining three composites.

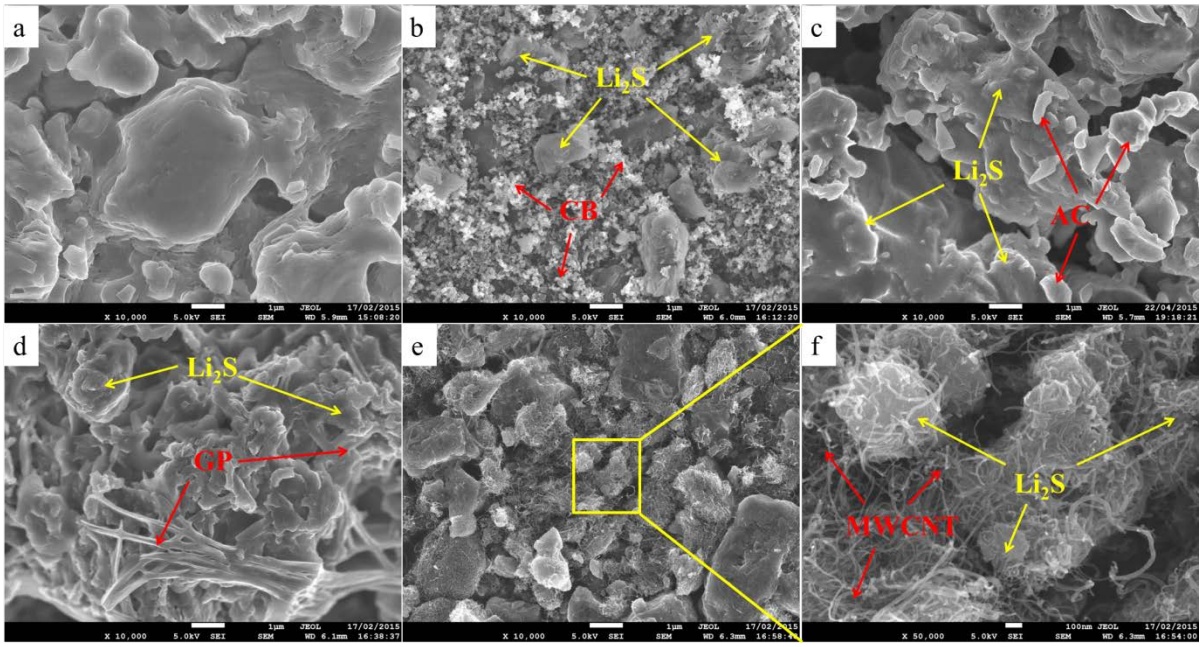

Figure 7.5 FESEM images of a) Li_2S, b) Li_2S-CB, c) Li_2S-AC, d) Li_2S-GP, and e, f) Li_2S-MWCNT composites (Scale bars are 1 µm for Figures-a, b, c, d, e and 100 nm for Figure-f).

For further confirmation of the distribution of the Li_2S particles and the carbon sources in the composite, energy dispersive spectroscopy (EDS) analysis was carried out and is shown in Figure 7.6. EDS mapping clearly shows that both sulfur and carbon coexist in the composite, and in most cases, they are embedded in each other.

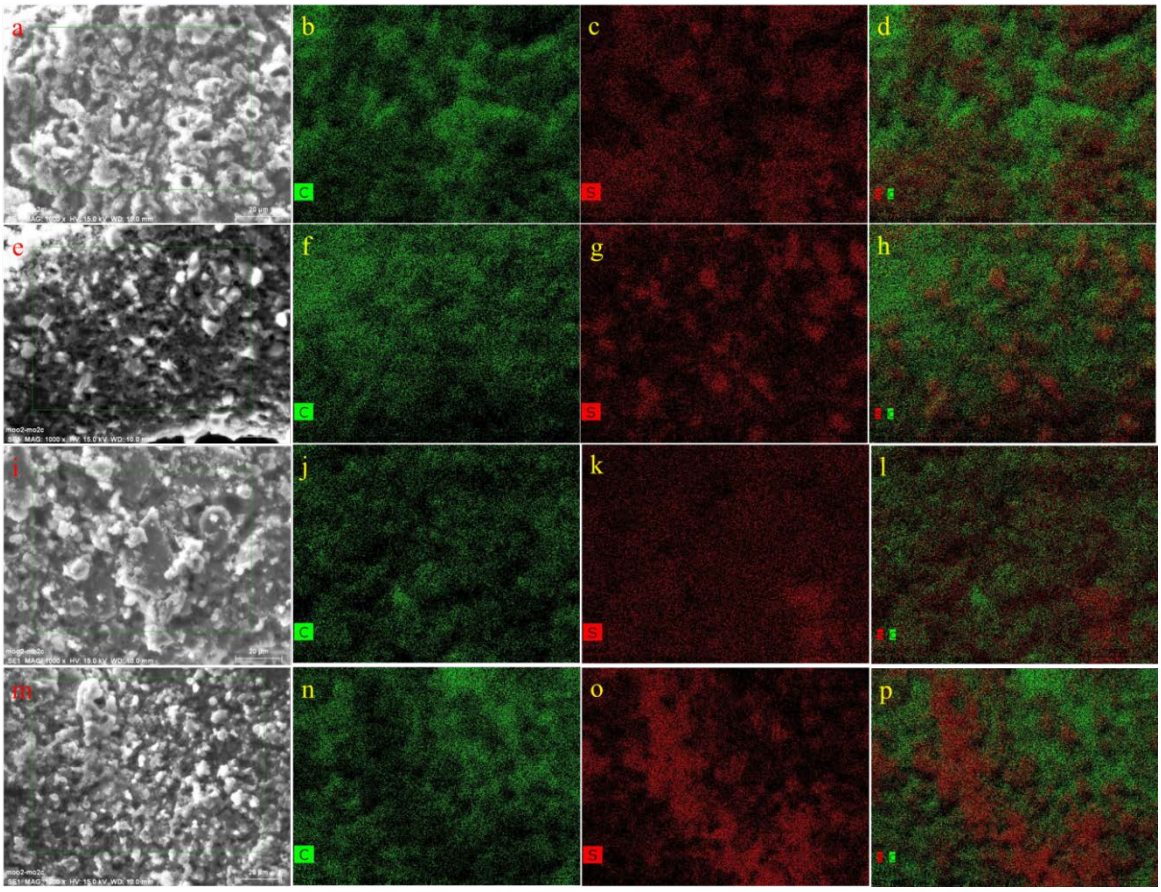

Figure 7.6 EDS mapping of a-d) Li_2S-CB, e-h) Li_2S-AC, i-l) Li_2S-GP, and m-p) Li_2S-MWCNT (Scale bars for all the figures are 20 µm).

Before analyzing the electrochemical performance of Li_2S-C composites cathode, it is worthwhile to mention that conventional Li_2S-C composite cathodes are prepared from slurry which contains active materials, binder, solvent, and other ingredients. This slurry is then pasted onto a two dimensional aluminium foil current collector. It is worthwhile to mention here that the aluminium foil current collector is a two dimensional (2-D) sheet and can be loaded with only a very limited amount of active materials, and in most cases, it can be loaded with 1 mg or less of the active material. Moreover, it is mandatory to add binder and solvent to achieve a firm bonding between the 2-D current collector and the active materials. Sometimes other ingredients are also used to achieve better interfacial bonding between the current collector and the active materials, [49, 257] which not only reduces the active

material content, but also increases the internal resistance of the cell. Furthermore, the binders, solvents, and other ingredients cost extra money, which could be a stumbling block for commercialization.

Table 7.1 Comparison of properties and performance of Li_2S-C composites for Li/S battery.

Discharge capacity (mAh/g $_{Li_2S}$)	Binder use	Active material (wt%)	Active material (mg/cm^2)	Current collector	Reference
250 after 50 cycles	Yes	60	NA	2-D Aluminium foil	[105]
650 after 80 cycles	Yes	NA	1.0	Carbon nano fiber	[106]
380 after 20 cycles	Yes	38	NA	Copper composite	[47]
600 after 100 cycles	Yes	60	1.0-1.5	2-D Carbon paper	[258]
550 after 400 cycles	Yes	60	NA	2-D Aluminium foil	[267]
650 after 150 cycles	Yes	NA	1.0	2-D Aluminium foil	[268]
500 after 50 cycles	Yes	40	1.0	2-D carbon paper	[256]
550 after 150 cycles	Yes	NA	1.0	2-D Aluminium foil	[259]
620 after 100 cycles	No	NA	1.0	MWCNT paper	[269]
300 after 95 cycles	Yes	55	0.96	2-D Aluminium foil	[270]
320 after 20 cycles	Yes	49	1.1-1.4	2-D Aluminium foil	[102]
450 after 150 cycles	No	NA	0.8-1.5	Graphene oxide layer	[260]
437 after 100 cycles	No	70	5.0-6.0	3-D Nickel foam	This work

Table 7.1 tabulates the relationships among the active material content, current collector, binder content, and the discharge capacity in the most recent papers investigating Li_2S-C composite cathode. It clearly shows that, for fabrication of Li_2S-C composite cathode, different binders were used in almost every case and achieved allowable discharge capacity. It is also noticeable from Table 7.1 that, in all the works on Li_2S that are currently available from open sources, their conventional 2-D current collector can barely be loaded with 1.5 mg/cm^2 active materials. To increase the active material content, a 3-D network or

framework needs to be considered. The use of 3-D conductive network materials in battery application is a promising feature that has already been used on several occasions. Xi et al. [51] used a 3-D graphene network to produce binder-free sulfur cathode. Zhao and Sa [271, 272] used 3-D Ni foam as a framework for the electrodeposition of sulfur materials and as current collector, respectively. All of them managed to achieve better electrochemical performance compared to that with a conventional 2-D Al-foil current collector.

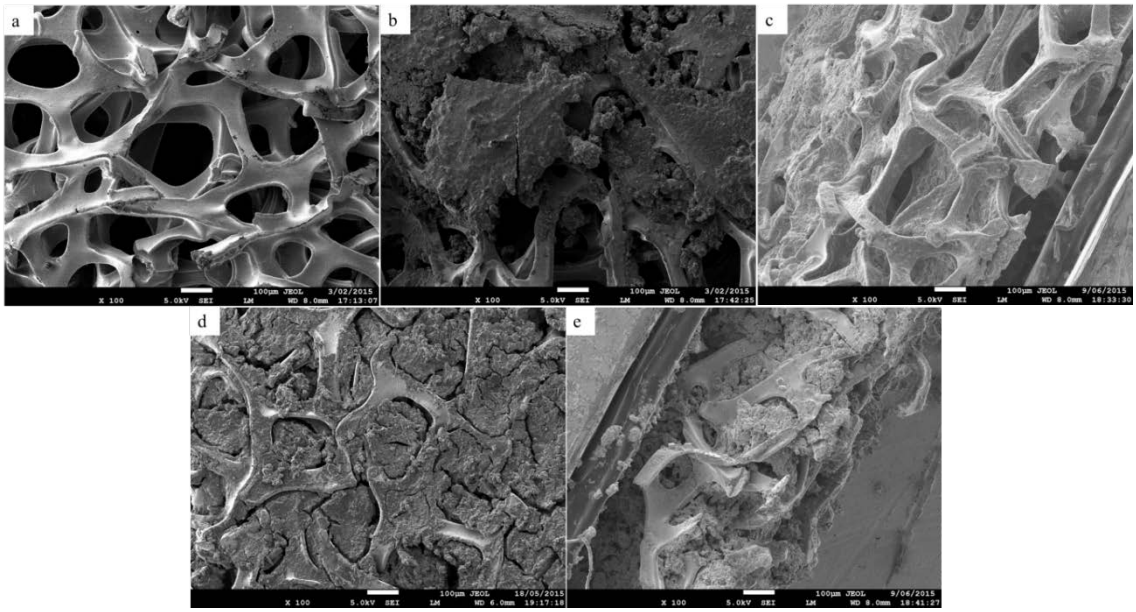

Figure 7.7 FESEM image of a) Ni-foam, and b, c) top view and side view images of Li_2S-MWCNT composite cathode, where the active material was loaded in Ni-foam through powder dispersion; d, e) top view and side view images of Li_2S-MWCNT composite cathode where the active material was loaded in Ni-foam through capillary deposition (Scale bars for all the figures are 100 µm).

3-D Ni-foam, which consists of several layers and many micropores, can accommodate a large amount of active materials and can maintain its structural integrity after active material loading. Figure 7.7a presents a micrograph of the pristine Ni-foam where a microporous 3-D layered network structure is clearly visible. The lodgment of the active material in the foam

has been done into two different ways, which are direct dispersion and capillary deposition. In both cases, the cathodes were pressed after the active material loading to achieve better mechanical confinement and interfacial bonding between the Ni-foam and the active material. Figure 7.7b and 7.7c respectively shows a top and side view of the morphology after direct active material dispersion (conventional dispersion method). From these two images, it is clear that the conventional deposition method is not suitable for loading high amount active material. The micro-sized Li_2S powder particles and carbon particles adhered to each other and failed to penetrate the Ni-foam pores. For this reason, most of the pores remained empty, and small amounts of active materials just adhered to the top of the Ni-foam surface. The side view (Figure 7.7c) shows that the materials cannot percolate to every layer, which reduces the active material content. On the other hand, the capillary deposition method can load more active material and provide better interfacial bonding. In the capillary deposition method, the active material can be loaded into each layer of the foam due to capillary action, which is unlikely to happen in the direct dispersion method. Figure 7.7d and 7.7e shows front and side views of a capillary deposited cathode and reveals that the active material is loaded into each layer of the foam. On top of that, due to capillary action, all the pores are completely filled by the active materials, which increased the active material content. It is important to mention here that DOL is an electrolytic compound that is used in the capillary deposition method as a solvent and is later evaporated, so that the active material is entrapped in the Ni-foam network. Moreover, DOL, which is liquid at room temperature (25 ^{o}C) and pressure (1 atm) does not react with the cathode surface and active materials.

With the help of this capillary deposition method, large amounts of active materials were deposited in the Ni-foam, and in every case, 5 mg/cm^2 and more (5 to 6 mg/cm^2) of the active materials were loaded in each electrode (9.5 mm diameter disk), which is the maximum

amount compared to the all other results that are available from open sources. After the active material loading process, the electrochemical performance of the electrodes was evaluated for all four different carbon sources, and the best Li_2S-C composite was found among them. Unlike sulfur-carbon cathode, Li_2S-C cathode is fabricated in the discharged state and needs to be activated before measuring its electrochemical performance.

For activating the Li_2S-C cathode, an upper high cut-off voltage (~ 4 V_{Li}) is usually applied by the researchers. They believed that the initial high cut-off voltage for charging promoted phase nucleation of the two-phase reaction between Li_2S and polysulfides [256]. At 4V, however, most of the ether-based electrolytes are not stable and start to dissociate. For this reason, researchers have tried to avoid a high cut-off voltage for the activation process [104]. They tried to use a redox-mediator in electrolyte, which can allow the recovery of most of the Li_2S theoretical capacity in the activation cycle at potentials as low as 2.9 V_{Li}.

Yang et al. [256] reported that the current density during first charging has a significant effect on the activation of the Li_2S-C cathode. They found a linear relationship between the overpotential and the current rate. They also claimed that the overpotential, which is the energy needed for phase nucleation to reduce the initial potential barrier, remains nearly constant and is quite small at low current. Inspired by their work, we used a very low current density (C/200) for the first cycle to activate the cathode. On top of that, we charged the cell to 3.5V instead of 4V for the first cycle. It is found that, in most cases Li_2S is activated at 3.5V when a very low current density is applied which will protect the electrolyte from being dissociated. In the following cycles, the cathode need not be activated at 3.5V, and hence, a conventional voltage window (1.7-3 V) was applied.

The charge discharge profile of the activation process is shown in Figure 6.8a, where the cell was charged to 3.5 V with a current density of C/200. In the charging profile, it is seen that,

the voltage is rapidly increased to 3.25V at the beginning of the charging and then dropped down to 3V followed by gradual increment to 3.5V. The initial rapid increment of voltage is known as the initial potential barrier of the cell which usually varies on the current density the charging. It is well known that the most suitable voltage window for ether-based electrolyte for the Li-S system is 1.5 V to 3 V, and Meini et al. [104] showed that the energy band gap between highest occupied molecular orbital (HUMO) and lowest unoccupied molecular orbital (LUMO) for ether-based electrolyte is around 4-4.5V but it can hardly be used this voltage window due to the formation of thick solid electrolyte interface (SEI). There is an inverse relationship between SEI thickness and electrolyte band gap. In most of the Li/S system, the SEI thickness is quite high which force to reduce the voltage window and beyond 3.6 V, the ether-based electrolyte in Li/S system starts to dissociate [273]. It is also shown in Figure 7.8a that, at 3.5 V upper cut-off voltages, the cell can achieve 990 mAh/g charge capacity, which is very close to Li_2S theoretical capacity (1166 mAh/g). So, it can be said from above discussion that, it is possible to activate Li_2S-C composites at 3.5V. This low voltage activation phenomenon has a substantial influence towards obtaining better discharge capacity.

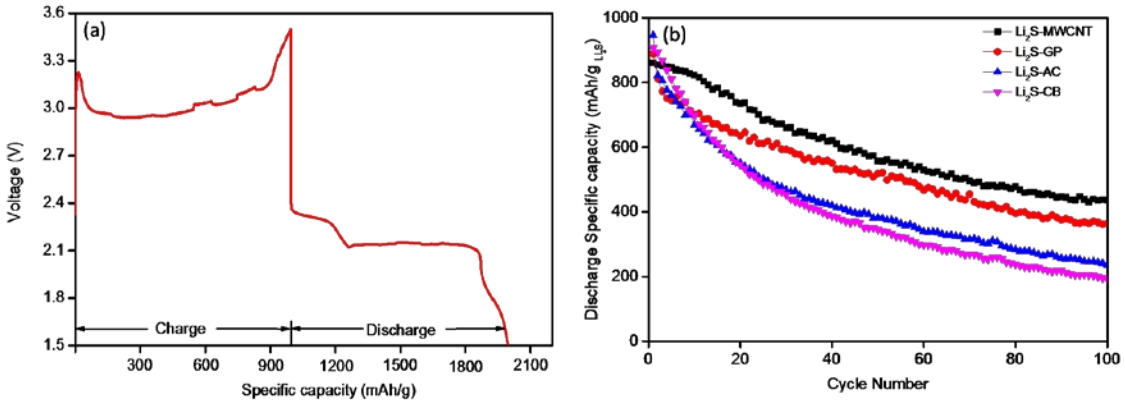

Figure 7.8 (a) Charge discharge profile of first cycle for activation of Li_2S-MWCNT composite (b) Cycling performance of Li_2S-C composites at the 0.1 C rate.

Beside the activation charging profile, Figure 7.8a shows the discharge profiles of the Li_2S-C composites, and as expected, the discharge profiles of the Li_2S-C composites for both activation processes are similar to the discharge profile of the conventional Li-S cell. In the discharge curves, two plateaus are observed, with the first plateau related to the transformation from elemental sulfur to long chain lithium polysulfides (Li_2S_n, $n \geq 4$), and the second plateau representing the reduction of long chain lithium polysulfides to short chain lithium polysulfides (Li_2S_n, $n < 4$). After the activation process, all four Li_2S-C composites were tested for cycling performance, and the results are shown in Figure 7.8b. Li_2S-AC and Li_2S-CB show higher initial capacity of 945 mAh/g and 906 mAh/g, respectively, compared to Li_2S-GP and Li_2S-MWCNT with 860 mAh/g and 888 mAh/g, respectively. Li_2S-MWCNT shows the highest capacity retention of 50.7%, however, followed by Li_2S-GP (40.9%), Li_2S-AC (25%), and Li_2S-CB (21.3%) after 100 cycles. It was expected from the morphology of this composite, where the Li_2S was fully covered and adhered to by MWCNT, that the Li_2S-MWCNT would exhibit better electrochemical performance compared to the other three composites. It is necessary to mention here that, compared to the other works on the Li_2S battery listed in Table 7.1, the discharge capacity has not significantly improved however, considering active material content which is 5 mg/cm^2; this is the highest discharge capacity that is available when compared to reports in open sources. It can be concluded here that Li_2S-MWCNT composite has better characteristics in terms of morphological and electrochemical performance, and in the following part of this paper; we shall focus only on Li_2S-MWCNT composite for further characterization and improvement.

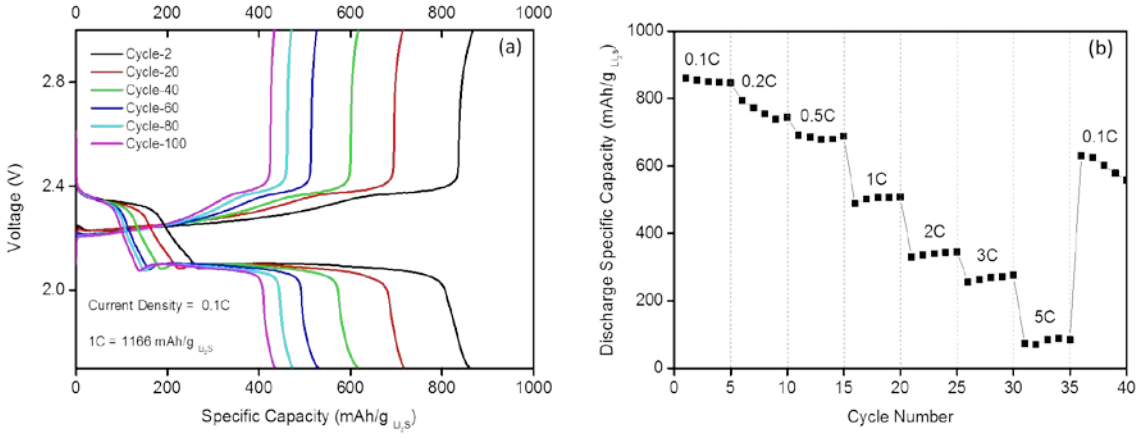

Figure 7.9 (a) Charge-discharge profiles, and (b) rate capability of Li_2S-MWCNT composite.

Figure 7.9a and 7.9b, respectively, shows representative charge-discharge profiles and the rate capability of Li_2S-MWCNT composite. The discharge plateau shows that there is no drastic voltage drop in the discharge profile, indicating very low polarization loss (both activation polarization and concentration polarization) along with internal impedance loss. The latter one can also be determined from electrochemical impedance spectroscopy (EIS), which will be discussed in a later part of the paper. Li_2S-MWCNT composite also shows high capacity at higher current density. The cells were tested at different current densities, varying from 0.1 C to 5 C, and the results show that, even at the 3C and 5C rates, the cells can exhibit a capacity of 300 mAh/g and 80 mAh/g, respectively. It is notable that, in most of the papers on Li_2S-C composite, the authors conducted their testing with a maximum current density of 2 C, and in most of cases, our Li_2S-MWCNT composite shows much better rate capability than in other works [258, 267]. This exceptionally high rate performance may be achieved because of the structural benefit of the 3-D network of Ni-foam along with better carbon sources. This combination not only improved the conductivity of the composite, but also maintained a 3-D conductive network that acted as a better current collector, as well as helping to utilize a higher amount of active materials. In Figure 7.9b capacity fading seems violent when the current density is back to 0.1 C from 5C. However, it is not true in the real

case and it can be explained in this way that, the capacity gain after 35 cycles with different current density is almost similar to the capacity after 35 cycles with 0.1C current density that had been shown in Figure 7.8b. This means that, varying the current density does not have any significant effect on capacity regaining as well as capacity fading.

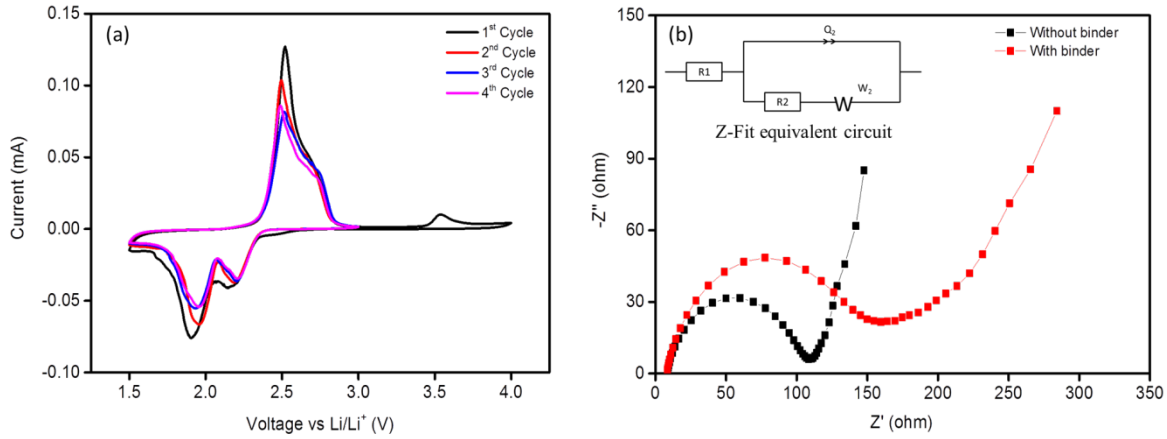

Figure 7.10 a) Cyclic voltammetry (CV) curves for the first 4 cycles and b) electrochemical impedance spectra (EIS) of Li_2S-MWCNT composite. The inset to the EIS spectra is the Z-Fit equivalent circuit.

Table 7.2 Z-fitted EIS results for Li_2S-MWCNT composite.

	Impedance values	R_e (Ω)	R_{ct} (Ω)	CPE (μF)	W ($\Omega.S^{-0.5}$)
Li_2S-MWCNT composite	**Without binder**	7.993	93.51	21.43	19.12
	With binder	7.322	154.8	21.98	45.35

Figure 7.10a shows cyclic voltammograms of Li_2S-MWCNT composite for the first 4 cycles with 0.05 mV s^{-1} scan rate, in which two reduction peaks and one oxidation peak are observed. The first cycle shows a small oxidation peak at 3.5 V, however, along with a very sharp peak at 2.5 V. Yang et al. [256] showed that the peak at 3.5 V indicates the necessity of overpotential to overcome the initial barrier. The EIS results shown in Figure 7.10b are

impedance spectra of Li_2S-MWCNT composite (with and without binder) as cathode, while the inset in Figure 7.10b shows the Z-fitted equivalent circuit for the composite, where the resistance (R), constant phase element (CPE ≈ Q_2), and Warburg impedance element (W) are included. R_e (~R1) and R_{ct} (~R2) represent the solution resistance of the electrolyte and the charge transfer resistance along with the surface resistance, respectively. Q2 represents the CPE, whichis related to the solid-state diffusion of Li^+ due to the formation of a double layer capacitor between the electrolyte and the cathode interface. W is the Warburg impedance element attributable to the diffusion of lithium ions in the active materials. The Z-fitted values of the EIS curves for Li_2S-MWCNT composite with binder and without binder are shown in Table 7.2. Both EIS curves show similar depressed semicircles with similar values of R_e and CPE. The charge transfer resistance (R_{ct}) and Warburg impedance (W), however, are much higher for Li_2S-MWCNT composite with binder than without binder. This is because the polymeric binders are electrical insulators, which impedes the Li ionic movement, as well as electron, movement inside the cell. This is because, linear-chain PVDF is a polar compound with a dipole moment of 2.1D and due to the high dipole moment, PVDF shows significant attraction to the positive Li ion which will impede Li-ion movement in the cathode material. It is important to mention here that the values of R_e and CPE remain the same for both cases, which is due to the structural benefit of the electrode. It is proposed that the 3-D Ni-foam network helps to diffuse Li^+ without increasing the thickness of the solid electrolyte interphase (SEI) and the double layer capacitor.

From Figure 7.8 and Figure 7.9, it is obvious that, as in the case of the Li-S cell, the capacity decay with cycle number is also an important issue for Li_2S-C composite. The main reason behind the capacity fading is the dissolution of polysulfide into the electrolyte, which causes the so-called shuttle phenomenon. To improve the initial capacity and the capacity retention,

a free-standing layer (FSL) of single-walled carbon nanotube (SWCNT) was inserted in between the separator and the cathode, which can increase the conductivity of the sulfur results, high amount active material utilization. This novel approach was first introduced by Manthiram's group [203], and later, it was also adopted by other groups [35, 204] to achieve higher initial capacity and better capacity retention for the Li-S battery. Although there are many similarities between elemental sulfur and Li_2S, this novel approach has not been used for Li_2S-C composite.

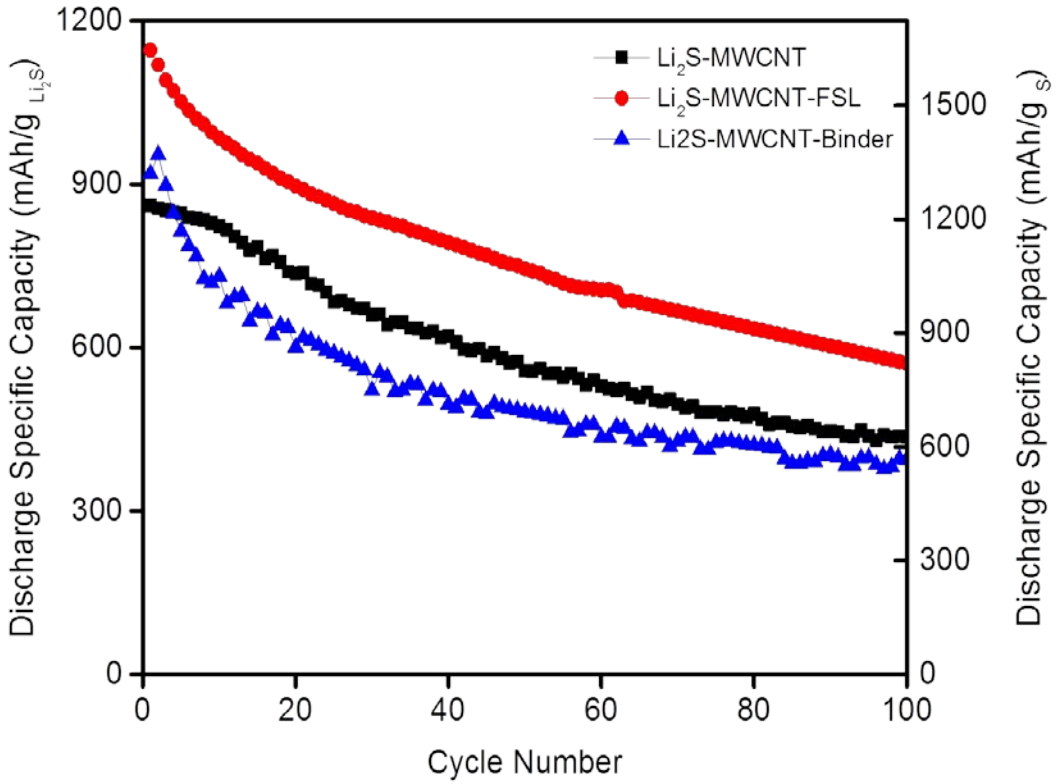

Figure 7.11 Cycling performance at the 0.1 C rate of Li2S-MWCNT composite with binder and FSL.

Figure 7.11 shows the cycling performance of the FSL-containing Li_2S-MWCNT composite, where the FSL was inserted in between the cathode and the separator. Moreover, the cycling performances of Li_2S-MWCNT composite with binder (10 wt% binder) and the bare Li_2S-

MWCNT composite are shown in the Figure for comparison to justify the EIS results that are shown in Table 7.2. The Figure shows that, with the insertion of a FSL, the initial capacity rises to 1146 mAh/g_{Li_2S}, and capacity of 571mAh/g_{Li_2S} is retained after 100 cycles, which is almost 13% higher than without FSL. It is also shown in Figure 7.11 that the addition of binder makes no significant difference to the cycling performance of the Li_2S-MWCNT composite. In terms of capacity retention, however, Li_2S-MWCNT shows 7% more capacity under the same conditions than binder-containing Li_2S-MWCNT composite.

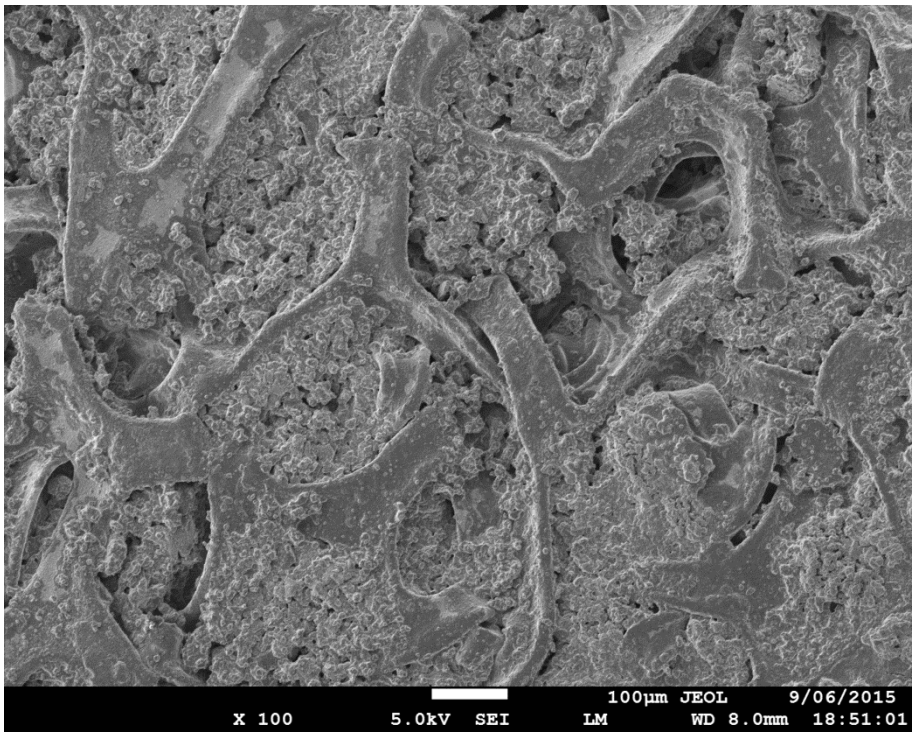

Figure 7.12 FESEM image of Li_2S-MWCNT composite confined in Ni-foam after cycling.

Figure 7.12 presents a FESEM image of binder-free Li_2S-MWCNT composite cathode after 100 cycles, and it clearly shows that the cathode maintains its structural integrity even after 100 cycles. This Figure also shows that, unlike the pristine cathode, the active material of the cathode after cycling does not show cracking and agglomeration. The reason behind this phenomenon is that the continuous contraction and expansion of the active material during cycling and the percolation of electrolyte through the cracks disintegrates the active material,

which increases the active surface area and facilitates the redox reactions, resulting in higher capacity. Hence, it can be said that the 3-D Ni-foam can not only hold a higher amount of active material, but also can maintain the structural integrity of the cathode with just its layered network structure, without the use of any binder.

7.4. Conclusion

Binder-free Li_2S-C composites were synthesized through a high energy ball-milling process with different carbon sources. These composites were then capillary-deposited in 3-D Ni-foam networks. Then, the composites were characterized physically, morphologically, and electrochemically. From the characterizations, it is found that Li_2S-MWCNT composite shows much better morphology and performances than those of other composites. Later, the performance of the Li_2S-MWCNT composite was further improved by inserting a vacuum-filtrated SWCNT free-standing layer in between the cathode and the separator. After insertion of the FSL, the initial capacity of the Li_2S-MWCNT composite was raised to 1146 mAh/g_{Li_2S}, which is equivalent to 1646 mAh/g_S for the Li-S system. Besides superior cycling performance, another important phenomenon is achieved in this work which is the loading of large amount active material (~5-6 mg/cm^2) into the 3-D Ni-foam electrode. The amount of active material that was loaded into each cathode was at least five times higher than that of conventional electrode with a 2-D aluminium-foil current collector. Furthermore, the structural integrity of the 3-D Ni-foam cathode without binder shows similar morphology compare to with binder 3-D Ni-foam cathode, even after 100 cycles.

Chapter 8. General conclusions and outlook

8.1. General conclusions

It has been mentioned several times in this thesis that the Li-S system has a number of promising features to replace the conventional Li-ion system that has been dominant for two decades. This promising system, however, has several severe shortcomings related to the anode, cathode, and electrolyte. The objective of this research work was to minimize these short comings, specifically on the cathode side, and to improve the electrochemical performance. The general conclusion of this research work is divided into four for parts for each individual subproject that was conducted.

It the first work, a systematic way of fabricating Li-S batteries that is suitable for large-scale production, as well as showing minimum shortcomings, has been demonstrated by applying a series of facile methods. The fabrication of porous sulfur was achieved by the industrially-oriented ball-milling method, followed by identification of superior carbon sources for that porous sulfur, by observing their physical, morphological, and electrochemical behaviour. This porous sulfur and a suitable carbon source can significantly minimize the volume expansion problem and conductivity deficiency. After that, a SWCNT free-standing layer was inserted to raise the discharge capacity of the best composite − the activated carbon–sulfur composite. This SWCNT can further improve the conductivity of sulfur and also can minimize the shuttle effect by preventing the movement of longer chain polysulfides. Finally, to retain capacity for a higher number of cycles, a new charging method was applied, which helped to retain the capacity at about 99%. We believe that this method will help to make the Li-S battery commercially viable in the near future, representing a major advance for energy storage devices.

In the second work, a modified chemical method, the spray precipitation method, efficiently produced fine and arbitrary-shaped sulfur particles that have very high surface area. This method was also used to fabricate a carbon-sulfur composite that showed high specific surface area along with a homogeneous distribution of sulfur in the carbon, with the sample denoted as the spray-precipitated carbon-sulfur composite. Because of the homogeneous distribution of sulfur and the high surface area of sulfur-carbon composite, the active material utilization and conductivity of the composite increased significantly. With the combination of these two properties, the spray-precipitated composite shows high discharge capacity with acceptable capacity retention. With the combination of the spray precipitation method and the new capacity-limited charging technique (charging up to 600 mA h g^{-1}), we managed to achieve more than 99% capacity retention after 100 cycles. For further improvement of the conductivity and to reduce the shuttle effect, a free-standing layer of SWCNT was applied in conjunction with the new charging technique, and we managed to achieve high capacity and also retained 91.6% of the initial capacity. Considering the significantly improved discharge capacity and capacity retention, we believe that this spray-precipitation technique, along with the fixed charging method, will represent a quantum leap for the large-scale production and commercialization of the Li-S battery.

In the third work, binder-free Li_2S-C composites were synthesized through a high energy ball-milling process with different carbon sources. By using Li_2S, which is in a fully lithiated state, the volume expansion problem can be fully resolved. Moreover, using it after ball milling with different carbon sources can minimize the conductivity problem of Li_2S. These composites were then capillary-deposited in a 3-D Ni-foam network. 3-D Ni-foam was used to load a high amount of active material, which is essential for commercializing the Li-S cell. From the physical, morphological and electrochemical data, it was found that MWCNT tends to improve the conductivity and active material utilization. Later, the performance of the

Li_2S-MWCNT composite was further improved by inserting a vacuum-filtrated SWCNT free-standing layer in between the cathode and the separator, which further improves conductivity and active material usage. After insertion of the FSL, the initial capacity of the Li_2S-MWCNT composite was raised to 1146 mAh/g_{Li_2S}, which is equivalent to 1646 mAh/g_S for the Li-S system. Besides superior cycling performance, another important phenomenon is achieved in this work, which is the loading of a large amount active material (~5-6 mg/cm^2) into the 3-D Ni-foam electrode. The amount of active material that was loaded into each cathode was at least five times higher than for the corresponding conventional electrode with a 2-D aluminium-foil current collector. Furthermore, the structural integrity of the 3-D Ni-foam cathode without binder shows similar morphology compare to the 3-D Ni-foam cathode with binder, even after 100 cycles.

In the fourth work, a reverse (water in oil) microemulsion technique was applied for fabricating a sulfur/carboxylated-graphene composite. The fabricated sulfur-graphene composite cathode, which contains only 6 wt% graphene, can dramatically improve the cycling stability as well as providing high capacity. This sulfur-graphene composite was later loaded on three-dimensional heteroatom-doped (boron and nitrogen) carbon cloth to achieve high active material content with better stability. The electrochemical data show that, even at high sulfur loading (~8mg/cm^2) on carbon cloth, this composite features 1256 mAh/g discharge capacity with more than 99% capacity retention.

8.2. Outlook

This doctoral thesis work has been mainly focused on the preparation of cathode materials with different fabrication techniques, especially mechanical milling and chemical reaction methods. The structure − property relationship of the synthesized composite has been investigated thoroughly, and the electrochemicalperformance was studied as well. Even

though sulfur-carbon composite cathode has been studied meticulously here, a number of challenges remain unsolved, which need to be solved before it is possible to commercialize lithium/sulfur batteries, especially for electric and hybrid electric vehicles. There are some directions listed below for further studies on the Li-S system that are likely to be fruitful.

1. The first thing that needs to be resolved is how to reduce the additive content. Most of the sulfur battery contains 50wt% or more additives (conductive carbons and binders) which do not make any contribution to the discharge capacity.
2. More study on the polysulfide dissolution problem. The well-known shuttle phenomenon is yet to be resolved completely. The polysulfide molecules are too small to completely prevent their migration by applying a carbon interlayer.
3. A thick electrode with high sulfur loading needs to be fabricated. To compete with current Li-ion technology, it is necessary to load more than 3 mg/cm^2 of sulfur into the cathode, whereas in most of sulfur-carbon composite cathodes, the electrode loading is only 1 mg/cm^2.
4. Understanding the anode side better. Li-metal has a safety issue problem, and attempts have been made to use it as anode for long time, but they are still unsuccessful. The formation of dendrites and reactivity with organic electrolyte are big challenges for Li-metal. Even though the Li-S system will operate within a low voltage window, there is no significant proof of eradicating the formation of dendrites.
5. More focus on the Li_2S cathode system. Li_2S/carbon composite is a very promising material for commercializing the Li-S system. Lithium-free anode (e.g. Sn, Ge, or some other alloy) can be used with Li_2S. It also suffers from several challenges such as having a high activation barrier along with low conductivity.

6. Scavenging the electrolyte more. It is believed by most of the relevant scientists that the success of Li-S system depends on the electrolyte. A suitable electrolyte can solve most of the challenges in Li-S system including the shuttle phenomenon and safety issues related to Li-metal.

Bibliography

1. Van Noorden, R., *A Better Battery.* Nature, 2014. **507**(7490): p. 26-28.
2. Meyer, B., *Elemental sulfur.* Chemical Reviews, 1976. **76**(3): p. 367-388.
3. Armand, M. and J.M. Tarascon, *Building better batteries.* Nature, 2008. **451**(7179): p. 652-657.
4. Whittingham, M.S., *Lithium Batteries and Cathode Materials.* Chemical Reviews, 2004. **104**(10): p. 4271-4302.
5. Manthiram, A., et al., *Rechargeable Lithium–Sulfur Batteries.* Chemical Reviews, 2014.
6. Scheers, J., S. Fantini, and P. Johansson, *A review of electrolytes for lithium–sulphur batteries.* Journal of Power Sources, 2014. **255**: p. 204-218.
7. Xu, W., et al., *Lithium metal anodes for rechargeable batteries.* Energy & Environmental Science, 2014. **7**(2): p. 513-537.
8. Wild, M., et al., *Lithium sulfur batteries, a mechanistic review.* Energy & Environmental Science, 2015. **8**(12): p. 3477-3494.
9. Manthiram, A., Y. Fu, and Y.-S. Su, *Challenges and Prospects of Lithium–Sulfur Batteries.* Accounts of Chemical Research, 2013. **46**(5): p. 1125-1134.
10. Wang, D.-W., et al., *Carbon-sulfur composites for Li-S batteries: status and prospects.* Journal of Materials Chemistry A, 2013. **1**(33): p. 9382-9394.
11. Zhou, G., et al., *A flexible nanostructured sulphur-carbon nanotube cathode with high rate performance for Li-S batteries.* Energy & Environmental Science, 2012. **5**(10): p. 8901-8906.
12. Su, Y.-S., Y. Fu, and A. Manthiram, *Self-weaving sulfur-carbon composite cathodes for high rate lithium-sulfur batteries.* Physical Chemistry Chemical Physics, 2012. **14**(42): p. 14495-14499.

13. Hagen, M., et al., *Lithium-sulphur batteries - binder free carbon nanotubes electrode examined with various electrolytes.* Journal of Power Sources, 2012. **213**: p. 239-248.

14. Rao, M., X. Song, and E.J. Cairns, *Nano-carbon/sulfur composite cathode materials with carbon nanofiber as electrical conductor for advanced secondary lithium/sulfur cells.* Journal of Power Sources, 2012. **205**: p. 474-478.

15. Zheng, G., et al., *Hollow Carbon Nanofiber-Encapsulated Sulfur Cathodes for High Specific Capacity Rechargeable Lithium Batteries.* Nano Letters, 2011. **11**(10): p. 4462-4467.

16. Zheng, G., et al., *Amphiphilic Surface Modification of Hollow Carbon Nanofibers for Improved Cycle Life of Lithium Sulfur Batteries.* Nano Letters, 2013. **13**(3): p. 1265-1270.

17. Rao, M., et al., *Carbon nanofiber-sulfur composite cathode materials with different binders for secondary Li/S cells.* Electrochimica Acta, 2012. **65**: p. 228-233.

18. Ahn, W., et al., *Synthesis and electrochemical properties of a sulfur-multi walled carbon nanotubes composite as a cathode material for lithium sulfur batteries.* Journal of Power Sources, 2012. **202**: p. 394-399.

19. He, G., X. Ji, and L. Nazar, *High "C" rate Li-S cathodes: sulfur imbibed bimodal porous carbons.* Energy & Environmental Science, 2011. **4**(8): p. 2878-2883.

20. Su, Y.-S. and A. Manthiram, *A facile in situ sulfur deposition route to obtain carbon-wrapped sulfur composite cathodes for lithium-sulfur batteries.* Electrochimica Acta, 2012. **77**: p. 272-278.

21. Zhang, C., et al., *Confining Sulfur in Double-Shelled Hollow Carbon Spheres for Lithium-Sulfur Batteries.* Angewandte Chemie-International Edition, 2012. **51**(38): p. 9592-9595.

22. Ji, X.L., K.T. Lee, and L.F. Nazar, *A highly ordered nanostructured carbon-sulphur cathode for lithium-sulphur batteries.* Nature Materials, 2009. **8**(6): p. 500-506.

23. Ji, L., et al., *Porous carbon nanofiber-sulfur composite electrodes for lithium/sulfur cells.* Energy & Environmental Science, 2011. **4**(12): p. 5053-5059.

24. Schuster, J., et al., *Spherical Ordered Mesoporous Carbon Nanoparticles with High Porosity for Lithium–Sulfur Batteries.* Angewandte Chemie International Edition, 2012. **51**(15): p. 3591-3595.

25. Wang, C., et al., *Dual core-shell structured sulfur cathode composite synthesized by a one-pot route for lithium sulfur batteries.* Journal of Materials Chemistry A, 2013. **1**(5): p. 1716-1723.

26. Yin, L., et al., *Dual-mode sulfur-based cathode materials for rechargeable Li-S batteries.* Chemical Communications, 2012. **48**(63): p. 7868-7870.

27. Park, M.-S., et al., *One-step synthesis of a sulfur-impregnated graphene cathode for lithium-sulfur batteries.* Physical Chemistry Chemical Physics, 2012. **14**(19): p. 6796-6804.

28. Evers, S. and L.F. Nazar, *Graphene-enveloped sulfur in a one pot reaction: a cathode with good coulombic efficiency and high practical sulfur content.* Chemical Communications, 2012. **48**(9): p. 1233-1235.

29. Zhao, M.-Q., et al., *Graphene/Single-Walled Carbon Nanotube Hybrids: One-Step Catalytic Growth and Applications for High-Rate Li-S Batteries.* Acs Nano, 2012. **6**(12): p. 10759-10769.

30. Wang, J.-Z., et al., *Sulfur-graphene composite for rechargeable lithium batteries.* Journal of Power Sources, 2011. **196**(16): p. 7030-7034.

31. Wang, Y.-X., et al., *Facile synthesis of a interleaved expanded graphite-embedded sulphur nanocomposite as cathode of Li-S batteries with excellent lithium storage performance.* Journal of Materials Chemistry, 2012. **22**(11): p. 4744-4750.

32. Wang, H., et al., *Graphene-Wrapped Sulfur Particles as a Rechargeable Lithium-Sulfur Battery Cathode Material with High Capacity and Cycling Stability.* Nano Letters, 2011. **11**(7): p. 2644-2647.

33. Li, N.W., et al., *High-rate lithium-sulfur batteries promoted by reduced graphene oxide coating.* Chemical Communications, 2012. **48**(34): p. 4106-4108.

34. Su, Y.S., et al., *A strategic approach to recharging lithium-sulphur batteries for long cycle life.* Nature Communications, 2013. **4**.

35. Wang, X.F., Z.X. Wang, and L.Q. Chen, *Reduced graphene oxide film as a shuttle-inhibiting interlayer in a lithium-sulfur battery.* Journal of Power Sources, 2013. **242**: p. 65-69.

36. Su, Y.S. and A. Manthiram, *Lithium-sulphur batteries with a microporous carbon paper as a bifunctional interlayer.* Nature Communications, 2012. **3**.

37. Moon, S., et al., *Encapsulated Monoclinic Sulfur for Stable Cycling of Li–S Rechargeable Batteries.* Advanced Materials, 2013. **25**(45): p. 6547-6553.

38. Wu, M., J. Jin, and Z. Wen, *Influence of a surface modified Li anode on the electrochemical performance of Li-S batteries.* RSC Advances, 2016. **6**(46): p. 40270-40276.

39. Wu, M., et al., *Trimethylsilyl Chloride-Modified Li Anode for Enhanced Performance of Li–S Cells.* ACS Applied Materials & Interfaces, 2016. **8**(25): p. 16386-16395.

40. Xu, K., *Nonaqueous Liquid Electrolytes for Lithium-Based Rechargeable Batteries.* Chemical Reviews, 2004. **104**(10): p. 4303-4418.

41. Dokko, K., et al., *Solvate Ionic Liquid Electrolyte for Li–S Batteries.* Journal of The Electrochemical Society, 2013. **160**(8): p. A1304-A1310.

42. Park, J.-W., et al., *Ionic Liquid Electrolytes for Lithium–Sulfur Batteries.* The Journal of Physical Chemistry C, 2013. **117**(40): p. 20531-20541.

43. Suo, L., et al., *A new class of Solvent-in-Salt electrolyte for high-energy rechargeable metallic lithium batteries.* Nat Commun, 2013. **4**: p. 1481.

44. Zhang, S.S., *Liquid electrolyte lithium/sulfur battery: Fundamental chemistry, problems, and solutions.* Journal of Power Sources, 2013. **231**: p. 153-162.

45. Azimi, N., et al., *Fluorinated Electrolytes for Li-S Battery: Suppressing the Self-Discharge with an Electrolyte Containing Fluoroether Solvent.* Journal of The Electrochemical Society, 2015. **162**(1): p. A64-A68.

46. Zhang, S., et al., *Recent Advances in Electrolytes for Lithium–Sulfur Batteries.* Advanced Energy Materials, 2015. **5**(16): p. n/a-n/a.

47. Hayashi, A., et al., *All-solid-state rechargeable lithium batteries with Li2S as a positive electrode material.* Journal of Power Sources, 2008. **183**(1): p. 422-426.

48. Cai, K.P., et al., *Nanostructured Li2S-C Composites as Cathode Material for High-Energy Lithium/Sulfur Batteries.* Nano Letters, 2012. **12**(12): p. 6474-6479.

49. Nagao, M., A. Hayashi, and M. Tatsumisago, *High-capacity Li2S-nanocarbon composite electrode for all-solid-state rechargeable lithium batteries.* Journal of Materials Chemistry, 2012. **22**(19): p. 10015-10020.

50. Cheng, J.J., et al., *Sulfur-Nickel Foam as Cathode Materials for Lithium-Sulfur Batteries.* ECS Electrochemistry Letters, 2015. **4**(2): p. A19-A21.

51. Xi, K., et al., *Binder free three-dimensional sulphur/few-layer graphene foam cathode with enhanced high-rate capability for rechargeable lithium sulphur batteries.* Nanoscale, 2014. **6**(11): p. 5746-5753.

52. Zhang, Y., et al., *Three-dimensional carbon fiber as current collector for lithium/sulfur batteries.* Ionics, 2014. **20**(6): p. 803-808.

53. Gong, Z., et al., *PEDOT-PSS coated sulfur/carbon composite on porous carbon papers for high sulfur loading lithium-sulfur batteries.* RSC Advances, 2015. **5**(117): p. 96862-96869.

54. Bruce, P.G., et al., *Li-O2 and Li-S batteries with high energy storage.* Nat Mater, 2012. **11**(1): p. 19-29.

55. Xu, R., J. Lu, and K. Amine, *Progress in Mechanistic Understanding and Characterization Techniques of Li-S Batteries.* Advanced Energy Materials, 2015. **5**(16): p. n/a-n/a.

56. Kazyak, E., K.N. Wood, and N.P. Dasgupta, *Improved Cycle Life and Stability of Lithium Metal Anodes through Ultrathin Atomic Layer Deposition Surface Treatments.* Chemistry of Materials, 2015. **27**(18): p. 6457-6462.

57. Park, M.S., et al., *A Highly Reversible Lithium Metal Anode.* Scientific Reports, 2014. **4**: p. 3815.

58. Qian, J., et al., *High rate and stable cycling of lithium metal anode.* Nat Commun, 2015. **6**.

59. Kolosnitsyn, V.S. and E.V. Karaseva, *Lithium-sulfur batteries: Problems and solutions.* Russian Journal of Electrochemistry, 2008. **44**(5): p. 506-509.

60. Wang, J., et al., *Sulphur-polypyrrole composite positive electrode materials for rechargeable lithium batteries.* Electrochimica Acta, 2006. **51**(22): p. 4634-4638.

61. Fu, Y. and A. Manthiram, *Enhanced Cyclability of Lithium-Sulfur Batteries by a Polymer Acid-Doped Polypyrrole Mixed Ionic-Electronic Conductor*. Chemistry of Materials, 2012. **24**(15): p. 3081-3087.

62. Choi, Y.J., et al., *Electrochemical properties of sulfur electrode containing nano Al2O3 for lithium/sulfur cell.* Physica Scripta, 2007. **T129**: p. 62-65.

63. Zu, C., et al., *Improved lithium-sulfur cells with a treated carbon paper interlayer.* Physical Chemistry Chemical Physics, 2013. **15**(7): p. 2291-2297.

64. Liang, C., N.J. Dudney, and J.Y. Howe, *Hierarchically Structured Sulfur/Carbon Nanocomposite Material for High-Energy Lithium Battery.* Chemistry of Materials, 2009. **21**(19): p. 4724-4730.

65. Younesi, R., et al., *Lithium salts for advanced lithium batteries: Li-metal, Li-O-2, and Li-S.* Energy & Environmental Science, 2015. **8**(7): p. 1905-1922.

66. Lin, T., et al., *Scotch-tape-like exfoliation of graphite assisted with elemental sulfur and graphene-sulfur composites for high-performance lithium-sulfur batteries.* Energy & Environmental Science, 2013. **6**(4): p. 1283-1290.

67. Larcher, D. and J.M. Tarascon, *Towards greener and more sustainable batteries for electrical energy storage.* Nat Chem, 2015. **7**(1): p. 19-29.

68. Erhardt, C., et al., *Proof of concept for a novel, binder-free and conducting carbon-free sulfur battery cathode: Composite electroformation of copper foil with incorporated polythiophene wrapped sulfur particles.* Journal of Power Sources, 2015. **296**: p. 70-77.

69. Zeng, Q., et al., *Electroactive cellulose-supported graphene oxide interlayers for Li–S batteries.* Carbon, 2015. **93**: p. 611-619.

70. Shi, J.-L., et al., *Template growth of porous graphene microspheres on layered double oxide catalysts and their applications in lithium–sulfur batteries.* Carbon, 2015. **92**: p. 96-105.

71. Fan, C.-Y., et al., *Fabrication of functionalized polysulfide reservoirs from large graphene sheets to improve the electrochemical performance of lithium-sulfur batteries.* Physical Chemistry Chemical Physics, 2015. **17**(36): p. 23481-23488.

72. Zhou, G.M., et al., *A graphene foam electrode with high sulfur loading for flexible and high energy Li-S batteries.* Nano Energy, 2015. **11**: p. 356-365.

73. Zhou, J.W., et al., *The impact of the particle size of a metal-organic framework for sulfur storage in Li-S batteries.* Journal of Materials Chemistry A, 2015. **3**(16): p. 8272-8275.

74. Ding, N., et al., *Key parameters in design of lithium sulfur batteries.* Journal of Power Sources, 2014. **269**: p. 111-116.

75. Chen, H., et al., *Rational Design of Cathode Structure for High Rate Performance Lithium–Sulfur Batteries.* Nano Letters, 2015. **15**(8): p. 5443-5448.

76. Zhao, Q., et al., *Sulfur Nanodots Electrodeposited on Ni Foam as High-Performance Cathode for Li-S Batteries.* Nano Letters, 2015. **15**(1): p. 721-726.

77. Brückner, J., et al., *Lithium–sulfur batteries: Influence of C-rate, amount of electrolyte and sulfur loading on cycle performance.* Journal of Power Sources, 2014. **268**: p. 82-87.

78. Li, X., et al., *Superior stable sulfur cathodes of Li-S batteries enabled by molecular layer deposition.* Chemical Communications, 2014. **50**(68): p. 9757-9760.

79. Yan, J., et al., *Long-Life, High-Efficiency Lithium–Sulfur Battery from a Nanoassembled Cathode.* Chemistry of Materials, 2015. **27**(14): p. 5080-5087.

80. Yu, X.Q., et al., *Direct Observation of the Redistribution of Sulfur and Polysufides in Li-S Batteries During the First Cycle by In Situ X-Ray Fluorescence Microscopy.* Advanced Energy Materials, 2015. **5**(16).

81. Yeon, S.H., et al., *Carbide-derived carbon/sulfur composite cathode for multi-layer separator assembled Li-S battery.* Korean Journal of Chemical Engineering, 2015. **32**(5): p. 867-873.

82. Shao, H., et al., *Improved electrochemical performance of sulphur cathodes with acylated gelatine as a binder.* RSC Advances, 2015. **5**(59): p. 47757-47761.

83. Zhang, Z., et al., *Titanium-dioxide-grafted carbon paper with immobilized sulfur as a flexible free-standing cathode for superior lithium–sulfur batteries.* Journal of Power Sources, 2015. **290**: p. 159-167.

84. Sun, Q., et al., *An Aligned and Laminated Nanostructured Carbon Hybrid Cathode for High-Performance Lithium–Sulfur Batteries.* Angewandte Chemie International Edition, 2015. **54**(36): p. 10539-10544.

85. Sun, Q., et al., *Engineering of Hollow Core–Shell Interlinked Carbon Spheres for Highly Stable Lithium–Sulfur Batteries.* ACS Nano, 2015. **9**(8): p. 8504-8513.

86. Liu, J., et al., *A Graphene-like Oxygenated Carbon Nitride Material for Improved Cycle-Life Lithium/Sulfur Batteries.* Nano Letters, 2015. **15**(8): p. 5137-5142.

87. Agostini, M., et al., *Polysulfide-containing Glyme-based Electrolytes for Lithium Sulfur Battery.* Chemistry of Materials, 2015. **27**(13): p. 4604-4611.

88. Zeng, L., et al., *Flexible copper-stabilized sulfur-carbon nanofibers with excellent electrochemical performance for Li-S batteries.* Nanoscale, 2015. **7**(25): p. 10940-10949.

89. Ding, B., et al., *Nanospace-Confinement Copolymerization Strategy for Encapsulating Polymeric Sulfur into Porous Carbon for Lithium–Sulfur Batteries.* ACS Applied Materials & Interfaces, 2015. **7**(21): p. 11165-11171.

90. Manthiram, A., S.-H. Chung, and C. Zu, *Lithium–Sulfur Batteries: Progress and Prospects.* Advanced Materials, 2015. **27**(12): p. 1980-2006.

91. Yan, N., et al., *Fabrication of a nano-Li+-channel interlayer for high performance Li-S battery application.* Rsc Advances, 2015. **5**(33): p. 26273-26280.

92. Zhou, G.M., Y.B. Zhao, and A. Manthiram, *Dual-Confined Flexible Sulfur Cathodes Encapsulated in Nitrogen-Doped Double-Shelled Hollow Carbon Spheres and Wrapped with Graphene for Li-S Batteries.* Advanced Energy Materials, 2015. **5**(9).

93. Gu, X., et al., *A conductive interwoven bamboo carbon fiber membrane for Li-S batteries.* Journal of Materials Chemistry A, 2015. **3**(18): p. 9502-9509.

94. Lin, C.-N., et al., *Understanding dynamics of polysulfide dissolution and re-deposition in working lithium–sulfur battery by in-operando transmission X-ray microscopy.* Journal of Power Sources, 2014. **263**: p. 98-103.

95. Yao, H., et al., *Improved lithium-sulfur batteries with a conductive coating on the separator to prevent the accumulation of inactive S-related species at the cathode-separator interface.* Energy & Environmental Science, 2014. **7**(10): p. 3381-3390.

96. Xu, J., et al., *Sulfur-graphene nanostructured cathodes via ball-milling for high-performance lithium-sulfur batteries.* Acs Nano, 2014. **8**(10): p. 10920-10930.

97. Wang, B., S.M. Alhassan, and S.T. Pantelides, *Formation of Large Polysulfide Complexes during the Lithium-Sulfur Battery Discharge.* Physical review applied, 2014. **2**(3).

98. Chung, S.-H. and A. Manthiram, *Bifunctional Separator with a Light-Weight Carbon-Coating for Dynamically and Statically Stable Lithium-Sulfur Batteries.* Advanced Functional Materials, 2014. **24**(33): p. 5299-5306.

99. Pang, Q., et al., *Surface-enhanced redox chemistry of polysulphides on a metallic and polar host for lithium-sulphur batteries.* Nat Commun, 2014. **5**.

100. Zhang, B., et al., *Enhancement of long stability of sulfur cathode by encapsulating sulfur into micropores of carbon spheres.* Energy & Environmental Science, 2010. **3**(10): p. 1531-1537.

101. Nagao, M., A. Hayashi, and M. Tatsumisago, *Sulfur-carbon composite electrode for all-solid-state Li/S battery with Li2S-P2S5 solid electrolyte.* Electrochimica Acta, 2011. **56**(17): p. 6055-6059.

102. Yang, Y., et al., *New Nanostructured Li2S/Silicon Rechargeable Battery with High Specific Energy.* Nano Letters, 2010. **10**(4): p. 1486-1491.

103. Fu, Y.Z., C.X. Zu, and A. Manthiram, *In Situ-Formed Li2S in Lithiated Graphite Electrodes for Lithium-Sulfur Batteries.* Journal of the American Chemical Society, 2013. **135**(48): p. 18044-18047.

104. Meini, S., et al., *The Use of Redox Mediators for Enhancing Utilization of Li2S Cathodes for Advanced Li-S Battery Systems.* Journal of Physical Chemistry Letters, 2014. **5**(5): p. 915-918.

105. Agostini, M., et al., *A Lithium-Ion Sulfur Battery Based on a Carbon-Coated Lithium-Sulfide Cathode and an Electrodeposited Silicon-Based Anode.* Acs Applied Materials & Interfaces, 2014. **6**(14): p. 10924-10928.

106. Zu, C., M. Klein, and A. Manthiram, *Activated Li2S as a High-Performance Cathode for Rechargeable Lithium–Sulfur Batteries.* The Journal of Physical Chemistry Letters, 2014. **5**(22): p. 3986-3991.

107. Mikhaylik, Y.V. and J.R. Akridge, *Polysulfide Shuttle Study in the Li/S Battery System.* Journal of The Electrochemical Society, 2004. **151**(11): p. A1969-A1976.

108. Wang, J., et al., *Sulfur-mesoporous carbon composites in conjunction with a novel ionic liquid electrolyte for lithium rechargeable batteries.* Carbon, 2008. **46**(2): p. 229-235.

109. Wang, L., et al., *Analysis of the synthesis process of sulphur-poly(acrylonitrile)-based cathode materials for lithium batteries.* Journal of Materials Chemistry, 2012. **22**(41): p. 22077-22081.

110. Li, G.-C., et al., *A Polyaniline-Coated Sulfur/Carbon Composite with an Enhanced High-Rate Capability as a Cathode Material for Lithium/Sulfur Batteries.* Advanced Energy Materials, 2012. **2**(10): p. 1238-1245.

111. Zhang, Y.G., et al., *Effect of mesoporous carbon microtube prepared by carbonizing the poplar catkin on sulfur cathode performance in Li/S batteries.* Journal of Alloys and Compounds, 2015. **619**: p. 298-302.

112. Zhang, C., et al., *A high-density graphene-sulfur assembly: a promising cathode for compact Li-S batteries.* Nanoscale, 2015. **7**(13): p. 5592-5597.

113. Zeng, Q.C., et al., *Dispersible percolating carbon nano-electrodes for improvement of polysulfide utilization in Li-S batteries.* Carbon, 2015. **93**: p. 161-168.

114. Zhang, S., et al., *Improving lithium-sulfur battery performance via a carbon-coating layer derived from the hydrothermal carbonization of glucose.* RSC Advances, 2015. **5**(63): p. 50983-50988.

115. Babu, G. and L.M. Reddy Arava, *Graphene-decorated graphite-sulfur composite as a high-tap-density electrode for Li-S batteries.* RSC Advances, 2015. **5**(59): p. 47621-47627.

116. Li, Y., et al., *Improving the electrochemical performance of a lithium-sulfur battery with a conductive polymer-coated sulfur cathode.* RSC Advances, 2015. **5**(55): p. 44160-44164.

117. Wang, H., et al., *Large-scale synthesis of ordered mesoporous carbon fiber and its application as cathode material for lithium–sulfur batteries.* Carbon, 2015. **81**: p. 782-787.

118. Duan, X., et al., *Improved rate ability of low cost sulfur cathodes by using ultrathin graphite sheets with self-wrapped function as cheap conductive agent.* Journal of Materials Chemistry A, 2015. **3**(15): p. 8015-8021.

119. He, G., et al., *Tailoring Porosity in Carbon Nanospheres for Lithium–Sulfur Battery Cathodes.* ACS Nano, 2013. **7**(12): p. 10920-10930.

120. Li, D., et al., *High Sulfur Loading Cathodes Fabricated Using Peapodlike, Large Pore Volume Mesoporous Carbon for Lithium–Sulfur Battery.* ACS Applied Materials & Interfaces, 2013. **5**(6): p. 2208-2213.

121. Ding, B., et al., *Encapsulating Sulfur into Hierarchically Ordered Porous Carbon as a High-Performance Cathode for Lithium–Sulfur Batteries.* Chemistry – A European Journal, 2013. **19**(3): p. 1013-1019.

122. Ma, Z., Q. Liu, and S. Wang, *Sulfur-graphene composite with molybdenum particles for stabilizing lithium-sulfur batteries.* RSC Advances, 2015. **5**(3): p. 2096-2099.

123. Su, Y.-S. and A. Manthiram, *Sulfur/lithium-insertion compound composite cathodes for Li–S batteries.* Journal of Power Sources, 2014. **270**: p. 101-105.

124. Zhou, W., et al., *Polydopamine-Coated, Nitrogen-Doped, Hollow Carbon–Sulfur Double-Layered Core–Shell Structure for Improving Lithium–Sulfur Batteries.* Nano Letters, 2014. **14**(9): p. 5250-5256.

125. Li, X., et al., *Tailoring interactions of carbon and sulfur in Li-S battery cathodes: significant effects of carbon-heteroatom bonds.* Journal of Materials Chemistry A, 2014. **2**(32): p. 12866-12872.

126. Zhang, Q., et al., *Review of carbon materials for advanced lithium-sulfur batteries.* New Carbon Materials, 2014. **29**(4): p. 241-264.

127. Li, F.-f., et al., *Preparation and electrochemical performance of a graphene-wrapped carbon/sulphur composite cathode.* New Carbon Materials, 2014. **29**(4): p. 309-315.

128. Ji, X.L. and L.F. Nazar, *Advances in Li-S batteries.* Journal of Materials Chemistry, 2010. **20**(44): p. 9821-9826.

129. Wei Seh, Z., et al., *Sulphur-TiO2 yolk-shell nanoarchitecture with internal void space for long-cycle lithium-sulphur batteries.* Nature communications, 2013. **4**: p. 1331-1331.

130. Evers, S., T. Yim, and L.F. Nazar, *Understanding the Nature of Absorption/Adsorption in Nanoporous Polysulfide Sorbents for the Li-S Battery.* Journal of Physical Chemistry C, 2012. **116**(37): p. 19653-19658.

131. Qu, Q.T., et al., *Strong Surface-Bound Sulfur in Conductive MoO2 Matrix for Enhancing Li-S Battery Performance.* Advanced Materials Interfaces, 2015. **2**(7).

132. Moon, S., Y.H. Jung, and D.K. Kim, *Enhanced electrochemical performance of a crosslinked polyaniline-coated graphene oxide-sulfur composite for rechargeable lithium–sulfur batteries.* Journal of Power Sources, 2015. **294**: p. 386-392.

133. Ma, J., et al., *Novel Large-Scale Synthesis of a C/S Nanocomposite with Mixed Conducting Networks through a Spray Drying Approach for Li-S Batteries.* Advanced Energy Materials, 2015. **5**(16).

134. Jing, H.-K., et al., *Protected lithium anode with porous Al2O3 layer for lithium-sulfur battery.* Journal of Materials Chemistry A, 2015. **3**(23): p. 12213-12219.

135. Zhao, C., et al., *Prussian blue-derived Fe2O3/sulfur composite cathode for lithium–sulfur batteries.* Materials Letters, 2014. **137**: p. 52-55.

136. Tao, X., et al., *Strong Sulfur Binding with Conducting Magnéli-Phase TinO2n–1 Nanomaterials for Improving Lithium–Sulfur Batteries.* Nano Letters, 2014. **14**(9): p. 5288-5294.

137. Wu, F., et al., *An effective approach to protect lithium anode and improve cycle performance for Li-S batteries.* ACS Applied Materials & Interfaces, 2014. **6**(17): p. 15542-15549.

138. Unemoto, A., et al., *Development of bulk-type all-solid-state lithium-sulfur battery using LiBH4 electrolyte.* Applied Physics Letters, 2014. **105**(8): p. 083901.

139. Liang, X., et al., *Highly dispersed sulfur in ordered mesoporous carbon sphere as a composite cathode for rechargeable polymer Li/S battery.* Journal of Power Sources, 2011. **196**(7): p. 3655-3658.

140. Rao, M., W. Li, and E.J. Cairns, *Porous carbon-sulfur composite cathode for lithium/sulfur cells.* Electrochemistry Communications, 2012. **17**: p. 1-5.

141. Weng, W., V.G. Pol, and K. Amine, *Ultrasound Assisted Design of Sulfur/Carbon Cathodes with Partially Fluorinated Ether Electrolytes for Highly Efficient Li/S Batteries.* Advanced Materials, 2013. **25**(11): p. 1608-1615.

142. Li, G., et al., *Sulfur/microporous carbon composites for Li-S battery.* Ionics, 2015. **21**(8): p. 2161-2170.

143. Peng, Z., et al., *Graphene-based ultrathin microporous carbon with smaller sulfur molecules for excellent rate performance of lithium–sulfur cathode.* Journal of Power Sources, 2015. **282**: p. 70-78.

144. Yan, J., et al., *Long-life, high-efficiency lithium/sulfur batteries from sulfurized carbon nanotube cathodes.* Journal of Materials Chemistry A, 2015. **3**(18): p. 10127-10133.

145. Zhang, C., et al., *Effect of Carbon Core Grafting on the Properties of Carbon-Sulfur Composite for Lithium/Sulfur Battery.* Journal of The Electrochemical Society, 2015. **162**(6): p. A1067-A1071.

146. Hao, Y., et al., *One step production of in situ nitrogen doped mesoporous carbon confined sulfur for lithium-sulfur batteries.* RSC Advances, 2015. **5**(40): p. 31629-31636.

147. Cheng, J.J., et al., *Sulfur/bamboo charcoal composites cathode for lithium-sulfur batteries.* RSC Advances, 2015. **5**(1): p. 68-74.

148. Hoffmann, C., et al., *Nanocasting hierarchical carbide-derived carbons in nanostructured opal assemblies for high-performance cathodes in lithium-sulfur batteries.* Acs Nano, 2014. **8**(12): p. 12130-12140.

149. Peng, H.-J., et al., *Strongly Coupled Interfaces between a Heterogeneous Carbon Host and a Sulfur-Containing Guest for Highly Stable Lithium-Sulfur Batteries: Mechanistic Insight into Capacity Degradation.* Advanced Materials Interfaces, 2014. **1**(7): p. n-a-n/a.

150. Wu, Y., et al., *Preparation of mesohollow and microporous carbon nanofiber and its application in cathode material for lithium–sulfur batteries.* Journal of Alloys and Compounds, 2014. **608**: p. 220-228.

151. Chen, X.a., et al., *Sulfur-Impregnated, Sandwich-Type, Hybrid Carbon Nanosheets with Hierarchical Porous Structure for High-Performance Lithium-Sulfur Batteries.* Advanced Energy Materials, 2014. **4**(13): p. n/a-n/a.

152. Tang, C., et al., *Nitrogen-doped aligned carbon nanotube/graphene sandwiches: facile catalytic growth on bifunctional natural catalysts and their applications as scaffolds for high-rate lithium-sulfur batteries.* Advanced materials (Weinheim), 2014. **26**(35): p. 6100-6105.

153. Zhang, B., et al., *Novel Hierarchically Porous Carbon Materials Obtained from Natural Biopolymer as Host Matrixes for Lithium–Sulfur Battery Applications.* ACS Applied Materials & Interfaces, 2014. **6**(15): p. 13174-13182.

154. Zhao, Y., et al., *Encapsulating MWNTs into hollow porous carbon nanotubes: a tube-in-tube carbon nanostructure for high-performance lithium-sulfur batteries.* Advanced materials (Weinheim), 2014. **26**(30): p. 5113-5118.

155. Jung, D.S., et al., *Hierarchical Porous Carbon by Ultrasonic Spray Pyrolysis Yields Stable Cycling in Lithium–Sulfur Battery.* Nano Letters, 2014. **14**(8): p. 4418-4425.

156. Schuster, J., et al., *Spherical Ordered Mesoporous Carbon Nanoparticles with High Porosity for Lithium-Sulfur Batteries.* Angewandte Chemie-International Edition, 2012. **51**(15): p. 3591-3595.

157. Ding, B., et al., *Chemically tailoring the nanostructure of graphene nanosheets to confine sulfur for high-performance lithium-sulfur batteries.* Journal of Materials Chemistry A, 2013. **1**(4): p. 1096-1101.

158. Liu, Y., H. Zhan, and Y. Zhou, *Investigation of S/C composite synthesized by solvent exchange method.* Electrochimica Acta, 2012. **70**: p. 241-247.

159. Shin, E.S., et al., *Sulfur/graphitic hollow carbon sphere nano-composite as a cathode material for high-power lithium-sulfur battery.* Nanoscale Research Letters, 2013. **8**(1): p. 1-8.

160. Xu, J., et al., *Sulfur–Graphene Nanostructured Cathodes via Ball-Milling for High-Performance Lithium–Sulfur Batteries.* ACS Nano, 2014. **8**(10): p. 10920-10930.

161. Takahashi, T., M. Yamagata, and M. Ishikawa, *A sulfur–microporous carbon composite positive electrode for lithium/sulfur and silicon/sulfur rechargeble batteries.* Progress in Natural Science: Materials International, 2015. **25**(6): p. 612-621.

162. Kaiser, M.R., et al., *A systematic approach to high and stable discharge capacity for scaling up the lithium–sulfur battery.* Journal of Power Sources, 2015. **279**(0): p. 231-237.

163. Xin, S., et al., *Smaller Sulfur Molecules Promise Better Lithium–Sulfur Batteries.* Journal of the American Chemical Society, 2012. **134**(45): p. 18510-18513.

164. Ji, X., K.T. Lee, and L.F. Nazar, *A highly ordered nanostructured carbon-sulphur cathode for lithium-sulphur batteries.* Nat Mater, 2009. **8**(6): p. 500-506.

165. Wang, D.-W., et al., *A microporous-mesoporous carbon with graphitic structure for a high-rate stable sulfur cathode in carbonate solvent-based Li-S batteries.* Physical Chemistry Chemical Physics, 2012. **14**(24): p. 8703-8710.

166. Jayaprakash, N., et al., *Porous Hollow Carbon@Sulfur Composites for High-Power Lithium–Sulfur Batteries.* Angewandte Chemie International Edition, 2011. **50**(26): p. 5904-5908.

167. Zhang, C., et al., *Confining Sulfur in Double-Shelled Hollow Carbon Spheres for Lithium–Sulfur Batteries.* Angewandte Chemie International Edition, 2012. **51**(38): p. 9592-9595.

168. Guo, J., Y. Xu, and C. Wang, *Sulfur-Impregnated Disordered Carbon Nanotubes Cathode for Lithium–Sulfur Batteries.* Nano Letters, 2011. **11**(10): p. 4288-4294.

169. Wang, H., et al., *Graphene-Wrapped Sulfur Particles as a Rechargeable Lithium–Sulfur Battery Cathode Material with High Capacity and Cycling Stability.* Nano Letters, 2011. **11**(7): p. 2644-2647.

170. Sun, H., et al., *A composite material of uniformly dispersed sulfur on reduced graphene oxide: Aqueous one-pot synthesis, characterization and excellent performance as the cathode in rechargeable lithium-sulfur batteries.* Nano Research, 2012. **5**(10): p. 726-738.

171. Dorfler, S., et al., *High capacity vertical aligned carbon nanotube/sulfur composite cathodes for lithium-sulfur batteries.* Chemical Communications, 2012. **48**(34): p. 4097-4099.

172. Zheng, J., et al., *Revisit Carbon/Sulfur Composite for Li-S Batteries.* Journal of The Electrochemical Society, 2013. **160**(10): p. A1624-A1628.

173. Zhang, Y., Y. Zhao, and Z. Bakenov, *A novel lithium/sulfur battery based on sulfur/graphene nanosheet composite cathode and gel polymer electrolyte.* Nanoscale Research Letters, 2014. **9**(1): p. 137-137.

174. Su, Y.-S. and A. Manthiram, *A new approach to improve cycle performance of rechargeable lithium-sulfur batteries by inserting a free-standing MWCNT interlayer.* Chemical Communications, 2012. **48**(70): p. 8817-8819.

175. Su, Y.-S., et al., *A strategic approach to recharging lithium-sulphur batteries for long cycle life.* Nat Commun, 2013. **4**.

176. Colthup, N.B., L.H. Daly, and S.E. Wiberley, *Introduction to infrared and Raman spectroscopy*. 1990: Academic press.

177. Brunauer, S., P.H. Emmett, and E. Teller, *Adsorption of Gases in Multimolecular Layers.* Journal of the American Chemical Society, 1938. **60**(2): p. 309-319.

178. Coats, A.W. and J.P. Redfern, *Thermogravimetric analysis. A review.* Analyst, 1963. **88**(1053): p. 906-924.

179. Du, G., *Nanostructured anode materials for lithium-ion batteries.* 2011.

180. Zheng, J., et al., *Revisit Carbon/Sulfur Composite for Li-S Batteries.* Journal of the Electrochemical Society, 2013. **160**(10): p. A1624-A1628.

181. Zu, C. and A. Manthiram, *Hydroxylated Graphene–Sulfur Nanocomposites for High-Rate Lithium–Sulfur Batteries.* Advanced Energy Materials, 2013. **3**(8): p. 1008-1012.

182. Wang, L., et al., *Covalent Bond Glued Sulfur Nanosheet-Based Cathode Integration for Long-Cycle-Life Li–S Batteries.* Nano Letters, 2013. **13**(12): p. 6244-6250.

183. Lin, Z., et al., *Lithium Polysulfidophosphates: A Family of Lithium-Conducting Sulfur-Rich Compounds for Lithium-Sulfur Batteries.* Angewandte Chemie-International Edition, 2013. **52**(29): p. 7460-7463.

184. Ji, L.W., et al., *Porous carbon nanofiber-sulfur composite electrodes for lithium/sulfur cells.* Energy & Environmental Science, 2011. **4**(12): p. 5053-5059.

185. Wang, L., et al., *Interface Chemistry Guided Long-Cycle-Life Li–S Battery.* Nano Letters, 2013. **13**(9): p. 4206-4211.

186. Kim, C.S., et al., *Importance of open pore structures with mechanical integrity in designing the cathode electrode for lithium–sulfur batteries.* Journal of Power Sources, 2013. **241**(0): p. 554-559.

187. Hagen, M., et al., *Development and costs calculation of lithium–sulfur cells with high sulfur load and binder free electrodes.* Journal of Power Sources, 2013. **224**(0): p. 260-268.

188. Jeddi, K., et al., *Stabilizing lithium/sulfur batteries by a composite polymer electrolyte containing mesoporous silica particles.* Journal of Power Sources, 2014. **245**(0): p. 656-662.

189. Song, M.-K., Y. Zhang, and E.J. Cairns, *A Long-Life, High-Rate Lithium/Sulfur Cell: A Multifaceted Approach to Enhancing Cell Performance.* Nano Letters, 2013. **13**(12): p. 5891-5899.

190. Li, X., et al., *Optimization of mesoporous carbon structures for lithium-sulfur battery applications.* Journal of Materials Chemistry, 2011. **21**(41): p. 16603-16610.

191. Zhou, G., et al., *A Graphene–Pure-Sulfur Sandwich Structure for Ultrafast, Long-Life Lithium–Sulfur Batteries.* Advanced Materials, 2014. **26**(4): p. 625-631.

192. Wang, H.L. and H.J. Dai, *Strongly coupled inorganic-nano-carbon hybrid materials for energy storage.* Chemical Society Reviews, 2013. **42**(7): p. 3088-3113.

193. Li, G.C., et al., *Sulfur/activated-conductive carbon black composites as cathode materials for lithium/sulfur battery.* Journal of Power Sources, 2013. **240**(0): p. 598-605.

194. Zhou, G., et al., *Fibrous Hybrid of Graphene and Sulfur Nanocrystals for High-Performance Lithium–Sulfur Batteries.* ACS Nano, 2013. **7**(6): p. 5367-5375.

195. Gillot, F., et al., *Ball milling synthesis of LixTiP4: Improvement of the electrochemical performances.* Ionics, 2003. **9**(1-2): p. 71-76.

196. Kim, D.-Y., et al., *Synthesis of VBO3–carbon composite by ball-milling and microwave heating and its electrochemical properties as negative electrode material of lithium ion batteries.* Journal of Alloys and Compounds, 2012. **542**(0): p. 132-135.

197. Panabière, E., et al., *Ball-milled Li7MnN4: An attractive negative electrode material for lithium-ion batteries.* Electrochimica Acta, 2013. **97**(0): p. 393-397.

198. Jhan, Y.R. and J.G. Duh, *Synthesis of entanglement structure in nanosized Li4Ti5O12/multi-walled carbon nanotubes composite anode material for Li-ion batteries by ball-milling-assisted solid-state reaction.* Journal of Power Sources, 2012. **198**(0): p. 294-297.

199. Kim, S.-B., et al., *Nanostructure cathode materials prepared by high-energy ball milling method.* Materials Letters, 2011. **65**(21–22): p. 3313-3316.

200. Jung, Y.S., et al., *Electrochemical reactivity of ball-milled MoO3−y as anode materials for lithium-ion batteries.* Journal of Power Sources, 2009. **188**(1): p. 286-291.

201. West, W.C., J. Soler, and B.V. Ratnakumar, *Preparation of high quality layered-layered composite Li2MnO3–LiMO2 (M = Ni, Mn, Co) Li-ion cathodes by a ball milling–annealing process.* Journal of Power Sources, 2012. **204**(0): p. 200-204.

202. Sivakkumar, S.R., A.S. Milev, and A.G. Pandolfo, *Effect of ball-milling on the rate and cycle-life performance of graphite as negative electrodes in lithium-ion capacitors.* Electrochimica Acta, 2011. **56**(27): p. 9700-9706.

203. Su, Y.S. and A. Manthiram, *A new approach to improve cycle performance of rechargeable lithium-sulfur batteries by inserting a free-standing MWCNT interlayer.* Chemical Communications, 2012. **48**(70): p. 8817-8819.

204. Jeong, T.-G., et al., *Free standing acetylene black mesh to capture dissolved polysulfide in lithium sulfur batteries.* Chemical Communications, 2013. **49**(94): p. 11107-11109.

205. Chew, S.Y., et al., *Flexible free-standing carbon nanotube films for model lithium-ion batteries.* Carbon, 2009. **47**(13): p. 2976-2983.

206. Zhao, X., et al., *Recovery from self-assembly: a composite material for lithium-sulfur batteries.* Journal of Materials Chemistry A, 2014. **2**(20): p. 7265-7271.

207. Gaffet, E., *Planetary ball-milling: an experimental parameter phase diagram.* Materials Science and Engineering: A, 1991. **132**(0): p. 181-193.

208. Takacs, L., *Self-sustaining metal-sulfur reactions induced by ball milling.* Journal of materials synthesis and processing, 2000. **8**(3/4): p. 181-188.

209. Lu, M., Y. Tian, and Y. Yang, *A comparison of electrochemical performance of natural graphite sulfurized by ball-milling and heat-treating as an anode for lithium ion batteries.* Electrochimica Acta, 2009. **54**(27): p. 6792-6796.

210. Liang, X., et al., *Split-half-tubular polypyrrole@sulfur@polypyrrole composite with a novel three-layer-3D structure as cathode for lithium/sulfur batteries.* Nano Energy, 2015. **11**(0): p. 587-599.

211. Wang, J.Z., et al., *Sulfur-graphene composite for rechargeable lithium batteries.* Journal of Power Sources, 2011. **196**(16): p. 7030-7034.

212. Xiao, L., et al., *A Soft Approach to Encapsulate Sulfur: Polyaniline Nanotubes for Lithium-Sulfur Batteries with Long Cycle Life.* Advanced Materials, 2012. **24**(9): p. 1176-1181.

213. Zheng, S., et al., *In Situ Sulfur Reduction and Intercalation of Graphite Oxides for Li-S Battery Cathodes.* Advanced Energy Materials, 2014: p. n/a-n/a.

214. Jia-jia, C., et al., *The preparation of nano-sulfur/MWCNTs and its electrochemical performance.* Electrochimica Acta, 2010. **55**(27): p. 8062-8066.

215. Qiu, L., et al., *Preparation and enhanced electrochemical properties of nano-sulfur/poly(pyrrole-co-aniline) cathode material for lithium/sulfur batteries.* Electrochimica Acta, 2010. **55**(15): p. 4632-4636.

216. Zhang, Y., Y. Zhao, and Z. Bakenov, *A simple approach to synthesize nanosized sulfur/graphene oxide materials for high-performance lithium/sulfur batteries.* Ionics, 2014. **20**(7): p. 1047-1050.

217. Sun, L., et al., *Sulfur Nanocrystals Confined in Carbon Nanotube Network As a Binder-Free Electrode for High-Performance Lithium Sulfur Batteries.* Nano Letters, 2014. **14**(7): p. 4044-4049.

218. Trautz, M., *Das Gesetz der Reaktionsgeschwindigkeit und der Gleichgewichte in Gasen. Bestätigung der Additivität von Cv-3/2R. Neue Bestimmung der Integrationskonstanten und der Molekül durchmesser.* Zeitschrift für anorganische und allgemeine Chemie, 1916. **96**(1): p. 1-28.

219. Cardillo, D., et al., *Highly porous hematite nanorods prepared via direct spray precipitation method.* Materials Letters, 2014. **117**(0): p. 279-282.

220. Jason, N.N., R.G. Chaudhuri, and S. Paria, *Self-assembly of colloidal sulfur particles influenced by sodium oxalate salt on glass surface from evaporating drops.* Soft Matter, 2012. **8**(14): p. 3771-3780.

221. Harvey, P.D. and I.S. Butler, *Raman spectra of orthorhombic sulfur at 40 K.* Journal of Raman Spectroscopy, 1986. **17**(4): p. 329-334.

222. Sadezky, A., et al., *Raman microspectroscopy of soot and related carbonaceous materials: Spectral analysis and structural information.* Carbon, 2005. **43**(8): p. 1731-1742.

223. Su, Y.-S. and A. Manthiram, *A facile in situ sulfur deposition route to obtain carbon-wrapped sulfur composite cathodes for lithium–sulfur batteries.* Electrochimica Acta, 2012. **77**(0): p. 272-278.

224. Wang, X., et al., *Nitrogen-doped graphene/sulfur composite as cathode material for high capacity lithium–sulfur batteries.* Journal of Power Sources, 2014. **256**(0): p. 361-368.

225. Wang, W.G., et al., *In situ sulfur deposition route to obtain sulfur-carbon composite cathodes for lithium-sulfur batteries.* Journal of Materials Chemistry A, 2014. **2**(12): p. 4316-4323.

226. Liang, X., et al., *High performance pure sulfur honeycomb-like architectures synthesized by a cooperative self-assembly strategy for lithium-sulfur batteries.* RSC Advances, 2014. **4**(69): p. 36513-36516.

227. Yin, Y.-X., et al., *Lithium–Sulfur Batteries: Electrochemistry, Materials, and Prospects.* Angewandte Chemie International Edition, 2013. **52**(50): p. 13186-13200.

228. Ahn, W., et al., *Synthesis and electrochemical properties of a sulfur-multi walled carbon nanotubes composite as a cathode material for lithium sulfur batteries.* Journal of Power Sources, 2012. **202**(0): p. 394-399.

229. Yuan, L., et al., *New insight into the discharge process of sulfur cathode by electrochemical impedance spectroscopy.* Journal of Power Sources, 2009. **189**(1): p. 127-132.

230. Chiang, Y.M., *Building a Better Battery.* Science, 2010. **330**(6010): p. 1485-1486.

231. Virden, A. and U. Willen, *Building a Better Battery.* R&D Magazine, 2011. **53**(3): p. 38-39.

232. Gur, I., K. Sawyer, and R. Prasher, *Searching for a Better Thermal Battery.* Science, 2012. **335**(6075): p. 1454-1455.

233. Kaiser, M.R., et al., *A Facile Synthesis of High-Surface-Area Sulfur–Carbon Composites for Li/S Batteries.* Chemistry – A European Journal, 2015. **21**(28): p. 10061-10069.

234. Kaiser, M.R., et al., *A methodical approach for fabrication of binder-free Li2S-C composite cathode with high loading of active material for Li-S battery.* Carbon, 2016. **103**: p. 163-171.

235. Barghamadi, M., et al., *Lithium-sulfur batteries-the solution is in the electrolyte, but is the electrolyte a solution?* Energy & Environmental Science, 2014. **7**(12): p. 3902-3920.

236. Chen, R., et al., *Graphene-Based Three-Dimensional Hierarchical Sandwich-type Architecture for High-Performance Li/S Batteries.* Nano Letters, 2013. **13**(10): p. 4642-4649.

237. Lu, S., et al., *Significantly Improved Long-Cycle Stability in High-Rate Li–S Batteries Enabled by Coaxial Graphene Wrapping over Sulfur-Coated Carbon Nanofibers.* Nano Letters, 2013. **13**(6): p. 2485-2489.

238. Xu, C., et al., *Graphene-based electrodes for electrochemical energy storage.* Energy & Environmental Science, 2013. **6**(5): p. 1388-1414.

239. Bagwe, R.P., et al., *Optimization of Dye-Doped Silica Nanoparticles Prepared Using a Reverse Microemulsion Method.* Langmuir, 2004. **20**(19): p. 8336-8342.

240. Capek, I., *Preparation of metal nanoparticles in water-in-oil (w/o) microemulsions.* Advances in Colloid and Interface Science, 2004. **110**(1–2): p. 49-74.

241. Yang, Y. and M.Y. Gao, *Preparation of Fluorescent SiO2 Particles with Single CdTe Nanocrystal Cores by the Reverse Microemulsion Method.* Advanced Materials, 2005. **17**(19): p. 2354-2357.

242. Koole, R., et al., *On the Incorporation Mechanism of Hydrophobic Quantum Dots in Silica Spheres by a Reverse Microemulsion Method.* Chemistry of Materials, 2008. **20**(7): p. 2503-2512.

243. Gibaud, S. and D. Attivi, *Microemulsions for oral administration and their therapeutic applications.* Expert Opinion on Drug Delivery, 2012. **9**(8): p. 937-951.

244. Guo, Y., et al., *Preparation and characterization of monoclinic sulfur nanoparticles by water-in-oil microemulsions technique.* Powder Technology, 2006. **162**(2): p. 83-86.

245. Yuan, S., et al., *Graphene-Supported Nitrogen and Boron Rich Carbon Layer for Improved Performance of Lithium–Sulfur Batteries Due to Enhanced Chemisorption of Lithium Polysulfides.* Advanced Energy Materials, 2016. **6**(5): p. n/a-n/a.

246. Lagourette, B., et al., *Percolative conduction in microemulsion type systems.* Nature, 1979. **281**(5726): p. 60-62.

247. Davies, R., D.E. Graham, and B. Vincent, *Water-cyclohexane-"Span 80"-"Tween 80" systems: Solution properties and water/oil emulsion formation.* Journal of Colloid and Interface Science, 1987. **116**(1): p. 88-99.

248. Kunieda, H. and N. Ishikawa, *Evaluation of the hydrophile-lipophile balance (HLB) of nonionic surfactants. II. Commercial-surfactant systems.* Journal of Colloid and Interface Science, 1985. **107**(1): p. 122-128.

249. Zhang, S.S., *Effect of Discharge Cutoff Voltage on Reversibility of Lithium/Sulfur Batteries with LiNO3-Contained Electrolyte.* Journal of The Electrochemical Society, 2012. **159**(7): p. A920-A923.

250. Dang, L., et al., *Three-dimensional honeycomb-like networks of birnessite manganese oxide assembled by ultrathin two-dimensional nanosheets with enhanced Li-ion battery performances.* Nanoscale, 2015. **7**(17): p. 8101-8109.

251. Mao, S., G. Lu, and J. Chen, *Three-dimensional graphene-based composites for energy applications.* Nanoscale, 2015. **7**(16): p. 6924-6943.

252. Lingappan, N., et al., *Growth of three dimensional flower-like molybdenum disulfide hierarchical structures on graphene/carbon nanotube network: An advanced heterostructure for energy storage devices.* Journal of Power Sources, 2015. **280**(0): p. 39-46.

253. Qie, L. and A. Manthiram, *A Facile Layer-by-Layer Approach for High-Areal-Capacity Sulfur Cathodes.* Advanced Materials, 2015. **27**(10): p. 1694-1700.

254. Lin, Z., et al., *Lithium Superionic Sulfide Cathode for All-Solid Lithium-Sulfur Batteries.* Acs Nano, 2013. **7**(3): p. 2829-2833.

255. Takeuchi, T., et al., *Preparation of electrochemically active lithium sulfide-carbon composites using spark-plasma-sintering process.* Journal of Power Sources, 2010. **195**(9): p. 2928-2934.

256. Yang, Y., et al., *High-Capacity Micrometer-Sized Li2S Particles as Cathode Materials for Advanced Rechargeable Lithium-Ion Batteries.* Journal of the American Chemical Society, 2012. **134**(37): p. 15387-15394.

257. Guo, J.C., et al., *Lithium-Sulfur Battery Cathode Enabled by Lithium-Nitrile Interaction.* Journal of the American Chemical Society, 2013. **135**(2): p. 763-767.

258. Nan, C.Y., et al., *Durable Carbon-Coated Li2S Core-Shell Spheres for High Performance Lithium/Sulfur Cells.* Journal of the American Chemical Society, 2014. **136**(12): p. 4659-4663.

259. Zheng, S.Y., et al., *In Situ Formed Lithium Sulfide/Microporous Carbon Cathodes for Lithium-Ion Batteries.* Acs Nano, 2013. **7**(12): p. 10995-11003.

260. Wang, C., et al., *Slurryless Li2S/Reduced Graphene Oxide Cathode Paper for High-Performance Lithium Sulfur Battery.* Nano Letters, 2015. **15**(3): p. 1796-1802.

261. Rolison, D.R., et al., *Multifunctional 3D nanoarchitectures for energy storage and conversion.* Chemical Society Reviews, 2009. **38**(1): p. 226-252.

262. Cheng, X.-B., et al., *Three-dimensional aluminum foam/carbon nanotube scaffolds as long- and short-range electron pathways with improved sulfur loading for high energy density lithium–sulfur batteries.* Journal of Power Sources, 2014. **261**: p. 264-270.

263. Rehman, S., S. Guo, and Y. Hou, *Rational Design of Si/SiO2@Hierarchical Porous Carbon Spheres as Efficient Polysulfide Reservoirs for High-Performance Li–S Battery.* Advanced Materials, 2016: p. n/a-n/a.

264. Li, X., et al., *Chemically Derived, Ultrasmooth Graphene Nanoribbon Semiconductors.* Science, 2008. **319**(5867): p. 1229-1232.

265. Kaiser, M.R., et al., *A Facile Synthesis of High-Surface-Area Sulfur–Carbon Composite for Li/S Batteries.* Chemistry – A European Journal, 2015: p. n/a-n/a.

266. Bahloul, B., et al., *Ab initio study of the structural, electronic and elastic properties of anti-fluorite Li2X (X = S and Te) compounds under pressure effect.* Computational Materials Science, 2014. **86**(0): p. 49-56.

267. Seh, Z.W., et al., *Facile synthesis of-Li2S-polypyrrole composite structures for high-performance Li2S cathodes.* Energy & Environmental Science, 2014. **7**(2): p. 672-676.

268. Seh, Z.W., et al., *High-capacity Li2S-graphene oxide composite cathodes with stable cycling performance.* Chemical Science, 2014. **5**(4): p. 1396-1400.

269. Fu, Y.Z., Y.S. Su, and A. Manthiram, *Li2S-Carbon Sandwiched Electrodes with Superior Performance for Lithium-Sulfur Batteries.* Advanced Energy Materials, 2014. **4**(1).

270. Han, K., et al., *Li2S-reduced graphene oxide nanocomposites as cathode material for lithium sulfur batteries.* Journal of Power Sources, 2014. **251**: p. 331-337.

271. Zhao, Q., et al., *Sulfur Nanodots Electrodeposited on Ni Foam as High-Performance Cathode for Li–S Batteries.* Nano Letters, 2015. **15**(1): p. 721-726.

272. Sa, Q. and Y. Wang, *Ni foam as the current collector for high capacity C–Si composite electrode.* Journal of Power Sources, 2012. **208**(0): p. 46-51.

273. Goodenough, J.B. and K.-S. Park, *The Li-Ion Rechargeable Battery: A Perspective.* Journal of the American Chemical Society, 2013. **135**(4): p. 1167-1176.

Appendix

Appendix A

Awards (June-2013 to December-2016)

1. 2013-2016 Excellerate Australia (former Auto CRC) PhD scholarship award, Institute for Superconducting and Electronic Materials, University of Wollongong
2. 2013-2017 International Postgraduate Tuition Award, University of Wollongong
3. 2016 ISEM Postgraduate Student Merit Award, University of Wollongong.
4. 2016 AIIM HDR Student Conference and International Travel Grants, University of Wollongong
5. Excellerate Australia (former Auto CRC) professional development fund 2015.
6. 3rd auto CRC technical conference image competition award.

Appendix B

1. Publications (June-2013 to November-2016)

1) **Kaiser, M. R.**, Chou, S., Wang, C. S., Liu, H. K., Dou, S. X, &Wang, J. H. "*Structure-Property Relationships of Organic Electrolytes and their Effects on Li/S Battery Performance*". **Advanced Materials**. 2017.

2) **Kaiser, M. R.**, Liang, X., Liu, H. K., Dou, S. X, &Wang, J. H. "*A Methodical approach for Fabrication of Binder-free Li_2S/C composite Cathode with High Loading of Active Material for Li-S Battery*". **Carbon**, Vol. 103, pp. 163-171, 2016.

3) **Kaiser, M. R.**, Liang, X., Konstantinov, K., Wang, J. H., Liu, H. K., & Dou, S. X. "*A Facile Synthesis of High Surface Area Sulfur-Carbon Composite for Li/S Batteries*". **Chemistry-A European journal. Hot paper**, Vol. 21 (28), pp. 10061-10069, 2015. **Back cover.**

4) **Kaiser, M. R**., Wang, J. H., Liang, X., Liu, H. K., &Dou, S. X. "*A systematic approach to high and stable discharge capacity for scaling up the Li/S battery*". **Journal of power sources**. Vol. 279, pp. 231-237, 2015.

5) **Kaiser, M.R.**, Ma, Z., Wang, X., Han, F., Gao, T., Fan, X., Wang, J.Z., Dou, S.X., Liu, H.K., and Wang, C.S. "*Synthesis of Sulfur/Graphene Composite by Reverse Microemulsion Method for Enhancing the Stability of the Lithium/Sulfur Battery*" (Submitted to Advanced Energy materials).

6) Liang, X., Zhang, M., **Kaiser, M. R**., Gao, X., Konstantinov, K., Tandiono, R., Wang, Z., Liu, H. K., Dou, S. X., & Wang, J. "*Split-half-tubular polypyrrole@sulfur@polypyrrole composite with a novel three-layer-3D structure as cathode for lithium/sulfur batteries*". **Nano Energy**. Vol. 11, pp. 587-599, 2015.

7) Liang, X., **Kaiser, M. R.**, Konstantinov, K., Tandiono, R., Wang, Z., Chen, C., Liu, H. K., Dou, S. X., & Wang, J. "*Ternary Porous Sulfur/ Dual-Carbon Architectures for Lithium/Sulfur Batteries Obtained Continuously and on a Large Scale via an Industry-Oriented Spray-Pyrolysis/Sublimation Method*". **ACS Applied Materials & Interfaces**, Vol. 8 (38), pp. 25251-25260, 2016.

8) Liang, X., **Kaiser, M. R**.,Gao, X., Konstantinov, K., Tandiono, R., Wang, Z., Liu, H. K., Dou, S. X., & Wang, J. "*High performance pure sulfur honeycomb-like architectures synthesized by a cooperative self-assembly strategy for lithium–sulfur batteries*". **RSC Advances**. Vol. 4 (69), pp. 36513-36516, 2014.

2. Conferences:

1) **Kaiser, M. R.**, Liang, X., Liu, H. K., Dou, S. X, & Wang, J. H. "*Capillary Deposition of Binder-free Li_2S-C composite in 3-D Ni Foam for High Performance Li-S Battery*". **18th International Meeting on Lithium Batteries**. Meeting Abstracts, 429-429. June 19-24, 2016. Chicago, Illinois, USA.

2) **Kaiser, M. R.**, Liang, X., Konstantinov, K., Wang, J. H., Liu, H. K., & Dou, S. X.(2014). "*Simple and Large-Scale Synthesis of Sulfur/Carbon composite: A Platform for Lithium/Sulfur Batteries Commercialization*". **Future Energy Conference**, Sydney, Australia. 3-5 November-2014.

3) **3rd Technical conference** arranged by Auto CRC, Melbourne, Australia.

3. Other activities:

a) 3 Minutes Competition in AIIM, Wollongong, Australia, Jun. 5, 2014.

b) Received certificate on Liquid Nitrogen Handling, Organized by University of Wollongong, Australia.

c) Received Certificate for First Aid Training, Organized by Barrington Training Service, Australia.